UNIVERSITÀ DEGLI STUDI DI PADOVA

Dipartimento di Ingegneria Industriale DII

Corso di Laurea Magistrale in Ingegneria dell'Energia Elettrica

Tesi di Laurea Magistrale in Ingegneria dell'Energia Elettrica

Ground fault current: Calculation of magnitude and its distribution in the neutral and ground paths

Relatore: Prof. Roberto Turri

Correlatore: Prof. Massimo Coppo

Laureando: Matteo Pettenò, 1205061

Anno Accademico 2019/2020

Acknowledgements

There are several people I would like to thank for this thesis experience: firsts of all, Prof. Roberto Turri, for the opportunity to develop this work and for the fruitful discussions on engineering and non-engineering topics, and Prof. Massimiliano Coppo, for his constant support and generous availability during the whole project.

Many thanks to all the people I have met in the laboratory during these months, for the advice, the occasions for confrontation and the friendship during work and breaks.

Finally, I want to thank my family and my friends, who have always believed in me and supported me, and because if I am the person I am today, I owe it to them.

Indice

i. List of symbols/abbreviations

Abbreviations

Follows a list of the main abbreviations used in the thesis. Others, used just once or with less frequency, are directly defined in the text.

ANSI	American National Standards Institute
CIGRE	Conseil International des Grands Réseaux Électriques
EMI	ElectroMagnetic Interference
FOP	Fall Of Potential
GDP	Gross Domestic Product
GIL	Gas Insulated Line
GMD	Geometric Mean Distance
GPR	Ground Potential Rise
HIF	High Impedance Fault
HV/MV/LV	High/Medium/Low Voltage
IEC	International Electrotechnical Commission
IEEE	Institute of Electrical and Electronics Engineers
LLG	Line to Line to Ground
OECD	Organization of Economic Cooperation and Development
OHEW	OverHead Earth Wire
PCC	Point of Common Coupling
PQ	Power Quality
QRA	Quantitative Risk Assessment
RES	Renewable Energy Source
SLG	Single Line to Ground
TS	Transition Station

Vectors and Matrices

Below is reported a list of vectors and matrices that are defined here to mark the used conventions or to introduce some parameters' names that are not generally used.

$\mathbf{Z_{(0)}}$, $\mathbf{Z_{(1)}}$, $\mathbf{Z_{(2)}}$	Subscripts used for the sequence quantities
$\mathbf{A}$	Incidence matrix
$\mathbf{B}$	Topology matrix
$\mathbf{C}$	Turns ratio matrix
$\mathbf{Y_{Branches}}$	Branches element admittance matrix
$\mathbf{Y_p}$	Primitive admittance matrix
$\mathbf{Y_T}$	Transformer's admittance matrix
$\mathbf{Y_0}$	Open-circuit losses admittance
$\mathbf{Y_O}$	Common node O admittance

ii. Abstract

The development of the electricity grid is increasingly oriented towards a widespread diffusion of electricity production from RES, which shifts the balance from a predominantly vertical structure to one in which generation units connected to low and mid voltage levels, even though of relatively small size, are becoming increasingly influential.

Although, of course, this development is also favoured by various incentives to support the production of energy from clean sources, at the transmission grid level the increasingly significant share of energy produced from RES compared to traditional power plants poses several technical issues, such as a more difficult voltage and frequency regulation in general requiring a higher coordination among the generation facilities and thus necessitating an evolution in grid management strategies in several aspects.

Within this wide panorama, it is necessary to maintain a high level of concentration on the most important issues such as safety: in fact, guaranteeing an adequate level of energy supply with quality and continuity is subordinated to ensuring the safety of plants and people. It is precisely in these issues that the main argument of the thesis intervenes, which concerns the fault currents within the transmission grid not only in its amplitude but also in its distribution, in case of ground fault, between the ground paths and the earthwire.

In this way, being able to know the value of the current that, in case of failure, flows through the ground system of a substation or in a tower footing, it is possible not only to efficiently design the above mentioned earthing systems but also to effectively predict the GPR levels reached, to avoid situations that could endanger people's health.

After a review of the state of the art of the fault conditions in the power systems and the main elements that influence them developed in Chapter 1, and a brief summary of the main standards for the fault current calculation with a subsequent comparison in Chapter 2, a system for the modelling of the electrical network based on multi-conductor representation will then be presented in the thesis, which basic theory and formulas are reported in Chapter 3: this method, through the particular representation of certain grid elements, is also able to integrate the management of asymmetric systems and sections with a different number of conductors.

Starting from this model, simulations will then be carried out at pre-fault and under fault conditions to analyse which parameters influence the current distribution. These simulations, first carried out on an elementary network and then applied on the portion of a real network, will also be carried out on commercial software such as Neplan and OpenDSS to validate the model developed in Matlab environment and to make a comparison on limits and potential of the implemented techniques, as will be reported in Chapters 4 and 5.

iii. Sommario

Lo sviluppo della rete elettrica è sempre più orientato verso una capillare diffusione della produzione di energia elettrica da fonte rinnovabile, che sposta l'equilibrio da una struttura prevalentemente verticale ad una struttura in cui le unità di generazione collegate ai bassi livelli di tensione, seppur di dimensioni ridotte, per via dell'elevato numero stanno diventando sempre più influenti.

Per quanto naturalmente questo sviluppo sia favorito anche tramite diversi incentivi a sostegno della produzione di energie da fonti pulite, a livello di rete di trasmissione la sempre più rilevante quota di energia prodotta da fonti rinnovabili rispetto alle tradizionali centrali elettriche pone delle difficoltà di gestione, come ad esempio una più difficoltosa regolazione di tensione e frequenza, in generale richiedendo un maggior coordinamento delle unità di generazione, necessitando dunque una evoluzione nelle strategie di gestione della rete sotto diversi aspetti.

All'interno di questo vasto panorama, è necessario mantenere alto il livello di concentrazione sui temi più importanti quali quello della sicurezza: l'assicurare un adeguato livello di fornitura di energia con qualità e continuità, infatti, deve essere subordinato alla garanzia della sicurezza degli impianti e delle persone. Proprio in queste tematiche interviene il principale argomento della tesi, che riguarda le correnti di guasto all'interno della rete di trasmissione non solo nell'ampiezza ma anche nella sua distribuzione, in caso di guasto verso terra, tra i percorsi nel terreno e la fune di guardia.

In questa maniera, infatti, potendo conoscere nel dettaglio il valore di corrente che in caso di guasto scorre attraverso l'impianto di terra di una sottostazione o la messa a terra di un sostegno è possibile non solo progettare al meglio il dimensionamento dei suddetti sistemi di messa a terra, ma anche poter prevedere efficacemente i livelli di GPR raggiunti al fine di evitare situazioni che possano mettere in pericolo la salute delle persone.

Dopo una revisione dello stato dell'arte delle condizioni di guasto nelle reti e dei principali elementi che le influenzano sviluppato nel Capitolo 1 e un rapido ma necessario riassunto sulle principali norme per il calcolo della corrente di guasto nelle reti con un successivo confronto inserito nel Capitolo 2, verrà quindi presentato nella tesi un sistema per la modellizzazione della rete elettrica basato sulla rappresentazione multi-conduttore, la cui teoria di base e le principali equazioni verranno descritte nel Capitolo 3. Questo metodo, tramite una particolare rappresentazione di determinati elementi, è in grado di integrare anche la gestione di sistemi asimmetrici e di sezioni con un differente numero di conduttori.

Partendo da questo modello, verranno poi svolte delle simulazioni a regime e in condizioni di guasto per analizzare quali parametri influenzano la distribuzione delle correnti. Queste simulazioni, dapprima svolte su una rete elementare e successivamente applicate su una porzione di rete reale, saranno svolte anche su software commerciali quali Neplan e OpenDSS per validare il modello sviluppato in ambiente Matlab e poter fare un confronto su limiti e potenzialità delle tecniche usate, come descritto nei Capitoli 4 e 5.

1 Introduction

1.1 Energy context and network evolution

In the last century, and particularly the second half of the twentieth century, global primary energy consumption has grown exponentially. Over the past 70 years, humanity has more than quintupled energy consumption, supporting economic and demographic growth through an energy system built mainly on the use of fossil fuels.

Based on the evolution of these numbers especially in recent years, numerous scenarios have been created and evaluated to better understand future developments. Among these, here are reported some data from the International Energy Outlook of 2019, considering the most balanced scenario which is the Reference case: it reflects current trends and relationships among supply, demand, and prices in the future; it is a reasonable baseline case to compare with cases that include alternative assumptions about economic drivers, policy changes, or other determinants of the energy system to estimate the potential impact of these assumptions. In this case, combined Gross Domestic Product (GDP) in the countries that are not part of the Organization of Economic Cooperation and Development (OECD) grows by 3.8% per year on average between 2018 and 2050, compared with 1.5% per year in the OECD countries (GDP per person is an indicator of a country's standard of living).

This and other constraints affect the growth of energy consumption, which is a key parameter for the future development of electricity generation and transmission systems. In the reference case, most of the increase in energy consumption comes from non-OECD countries, where strong economic progress, increased access to marketed energy and rapid population growth lead to rising energy consumption. On the other hand, in OECD countries the progress in energy consumption is slower as a result of relatively slower population and economic growth, higher improvements in energy efficiency, and slower expansion in energy-intensive industries. Fig. 1-1 shows the prevision of energy consumption in non-OECD countries, which increases nearly 70% between 2018 and 2050, in contrast to a 15% increase in OECD countries [1].

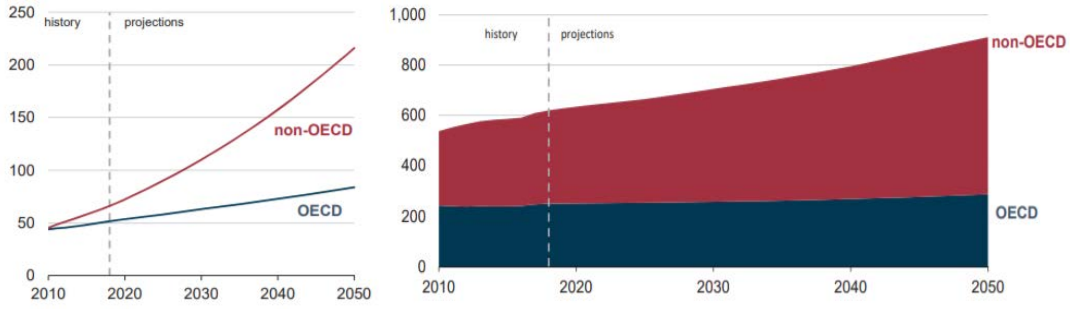

Figure 1-1: On the left the world GDP in trillion dollars with Purchasing Power Parity, on the right world energy consumption in quadrillion British Thermal Units [1].

The main problem related to these values and their predictions is how the end-use energy consumption (end-use fuels include those consumed in the industrial, transportation and buildings sectors and exclude fuels used for electric power generation) is distributed among the various energy sources. As shown in

Fig. 1-2, fossil fuels are still the main energy source, since coal continues to be an important end-use fuel in industrial processes, such as the production of cement and steel, and liquid fuels, because of energy density and cost, continue to be the predominant transportation fuel and an important industrial feedstock. While, for the diffusion of electricity use, it's rapidly increasing primarily in the industrial and transportation sector, respectively, as a result of the automation of industrial processes and the increasing use of electric vehicles [1].

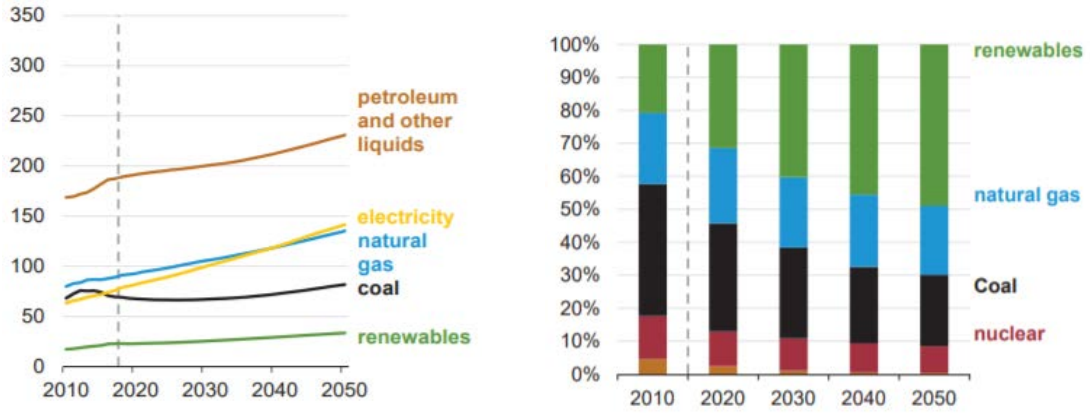

Figure 1-2: On the left the end-use energy consumption by fuel in quadrillion BTU, on the right the share of net electric generation [1].

The crucial issue associated to these numbers is that the production of energy from fossil sources is one of the central responsibility for the anthropogenic greenhouse gas emissions (including CO_2), widely recognized as the cause of significant environmental and climatic impacts, including the increase in the global average temperature (it's estimated a growth trend of + 0.2 °C per decade due to human actions [2]) and the intensification of natural catastrophic events.

That is why in recent years it has been chosen internationally to invest in energy efficiency and energy production from renewable sources. To achieve certain objectives and protect the environment, international agreements such as the one at the 2015 Paris Conference [3], and short-medium term projects such as "Europe 2020 strategy" (20% cut in greenhouse gas emissions from 1990 levels, 20% of EU energy from renewables, 20% improvement in energy efficiency [3]) and "Clean Energy for all Europeans Package" (40% greenhouse gas emission reductions, 32% in renewable energy, 32.5% for energy efficiency [4]) for 2030 have been established.

However, this transformation is not zero-impact for the electrical system and involves several challenges to be addressed for the transition process to be carried out continuously and efficiently, while maintaining high levels of service quality and avoiding an excessive increase of costs. Changes in the context already cause significant effects on the network management activities, that require at any given moment the balance between electricity production and demand, to ensure that users have a safe, constant, and reliable supply of energy.

Here are some examples of the main variations:

- Plant connection: RES plants are generally interfaced with the grid through static converters (inverters), which, unlike the rotating machines typical of traditional generation, provide a

much lower inertia and hence are unable to provide the same support to the grid's stability (in terms of frequency and voltage), in the case of perturbations.

- Non-programmability of the plants: the production of electricity from RES does not follow the dynamics of the energy requirement for consumption, but rather dynamics typical of the availability of the primary energy source which is, by its nature, intermittent, due to both slow and predictable variations (weather forecasts) and sudden and unpredictable changes (e.g. clouds passage for photovoltaic generators or wind changes in magnitude and direction for wind turbines). The system is also "structurally" exposed to periods in which the production from RES exceeds the need for electricity (over-generation) with the consequent need to either reinforce the power lines or install adequate storage capacity.
- Plant location: RES plants, in particular wind power, are often located far from consumption centres, causing an increase in transmission grid congestion. Also, the fact that a substantial part of RES plants is connected to MV/LV distribution networks is bringing new problems in the management of the electricity system, such as the reduction of the selectivity of protection systems and the possible inadequacy of monitoring systems and automation systems designed for unidirectional operation.
- Climate change: the increased frequency of extreme climate events, already perceptible today, causes a higher probability of significant damage to the country's infrastructure, including electricity transmission ones, which leads to the risk of increased network failures.

As mentioned above, the power grid is going through a period of necessary evolution characterized by an operation that goes against beliefs once considered immutable (unidirectional power flow, passive grid), and by new parameters with a strong variability. Within this wide picture, it is necessary not to lose sight of what are the essential constraints: the reliability of the system and human safety. It is, therefore, necessary, now more than ever, to better understand the consequences of faults and the distribution of ground fault currents to correctly coordinate protection systems and minimize the risk of personal injury.

1.2 The need for ground current distribution evaluation

Nowadays electricity is increasingly seen as a real commodity, which must meet certain quality criteria required by the customer who pays for it. The study of Power Quality is referred to as a set of measures to be considered in the design and management of the electricity grid to ensure an adequate supply of energy that guarantees certain standards. In recent years, the task of maintaining a high level of PQ has become more difficult due to the presence of more sensitive devices in the network, which suffer more from the presence of disturbances and become, in turn, a source of distortion, and the spread of Distributed Generation with the arrival of the new figure of the prosumer (producer + consumer) that has led the network to no longer be solely passive and no longer have a unidirectional power flow.

PQ can be divided into Voltage Continuity, linked to energy availability, and Voltage Quality, related to the presence of "low-frequency disturbances" in the network [5]. To oppose adequate maintenance of the required values, there are a series of perturbation events that modify the voltage in the network: as reported in Fig. 1-3, these can be distinguished in events that modify the waveform (harmonic content), events that vary the frequency, events that cause dissymmetry, and finally events that modify the amplitude and that, according to the percentage variations and duration, are distinguished in various types such as fluctuations, voltage dips, interruptions, overvoltage and others.

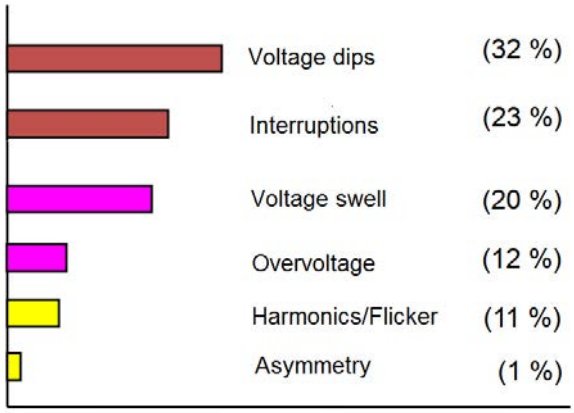

Figure 1-3: Statistics concerning the complaints of the electricity network's users [5].

The main problems for consumers are voltage dips and interruptions, and these are largely caused by grid failures. There are different types of electrical faults, ranging mainly from short circuits to overloads, due to internal causes, as in the case of switching transients, or external causes, such as those due to direct or indirect lightning strikes. The same short circuits are then classified in net or not net, in case that an active part comes into contact with a part with a different voltage through negligible and non-negligible impedance respectively, and, according to the number of phases involved, in single-phase, two-phase, three-phase and combinations of these [6]. A proper knowledge of these phenomena and the resulting current distribution they cause in the grid and its surroundings is therefore necessary for the maintenance of a high level of PQ, being able in many cases to limit their frequency and in some cases even predict their occurrence.

It is necessary to point out that with the rapid development of the new industry, the occurrence of a voltage sag can cause significant economic loss due to the trip of industry process: in fact computers, programmable logic controllers, electromagnetic switches and other equipment, which are widely used in the new industry, are greatly affected by voltage sag, which is defined by the Institute of Electrical and Electronics Engineers (IEEE) as “an event in which the root mean square value of voltage drops rapidly between 10% and 90% of the rated value and the duration lasts from 0.5 cycle to 1 min” [7].

Obtaining information on network faults and their correlation with voltage sags can help to take measures to reduce the financial loss due to voltage sag: from the system operator’s side, voltage sag frequency can provide information for the maintenance and the reconstruction of the power system,

while, from the user's side, the knowledge of voltage sag frequency can help sensitive users to select the point of common coupling (PCC) with less sag severity [8]. Duration is an important characteristic of voltage sag and is usually determined by the fault clearance time; other parameters that influence voltage sags' characteristics are the resistance and the type of faults, which have been widely discussed in detail in many papers, and fault locations. Although engineers design the transmission lines aiming to have a uniform fault distribution, because of the exposure to adverse environmental conditions the fault rate of some parts of the line may be higher than others, leading to a non-uniform distribution of faults as reported in Fig. 1-4 [9].

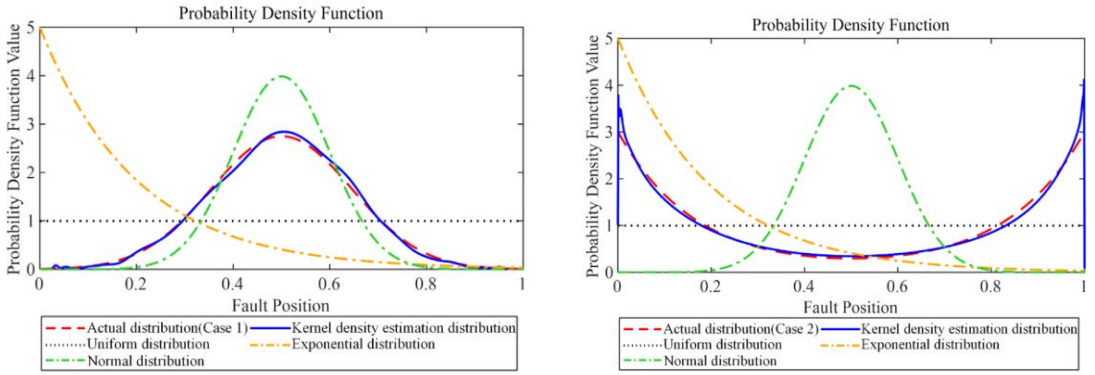

Figure 1-4: Several probability density functions of line fault under different methods in normal (left) or valley (right) basic case to evaluate the contributions of different fault locations to the probability density function [8].

To better understand these phenomena, two techniques can be used: past performance measuring (monitoring) and future performance prediction. The former is a process in which data are stored and analyzed, for which reason it finds fewer application in the case of continuous network changes also considering that, since faults occur randomly, voltage sags monitoring for a single area requires a long time to be completed. The latter is based on several probabilistic techniques such as stochastic simulation, analytical technique (which represents the power system employing mathematical models and estimates reliability indexes using direct mathematical solutions) and the method of fault positions, which estimates the frequency of voltage sags in electrical networks [10].

A further element for which the analysis and modelling of faults in the network and earthing systems are of fundamental importance to determine the distribution of fault currents is human safety. AC transmission lines' grounding systems provide low impedance paths to dissipate fault currents without excessive damage to facilities. When a single-phase ground fault occurs, the current follows two return paths, ground wires and towers' footing systems: the latter generates an increase in the potential at the base of all connected structures which leads to the risk of electrical shock to nearby people.

In the same way, the distribution system, due to its extension and increased susceptibility to short circuit events, suffers many more failures than the transmission system, and of these more than half concern the ground connection. Although the amplitude of the fault currents is lower than those of the transmission system, the fault clearance times are much longer: they range from 10's-100's ms in the transmission line, depending on the distance of the fault section from the protection [11], to values close

to one second for the distribution lines conditioned by particular neutral management approaches (e.g., a system earthed via Petersen coil allows longer fault clearance times because the current value is kept very low) [12].

The above-mentioned increase in the potential of the ground system compared to the remote ground, which can be touch or step voltage, is generated between different points inside or outside an installation (e.g. a substation) and can cause electrocution in the presence of people. If the magnitude of these voltages and the duration of the shock are high enough, they can cause severe shock, asphyxia, or even cardiac fibrillation and death.

Although the trend of deaths and injuries caused by these events has been declining in recent years thanks to increased investment and a better understanding of the phenomenon, it is a number that still needs to decrease, as shown in Fig. 1-5.

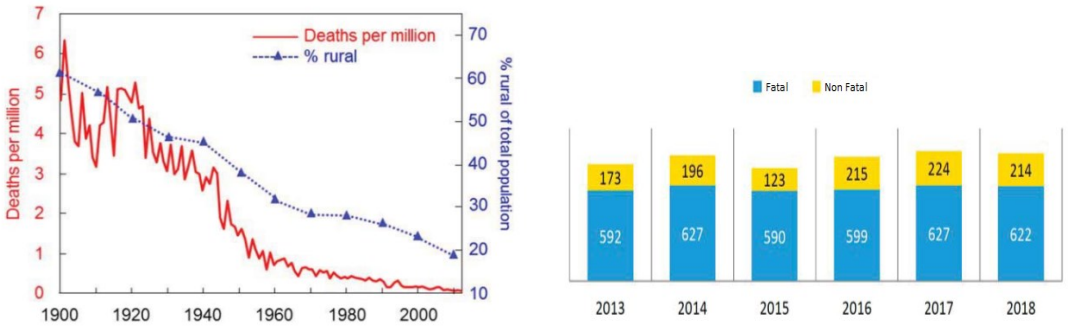

Figure 1-5: On the left the annual mortality rate from lightning in the USA; on the right, fraction of fatal and non-fatal outcomes from electric shock accidents in Brazil [13].

However, due to the hazardous nature of many processes, it is infeasible to eliminate the risks. A balance, that would secure the benefits gained by the practice of the hazardous activity, while retaining the risk to acceptable levels, is desirable, following the "As Low As Reasonably Possible" principle, as suggested by CIGRE B2 Study Committee [13]. It has been proven, over the past few years, that fault location, clearance time, soil resistivity, fault current magnitude, location of the person in time of shock, and current path are some of the parameters that lead to a statistical variation and that should be considered in the safety analysis of an earthing system, instead of the standard " worst-case scenario" values [14]. Therefore, a more rigorous and comprehensive procedure of probabilistic risk assessment of the earthing systems is required to reduce risk as much as possible trying to maintain acceptable costs.

Unfortunately, these are not the only considerations and analyses that need to be made to assess the safety of a line: for instance, when a fault to ground occurs in HV/MV substations supplied by a combined overhead-cable line, a significant part of the ground-fault current flows through the sheaths of the earthing cables and finally discharges into the ground at the transition station (TS), where the cables are connected to the overhead line. This is due to the difference in mutual coupling factors for overhead lines and cables, which results in only a small portion of current carried by cable sheaths to continue towards the source through the overhead ground wire; instead, a large portion of this current

flows in the ground surrounding the ground electrode and continues towards the source through the earth.

This phenomenon, represented in Fig. 1-6 and called "fault application transfer", was noted for the first time in 1988 concerning safety problems related to the increase in the potential of the ground in transition station in Rio de Janeiro, in which shocks and damage to equipment were recorded as a result of ground faults in a remote substation up to 12 km away [15]. Several tests have been carried out, based on measurement campaign of the ground fault current distribution at substations with combined overhead-cable transmission lines, which have reported that more than 25% of the current flows between TS's ground electrode and the adjacent area causing high and dangerous voltage values, especially in dense urban areas.

Therefore, it is necessary to carefully consider the effects of this phenomenon in the design and testing phase of a substation, both for more efficient and economical design and for safety in the substation. It should be considered that this phenomenon is expected to increase for a few reasons [16], among which:

- the use of underground transmission cables in modern HV installations continuously increases due to technical and environmental reasons, so that combined overhead-cable transmission lines are becoming more frequent in current applications;
- an overhead-underground TS occupies a very small area compared to a conventional substation and therefore its relatively small and high resistance ground electrode may be inadequate to keep the ground potential rise (GPR) within safe limits in case of fault current transfer, also considering the ever-increasing fault current values;
- optics fibres for telecommunication systems are even more frequently located within ground wires on high-voltage overhead transmission lines. The effects of "fault application transfer" on the GPR at TS and nearest towers can expose workers to unsafe conditions during maintenance of optical ground wires on the towers where the equipment boxes are located.

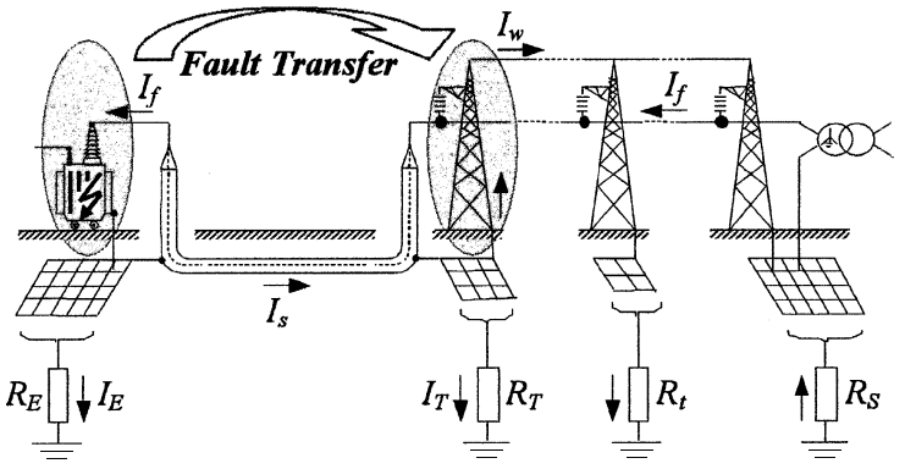

Figure 1-6: "Fault application transfer" at a substation fed by a combined overhead-cable line [16].

A further reason to deepen the knowledge on the distribution of fault currents is the presence of metal structures in the ground: these must not only be considered in the analysis as they modify the distribution, as will be seen in the next paragraph, but they can also suffer unexpected damages due to high voltage or current values and cause further problems to the human safety.

Considering, for example, a failure near a railway track, the presence of coupling due to the ground fault of the power system with the multiconductor network of the railway system is a serious problem not only for people's safety but also for small power equipment such as signalling and telecommunication cables.

Perhaps even more evidently, often due to the similarity of the criteria for the choice of industrial and oil/gas power transmission paths, there are often situations of parallelism or crossing between the transmission lines and the pipelines. This involves several coupling effects with the pipelines, respectively of capacitive nature in the case of an aboveground pipeline, of inductive nature due to the variation in time of the magnetic field caused by the transmission lines (which involves both aboveground and underground pipelines), and then of resistive nature in the case of earth faults and lightning strikes with high levels of current flowing to the ground. This often increases the potential of the tower base and the surrounding terrain, interfering with personal safety, resulting in significant stress voltage across the pipeline's coating which can lead to arcing phenomena with consequent corrosion of coating or pipeline, and changing the normal functionality of the pipeline's cathodic protection systems.

The phenomenon of electric arcs affects not only the metal structures outside the electrical network but also the electrical network itself. When an overhead power line breaks physically and falls to the ground, or comes into contact with the ground through any object, it leads to a concept called high-impedance failure, often accompanied by an electrical arc, which can lead to hazards, damage to electrical equipment or risk to human life. According to the Power System Relaying and Control Committee of the Institute of Electrical and Electronics Engineers (IEEE PSRC), a HIF is defined as "an unwanted electrical contact of an excited conductor with a non-conductive surface that limits the fault current to a lower level making it undetectable by conventional analysis" [17].

As reported by the various examples and considerations in this regard, it is clear that, due to the complex nature of the phenomenon, the various factors that influence it, and, above all, the direct consequences that it can have on people's health, a more in-depth study of the distribution of fault currents is necessary.

In the past, analyses of this kind were based on collecting data from years of failure on a given section of the line and tests carried out to conclude how the nature of the failure and the characteristics of the line were related to fault current's magnitude [18]. A technique like this takes an enormous amount of time, which is why nowadays, thanks to technological and informatics development, simulations to validate line models, ground systems, and network scenarios are performed using software.

In this thesis, therefore, a complete grid model will be presented, and several simulations will be carried out to better understand which are the key parameters that influence the fault current distribution to obtain a deeper knowledge of the phenomenon and to be able to limit its dangerousness.

1.3 Factors influencing the ground current distribution

Among the various elements that influence the ground current distribution, the main ones can be classified in the following categories:

- Type and topology of the line
- Failure type, failure distance, different generation-load scenarios
- Earth system
- Soil resistivity

Since the basis for the calculation of the breakdown current distribution is the modelling of the involved circuit, which largely consists of the transmission line and its parameters, the type of line undoubtedly changes the current values. If we consider, for example, a pi-model representation of the line, to calculate the values of transverse admittances and longitudinal impedances it is necessary to know the diameter of each of the phase conductors (the equivalent ones in the case of bundles), their arrangement with the resulting geometric mean distance, the knowledge of the material properties (including insulators in cables' case) and the operating temperatures. These elements vary the overall impedances of current's paths modifying the distribution.

Besides the obvious difference in calculating these values in the case of overhead line, cable, or GIL, this procedure can be further complicated by the presence of several lines with different characteristics or of different nature that require the evaluation of mutual relevant parameters. These cases are far from being rare and often occur when a new substation is connected to an existing one, or when, as happens more and more frequently in an urban and suburban environment, the new lines are buried cables that are connected to an existing overhead line: when a ground fault occurs, these lines create a complex electrical circuit with a high number of galvanically and inductively coupled elements that make the whole problem more complicated [19].

Another component that modifies these circuits is the overhead earth wire (OHEW), which connects the earth system of the various transmission poles with substation earth: this plays an important role when it comes to fault current distributions and it protects the transmission main lines from lightning strikes. A further coupling factor is thus introduced, this time between the OHEW and the faulty phase, that causes the substation fault current's division into two sub-currents of which the percentage that flows through the OHEW depends on the coupling factor, on the value of the substation ground resistance and on the impedance of the OHEW, which, in turn, depends on the material, the length, the distance between the wire and the faulty phase and the ground resistivity [20].

Below are presented in a more detailed way some of the above-mentioned parameters that, as for the conductors of the transmission line, modify the impedance of the circuit [21]:

- Effect of the average geometric distance: the greater the distance between the earth cable and the faulty phase conductor, the smaller the magnetic coupling between them, resulting in a greater share of current flowing through the earth system with a consequent higher GPR, higher

touch and step voltage and transferred potential phenomenon. Thus, to have a safe and economic design of the grounding grid, more current should be diverted via earth wire.

- Effect of section and material: the section of the cable and the properties of the material used to make the OHEW (steel, aluminium, etc.) modify the resistance; the higher the geometric mean radius of earth wire and conductivity, the more current will be diverted via earth wire.
- The number of spans/length of OHEW: tests carried out to illustrate the influence of these parameters, which results are reported in Fig. 1-7, have shown that the current carried by the OHEW to the remote source which fed it rapidly decreases as its length increases up to several kilometres, above which the value has only smaller variations.

This not only affects the distribution of currents but needs also to be considered because this current portion energizes the grounding of the various transmission pylons, leading to unsafe step or touch voltage values.

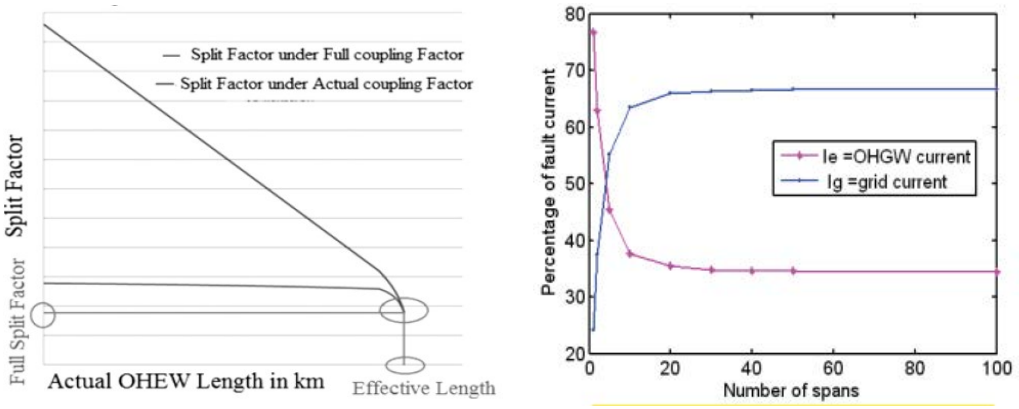

Figure 1-7: Split factor for non-continuous OHEW when using the full and the actual coupling factor on the left *[20]*; the percentage of fault current diverted via OHEW vs the number of spans on the right [21].

Still talking about circuits, as already mentioned in the previous paragraph, there are other metal structures present in the vicinity of the power line (either above or underground) which, through the phenomenon of mutual coupling, may interfere in the distribution of the fault current: the different couplings due to the presence of pipelines, conductors for railway transport system or conductors dedicated to the transport of signals or information have already been mentioned. In fact, in the case of single-phase to ground fault, the electromagnetic interference (EMI) generates inductive coupling for the current flowing in the phases and the ground wire and resistive coupling for the current going to the ground through the tower footing impedance. Since they cause considerable changes compared to an analysis that does not take these elements into account, in Fig. 1-8 are reported the results that numerically confirm that these contributions have not to be underestimated.

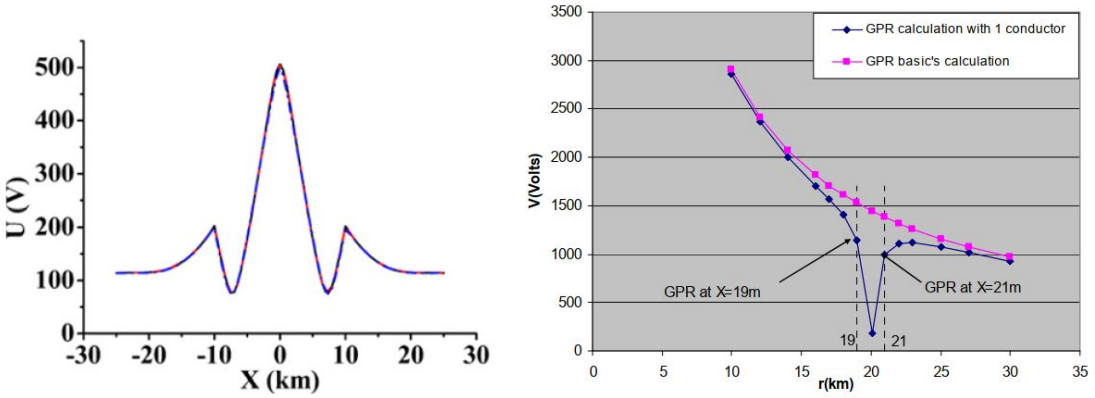

Figure 1-8: Pipeline stress voltage whit fault in 0 Km on the left [22], classical grounding calculation vs calculation with railway conductor on the right [23].

When carrying out the analyses for the calculation of the breakdown current distribution, it is also necessary to take into account a series of factors linked to the state of the grid at the time of failure and the characteristics of the failure itself, which, unlike the parameters discussed above, are quantities associated to a greater degree of uncertainty. For this reason, various statistical techniques based on the probability of current distribution are used, including, for example, analyses based on Monte-Carlo simulation, a simple method to implement providing reliable results: analyses of this type require to reproduce the random variability of certain parameters within the program's algorithms, leading to analytical and computational difficulties as the size of the problem increases.

These elements can be separated between those related to the transmission network and those related to the failure. To the first category belong, for example, all the random variations of the transmission facilities, that can be predicted by historical data regarding, for example, maintenance and planned disconnections during fixed periods of the year. In addition to this, it is necessary to consider the constant evolution of the load and generation scenarios. In this type of analyses, load representation is often acceptably neglected, although potentially being a factor is determining the pre-fault operating conditions, while representing the generation scenario, that is closely related to the expected system demand, is particularly important, given its impact on fault current values. To simulate the different scenarios and their consequences on the current distribution, it is possible to rely on daily or monthly average load diagrams, to include in the model the generation plants both in service and in reserve; the same scheduled maintenance interruptions of the production units should be consulted, based on the average daily load forecast [24].

To the second group belong the fault type, influencing the number of phases involved and the frequency of fault occurrences, the moment in which it happens, that has an impact, as seen above, on generation and transmission facilities, which need to be included in the network model as well as the fault impedances that may vary due to seasonal variations, and the fault location, which modifies the fault impedance. Several papers can be found in literature about this last parameter, showing that, in the case of the overhead line model, the fault location influences the division of the current between the tower

and ground-wire presenting the minimum value in case of failure at the middle section of the transmission line [25]. For the selection of the probability of the occurrence of a failure, one can rely on historical data, if this is available, otherwise one can consider the probability proportional to the length of the line concerning the area considered [26].

The last component that has to be considered for the distribution of the ground-fault current, and perhaps the most important, is the impedance of the grounding systems, on which depends the portion of the current flowing through the local grounding with all the aforementioned consequences on GPR, touch and step voltage and their relative level of risk. In recognition of this, the standards that a grounding system must guarantee have to be checked and verified several times, through minor assessment as visual inspection and ground continuity test, or major assessment as a test with the current injection to simulate a ground fault [27].

Moreover, due to the direct proportionality between the current amplitude and the risk for the safety of people, different strategies are used to reduce the capacitive component of the ground-fault current, through automatic compensation coil or manually adjustable reactor with a parallel low-Ωic resistor. There are several advantages in having a system with this type of compensation among which the relatively low cost compared to the avoided expenses, lower voltages inside the plant, maintenance of the protection system, and exclusion of the intermittent overvoltage phenomenon; all this despite the disadvantage that every failure, even transitory, can cause an outage of the power supply, with consequent decrease of the PQ [28].

According to the IEEE definition of the earth system, this is a set of various electrical connections to the earth mass consisting on the one hand of a series of conductors connecting metal components that do not carry current to the earth system as a form of prevention against high fault currents in machines and equipment, and on the other hand of the actual connection of the electrical system conductors for the protection of the system itself. The task of providing a short resistance path for currents is performed by the conductive metallic earth rods, horizontal or vertical (vertical ones are more efficient as they disperse current at greater depths), whose resistance depends on geometric properties. Tests have also been carried out to evaluate the influence of the number of vertical rods used in an earthing system, demonstrating that the more the vertical driven rods number increase, the more the value of the surface potential at the ground surface decrease with enhanced benefits in case of connections between the vertical driven rods, due to the decreasing of the whole grounding system resistance [29].

In grid short circuit failures, the distribution of the fault current through the earth is therefore largely dependent on tower footing resistance: the lower this value, the greater the amount of current dissipated through the earth by reducing the grid current. Typical values for EHV lines are generally 10 Ω to 20 Ω, numbers suitable for lightning protection. Tests show that there is a significant increase in current through the OHEW with the reduction of the tower foot resistance below 20 Ω while above this value, the magnitude of the current remains largely unchanged. The resistance of the earthing system depends on the shape and the size of the earthing grid and on soil resistivity. Soil resistivity is a parameter that can be determined experimentally by several methods including the Wenner method, the Schlumberger-Palmer method, and the Fall-Off Potential (FOP) method: this topic will be further discussed in a more

detailed way, both as regards the methods to obtain the values and as regards its modelling for simulations, in the next section. Moreover, this parameter is often considered uniform, while in nature such a possibility does not exist due to the inhomogeneity of the structure and the widespread layered composition of substances with different properties.

To give an idea of how these parameters influence total resistance, one of the several formulas present in the literature, Sverak's one, is reported below for its simplicity:

$$R_{G(IEEE)} = \rho \left\{ \frac{1}{L_t} + \frac{1}{\sqrt{20A}} \left[1 + \left(\frac{1}{1+h\sqrt{\frac{20}{A}}} \right) \right] \right\} \quad (1.\ 1)$$

where ρ it's the uniform soil resistivity, L_t is the total length of buried conductors, A is the grid area and h is the depth of the grid into the ground. Tests were carried out to see the influence of the ground system's shape on the main parameters regarding the safety of people, and the results reported in Fig. 1-9 showed that between rectangular, triangular, L and T shape, the L-shape gives the lowest values of grid resistance and is the best configuration for step voltage and GPR, while slightly better are the touch voltage values in the case of rectangular shape [30].

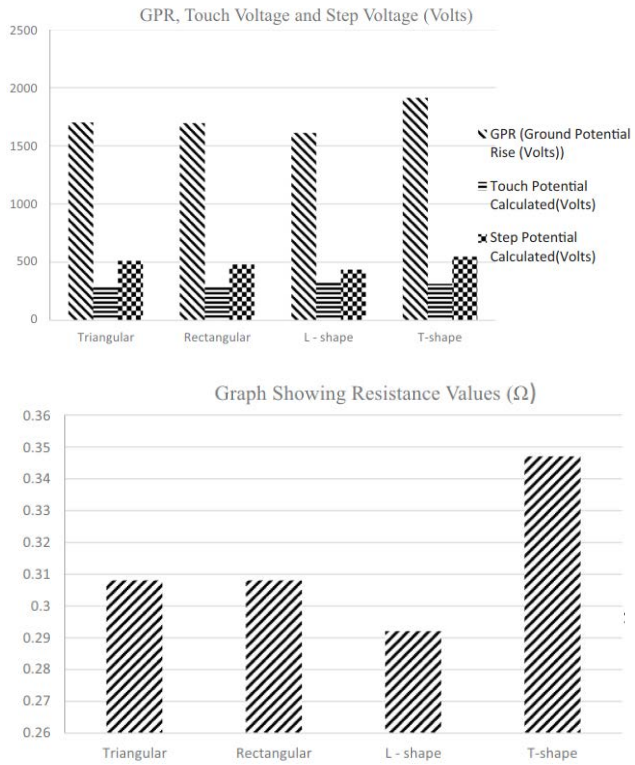

Figure 1-9: Values of GPR, voltage step, touch step and resistance for different shapes [30].

Besides, the use of counterpoises is recommended in the case of high resistivity terrains: these are conductors buried horizontally in the ground at a slight depth connected to the tower foundation grillage in the match to some angle or side. To make the system more effective, instead of using a single long

conductor, several counterpoises of reduced length can be used. In doing this it is necessary to take into account that, although the addition of these buried conductors increases the earthing grid performance, on the other hand, there is the possibility of reaching a saturation point with a consequent drop in the results due to the proximity and induction effects between the conductors, which would only lead to an unnecessary extension of the risk area. The proximity effect is the increase of the impedance of buried conductors due to their mutual resistance, as the current carried by a conductor causes a voltage increase in the other one reducing its capability to further dissipate current; furthermore, the presence of counterpoises in parallel causes an induced electromagnetic force with a result similar to the injection at regular intervals of current in the conductor. For this, when more than one counterpoise is installed, the maximum benefit is obtained where they extend in different directions from the earth grid as reported in Fig. 1-10.

Counterpoise is not the answer in all situations, and for the above-mentioned cons need to be carefully taken into account the earthing systems' location. While if located in a rural area, very little third-party infrastructure need to be considered and counterpoise can often be safely used to achieve desired results, when installed into more densely populated areas, the management of touch voltages and other elements interference coordination becomes very difficult and, in some case, even prohibitive.

This is why over the years, new solutions have been proposed and tested in addition to traditional ones such as: the installation of the counterpoise at a greater depth to increase the quantity of soil around the conductor and the distance from the walking surface; the installation of covered sections within the counterpoise to shield third party equipment, even though this approach requires, in turn, knowing in advance the location of each device at the design stage and the installation of the counterpoise into a feeder cable trench, which offers greater coverage in exchange for increased costs. Among these, some of the most common are the installation of the counterpoise bonding it to the substation earthing system via a feeder cable, so to economically and easily protect it through the feeder cable trench, or running the counterpoise within a feeder cable trench and bonding it to the feeder cable screen at the far end of the cable and to the earth grid, maximizing the auxiliary earth fault return paths' efficiency [31].

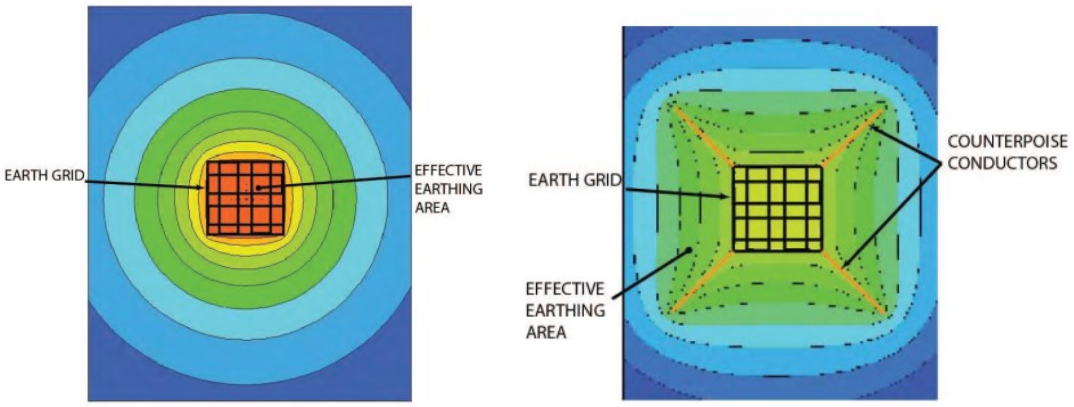

Figure 1-10: Traditional earthing system efficiency on the left and counterpoise position for maximum benefit on the right [31].

1.4 Effect of faults on Ground Potential Rise (GPR)

The ground potential rise is defined as "the product of a ground electrode impedance, referenced to remote earth, and the current that flows through that electrode impedance" in IEEE Std. 367-2012 [32]. Considering that the GPR depends on these parameters, it is a function of the zero-sequence current, which is present only in the case of Single Line to Ground (SLG) or Line to Line to Ground (LLG) faults. GPR is concerned when a large amount of electricity enters the ground due to a line failure or a lightning strike: in case of failure, the fault current at fundamental frequency falls from the fault point trough the earthing system and shield wires, depending on the parameters discussed on the previous section. In standard conditions, the grounded electrical components work at a potential nearly identical to the remote earth one, but, during one of the above-mentioned events, the current flowing through the grounding grid causes an increase in potential (GPR means the maximum electrical potential value of the ground system with respect to the remote earth one): this phenomenon can be risky both for people and equipment since in unusual circumstances tens of kV can be reached.

Although they are not the main focus of the thesis and will not be further investigated later, it is worth underlining the importance of the problem of lightning strikes on the grid both for its randomness and for the high current values that can be reached (the standard lightning current waveform has a peak in 1.2 μs and the half-value in 50 μs, while distribution curve of lightning currents has a scale ranging from 60 to 240 kA), considered the high ceraunic level present in Italy (on average about 3 lightning strikes per km^2 per year, obviously with greater concentration in mountainous areas) [33]. For this reason, to protect the overhead phase conductors there are one or more OHEW, placed above the phase conductors and often containing the optical fibre, to limit the number of direct lightning strikes to the phase conductors within the protection angle of the OHEW (30-40°) to 5%. Since these conductors are electrically connected to the towers, they put in electrical parallel the towers individually earthed reducing the overall earth resistance of the line. As these events also cause a considerable increase in potential depending on the lightning current and the respective impedance, the value of which exceeds that of the pylons' earthing, numerous analyses are carried out since, depending on the fault type (direct, on the pylon or on the guard rope), there are different circuits for the propagation of these travelling waves resulting in different values.

Much more important for the development of the topic of earth fault current distribution is the distribution of currents in the ground due to short-circuit failures in the grid, for which some parameters have already been discussed and others will be explored later.

In addition to the necessary analysis of these phenomena for better network operation and for the direct implication they have on human health, the GPR values are also used for the development specifications of the network protections and components, vital elements for safe and continuous operation of the grid. Several studies have been carried out on how to calculate the impedance related to GPR, as its evaluation in the case of ground faults in a grid requires managing a high amount of data and therefore must rely on computer simulations though adequate models.

The most accurate method for the evaluation of the GPR of a grounding system is the FOP method, although in certain areas such as urbanized ones it is not feasible: this is based on measurements of the ground potential with respect to the GPR with increasing distances from the grounding system, obtaining a voltage profile with respect to the distance that is then analyzed differently in case of the linear model (homogeneous soil resistivity, negligible grounding system's size in respect to the used spaces, point current source) or the compensated one (without the negligible size assumption and considering conductive couplings) [34].

FOP response usually presents two distinct sections separated by a knee as shown in Fig. 1-11, of which the part closest to the ground system has a trend whose analysis is more complex due to the dependence on the geometric parameters of the system itself, while the other part has a trend which approaches a hyperbolic distance relationship. For data processing, GPR estimation software are used, whose reliability is based on the estimation of knee point, as the inclusion of data points before it would complicate the curve fitting, and the influence of measurement errors and local soil variations, which may lead to erroneous data which need to be eliminated. For the solutions of these complications several methods are applied to assess the estimated errors and for determining proper data such as First-Order Least Squares Minimisation Method or Second-Order Least Squares Minimisation Method.

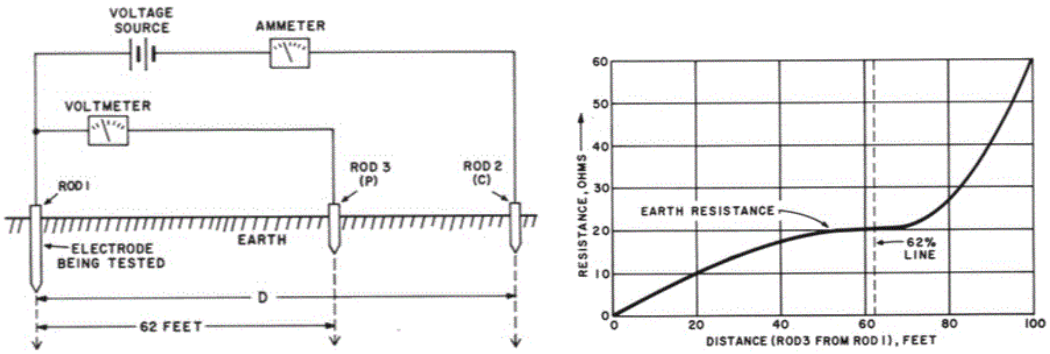

Figure 1-11: On the left the FOP test setup, on the right FOP response [34].

In the following, the parameters that influence the GPR the most will be addressed: from the definition by IEEE, it is directly dependent on the value of the fault current, therefore on the various parameters described in the previous section; therefore, only the parameters that were not discussed previously or those that were only mentioned will be treated.

Having already described the influence of the resistance of the ground system, more in-depth considerations regarding the position where the fault occurs in one of the many towers between two substations need to be done. As it is natural to think, but it is worth noting, the higher GPR value is always obtained at the tower where the failure occurred, this level being proportional to the tower resistance. Tests performed on a transmission network showed that, for tower footing resistance values below 80 Ω, the GPR peak at the tower closer to a local substation were higher than at others, while for

a higher resistance value the trend is shifted towards the other direction, creating a non-linear relationship for peak GPR values vs. tower number as reported in Fig. 1-12 [35].

This depends on the fact that when tower footing resistance increases, the increase of the ratio between it and the equivalent impedance of ladder networks at either side seen from the fault point may not be the same. It is also shown that an SLG fault at a tower is more severe than one at the substation, with a resulting much higher GPR that will involve both substations, even with different values.

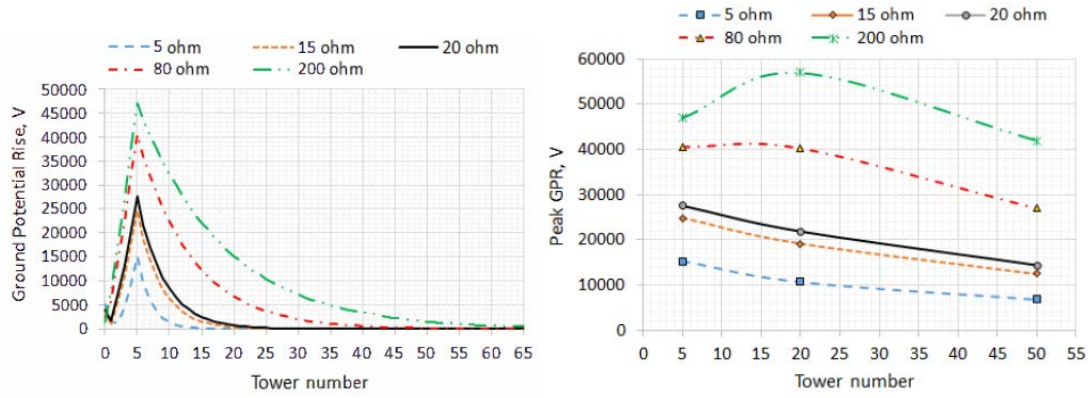

Figure 1-12: Graphs showing the influence of tower number and tower footing resistance on GPR [35].

Further researches have also been carried out to consider variations in GPR according to the type of ground fault, although LLGs are much more infrequent than SLGs, and according to the phase considered faulty: the results have confirmed that in the case of SLG the fault current through earthing systems and ground wires values are slightly higher than those in case of LLG and that the phase considered does not affect the values so it is reasonable to consider, as recommended by standards, the phase furthest from the ground wire to have more current through the earthing system with a consequent higher GPR.

In the previous section, the effects of span length on the fault current distribution have already been mentioned, and now are mentioned also its effect on the GPR reported in Fig. 1-13. The larger is the average span, and the larger is it the GPR while the smaller becomes the earth wires current, showing a noticeable difference with not so distant values of span even if the effect on the footing fault current appears to be minimal [35].

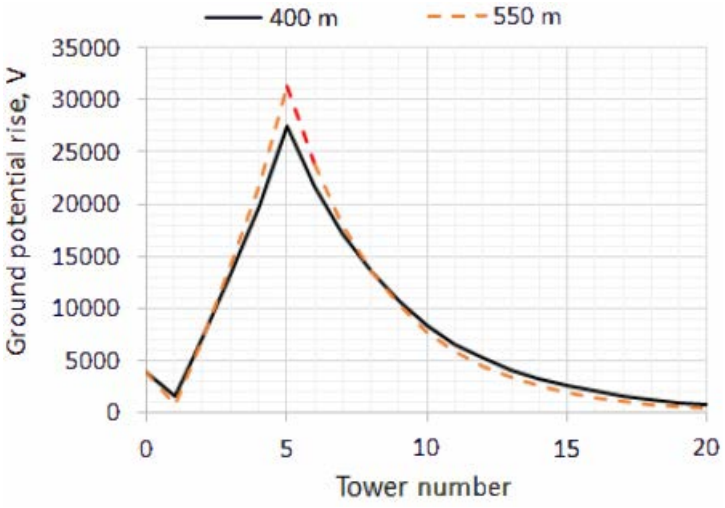

Figure 1-13: Influence of different values of average span on GPR [35].

Among the considerations regarding grounding systems and the GPR phenomenon, one of the main elements to be treated is soil resistivity. The soil plays an important role in the absorption of the fault current as is one of the parameters that varies the overall resistance of the ground system, as well as its influence on the rate of galvanic corrosion of metal structures in contact with the soil. The soil is by nature composed by the alternation of dissimilar horizontal and vertical layers characterized by different thicknesses, material composition, chemical characteristics, consistency, temperature, and humidity rate. The latter is particularly important as an increased concentration of electrolytes will lead to a lower resistivity of the soil [36]. Typical values of soil resistivity vary between 2 to 10000 Ωm, but more extreme numbers are not unusual.

For practical evaluation of soil resistivity's values, the Wenner Method is the most popular, due to several advantages such as the capability of obtaining data from deep layers without reaching it with the drive rods, the invariance at test pins' resistance, the presence of holes created by them, and the relatively easy and light test equipment. The test consists in placing probes in a straight line and equally spaced at different soil depth for each measurement, then use wire conductors to connect the meter and probes: two outer probes are connected to the meter to inject constant current to the ground, while two inner probes measure voltage drop due to current flows through the earth.

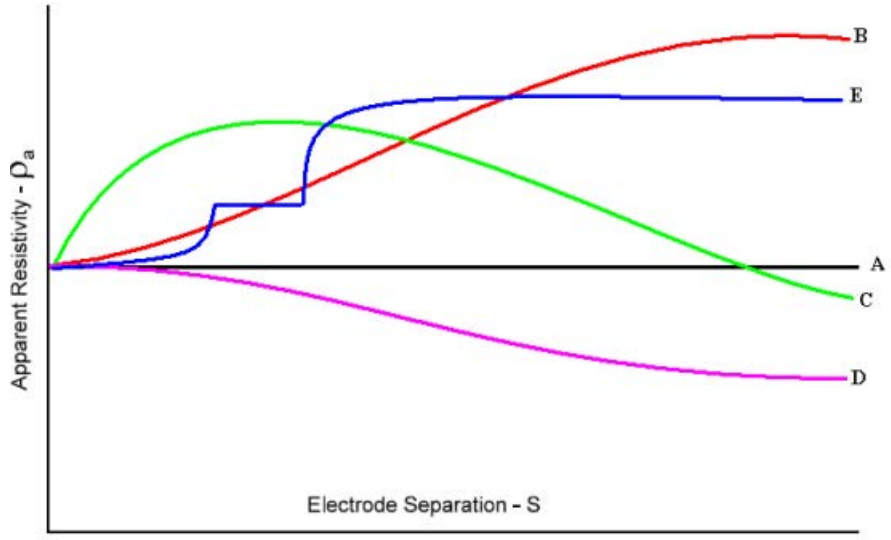

Figure 1-14: Curve (A) represents homogenous resistivity, curve (B) represents a low resistance layer overlaying a higher resistivity layer, curve (C) represent a high resistivity layer between two low resistivity layers, curve (D) represents a high resistivity layer overlaying a lower resistivity layer, curve (E) represents a low resistivity layer over a high resistivity layer with vertical discontinuity [37].

Generally, the use of a uniform soil resistivity structure is a huge simplification as it has a very rare occurrence in practice: it could be applied just in case of small variation through the average value calculation or the midrange (mean of the highest and lowest values). However, according to IEEE standards, a more accurate representation of soil resistivity could be obtained using a two-layer model or considering different behaviours as shown in Fig. 1-14. Common situations lead to the presence of a high resistivity layer above a lower one or the opposite, varying the strategy needed to improve the performance of the system (for instance in the first case it's better to use vertical rods while in the second one would be better a mesh grid eventually with counterpoises).

The application of two-layer soil structure for the earth grid calculation can be based on two methods: evaluation of earth grid resistance passing through mesh grid and electrode combined calculation, or the computation of apparent soil resistivity with the formulas given below for completeness [37].

For the negative value of K:

$$\rho_a = \frac{\rho_1}{\left[1+\left(\frac{\rho_1}{\rho_2}-1\right)*\left(1-e^{\overline{-k(d+2h)}}\right)\right]} \quad (1.\ 2)$$

For the positive value of K:

$$\rho_a = \rho_2\left[1+\left(\frac{\rho_2}{\rho_1}-1\right)*\left(1-e^{\frac{-1}{k(d+2h)}}\right)\right] \quad (1.\ 3)$$

where ρ_2 is the bottom layer soil resistivity, ρ_1 is the top layer soil resistivity, d is the depth of the top layer, h is the grid depth and K is the reflection factor computed by:

$$K = \frac{\rho_2-\rho_1}{\rho_2+\rho_1} \quad (1.\ 4)$$

In addition to the previously mentioned methods to reduce the overall resistance of the soil system, such as the use of short length radial conductors bonded at the injection points and the use of vertical rods to terminate radial conductors, which is particularly convenient in low-medium soil resistivity ground, is

now added an appropriate engineered treatment of the soil around the earth system, for example through the study of a particular composition of low resistivity materials in the soil, or the simpler but still very effective maintenance of a good moisture level, which effects are reported in Fig. 1-15.

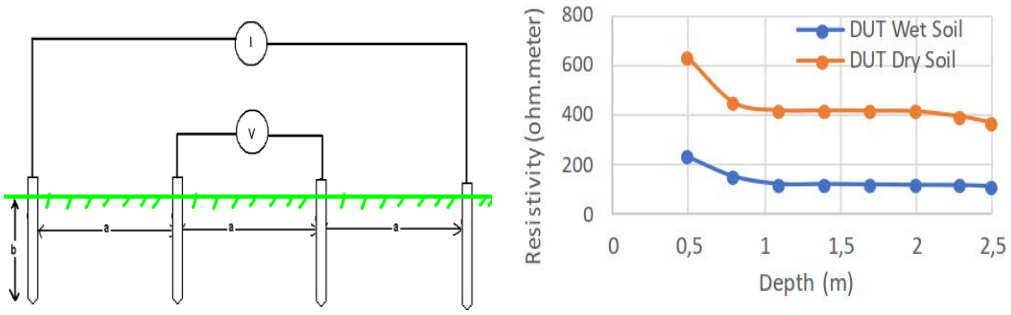

Figure 1-15: Wenner method setup and results of different levels of moisture on soil resistivity [37].

However, even in case of a correct design of the earthing system and appropriate expedients to limit the GPR, many causes can lower grid performance as time goes by, leading to an increase in GPR further aggravated in case of high fault currents. Some of the possible causes of failure that can increase GPR are for example melting, fusing, arcing, burning, drying of the soil, thinning or pollution of the protective surface layer, altered current distribution, corrosion of conductors, or neutral wire's connection failure.

Of this list, the most dangerous are certainly those that occur as a result of a system failure, which is further made harmful by the presence of high fault currents: these can significantly reduce the fusing time of conductors:

$$t_c = \left(\frac{A}{I_G * D_f * K_f}\right)^2 \quad (1.5)$$

(where A is the cross-section of the conductor, I_G is the single-line phase-to-ground rms fault current, D_f is the decrement factor and K_f is the material-fusing constant) increasing its chance to be subject to fusing, melting, or other forms of thermal and mechanical damage [38].

Including this extensive discussion about GPR and the various factors influencing it was considered necessary as it is strongly linked to network efficiency and people protection. A careful analysis of these phenomena is often necessary when designing a new plant or expand an existing one [39], and even more when considering unexpected phenomena that may threaten the safety of people: just think, for example, of the fault application transfer phenomenon, which may involve risks not foreseen in a first analysis, or the fact that the widespread diffusion of the telecommunications system in urban areas, which standards for lightning protection are mainly focussed on equipment protection, may lead in anomalous condition to a severe GPR which can drastically increase voltage gradients in the earth hence finding its way through the neutral and the earth electrodes into nearby dwellings [40].

Due to all these changes in the power system, as well as the several factor's influences such as temperature and moisture level, recently measurement systems for real-time GPR and ground resistance

monitoring have been proposed. This would bring benefits such as notifications of substation grounding system's impedance variation, real-time evaluation of step and touch voltage, and enhanced probabilistic characterization of the system's performance which provides useful tasks for probabilistic risk analysis [41].

1.5 Quantitative Risk Assessment (QRA)

As mentioned at the beginning of this chapter, in the modern society the role of the power system has become of critical importance as the industry is globally based on electrically powered machines and the rise of automation will only intensify the situation, as any outage in power supply has a deep economic impact which can be easily quantified. Therefore, in recent years there has been an increased focus on asset management within the electricity distribution sector, to reach an adequate level of competence and to ensure short- and long-term risk management.

Most of the work on risk management in distribution system has been mainly focused on reliability, certainly of vital importance also due to the strict laws that are applied there: in fact, one of the main risk factors is voltage instability, which can lead to voltage's drop at load bus at a level at which the voltage control mechanism cannot bring it back to its nominal value, called the Saddle Node Bifurcation Point (SNB) or Critical Point in the curves Active Power-Voltage (P-V) or Reactive Power-Voltage (Q-V). For this, novel approaches have been developed to identify and assess voltage stability risk, including intermittent renewable generation and time-variable loads: based on the iterative calculation of the SNB at a given time whose data are used as a training set for support vector machine classifiers, can build voltage stability risk probability distribution using Monte-Carlo simulations with stochastic load profiles, showing advantageous scalability to wider networks [42].

Nevertheless, these companies need to face also other relevant risks which typically have a more intangible nature such as safety risk, environmental risk, vulnerability risk, and regulatory risk. These risk categories can be further differentiated due to their impact, which could be local in case of "concentrated" incidents, system-level if failure in components provides widespread influence on extensive parts of the transmission system, corporate-level if the main impact is on business [43]. While, for most of these risks, a decision can be taken without including all the other risk aspects, for a better result more than one risk should be considered keeping into account that often the optimal solution for one risk will not be favourable for others, leading to the analysis of a compromise.

Risk assessment is defined as "a multi-stage process used to determine the magnitude of a threat (risk) of loss, in its widest sense, to assist management decision making. An assessment should determine whether the risk is tolerable, taking into account existing control measures. If they are not adequate, the assessment should recommend more effective measures" [44]. Qualitative risk assessment and Quantitative Risk Assessment (QRA) are used to assess and manage the risk of failures and equipment damage that have the potential to cause unsafe conditions: each method offers his advantages and disadvantages, so they will both shortly be described and analyzed.

Qualitative risk assessment is defined as the process of characterizing hazards within risk categories by estimating the severity and probability of occurrence: it is a relatively simple procedure with several shortcomings, but it can be useful for preliminary consideration in the design phase of a project and to provide input to quantitative analysis. This process is typically characterized by a two-dimensional risk matrix as the one shown in Fig. 1-16 as an example, which presents the estimated severity of the potential outcome on the y-axis and the estimated probability of occurrence on the x-axis. Unfortunately, often the number of choices typically used it's not enough to allow an adequate determination of risk values, and the subjectivity which lies behind the choice it's almost impossible to avoid. Therefore, although this type of risk assessment can still lead to good results, there is an increasing tendency to use QRA, which provide more concrete results also in terms of the cost-benefit of interventions.

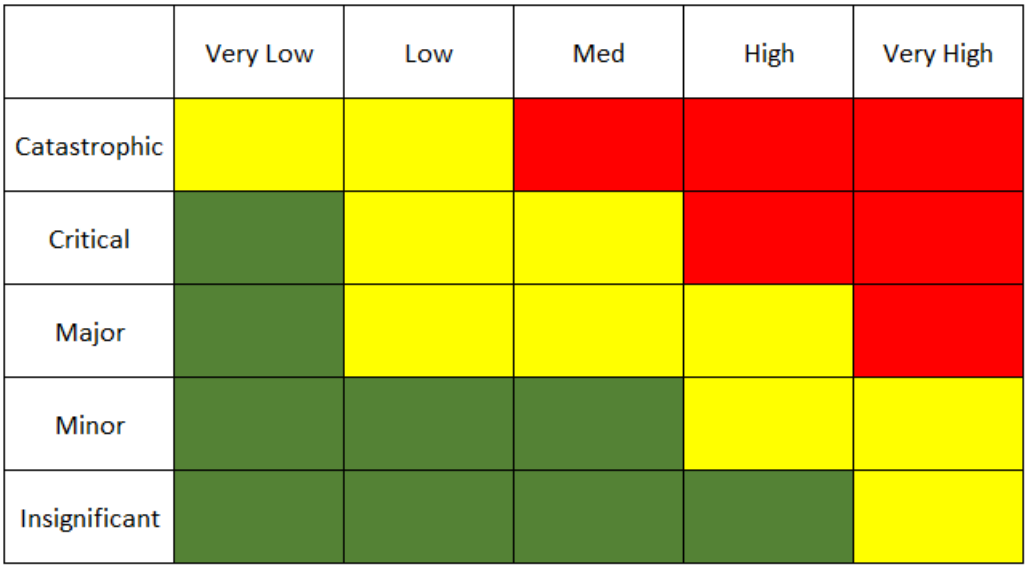

Figure 1-16: Typical qualitative risk assessment two-dimensional matrix.

QRA is defined as the process of assessing hazards using statistical techniques, such as Life Data Analysis and Monte-Carlo simulation: identification of possible hazards, quantification of the likelihood that the hazard materializes, and the severity of the consequences are the parameters that define risk. Although it requires a fair amount of data and a good level of statistical education, this method can accurately predict the danger of future element failures and also provide a comparative evaluation of the effectiveness of multiple corrective action scenarios, which may be used in justifying the cost of preventative safety actions [45].

Although in some fields there is scepticism in using these statistical methods with a consequent fallback in more "familiar" strategies, in power system, because of the various dangers due to the high voltages, electrical safety is a prime concern so that both qualitative and quantitative analysis are used to manage these risks. In fact, among the previously mentioned risks, the one on the safety of people is certainly the most important, and the high unpredictability of the parameters that characterize it, combined with

the different effects that it can have on human health, has made it the one most widely discussed in the literature and regulations around the world; for this, the main issues related to it will be now treated.

There are different consequences of electric current on the human body, which can range from slight burns to dangerous cases of asphyxia and ventricular fibrillation, depending on the amplitude of the current and the duration of the shock. Among these, the main cause of death from electrocution is considered ventricular fibrillation: based on animal experiments, this heart condition has been extensively analyzed to estimate the probability of death from electric shock and create current and duration thresholds.

Studies have also been carried out to understand the different effects between continuous and alternating currents, analysing in the latter how the frequencies' variation between 15 and 100 Hz modified the effects on the human body: the international standard IEC 479-1 offers a detailed description on this.

A very important limit value is the perception threshold, defined as the minimum value of current that on contact causes any sensation to the person through which it flows. The extent of this body current threshold depends on various parameters, such as the contact area of the body, the contact conditions and the physiological characteristics of the individual. The reaction threshold, i.e. the minimum value of the contact current that causes an involuntary muscle contraction, is considered, regardless of time, 0.5 mA.

The following level of muscle contraction related to the current is immobilization, due to the effect of current flowing on the muscles and associated nerves or parts of the brain, which causes the human body or part of it to be unable to move voluntarily: the value of the current that can have this effect depends on the volume of the muscles, as well as the part of the brain and the type of nerves involved. This phenomenon can have very serious consequences because an involuntary contraction of the muscle around an electrical component and subsequent immobilization can significantly lengthen the shock time and aggravate its effects.

The threshold for ventricular fibrillation is the minimum value of the current through the body that causes ventricular fibrillation. Exceeding this limit can be fatal because it causes the blood flow to stop, resulting in a lack of oxygen transport within the body. This can only happen if the shock occurs during the period of vulnerability of the heart, described in various scientific texts as a relatively small part of the cardiac cycle during which the cardiac fibres are in a state of uneven excitability that causes ventricular fibrillation if they are excited by an electric current of sufficient magnitude. The parameters that influence this value are highly physiological, for example, the anatomy of the body and the state of cardiac function of the individual [46].

It is sometimes and wrongly assumed that when a conductor is earthed, then it is safe to touch it but, as before deeply discussed, as a consequence of a fault, the GPR phenomenon can lead to unsafe conditions in the proximity of the substation, causing potential differences in points inside and outside the installations that can be risky when human bridges these points.

There are different electrocution scenarios as represented in Fig. 1-17, depending on person position and current's path:

- Touch voltage: “The part of the earth potential rise due to an earth fault which can be picked up by a person, assuming that the current is flowing via the human body from hand to feet” [47].
- Step voltage: “The part of the earth potential rise due to an earth fault which can be picked up by a person with a step-width of 1 m, assuming that the current is flowing via the human body from foot to foot” [47].
- Source voltage for touching also called prospective touch voltage: “The voltage which appears during an earth fault between conductive parts and earth when these parts are not being touched” [47].
- Mesh voltage: “The maximum touch voltage within a mesh of a ground grid” [48].
- Transferred voltage: “A special case of the touch voltage where a voltage is transferred into or out of the substation from or to a remote point external to the substation site” [48].

Of this list, the first two are certainly the most known, and of the two, step voltages are generally considered less dangerous than touch voltages. It has been scientifically proven that the human body can withstand higher currents for a path from one foot to the other; moreover, for any position, the step voltage is lower than the contact voltage, so for the safety of a system it is sufficient to make it safe for the touch voltage. However, there may be places where there is no danger of touch voltage (i.e. unexposed metal objects), but step voltages may occur.

As already mentioned in the previous section, the resistance of the earthing system for high voltage systems should be such that the rise of earth potential is “As Low As can be Reasonable Possible”: maximum values of GPR are indicated to provide general guidelines, for example, the potential-rise should not exceed 430 V rms for short duration earth faults, or 650 V rms if the fault is cleared in less than 0.2 s. For this, apart from the several actions that can be applied to reduce the overall impedance of the system that have been previously discussed, some practices are also implemented to increase the resistance of accidental path so that a lower level of current would pass through the human body: some of these strategies are for instance the application of a layer of gravel on substation’s surface, which guarantees a high resistance layer even under wet conditions, or the use of gloves or special boots that, considered as additional series resistances, have a significant effect on the tolerability of touch and step voltages, and for this various standards consider them when calculating allowable voltages.

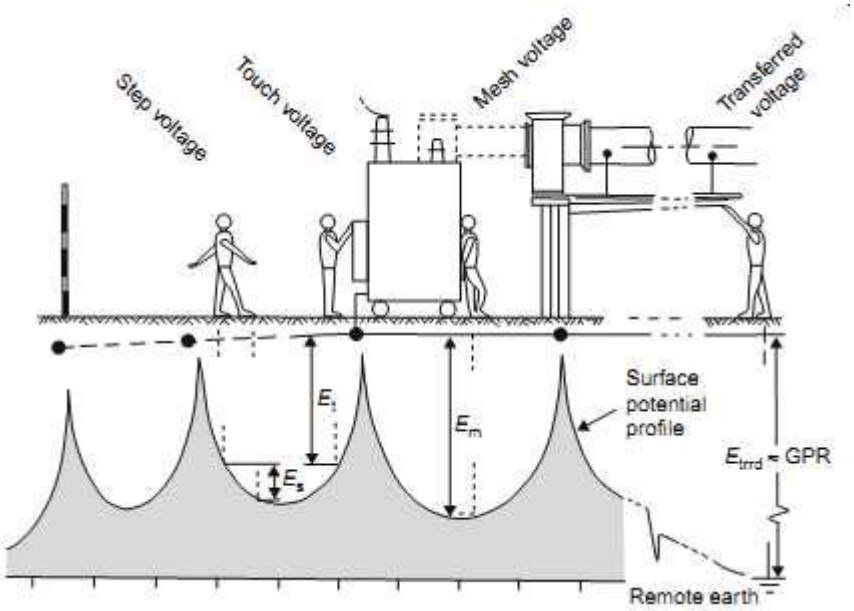

Figure 1-17: Graphical representation of several dangerous electrocution scenarios [6].

After this rapid mention of the main risks for the interaction between the human body and the electric current, it's now presented the application of the QRA in the field of the transmission system, describing its principles and some models present in the literature. Being the main risk in an earthing system the death from electrocution, the individual risk is computed as the product between the probability of earth potential rise, the probability of human presence and the probability of ventricular fibrillation.

Several examples of probabilistic risk assessments of step and touch potentials in the proximity of transmission line structures can be found in various papers, based on the use of probabilistic analysis programs. To evaluate the possibility of GPR, the Monte-Carlo simulation method is often applied, which calculates the probability distributions of line currents and voltages taking into account the random variations in the system generation, the operating conditions of the transmission and the time, place and type of failure: different types of distribution can be used for the duration of the failure to sample the possible duration of the shock [49]. This leads to the generation of the "applied voltage" distribution. Then it's computed the "withstand voltage" distribution, in which different approaches can be used and in which there are key parameters such as the impedance of the body, that can be a single value (standard 1000 Ω) or can be related to the voltage level, and the resistance between ground and foot which proportional to soil resistivity.

The probability of presence is the probability that a ground fault occurs in the area under examination and that a person is present exactly at the time of the fault: for its evaluation, it is assumed that the number of ground faults occurring in certain periods follows Poisson's distribution so the value is derived from the number of ground faults in a given period and the average annual frequency of ground faults assuming that, if a person is present, he will be exposed. It's worth noting that the exposure varies if we are considering step or touch voltage, as in one case the total time of a person coming in contact with a metallic structure need to be considered, while in the other case the time that a person will be

close to a substation needs to be estimated. Further developments were carried out successively by introducing other random parameters into the simulations, such as the introduction of the frequency and duration of ground faults and the frequency and duration of human presence in the hazardous area [46]. Of interest is the concept of probability of ventricular fibrillation and how different strategies have been developed over the years to arrive at international standards that still show discrepancies.

In the beginning, after the work of various authors based on experimental tests, the 1/2 percentile lines of the maximum non-fibrillating current and the minimum fibrillating current were derived. So, selecting 50 Kg as the standard weight of the victim, Dalziel equation was refined:

$$I = \frac{n}{\sqrt{t}} \tag{1. 6}$$

where *n* varies between 116 and 185 and *t* between 8.3 ms and 5s.

Further tests carried out on different species and with different weights have been used to develop the nowadays applied probability current curves. According to these tests, the IEC TC64 Working Group 4 developed the fibrillation thresholds curves applicable to humans of 5%, 50%, and 95% probability, subsequently adding an even more conservative limit below the "5%" known as safety curve: these curves, reported in Fig. 1-18 are nowadays slightly different from the original ones and the "95%" curve is now omitted.

Also IEEE Standard 80 provide limits of allowable body current, establishing two limits based on different weights still with the allowable body current as a function of exposure duration. As shown in the figure, the limits have different shapes meaning that different results are obtained: there is a part of the 50-kg limit which has negligible fibrillation probabilities in respect of the safety curve (more or less between 100 and 200 ms) while a part of the 70-kg line considers fibrillation probabilities greater than 50% (between 1 and 2 s of exposure time).

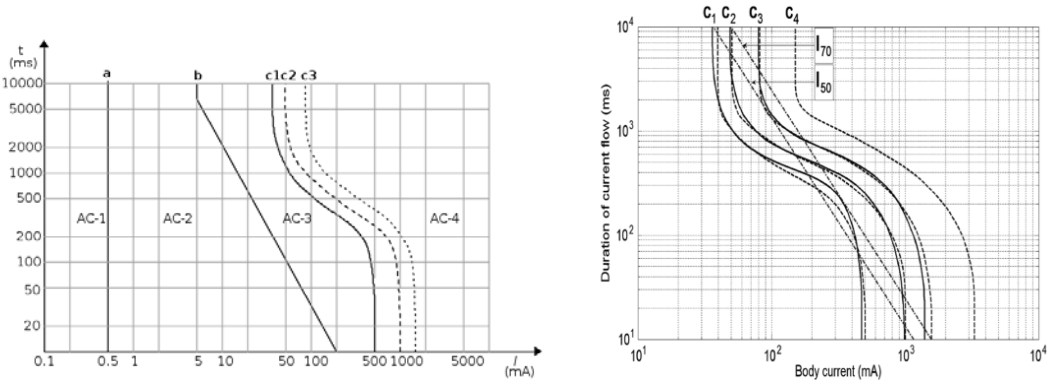

Figure 1-18: On the left the IEC limits with also most recent zone, respectively the AC-1 zone, in which the current may be perceptible without any reaction, AC-2, where there is normally no dangerous pathological phenomena up to the tetanisation threshold, and AC-3 in which usually reversible pathophysiological effects happens such as muscle contractions, breathing difficulties or arrhythmias. On the right the superposition of different standards limits [50].

Further developments can be made by building 3-D surfaces of safety limits based on the variation of other parameters as reported as examples in Fig. 1-19, which modify the reaction of the human body and the total impedance of the current circuit: among these, there are those already mentioned for the

evaluation of earthing system impedance, such as soil resistivity, mesh density and grid area, others related to body impedance, which is highly affected by the path of the current through the body showing quite different values and risk levels if the contact happens with both hands, both feet, one hand and one feet or other body parts such as back or chest, and then the ones related to electrical values of current and voltage magnitude [50].

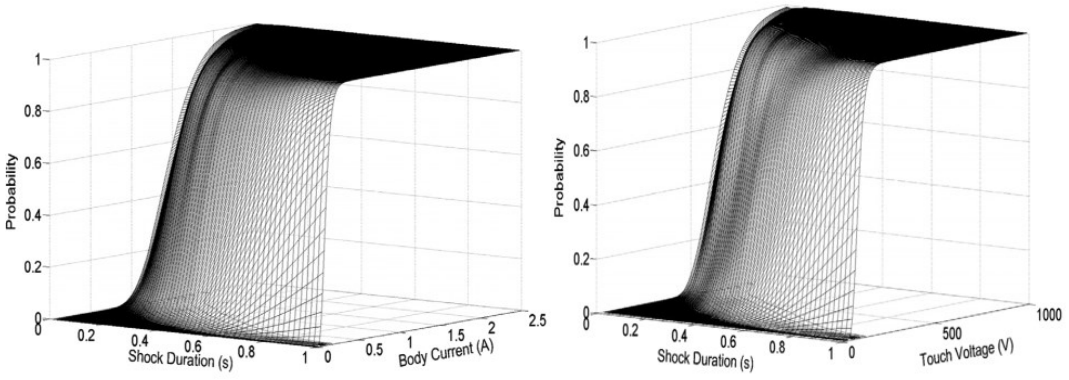

Figure 1-19: 3-D limits surface for ventricular fibrillation probability depending on the current magnitude and touch voltage [50].

2 Network modelling and fault calculation according to international standards

2.1 Standard IEC 60909

Since the final purpose of the thesis is to present a robust and reliable model to be used for the calculation of the ground-fault current distribution, it is necessary to analyse the rules for the calculation of fault currents in three-phase a.c. systems. Such rules represent the benchmark on which to base any further development in this field, setting the basic assumptions for the construction of the models.

The two most important international standards that will be briefly described and then compared, are respectively the European IEC 60909 and the American ANSI/IEEE 37.010.

Among the whole guidance given by IEC 60909 "Short-circuit currents in three-phase a.c. systems" [51], this chapter will focus on the most important aspects taken from part 0, which is the one that is applicable for short-circuit calculation in case of low or high voltage three-phase a.c. systems at the nominal frequency of 50 or 60 Hz.

This section of IEC 60909 establishes a general, feasible and brief procedure leading to generally enough accurate results, applied both in case of balanced or unbalanced short circuits. For this calculation method, an equivalent voltage source at the short-circuit location is introduced, without excluding other methods such as the superposition method, which can be adjusted to particular circumstances and need to give at least the same precision.

In case of SLG fault, two cases must be distinguished regarding their different physical properties and effects, which result in changed requirements for their calculation: the first case is applied when the SLG short-circuit occurs in a solidly earthed neutral system or an impedance earthed neutral system, the second one when an SLG fault occurs in an isolated neutral earthed system or a resonance earthed neutral system; the latter is analysed in IEC 60909 part 3.

This standard suggests, except for certain specific circumstances, to compute always two short-circuit current values: the maximum one, which determines the capacity of electrical equipment, and the minimum one, which is, for instance, a basic data in fuses selection, protective devices setting and motors' run-up checking.

For the calculation of short-circuit currents according to standards, a series of definitions, mainly taken from IEC 60050(131) [52], is given below, regarding quantities which will be subsequently applied, some of which are illustrated in Fig. 2-1:

- Short circuit: "Accidental or intentional conductive path between two or more conductive parts forcing the electric potential differences between these conductive parts to be equal or close to zero".
- Prospective (available) short-circuit current: "Current that would flow if the short circuit were replaced by an ideal connection of negligible impedance without any change of the supply".

- Symmetrical short-circuit current: “Root mean square value of the a.c. symmetrical component of a prospective short-circuit current, the aperiodic component of current, if any, being neglected”.
- Initial symmetrical short-circuit current I_k": “r.m.s. value of the a.c. symmetrical component of a prospective short-circuit current, applicable at the instant of short circuit if the impedance remains at zero-time value”.
- Decaying (aperiodic) component $i_{d.c.}$ of short-circuit current: “Mean value between the top and bottom envelope of a short-circuit current decaying from an initial value to zero”.
- Peak short-circuit current i_p: “Maximum possible instantaneous value of the prospective short-circuit current”, which magnitude varies in accordance with the moment in which the fault occurs and by normative is computed in the instant at which the greatest possible short-circuit current exists, without considering sequential short circuits.
- Symmetrical short-circuit breaking current I_b: “r.m.s. value of an integral cycle of the symmetrical a.c. component of the prospective short-circuit current at the instant of contact separation of the first pole to open of a switching device”.
- Steady-state short-circuit current I_k: “r.m.s. value of the short-circuit current which remains after the decay of the transient phenomena”.
- Symmetrical locked-rotor current I_{LR}: “Highest symmetrical r.m.s. current of an asynchronous motor with locked rotor fed with rated voltage U_{rM} at rated frequency”.
- Subtransient voltage E" of a synchronous machine: “r.m.s. value of the symmetrical internal voltage of a synchronous machine which is active behind the subtransient reactance X_d" at the moment of short circuit”.
- Subtransient reactance X_d" of a synchronous machine: “Effective reactance at the moment of short circuit, which saturated value is taken for short-circuit currents calculation”.
- Minimum time delay t_{min}: “Shortest time between the beginning of the short-circuit current and the contact separation of the first pole to open of the switching device”.
- Thermal equivalent short-circuit current I_{th}: “The r.m.s. value of a current having the same thermal effect and the same duration as the actual short-circuit current, which may contain a d.c. component and may subside in time”.

To have complete knowledge of short-circuit currents, a calculation of its magnitude at fault location as a function of time from the beginning to its end should be done. Luckily, in most practical cases this is not necessary, and only the computation of some specific quantities is required: it is useful to know the rms value of the symmetrical a.c. component and his peak value, which mainly depends on the frequency and on the time constant of the decaying aperiodic component, that is on the ratio between X and R of the short-circuit impedance.

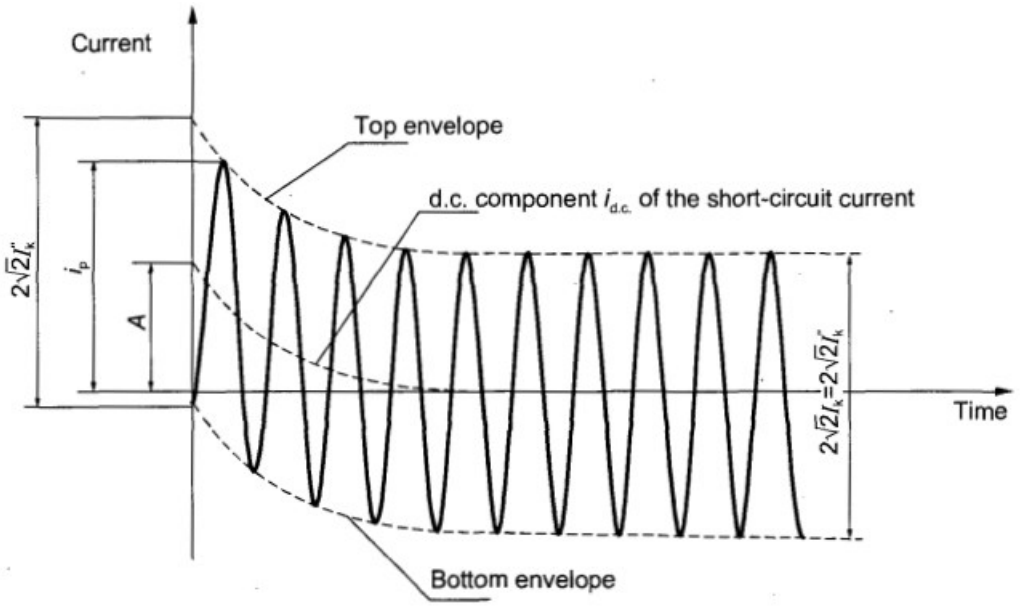

Figure 2-1: Short-circuit current in case of far-from-generator short circuit with constant a.c. component [51].

Some simplifications are needed for the calculation of maximum and minimum values of short-circuit currents that, even if they are not strictly true for all the power systems considered, still lead to acceptable results:

- For the whole duration of the short circuit, the type of fault involved does not change.
- For the whole duration of the short circuit, the network involved does not change.
- Transformers' impedance is referred to the tap-change main position, thanks to the further introduction of the impedance correction factor for network transformers.
- Arc resistances are neglected.
- All line capacitances, shunt admittances and non-rotating loads which do not influence the zero-sequence system are neglected.

It is necessary to underline that, when computing short-circuits currents in systems with different voltage levels, all values need to be transferred at the same voltage level, which is usually done when calculating the current; of course, if values are in per unit, no transformation is needed if systems are coherent: equipment's impedances in subordinated or superimposed networks need to be multiplied or divided by the square of the transformation ratio t_r, while currents and voltages need to be converted by it.

As already mentioned, the method applied for these calculations is based on the substitution of power sources with equivalent voltage sources, while all the others elements such as network feeders, transformers, synchronous and asynchronous motors are replaced by their internal impedances: this technique has the advantage that it can be applied in all cases, requiring information about loads, operational data, tap-changer position, excitation of generators and so on; while doing this, usually shunt admittances like line capacitances and passive loads are not considered. To model this voltage source, the c_{max} and c_{min} multipliers are introduced by IEC: in absence of other

national standards, c_{max} should be chosen as 1.05 or 1.10 in LV networks or 1.10 in MV/HV networks according to the fact that the highest voltage in an undisturbed situation does not differ on average from these values, while for c_{min} respectively the value 0.95 and 1.00 should be chosen.

These calculations are further simplified using symmetrical components, both in balanced and non-balanced short circuits, postulating that the electrical equipment has a balanced structure as in transposed overhead lines' case. Although being an approximation, this assumption is still valid for limited asymmetry in the power line structure.

With this method, the currents in each line conductor are found by superposing the currents of the three symmetrical component systems, which are respectively positive-sequence current $\mathbf{I_{(l)}}$, negative-sequence current $\mathbf{I_{(2)}}$ and zero-sequence current $\mathbf{I_{(0)}}$ through the following formulation with the line conductor L_1 taken as reference:

$$\boldsymbol{I_{L1}} = \mathbf{I}_{(1)} + \boldsymbol{I}_{(2)} + \boldsymbol{I}_{(0)} \tag{2. 1}$$

$$\boldsymbol{I_{L2}} = \boldsymbol{a}^2\mathbf{I}_{(1)} + \boldsymbol{a}\boldsymbol{I}_{(2)} + \boldsymbol{I}_{(0)} \tag{2. 2}$$

$$\boldsymbol{I_{L3}} = \boldsymbol{a}\mathbf{I}_{(1)} + \boldsymbol{a}^2\boldsymbol{I}_{(2)} + \boldsymbol{I}_{(0)} \tag{2. 3}$$

where:

$$\boldsymbol{a} = -\frac{1}{2} + j\frac{\sqrt{3}}{2} \quad ; \quad \boldsymbol{a}^2 = -\frac{1}{2} - j\frac{\sqrt{3}}{2} \tag{2. 4}$$

For this, the short-circuit impedance at the fault location has a positive-sequence component $\mathbf{Z_{(1)}}$, a negative-sequence component $\mathbf{Z_{(2)}}$ and a zero-sequence component $\mathbf{Z_{(0)}}$. The first two are obtained by applying a symmetrical system of voltages of positive or negative sequence phase order to the short-circuit location, and these values differ only in case of rotating machines while are generally taken equally when calculating far-from-generator short circuits; $\mathbf{Z_{(0)}}$ instead, is obtained by applying an a.c. voltage between the three short-circuited line conductors and the joint return. As mentioned, when calculating $\mathbf{Z_{(0)}}$ in MV/HV systems, the zero-sequence capacitances of lines and the zero-sequence shunt admittances are neglected: these are considered only for resonant earthed systems, isolated neutral systems and earthed neutral systems with an earth fault factor higher than 1,4; this assumption leads to results which are slightly higher than the real short-circuit currents' values.

When calculating maximum short-circuit currents, several conditions are included to obtain the maximum allowable current's value, such as: the voltage factor c_{max}, the choice of system configuration, external networks' equivalent impedance, power plants contribution that lead to the maximum value of current in the fault location, the inclusion of motors and the calculation of lines' resistance at a temperature of 20°C.

On the other hand, when calculating minimum short-circuit currents, the opposite choices to the previous ones need to be taken, and the formula for lines' resistance becomes the following:

$$R_L = [1 + \alpha(\theta_e - 20°C)] * R_{L20} \tag{2. 5}$$

where R_{L20} is the resistance computed at 20°C, θ_e is the conductor temperature in degrees Celsius at the end of the short-circuit duration and α is a factor equal to 0,004 K^{-1}, number that is valid with sufficient accuracy for copper, aluminium and aluminium alloy, even though for more accurate results different values should be used depending on line's conductors material.

It will now be shortly presented the methodology imposed by this standard for modelling and calculation of the impedances of the various network's components, reporting only the main formulas and some of the various assumptions that are applied to simplify these calculations:

- **Network feeders:** In case of three-phase short circuit fed from a network which initial symmetrical short-circuit current at the connection point Q is known, then the equivalent impedance of the network can be determined by:

$$\boldsymbol{Z_Q} = \frac{c\boldsymbol{U_{nQ}}}{\sqrt{3}\boldsymbol{I''_{kQ}}} \tag{2. 6}$$

  If the high-voltage feeders with nominal voltages above 35 kV are fed by overhead lines, it's assumed that the equivalent impedance is a pure reactance while, if no accurate value is known, the relation $R_Q = 0.1\ X_Q$ where $X_Q = 0.995\ Z_Q$ can be used.

- **Transformers:** The positive-sequence short-circuit impedances of two-windings transformers can be calculated from transformer data as follows:

$$\boldsymbol{Z_T} = \frac{u_{kr}}{100\%}\frac{U_{rT}^2}{\boldsymbol{S_{rT}}} \tag{2. 7}$$

  with:

$$R_T = \frac{P_{kT}}{3I_{rT}^2} \tag{2. 8}$$

  For large transformers, the resistance is small so that the standard allows to neglect it, unless the peak short-circuit current or the d.c. component has to be calculated.

  In the case of three-winding transformers, the positive-sequence short-circuit impedances can be calculated by the three short-circuit impedances (referred to side A) obtained through:

$$\boldsymbol{Z_{MN}} = \left(\frac{u_{RrMN}}{100\%} + j\frac{u_{XrMN}}{100\%}\right) * \frac{U_{rTA}^2}{\boldsymbol{S_{rTMN}}} \tag{2. 9}$$

  where M and N are each time different transformer sides and the third side is left open, by the following equation:

$$\boldsymbol{Z_M} = \frac{1}{2}\left(\boldsymbol{Z_{MN}} + \boldsymbol{Z_{MP}} - \boldsymbol{Z_{NP}}\right) \tag{2. 10}$$

  meaning that, for the value of one side's impedance, half the sum of the two short-circuit impedances in which the side is included minus the one in which is excluded needs to be done.

  For two- and three-winding network transformer, an impedance correction factor needs to be applied, which, in case of absence of long-term operating conditions of the transformer before the fault, can be obtained by the formula:

$$K_T = 0.95\frac{c_{max}}{1+0.6x_T} \tag{2. 11}$$

that is one value in case of two-winding, while for three-winding three impedance correction factors can be computed with the same equation, one for each couple of sides. These factors shall be applied also to negative- and zero-sequence impedance in case of unbalanced fault currents, even though the $\mathbf{Z_N}$ impedances between transformers' star-point and earth are added as $3\mathbf{Z_N}$ in the zero-sequence system without the correction factor.

- **Overhead lines and cables:** The positive-sequence short-circuit impedance $\mathbf{Z_L}$ can be easily estimated by conductor data, and specific standards exist for the measurement of positive- and zero-sequence impedances, often obtainable once one of the two values is computed through the knowledge of the ratio between the zero- and the positive-sequence impedance from constructors' catalogues, as for the material properties and nominal sections.
  For the reactance per unit length, the standard recommends using the following equation:

$$X'_L = 2\pi f \frac{\mu_0}{2\pi}\left(\frac{1}{4n} + ln\frac{GMD}{r}\right) \quad (2.\ 12)$$

- **Short-circuit limiting reactors:** According to the standard, short-circuit current-limiting reactors should be treated as part of the fault impedance and can be considered as geometrically symmetrical, assuming that all sequence impedances are equal, and its impedance can be calculated as follows:

$$\boldsymbol{Z_R} = \frac{u_{kR}}{100\%}\frac{U_n}{\sqrt{3}\boldsymbol{I_{rR}}} \quad (2.\ 13)$$

  and is usually advised to neglect the resistance value, leading to $Z_R \simeq X_R$.

- **Synchronous machines:** For the calculation of the initial symmetrical short-circuit currents in case of network fed directly from generators without unit transformers, the standard provides formulations for the values of each sequence impedance. In the case of positive-sequence, the following impedance must be used:

$$\boldsymbol{Z_{GK}} = K_G\,(R_G + jX''_d) \quad (2.\ 14)$$

  with the correction factor:

$$K_G = \frac{U_n}{U_{rG}} * \frac{c_{max}}{1+X''_d\ sin\,\varphi_{rG}} \quad (2.\ 15)$$

  needed because the equivalent voltage source is used instead of the subtransient voltage. Simplified values are also provided for the fictitious resistance which may be applied for the calculation of peak short-circuit currents and the decay of a.c. and d.c. components, get without considering the influence of windings temperature.
  For the negative- and zero- sequence impedances similar equations are applied:

$$\boldsymbol{Z_{(2)GK}} = K_G\left(R_{(2)G} + jX_{(2)G}\right)\ ;\ \boldsymbol{Z_{(0)GK}} = K_G\left(R_{(0)G} + jX_{(0)G}\right) \quad (2.\ 16)$$

  where if the values of X_d" and X_q" are different, the standard allows the use of the mean value between them.

Synchronous motors with voltage regulation and synchronous compensators considered when calculating the initial symmetrical short-circuit current, the peak short-circuit current, the symmetrical short-circuit breaking current and the steady-state short-circuit current, are treated in the same way as synchronous generators.

- **Power station unit:** For the calculation of power station unit whole impedance, two different equations are given, that need to be applied respectively in case of presence or absence of on-load tap changer. The first one is the following:

$$\boldsymbol{Z_S} = K_S\,(t_r^2\,\boldsymbol{Z_G} + \boldsymbol{Z_{HTV}}) \tag{2. 17}$$

with the correction factor:

$$K_S = \frac{U_{nQ}^2}{U_{rG}^2} * \frac{U_{rTLV}^2}{U_{rTHV}^2}\,\frac{c_{max}}{1+|x_d'' - x_T|\,\sin\varphi_{rG}} \tag{2. 18}$$

with appropriated modification in case of well-established operating voltage from the long-term operating experience of the system or variation of the operating voltage at generator's terminals.

If only overexcited operations are expected, then for the calculation of unbalanced short-circuit currents the correction factor K_s should be used for positive-, negative- and zero-sequence system impedances, except for the last one which does not need the correction factor if, as already seen before, an impedance between transformer's star-point and earth is present. On the other hand, if underexcited operation is expected at some time, then the application of K_s may lead to results at the non-conservative side, requiring special considerations and methods. The same equation can be applied also in case of power station units without on-load tap changer, but with a different correction factor which is the following:

$$K_{SO} = \frac{U_{nQ}}{U_{rG}\,(1+p_G)} * \frac{U_{rTLV}}{U_{rTHV}} * (1 \pm p_T)\,\frac{c_{max}}{1+x_d''\,\sin\varphi_{rG}} \tag{2. 19}$$

where $1 \pm p_T$ is needed when the transformer has off-load taps permanently used: if not, p_T can be taken equal to zero; the sign minus is chosen only if the highest partial short-circuit current is searched.

- **Asynchronous motors:** Medium- and low-voltage motors contribute to the initial symmetrical short-circuit current, to the peak short-circuit current, to the symmetrical short-circuit breaking current and to the steady-state short-circuit current Ik. Nevertheless, the standard allows neglecting its effects in low-voltage power supply system in the calculation of I_k" if their contribution is not higher than the 5% of the initial short-circuit current value calculated without motors:

$$\sum I_{rM} \leq 0.01\,I_{kM}'' \tag{2. 20}$$

This can only be done if these motors are not switched in at the same time.

If their values must be considered in the analysis, the impedance $\mathbf{Z_M}$ of asynchronous motors in the positive- and negative-sequence systems can be obtained by:

$$\boldsymbol{Z_M} = \frac{1}{I_{LR}/I_{rM}} * \frac{U_{rM}^2}{\boldsymbol{S_{rM}}} \quad (2.\ 21)$$

while, if needed, the zero-sequence system impedance shall be given by the manufacturers. Even in this case, simplified values of the relation between motors resistance and reactance are given by the standard, based on motors power per pair of poles.

For a correct analysis of the inclusion of motors impedance in the system, the standard gives a formulation with which to recognize the possibility to neglect motors' presence or not in the network in which the short circuit occurs:

$$\frac{\sum P_{rM}}{\sum \boldsymbol{S_{rT}}} \leq \frac{0.8}{\left|\frac{c100\ \sum \boldsymbol{S_{rT}}}{\sqrt{3}\, U_{nQ}\, I''_{kQ}} - 0.3\right|} \quad (2.\ 22)$$

Also, motors connected to the busbar by cables, even if with different properties, for simplification are usually combined into a single equivalent motor.

- **Static converters:** Reversible static converter-fed drives are considered for short circuits calculation only if the rotational masses of motors and static equipment provide a reverse transfer of energy at the fault time, contributing only to I_k" and i_p values. In such a case, they can be treated as asynchronous motors with $I_{LR}/I_{rM} = 3$ and $R_M/X_M = 0{,}10$ with $X_M = 0{,}995$ $\mathbf{Z_M}$.
- **Capacitors and non-rotating loads:** As already mentioned, the standard allows for line capacitance, parallel admittance and non-rotating loads to be neglected. For this, the discharge current of shunt capacitors may be neglected even for the calculation of peak current, and also the effect of series capacitors can be neglected, especially if they are equipped with voltage-limiting devices in parallel. For HV transmission systems, special considerations are needed for capacitor banks and filters when calculating a.c. short-circuit currents.

All these impedances formulations, whose only main features have been mentioned above, are then used by the standard for short-circuits currents calculation: the method is based on a conversion of the system by network reduction in a circuit made by several short-circuit impedances that, for the final equations, are reduced to a single equivalent impedance at the short-circuit location, which is accurately processed according to the type of fault and, consequently, the sequences involved. The only current for which this process is not allowed is the peak current, for which is necessary the distinction between networks with or without parallel branches.

As already mentioned, there is a difference between fault far-from generator and near-to generator: in both cases, the current is composed of two parts; one is for both the aperiodic d.c. component, that begins whit its initial value and then decays to zero, while the other is the a.c. component, with constant amplitude during the whole fault in the first case or with a decaying amplitude in the second case. However, in both cases, for the calculation of I_k" it is allowed to take $\mathbf{Z_{(1)}} = \mathbf{Z_{(2)}}$. While doing these

calculations for I_k'', the presence of fuses and current-limiting circuit-breakers to protect substations is initially neglected.

The standard provides, in the last section, all the useful formulas for the calculation of the previously defined currents, for the various types of failure and the different conditions in which it occurs, according to the position and state of elements such as generators and transformers; main formulas between these will be reported in the comparison section, but the complete procedures are easily available from [51]. Particular attention is paid to the distinction between meshed and non-meshed networks, as in the second case the radially-connected sources that are contributing to the short-circuit current need to be considered separately to obtain I_k'' as the sum of the individual branch short-circuit currents. It is also consented from the regulation, within the accuracy of the standard, to determine the current as the sum of the absolute values of the partial short-circuit currents.

For the various cases, approximations are provided that can simplify the calculations or overcome the lack of information, and useful graphs to obtain parameters of the currents' formulas such as the R/X or X/R ratio for i_p, μ factor for I_b, λ_{max} and λ_{min} for maximum and minimum steady-state short-circuit current and others.

2.2 Standard ANSI/IEEE C37.010

This standard is applied for ac high-voltage circuit breakers, rated following other guides such as ANSI/IEEE C37.04 and ANSI C37, while for circuit breakers manufactured to meet other standards it is necessary to apply specific procedures adapted to their use. This guide is intended for general use in the application of circuit breakers in Usual Service Conditions, even though some advice is given for unusual circumstances, such as in case of very high altitude, the exposure to particularly dangerous chemical agents, or natural elements that may limit its efficiency or damage the equipment.

The application of circuit breakers in electrical networks requires attention to many technical factors to avoid the misapplication, preventing the component from performing its regular load current-carrying and short-circuit breaking function.

However, since it can be used in other applications where switching requirements may be a determining factor in the selection, special attention must be paid to the relevant variables and permitted ranges to make an optimal choice.

Of these quantities, below is only given a brief list/description to make known the main considerations on which the guide focuses [53], to better develop the short circuit part later on.

- **Maximum Voltage for Application:** It represents the upper limit for the operation to avoid damaging.
- **Voltage Range Factor:** Same as the previous but considering also a lower limit, even though in most cases the voltage range is not different from the commonly used one.
- **Frequency:** The standard frequency is 60 Hz; special consideration should be given to applications at other frequencies as the interruption of fault current at a different frequency may require modification to the main mechanism to change opening speed.

- **Continuous Current:** The guide pays particular attention to the current values of the loads which must not exceed the rated continuous current, except for short time intervals in specific situations such as motors or synchronous condensers starting. Due to this, the standard gives some advice on how to verify the suitability of the circuit breaker to the environment in which it operates, especially as regards its function, the presence of other equipment in the vicinity and the temperature. The rated continuous current is computed considering an environmental temperature of 40° C, meaning that higher temperatures require a reduction of the transported current, and various measures must be taken to prevent the operating temperature from exceeding the permitted limits, such as an appropriate cable sizing to avoid exceeding cable insulation's temperature limit and the operation of the circuit breaker at lower current values than the rated ones. The last expedient, maintained for a relatively long time, allows the system to exceed the continuous current rating limit without exceeding the temperature limit for a short time, whose value depends on the amplitude of the current normally carried and that can be obtained from tables with standard values or through specific formulas.
- **Rated Dielectric Strength:** Circuit breakers are tested to withstand a voltage higher than the rated maximum for 1 min at the nominal frequency, to provide a margin of safety for deterioration or light contamination. Impulse voltage withstand tests are also carried out to check the efficiency of the insulation level against dielectric failure or similar events.
- **Standard operating duty:** If the actual duty cycle is different from the standard one, appropriate rating factors must be applied.
- **Interrupting time:** Defined as "the time between trip circuit energization and power arc interruption on an opening operation", is used to classify circuit breakers by their speeds and require different considerations depending on the performed operation and current's value.
- **Permissible Tripping Delay:** A value which needs to be considered to avoid thermal damage during close, carry and interrupt sequence, which limit depends on short-circuit current's amplitude.
- **Reclosing Time:** High-speed reclosing is often applied on radial lines to minimize line outages' effects, as in most case a reclosure after 0.5 s prevent any adverse effect for residential and commercial customers. Several definitions are given by the guide, as enough dead time must be guaranteed before line re-energization for the arc path to be deionized, a value that considerably varies for other elements' presence (synchronous motors, static capacitors).
- **Short-circuit Rating:** The standard describes, with the help of some examples and referrals to others ANSI guides, the short-circuit current capabilities that must not be exceeded; among these, asymmetrical requirements need to be carefully checked as, even if normally a circuit breaker having adequate symmetrical interrupting capability will also have adequate capacity to meet all of the related requirements, particular conditions such as a great contribution from motor load or an X/R ratio higher than 15 will result in a slower decrement rate for the asymmetrical current.

- **Line Closing Switching Surge Factor:** Due to the transient overvoltage following the energization of an OH transmission line, circuit breakers are specifically designed to control the voltage peak value to a value lower than this limit in at least 98% of times. As the establishment of this factor is governed by random-variation elements such as time differences between completion of the circuit path in each phase, source voltage's instantaneous value and system's parameters, a statistical analysis is briefly carried out in the guide.

Other factors of minor importance are deepened in the standard, such as out-of-phase switching current rating, shunt reactor current switching, excitation current switching, mechanical life, rated control voltage and fluid operating pressure.

Of course, one of the most important requirements needed for the circuit breaker application is the evaluation of the short-circuit current. For these calculations, "it must be assumed that a short circuit on any ac system can produce the maximum offset (d.c. component) of the current wave" by the guide, that successively decays into a symmetrical current which rate of decay is affected by fault location and system L/R ratio. To meet these considerations, circuit breakers are projected to properly interrupt both symmetrical and asymmetrical current with the relationship reported in Fig. 2-2.

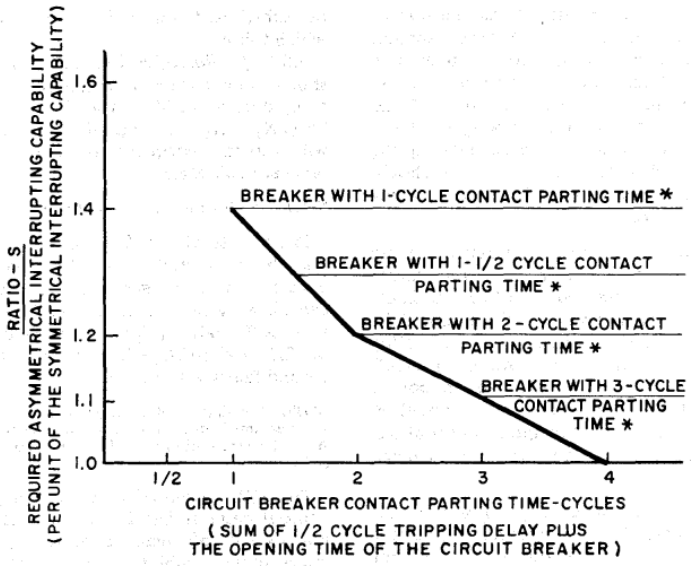

Figure 2-2: Asymmetrical and symmetrical current relationships from [53].

For the short-circuit current computation, the analysis is performed, for the ANSI standard, in three different networks, namely ½ cycle, 1 ½ to 4 cycles and 30 cycles: in the first one the subtransient network's reactance is used for the calculation, in the second the transient network's reactance is used to calculate the fault current after 4 cycles of fault occurrence, while in the last one the steady-state reactance of network's component is used for steady-state short-circuit current's calculation.

Since several methods can be applied to perform these calculations, from the most rigorous and complex to the most approximate, the standard first describes a simplified method that is based on the calculation of the E/X ratio only, and then a more accurate version of the same method, useful if more precise results are needed.

E/X simplified method requires only the easy computation of this ratio, where E is the line-to-neutral value corresponding to the highest typical operating voltage at the circuit breaker location and X is the lowest system reactance value, viewed from fault point and varying on fault type and on the rotating machines' behaviour, which reactances values are reported in a table for several types of rotating machines. The use of this procedure without considering the system resistance value is suggested by the standard only if the E/X value does not exceed 80% of the symmetrical interrupting breakers' capability. For greater accuracy, the guide suggests the application of a more complete procedure involving steps for applying other factors to E/X calculation including, in this way, fault location and X/R ratio, for which is further specified that, for practical proportions, both procedures of reducing the reactance to a single value neglecting the resistance and vice versa lead to accurate results. After the computation of E/X current, it should be multiplied by specific factors which take into account fault types, a.c. and d.c. decay effects, contact parting times and breaker's cycle number. These values, in absence of exceptions that go beyond the cases permitted by this standard, can be obtained from the related graphs which maximum correction factor in most practical applications is 1.25 that forms the basis for the abovementioned value of 80%.

On the other hand, to use the equivalent X/R ratio, the standard recommends obtaining important electrical devices' resistance value from manufacturers, whereas, in the absence of that, approximated values are suggested from specific tables, which must be converted to normal operating temperature.

The appendix presents, in a more detail way, the method used to derive the correction factors to be applied to E/X method which is based on system X/R at fault point. It is suggested to apply it thanks to its great accuracy, even if is considered a semi-rigorous procedure, if by doing the simplified calculation the results of short-circuit current exceed 80% of the circuit breaker symmetrical interrupting capability in case of three-phase and standard SLG faults, while the value 70% is taken as a limit in case of SLG fault supplied predominantly by generators at their voltage. It is further underlined that, as the method does not account for any decay of short-circuit current's symmetrical component, it often offers overly conservative results, especially for near-to-generator faults.

The charts from which the factors are derived are reported in Fig. 2-3: these are based on calculated decrement of both a.c. component and total short-circuit current. From rigorous calculation, it is shown that for remote faults or near-to-generation faults characterized by a substantial contribution from a remote system, the a.c. decrement might be very low but again, the assumptions of computing values regardless of fault location is going to give overly conservative results.

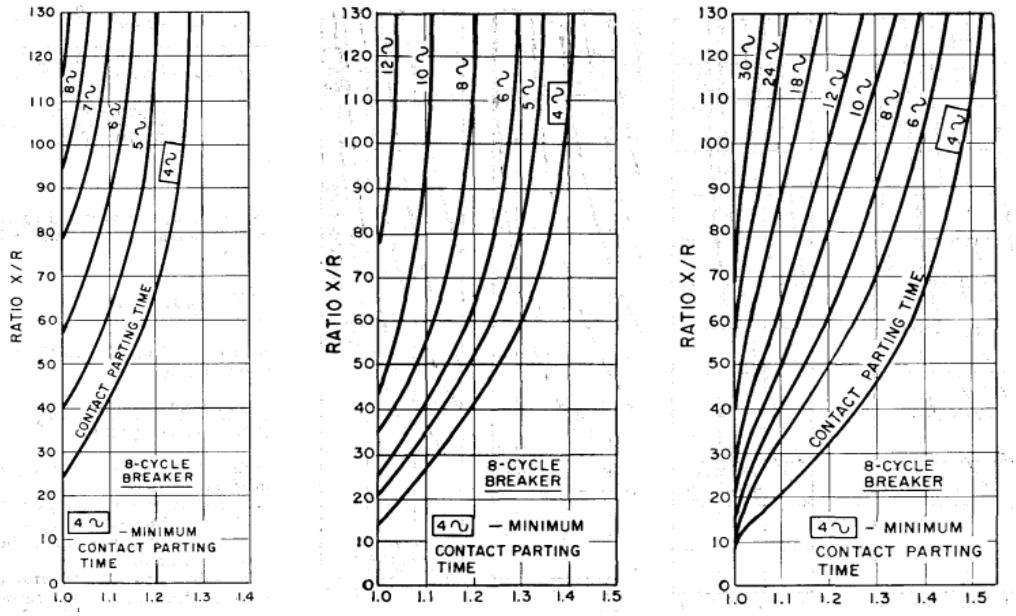

Figure 2-3: From left to right, respectively, three-phase fault and SLG multiplying factors, including a.c. and d.c. decrement effects, while the last one shows three-phase fault and SLG multiplying factors including only the d.c. decrement effects [53].

Among the various figures present in the A-Appendix of the standard, the most important two are reported for completeness in Fig. 2-4, representing respectively the relationship between the symmetrical and asymmetrical component (no a.c. decrement) as a function of X/R with several contact parting times, and the modifications of these curves to take into account the decay of fault current's symmetrical component: a part of the latter shows it at various time intervals after fault beginning, in which, to remain on the conservative side, the points showing the least ac decrements were preferred to get the curves, avoiding issues with machines' variations and system constants.

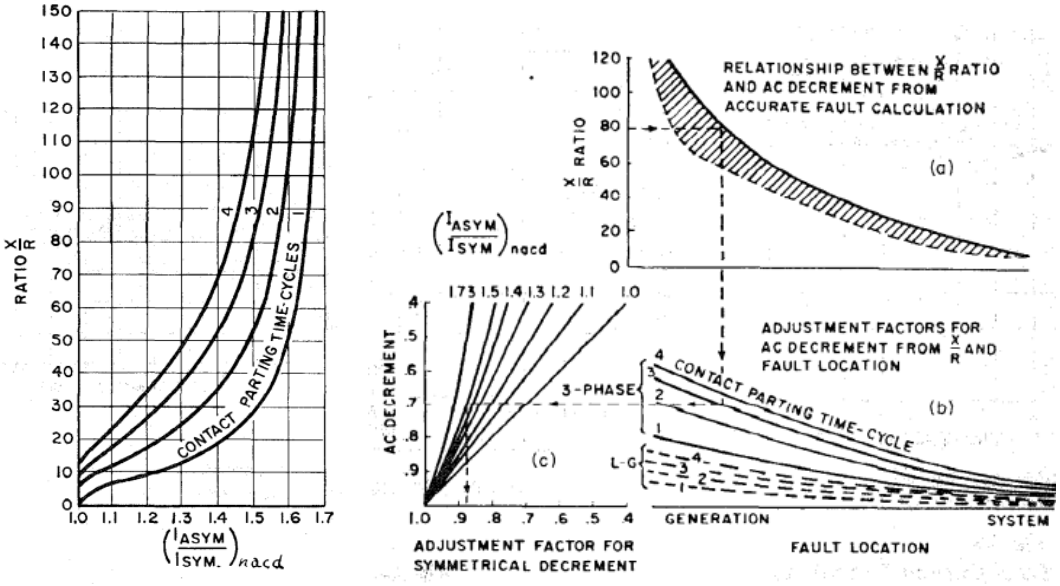

Figure 2-4: Figure 5 and 7 of [53], representing respectively the relationship of asymmetrical and symmetrical current ratio in respect of X/R for several contact parting times and the relationship between X/R and ac decrement factor.

2.3 Comparison between IEC 60909 and ANSI/IEEE C37.010

As can already be noticed from the description of the individual European and American standards, there are several differences concerning the definitions of the quantities involved, the formulas used to calculate them and the assumptions that are applied to network's model. Since in this period engineering services exchange between continents is increasing [54], the question of differences between standards has become even more important. Another very relevant factor is related to circuit breaker's testing, which costs in many cases can easily reach tens of thousands of dollars making it uncomfortable to have to do two rounds of testing for the two standards, also because a design optimized for one type of standard will not have the same effectiveness if evaluated with the other, leading to a reduction in ratings [55]. For these reasons, it was deemed necessary to make a brief but as much as possible complete comparison between the two standards, to highlight the discrepancies and the effects that have on currents values.

The first differences are evident as soon as the model aspects for a.c. and d.c. decaying components are presented by the two standards. While computing the symmetrical interrupting currents, ANSI standard recommends multipliers for rotating equipment's subtransient and transient reactances as reported in Table 2-1, as a function of duty type and machine's size and speed but without considering the distance between the machine and the fault. Particular procedures must be considered in case of low voltage standard, that in case of an X/R ratio at the fault point higher than 6.6 requires others multiplying factors for the symmetrical rating to be compared to tested values [56]. On the other hand, IEC does not recommend a priori adjustment; in fact, it does not rely on curves for modelling the a.c. decaying for generating stations, like ANSI C37.010, but directly considers the abovementioned characteristics, including fault location and machine proximity, when modelling a.c. decrement for rotating loads [57]. This will also lead to one of the many discrepancies in the data required by the two methods, which in this case consists on rpm and hp rating information for ANSI factors and rated real power per pole information for IEC models.

Criterion	Multipliers for first cycle duty	Multipliers for breaking current
Synchronous machines		
turogenerators	1,0	1,0
synchronous motors	1,0	1,5
Induction machines		
> 735,5 kW and ≤ 1500 turns/min	1,0	1,5
> 183,9 kW and ≤ 3000 turns/min	1,0	1,5
≥ 36,8 kW	1,2	3
< 36,8 kW	∞	∞

Table 2-1: Values of reactance multipliers to calculate the first cycle and breaking current from ANSI 37.010 [53].

Concerning asymmetrical currents, ANSI recommends the application of multipliers to the symmetrical current, which values require the computation of X/R ratio at the fault point through a calculation in which is suggested to separate resistance and reactance networks; IEC guidelines do not share the concept of a single X/R ratio, preferring the use of more X/R ratios applied through superposition in case of more independent sources. This separation procedure, which allows avoiding calculations with complex numbers, is justified by the American standard by the fact that even the more complicated and time-consuming calculation will not lead do correct results since in a network with several sources, each sources' branch has a distinct decay's time constant of aperiodic component [58].

Directly related to this X/R ratio, there is also an issue concerned about network configuration: while for ANSI there are not direct references on differences in methods for radial or loop systems, IEC makes a clear distinction between the two cases, applying a simple scalar or vectorial sum for contribution in non-meshed networks [59], while providing three different methods for contribution flowing through meshed grids. The classification between these methods, which are used for the calculation of k required for peak current, is based on this ratio: in the A-Method, known as "dominant ratio", k is determined by taking the smallest ratio from all network's branches with 80% of current at nominal voltage; in the B-Method, known as " equivalent ratio at the fault point", the previous value is modified with a 1.15 safety factor to account for inaccuracies; in the C-Method, known as "equivalent frequency" method, the ratio is computed at a lower frequency and then multiplied by a frequency-dependent multiplying factor [60].

Considering now another aspect, for the evaluation of breaker's rated short-circuit currents the ANSI standard recommends a 1.0 p.u. pre-fault voltage, including adjustment of the current with the correction impedance factor K only in case of operating voltages different from breaker's rated maximum voltage. On the other hand, IEC introduces the application of the c multiplying factor for the initial symmetrical current evaluation as reported in Table 2-2, accounting several aspects such as transformer taps, worst case pre-fault voltage conditions, system loads and shunts and others, allowing the determination of an equivalent voltage source at the fault location. These values, that change for maximum and minimum fault currents evaluations and depend also on network nominal voltage, are considered as one of the main reasons of the different results on currents magnitude obtainable through these standards.

Nominal voltage Un	Voltage factor c	
	maximum short-circuit current	minimum short-circuit current
Low voltage: 100 to 1000 V	1,05 1,10	0,95
Medium voltage (up to 35 kV)	1,1	1
High voltage (>35 kV)	1,1	1

Table 2-2: Values of voltage factor c recommended in [51].

As far as transformers are concerned, and as already mentioned in the dedicated section, IEC 60909 describes procedures for transformers' modelling in case of primary and secondary rated voltages

different from the system's voltage levels, deepening the issue for power station units' modelling and providing in the Appendix A many examples of transformers with nominal turns ratio different than system voltage levels' ratio. Regarding this theme, the ANSI standard does not give any indication.
Another important factor of distinction between the two standards concerns the relative position between electrical machines and fault location. The distance of synchronous and induction motors is not considered by ANSI in their calculation on interruption currents, as motors are represented by fixed impedances; on the other hand, for generators, it's applied a rule that defines them as remote if the short-circuit location is more than two transformers away or if the reactance between these two positions is greater than 1.5 times generator's subtransient reactance. If these cases are not verified, the generator is considered as local. This distinction is important for ANSI calculation as the application of a.c./d.c. decrement factor rather than the only d.c. decrement factor is determined by whether source contributions are mainly remote or predominantly local. For IEC 60909, during breaking currents computation, motors are considered near if the sum of all their currents contribution I_{kG}" is larger than 5% of total I_k" obtained without motors; otherwise, are all retained as far. For synchronous machines is applied a similar rule that considers its as near if I_{kG}" exceeds twice their rated current.
Since there are several differences about the calculation methods of the main currents, already defined in the respective sections of the standards, a comparison between the various types is made below, showing the most important formulas to highlight the distinctions:

- **Initial fault currents:** It has previously been reported I_k" definition and network configuration, here is reported also the equation used to obtain it:

$$I_k'' = \frac{c\, U_n}{\sqrt{3}\sqrt{R_k^2 + X_k^2}} \tag{2. 23}$$

  The equivalent of the initial symmetrical short-circuit current in ANSI is the so-called first duty cycle, defined as "the maximum cumulative value of the symmetrical short-circuit current in the first cycle after the occurrence of short circuit", and its value is obtained with the already discussed E/X ratio, where X is the value at fault time.
  Both currents are symmetrical and can be easily compared, but as will be further enhanced through some reported results, I_k" is usually higher, both for c and subtransient impedances contribution.
- **Closing/latching currents:** These asymmetrical fault currents are computed at half cycle after the short circuit, using the same network as for the first cycle duty and applying a 1.6 multiplier for asymmetry as recommended by ANSI, while the calculation of similar value is not performed in IEC standard.
- **Peak currents:** Having already described the differences regarding the X/R ratio and the methods applied in IEC, here are reported the equations used respectively for IEC and ANSI calculation of peak currents:

$$I_p = \sqrt{2}\, k\, I_k'' \tag{2. 24}$$

where k in the A-method can be read from the graphs or computed as:

$$k = \sqrt{2}\left(1.02 + 0.98\, e^{-3\frac{R}{X}}\right) \quad (2.25)$$

The equivalent in ANSI is:

$$\boldsymbol{I}_{peak} = \sqrt{2}\, I_{sym}\left(1 + e^{\frac{2\pi\tau}{X/R}}\right) \quad (2.26)$$

where the first step is relative time tau calculation through:

$$\tau = 0.49 - 0.1\, e^{-\frac{X/R}{3}} \quad (2.27)$$

- **ANSI interrupting vs. IEC breaking currents:** Calculation of short-circuit breaking current, according to IEC 60909, requires a distinction between short-circuit near-to and far-from generator, as in the first case I_{bG} has a value lower than the initial one and can be computed as:

$$I_{bG} = \mu_G I_k'' \quad (2.28)$$

where μ_G factor depends on the ratio between the initial fault current coming from the source and the generator's rated current and on the minimum time delay; these values can be read by a dedicated graph trough linear interpolation with appropriate corrections for lower t_{min} values. For motors, the equation is the same, of course with currents and parameters referred to the motor, with the addition of a q factor depending on engine power per pair of poles in MW and t_{min}.

In case of a far-from-generator short circuit, if the condition is verified with both reactances converted to the voltage level of the network at fault location, I_{bG} is equal to I_k". It can be seen from the graphs present in the standard that the μ factor decays exponentially with respect to the ratio between the currents with a decay which decreases as the t_{min} is smaller; the q factor, instead, is a natural logarithmic function which decay is faster the larger is machine power per pole pairs [61].

In ANSI, the equivalent of I_{bG} is the so-called interrupting current I_{sc} which is calculated in the same way as the first cycle's one but with recalculated reactances trough specific multipliers. A comparison between the results offered by the two standards underlines that for short clearing times IEC reactances tend to be smaller than ANSI ones while for longer times reactance adjustment's effect becomes prevalent.

For the calculation of asymmetrical fault currents, ANSI guidelines recommend the application of multipliers which are obtained by two sets of curves (one for local fault, one for remote) based on minimum time delay and X/R ratio. IEC does not rely on curves but applies similar procedures to the ones used for peak current to obtain the d.c. component of short-circuit current through:

$$i_{d.c.} = \sqrt{2}\, I_k''\, e^{-2\pi f t \frac{R_k}{X_k}} \quad (2.29)$$

Results comparison shows that, if it is taken I_{bG} equal to I_k'', IEC asymmetrical current is higher than ANSI's one, mainly due to the lack of a.c. decay modelling which, if considered during calculations, leads to much more similar values.

- **ANSI delayed vs. IEC steady-state currents:** Both standards agree on the issue that transient effects are not to be modelled, but IEC provides for a series of clauses that, depending on the type of duty, requires generators excitation system representation. These clauses, that may also be applied to synchronous motors, depart considerably from ANSI procedures, leading to more pessimistic results especially in case of a near-to-generator fault.
- **Circuit breaker performance test:** It is worth noting that, concerning circuit breakers tests, similar terms do not necessarily result in similar concepts in these standards, leading in general to the requirement of a more stringent performance for ANSI standard. For instance, several of the allowable temperature rise limits considered in ANSI are from 5 to 10°C lower than IEC standard, ANSI test duration of 3 s is considerably higher than the 1 s used in IEC, ANSI requirements for a peak current of 2.7 times higher than rated fault current is different from the 2.5 of IEC, and some procedures are applied only in ANSI such as the requirement for latching against rated closing current, that consists in carrying the rated current for 2 s and then interrupting it, that is not present in IEC guidelines [55].

As many of the currently available software for short-circuit simulations and calculations include both standards, here is proposed a shortlist of elements for which different sets of data are needed:

- IEC recommends, for unbalanced faults, the modelling of negative sequence impedance that might necessitate the negative sequence matrix computation, leading to a computational burden usually not undertaken for ANSI analysis.
- Even though both guidelines agree on most of the data needed for zero-sequence series impedance and on assumptions that can be applied to simplify problem's complexity, still there are some differences such as the adjustment of zero-sequence generator impedance and the modelling of zero-sequence line shunts, required only for resonant grounded and isolated system, that are considered only by IEC.
- For generators, there are some data needed, in particular circumstances, only by IEC, such as saturated leakage reactance for system's excitation response modelling and pre-fault power factor, while ANSI might require generator's transient reactance for time-delayed considerations.
- Almost all of the induction and synchronous motor information that are needed for its modelling in the network are the same, but it has always to be considered that many of this data may not be imported from one system to the other as for several quantities the unit of measurement is not the same and, in some case, slightly different elements are used in similar equations (ANSI X_d'' versus IEC ratio of load to locked rotor current [57]).

As evidenced by this brief comparison, there are many differences between the approaches used by the two standards for the calculation of short-circuit and circuit breaker interruption currents, some with a negligible weight but others more relevant, ranging from the concept of how the network is represented in the various duty types to how certain quantities are defined. To file these discrepancies, to avoid the abovementioned problems and to limit the inconveniences, recent years revisions of ANSI/IEEE standards have led to changes implemented to harmonize with IEC guidelines [62]. Many fields have seen changes introduced, including transient recovery voltage profiles, voltage range factor, classifications and, concerning short-circuit calculations, peak ratings: for this has been defined that maximum peak current does not occur at the half-cycle in the phase with the maximum initial d.c. component unless the fault occurs on a purely inductive circuit; exact time for peak and more detailed instructions are given for more precise calculation, whose insights go beyond the purpose of this review, but that has been mentioned to show how this field is still evolving.

2.4 Results

The comparison carried out in the previous section is based on a careful reading of the two standards and related papers, from which the main differences, both for the formulas applied in the calculations and for grid elements' representation, with the relative simplifications and conditions for neglecting them, are listed. With the aim of integrating the discussion with practical results under the two approaches, a simple circuit, shown in Fig. 2-5, has been built in the commercial software NEPLAN to compare fault current values following the two different standards, respectively IEC 60909, the second edition of 2015 and ANSI C37.010.

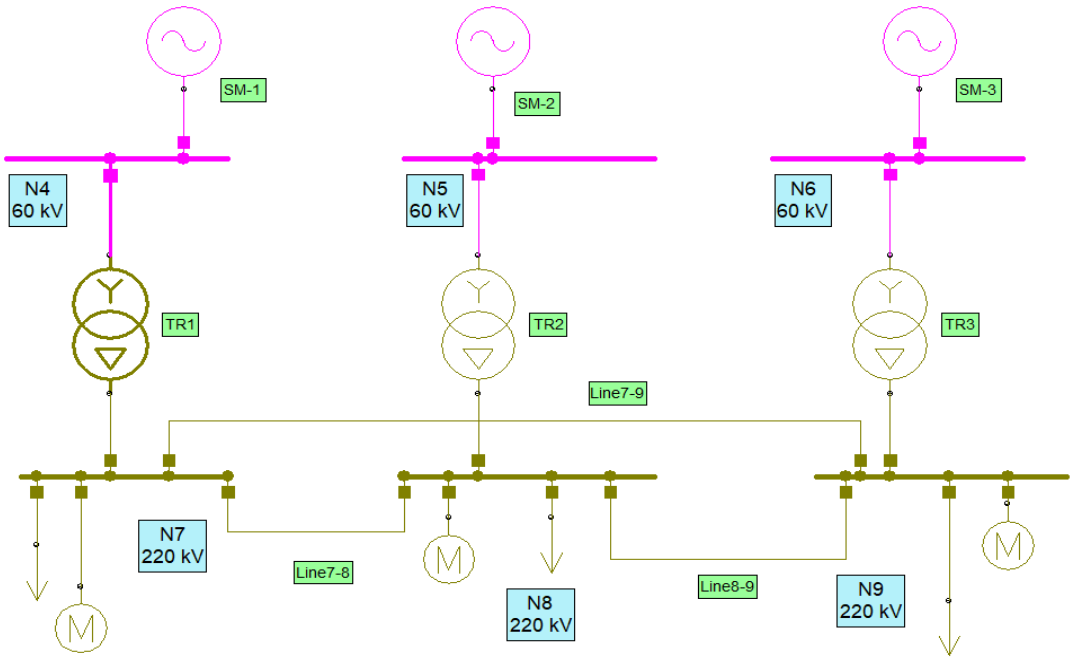

Figure 2-5: Network's scheme.

Although the grid is simple and has few loads, rotating machines have been included in addition to static loads to quantitatively verify the result of the different approaches proposed by the standards. The results of SLG and three-phase faults are shown in Figg. 2-6 and 2-7. The faults have been simulated along Line 7-9, and since the results are symmetrical for each half of the line, with respect to the middle point, the values have only been reported for the first segment between Node 7 (0 km) and the middle of the line (20 km).

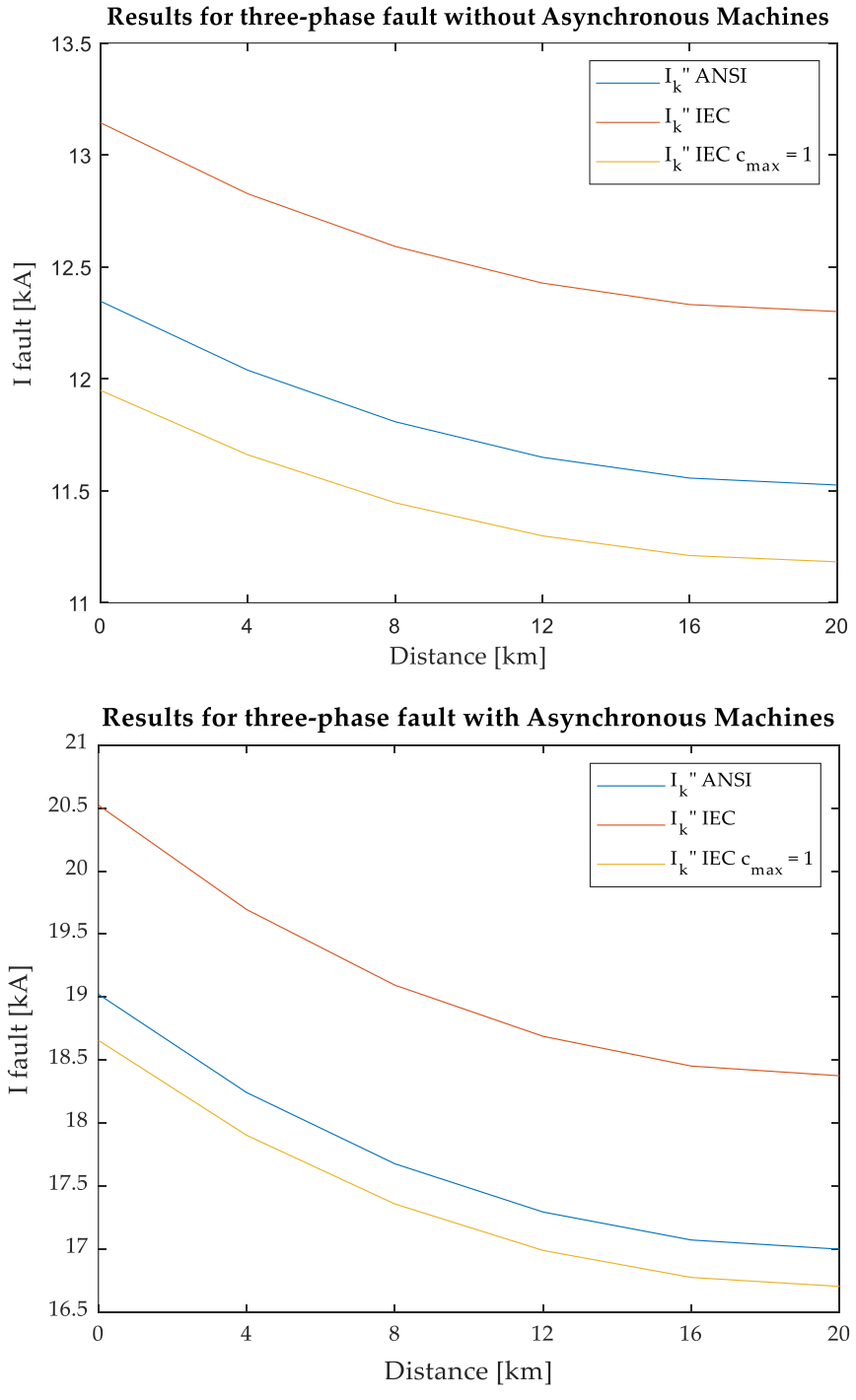

Figure 2-6: Results for three-phase fault obtained with NEPLAN short-circuit analysis.

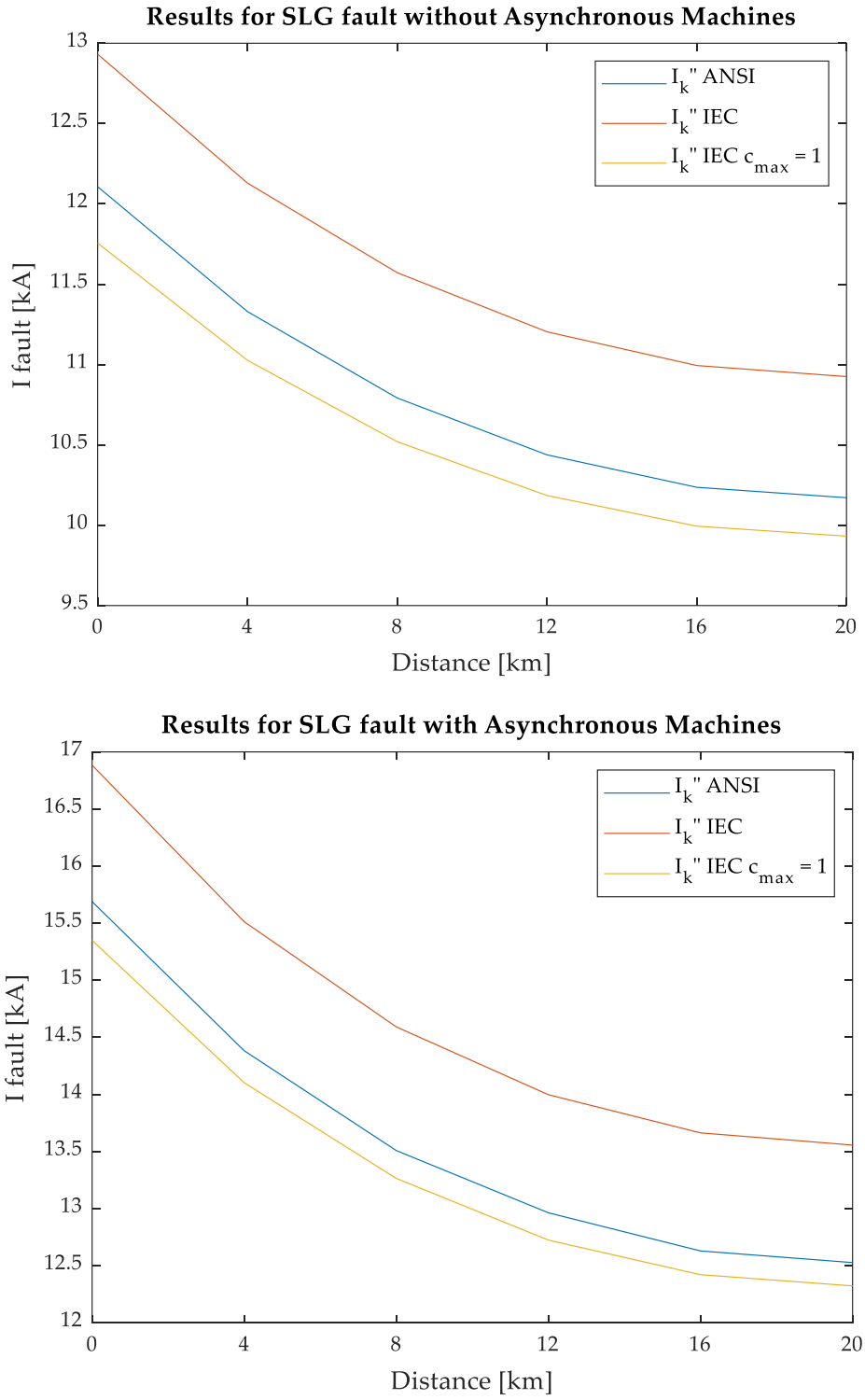

Figure 2-7: Results for SLG fault obtained with NEPLAN short-circuit analysis.

As shown in the graphs, all currents computed using IEC 60909 are generally higher (in this case all values are between 6% and 7.5% higher) than those calculated using ANSI 37.010: this effect is mainly due, as mentioned in the relative section, to the voltage factor c. For this reason, in Figg. 2-6 and 2-7 the values obtained through IEC standards but with the imposition of the c_{max} factor equal to one have

also been reported, showing how much this value influences the final results as, in this case, the ANSI results are even higher than IEC ones. The other relevant factor is the presence in the network of asynchronous machines. As it could be noticed in these figures and that is even more evident when computing the differences, their presence leads to generally higher fault current values, and the difference between IEC and ANSI results increases of one percentage point.

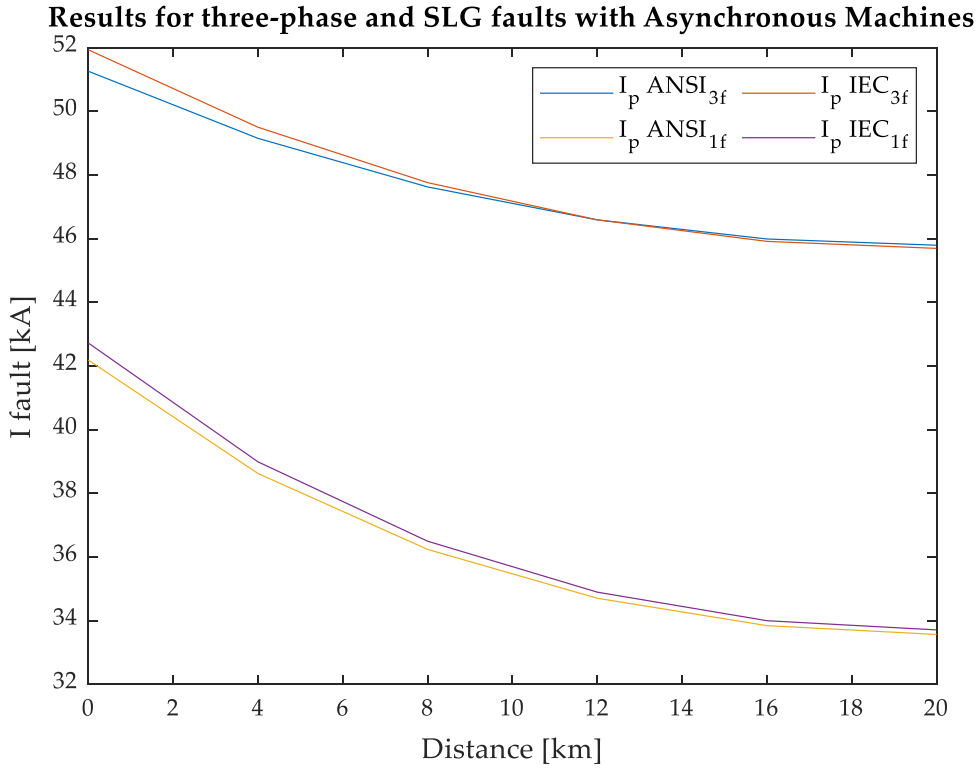

Figure 2-8: Results for both SLG and three-phase faults obtained with NEPLAN for peak currents values, obtained, in the case of the IEC standard, with c_{max} automatically selected (meaning equal 1.1).

Also the i_p values have been reported for completeness. As it can be noticed from the graphs, these values have a much more similar trend than the previous cases. There are no general rules on which the standards provide the peak value because it is strongly influenced by the system's X/R ratio.

3 Multi-conductor modelling of power systems elements

For the calculation of fault currents, but also the solution of power flow algorithms, a complete but at the same time flexible representation of the network is necessary. In the last century, the exponential development of transmission theories has led to a continuous modification of the techniques used for circuits analysis and simulations, starting from the formulas proposed by Carson for the calculation of the impedance of the ground-fault current return circuit, passing through methods based mainly on matrix calculations (both impedance and admittance matrices) and arriving in the recent years at the application of new power flow solution methods such as the backward-forward sweep method, the Gauss Z_{Bus} method and the Newton-Raphson method.

The last methods are just mentioned and will not be further discussed in the thesis, since the scope is mostly on developing the grid elements' models for fault regime analysis. This is obtained by means of nodal admittances matrix method, developing a novel procedure for solving the problem as will be illustrated later. For this reason, among the various methods described in the literature, studied and elaborated by different authors, just some of the most important ones with their main innovations and advantages are presented below, as an overview of all the known methods is not in the aim of this work and can be found in review papers available in literature.

Papers that need to be mentioned include DeSieno's article [63], based on a distributed parameter network modelling, Meliopoulos' article [64], in which an equivalent model integrating the earth conductor and the soil into the system is described and solved through modified nodal analysis method application (the model is obtained by solving Laplace's equations and the paper presents also some techniques for size reduction based mainly on the grouping of system segments into groups containing segments with similar characteristics), and the Dawalibi's [65], Popovic's [66] and Weizenfeld's [67] articles, developed on a sequence-based representation of the network (both with concentrated and distributed parameters) and with the application of the double-sided elimination method to solve the problem of the limited sizes.

However, the various methods present some simplifications that, although necessary to reduce the structural and numerical complexity, prevent from generalizing the modelling approach in all the possible network configurations: in Weizenfeld's paper the various subsystems of a line are treated as an equivalent one, only representing the mutual couplings between phase conductors and the neutral, leading to higher current values and not allowing a complete representation of the actual distribution of the fault current. In Popovic's one, in addition to the simplifications already seen in the previous chapter, implicit in the theory of sequences, there is the consideration of towers' footing resistances as constants and all equal to the average value, with a consequent error that is the heavier the closer the failure occurs to one of them. For this, the paper proposes both distributed and lumped parameters procedures, with their pros and cons and a comparison between the results.

A further development worth to be mentioned is reported in the article by Nahman and Dordevic [68], in which there is an evolution of the symmetrical components method that through a multiport representation of the main elements of the system allows the inclusion in the model of components such

as ground systems and switching stations, then appropriately interconnected through the application of Kirchhoff's laws. Of course, being the method based on symmetrical components, it assumes phase transposition for all the lines, thus allowing to limit the size of the problem to be solved and to make it particularly advantageous for the iterative calculations required, but avoiding to treat individually phase quantities, which require a more complex approach but allow a more realistic representation.

However, the first numerical approaches that have been developed and applied for the power flow calculation were based on impedance and admittance matrices used in iterative methods. Between the two, to create an exhaustive model of the network and to solve load flow problems and, through appropriate modifications, to calculate fault currents, there has been a shift towards the use of the nodal admittance matrix. The latter allows to represent the transmission grid and its elements in a widespread way and is characterized by a great sparsity and the possibility to be built automatically: these properties make it more suitable for this application than those based on the impedance matrix which, on the opposite, although buildable automatically, is a dense matrix, with consequent storage and complexity problems.

Even though these methods, due to the scarce reliability of the admittance matrix method and to the high storage requirement and low-speed performance of the impedance matrix method, have been substituted by more recent ones, which have been already mentioned, below will be explained in a more detailed way the characteristics of the admittance matrix and its construction, as the basis of the algorithm development.

The potential of this matrix and its properties are still subject of study, mainly focused on the ability of this matrix to represent multiphase systems comparing the results with a single-phase configuration, and on the different methods of reducing the size of the matrix [69] [70]. Among these, there is, for example, the Kron reduction method that is frequently used for the analysis of multi-machine power systems where, under certain assumptions, allows to reduce the size of networks composed of hundreds or thousands of elements by lightening the computational weight. Subsequently, the properties of the matrix and its application for network modelling will be better presented, but here it's shortly introduced to show its basic construction method and how it can be made automatically.

The simplest technique for the construction of the nodal admittances matrix is the inspection method: since it is based on the visual observation of the connections between the circuit nodes, it is a technique not suitable for the implementation of automation strategies of the procedure, but it is still valid to explain the essential points on which it is based.

Let's consider, for instance, a very simple system formed only by a few nodes and with a π-representation of the network elements, like the one in Fig. 3-1. The evolution of this system neglecting the derived components leads to the new representation in which there are no ground connections: this is a valid simplification because often the shunt quantities have negligible values, but that obviously will not be applied in the complete method presented step by step in the next sections.

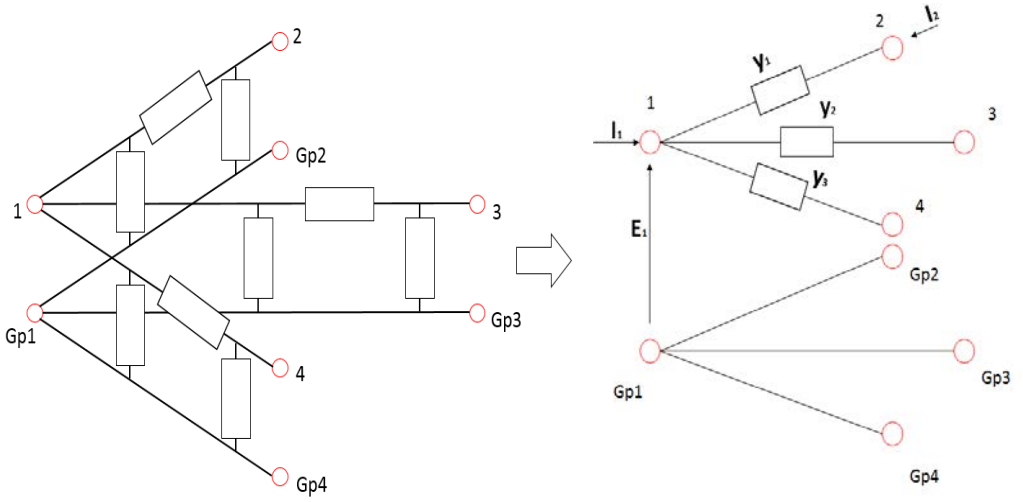

Figure 3-1: Simple 4-port system with its π-representation and the representation where shunt elements are neglected.

The convention of positive current entering from the nodes is applied to the system and the various longitudinal admittances and node potentials between the node itself and its ground gate are defined. To derive the individual terms of the matrix at the nodal admittances, which will have dimension $n \times n$ with n the number of the circuit's nodes, the following formula between phasors is applied:

$$\boldsymbol{Y_{r,s}} = \frac{\boldsymbol{I_r}}{\boldsymbol{E_s}} \tag{3.1}$$

where the application of the voltage generator between node s and its ground port and the consequent evaluation of the current circulating through node r is carried out by short-circuiting the other ports. As it can be easily derived from this circuit, if the formula is applied to compute the auto-admittance of node 1, the circuit shows the parallel between the admittances 1, 2 and 3. For the other nodes the same strategy is applied, leading to the valid statement that in the building process of the nodal auto-admittances, which will represent the diagonal of the total matrix, only the elements that converge to the node are considered. While applying the same process for the computation of the mutual admittances between nodes, the achieved result is that in its definition are considered only the elements that are between these nodes, that, for the before mentioned sign convention, are taken with a negative sign. This is the final result for the considered system:

$$\boldsymbol{Y} = \begin{bmatrix} \boldsymbol{y_1 + y_2 + y_3} & \boldsymbol{-y_1} & \boldsymbol{-y_2} & \boldsymbol{-y_3} \\ \boldsymbol{-y_1} & \boldsymbol{y_1} & 0 & 0 \\ \boldsymbol{-y_2} & 0 & \boldsymbol{y_2} & 0 \\ \boldsymbol{-y_3} & 0 & 0 & \boldsymbol{y_3} \end{bmatrix}$$

which emphasizes some of the most important properties of this matrix such as its sparsity, the fact that is symmetrical (if the element of the network is reciprocal) and that is always defined even without transversal elements; of course the sparsity is more obvious in a larger system and the more the grid is meshed, the more the matrix will be sparse.

Applying the same strategy, but now considering the impedances of the system and therefore applying the inverse formula with respect to the previous one, i.e. inserting a current generator on the considered node and evaluating the respective voltage considering the other nodes as open, it is immediately evident that, since the current cannot circulate, the impedance value is infinite; therefore the impedance matrix first of all needs the presence of a ground connection, so it is not always defined. Moreover, even after having added a further transverse admittance $\mathbf{y_4}$ between node one and its ground port to allow the current circulation, the result shows that the matrix is dense and that for how is built, a change for example to $\mathbf{y_4}$ will affect the values of many elements in the matrix; by bringing this concept into a much larger network, the result is that a change at one point in the network can lead to changes in matrix's values in positions even far away from that node.

$$\boldsymbol{Z} = \begin{bmatrix} \frac{1}{\boldsymbol{y_4}} & \frac{1}{\boldsymbol{y_4}} & \frac{1}{\boldsymbol{y_4}} & \frac{1}{\boldsymbol{y_4}} \\ \frac{1}{\boldsymbol{y_4}} & \frac{\boldsymbol{y_1}+\boldsymbol{y_4}}{\boldsymbol{y_1 y_4}} & \frac{1}{\boldsymbol{y_4}} & \frac{1}{\boldsymbol{y_4}} \\ \frac{1}{\boldsymbol{y_4}} & \frac{1}{\boldsymbol{y_4}} & \frac{\boldsymbol{y_2}+\boldsymbol{y_4}}{\boldsymbol{y_2 y_4}} & \frac{1}{\boldsymbol{y_4}} \\ \frac{1}{\boldsymbol{y_4}} & \frac{1}{\boldsymbol{y_4}} & \frac{1}{\boldsymbol{y_4}} & \frac{\boldsymbol{y_3}+\boldsymbol{y_4}}{\boldsymbol{y_3 y_4}} \end{bmatrix}$$

Returning now to the nodal admittances' matrix, to automate the construction procedure of the matrix it is necessary to pass from the quantities referred to the branches to those referred to the nodes. Applying the definition of voltage to potentials and obtaining the current entering the node as the vector sum of the branch currents, the following formulas are obtained:

$$\boldsymbol{v_b} = \boldsymbol{A}\, \boldsymbol{e_n} \tag{3.2}$$
$$\boldsymbol{i_n} = \boldsymbol{A^T}\, \boldsymbol{i_b} \tag{3.3}$$

where **A** is defined as incidence matrix, a matrix which the only non-zero elements are ones with the relative sign, and for this small example is equal to:

$$\boldsymbol{A} = \begin{bmatrix} 1 & -1 & 0 & 0 \\ 1 & 0 & -1 & 0 \\ 1 & 0 & 0 & -1 \end{bmatrix}$$

Combining the formula of the admittance with the two just presented, and defining $\mathbf{Y_p}$, primitive admittance matrix representing the link between branches' currents and voltages, it is finally obtained the following:

$$\boldsymbol{i_n} = \boldsymbol{Y_n}\, \boldsymbol{e_n} = \left(\boldsymbol{A^T}\, \boldsymbol{Y_p}\, \boldsymbol{A}\right) \boldsymbol{e_n} \tag{3.4}$$

which finally correlates nodal quantities, which are easier to consider and calculate for computer processing.

Going beyond this simple example, it is now shortly defined the Y primitive for a single element. Each element of the circuit is considered as an element between two terminals, which always need to be specified to locate the element in the network: each terminal is composed by several ports equal to the number of branches between the terminals (in this case p for the first terminal and q for the second terminal), that represent the points of connection between each conductor and the bus. Once the voltages of each branch are defined through the bus's reference for each terminal, and the injected currents that are linked to the branches are considered with the same convention used previously, then these currents are related to the branches' voltages through the Y primitive, which dimension is the total number of branches by the total number of branches, in this case $(p + q) \times (p + q)$.

One important feature of this matrix is that it is always symmetrical so that, for this generic element, can be split into four submatrices which are respectively two submatrices containing each terminal self and transference admittances, and two submatrices constituted by the mutual admittances between the two terminals in which every single element has an index of the first terminal and an index of the other terminal. The result is presented in this form to highlight the submatrices:

$$\begin{bmatrix} \boldsymbol{I_1} \\ \vdots \\ \boldsymbol{I_p} \\ \boldsymbol{I_{p+1}} \\ \vdots \\ \boldsymbol{I_{p+q}} \end{bmatrix} = \begin{bmatrix} \boldsymbol{y_{11}} & \cdots & \boldsymbol{y_{1p}} & \boldsymbol{y_{1(p+1)}} & \cdots & \boldsymbol{y_{1(p+q)}} \\ \vdots & \ddots & \vdots & \vdots & \ddots & \vdots \\ \boldsymbol{y_{p1}} & \cdots & \boldsymbol{y_{pp}} & \boldsymbol{y_{p(p+1)}} & \cdots & \boldsymbol{y_{p(p+q)}} \\ \boldsymbol{y_{(p+1)1}} & \cdots & \boldsymbol{y_{(p+1)p}} & \boldsymbol{y_{(p+1)(p+1)}} & \cdots & \boldsymbol{y_{(p+1)(p+q)}} \\ \vdots & \ddots & \vdots & \vdots & \ddots & \vdots \\ \boldsymbol{y_{(p+q)1}} & \cdots & \boldsymbol{y_{(p+q)p}} & \boldsymbol{y_{(p+q)(p+1)}} & \cdots & \boldsymbol{y_{(p+q)(p+q)}} \end{bmatrix} \begin{bmatrix} \boldsymbol{V_1} \\ \vdots \\ \boldsymbol{V_p} \\ \boldsymbol{V_{p+1}} \\ \vdots \\ \boldsymbol{V_{p+q}} \end{bmatrix} \quad (3.5)$$

Similarly, if our element was connected to a single node, as in the case of a load, the Y primitive would have dimension $n \times n$ (with n number of branches of the terminal), that in comparison to the previous example is the matrix containing the self admittances of the first terminal. The same principle applies for any element: if we consider a generic element connected to M terminals with an arbitrary number of conductors each, the Y primitive is composed by M times M submatrices, of which M are in the diagonal representing the self admittances.

Then, if we consider a generic network composed by many elements and nodes, all properly defined, to pass from the single element Y primitive matrix to a complete Y system matrix, the rule is simple: each submatrix of each Y primitive matrix is added to the Y matrix in the corresponding area.

Despite this rapid digression on the admittance matrix and the construction of the primitive matrix of an element, it is worth reporting how not all the methods applied in these years are based on the use of the nodal admittance matrix: there are several papers in the literature that present variations of the impedance matrix that, with appropriate modifications, allows the representation of three-phase components such as transformers and voltage regulators, with the possibility of dealing with power flow problems in meshed and unbalanced networks [71].

Within this thesis, a power flow method, that allows the representation of a generic multi-phase circuit, is presented based on the construction of the admittance's matrices of the various circuit's components and integrated with special features that allow, for example, the modelling of switches at the bus or the interconnection between systems with different voltage levels or number of phases thanks to a multi-

port representation of the transformers. This tool makes it possible to analyse how variations in the generation or in the loads connected to the network modify the grid behaviour in the event of faults, and thanks to the multi-conductor representation, which will be presented in detail in the next section, all mutual coupling and reciprocal influences between the phases are taken into account, making it possible to represent any circuit even with an asymmetrical structure and unbalanced operation.

These and other peculiarities that will be illustrated during the thesis allow this algorithm an easy implementation and intrinsic robustness also in the case of ill-conditioned systems such as LV networks with high R/X ratios.

3.1 Transmission line model

Of the several elements that need to be modelled to represent a network, this section will focus on the transmission line model [72]. The branch elements are represented through an n-phase π-model as mentioned before: this means that, considering a three-phase branch with neutral conductor between two nodes, each phase conductor and neutral conductor has its self-impedance, and, as shown in the figure below, between each combination of conductors there will be the corresponding mutual impedance named according to the conductors which they are related to; as we consider a π-model of the line, the total lines admittances are split and considered half of it at the beginning of the line and the other at the end of the line, for both self and mutual admittance, as shown in Fig. 3-2.

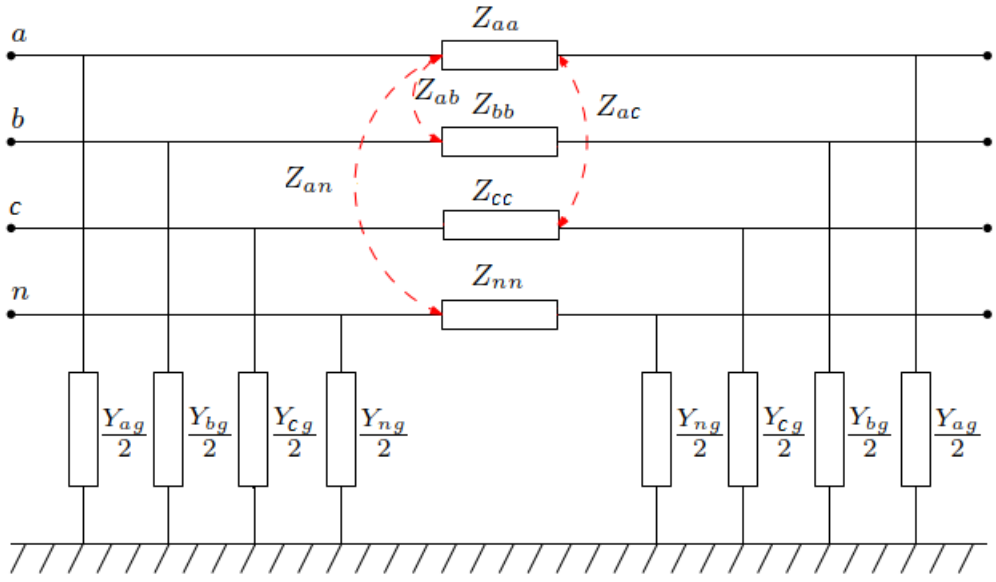

Figure 3-2: Graphical representation of the π-model of a three-phase system with neutral wire; in the picture have not been drawn, to avoid confusion, mutual impedances of phases different from a-phase and the mutual admittances that would be between each couple of conductors and split in half too.

By using the same convention as above, with currents taken as positive if entering the lines, it is easy to obtain the following equation for phase a:

$$\Delta \boldsymbol{V_a} = \boldsymbol{V_{a1}} - \boldsymbol{V_{a2}} = \boldsymbol{Z_{aa}} * \boldsymbol{I_a} + \boldsymbol{Z_{ab}} * \boldsymbol{I_b} + \boldsymbol{Z_{ac}} * \boldsymbol{I_c} + \boldsymbol{Z_{an}} * \boldsymbol{I_n} \qquad (3.6)$$

where $\mathbf{V_{a1}}$ and $\mathbf{V_{a2}}$ are the phase a voltage for the first and the second node respectively (with respect to the common zero voltage reference) and the currents are considered positive if entering.

This easily leads to the matrix expression:

$$\begin{bmatrix} \Delta V_a \\ \Delta V_b \\ \Delta V_c \\ \Delta V_n \end{bmatrix} = \boldsymbol{Z} \begin{bmatrix} I_a \\ I_b \\ I_c \\ I_n \end{bmatrix} \tag{3.7}$$

where is now considered only the part of the current which is flowing through the longitudinal impedance, and **Z** is the impedance matrix, symmetrical and composed by self impedance on the diagonal and mutual impedance outside of it.

Using these formulas and remarking that the two currents vectors flow in opposite directions, we can express the relation between these longitudinal currents and the voltages as:

$$\boldsymbol{Z^{-1} * V_1 - Z^{-1} * V_2 = I_{L1}} \tag{3.8}$$

$$\boldsymbol{-Z^{-1} * V_1 + Z^{-1} * V_2 = I_{L2}} \tag{3.9}$$

where $\mathbf{I_L}$ are the longitudinal components of the whole currents entering the nodes.

Similarly, as the shunt capacitive and conductive links have been split into two equal parts and lumped at the beginning and the end of the line's section, is obtained:

$$\boldsymbol{I_{T1} = \frac{Y_t}{2} * V_1} \tag{3.10}$$

$$\boldsymbol{I_{T2} = \frac{Y_t}{2} * V_2} \tag{3.11}$$

where $\mathbf{I_T}$ are the transversal components of the whole currents entering the nodes.

These finally lead to the matrix that represents the link between voltages and currents of the ports of the branch element, $\mathbf{Y_{branch}}$:

$$\boldsymbol{Y_{branch}} = \begin{bmatrix} \boldsymbol{Z^{-1} + \frac{Y_t}{2}} & \boldsymbol{-Z^{-1}} \\ \boldsymbol{-Z^{-1}} & \boldsymbol{Z^{-1} + \frac{Y_t}{2}} \end{bmatrix} \tag{3.12}$$

The construction of the **Z** and **Yt** matrices is based on the Carson-Clem formulation for an n-phase branch, that computes both the self and mutual impedances (results in Ω/km) by:

$$z_{i,i} = r_i + r_e + \pi^2 * 10^{-4} * f + j4\pi * 10^{-4} * f * \ln\left(\frac{2*D_e}{d_i}\right) \tag{3.13}$$

$$z_{i,j} = r_e + \pi^2 * 10^{-4} * f + j4\pi * 10^{-4} * f * \ln\left(\frac{D_e}{d_{i,j}}\right) \tag{3.14}$$

where r_i is the DC resistance of the conductor [Ω/km], d_i is the phase conductor diameter [m], $d_{i,j}$ is the mutual distance between conductors i and j [m], and r_e and D_e are the quantities referred to the earth return path, respectively its resistance [Ω/km] and depth [m], computed trough:

$$r_e = \pi f * 10^{-4} \tag{3.15}$$

$$D_e = 659 * \sqrt{\frac{\rho}{f}} \tag{3.16}$$

where ρ is soil conductivity [Ωm], which typical value is 100 Ωm.

The matrix **Yt**, on the other hand, is computed through the knowledge of the conductivity of the conductor, which has to be provided to the software, and the application of Maxwell's potential coefficients for the calculation of self and mutual capacitance using the method of images. Considering

our conductors and their images with respect of the earth, and referring with S to the distances between a real conductor and other conductors' images and D as the distance between two real conductors, the self and mutual potential coefficients [km/F] are calculated by:

$$P_{i,i} = \frac{1}{2\mu\varepsilon_0 * 1000} * \ln\left(\frac{S_{i,i}}{r_i}\right) \tag{3.17}$$

$$P_{i,j} = \frac{1}{2\mu\varepsilon_0 * 1000} * \ln\left(\frac{S_{i,j}}{D_{i,j}}\right) \tag{3.18}$$

where ε_0 is the free space permittivity in F/m, while the other quantities have already been described; then the **C** matrix is obtained by doing the inverse of **P** matrix.

Once the branches' admittance matrix is computed for every single longitudinal element, the complete system's nodal admittance matrix can be built through an incidence matrix defining the network's topology.

3.2 Transformer model

The transformer is a particularly important element within a multiphase multi-conductor system and its representation is far from being trivial: in the literature, there are several examples of applied strategies, based on different references such as the αβ0 stationary system, the dynamic dq0 system and the sequence frame; however, modelling obtained through the admittance matrix allows a better definition of mutual couplings. In this section will be presented the procedure to model the transformer in the system with some practical examples. The steps to build the model of a generic multi-phase transformer, allowing elaborations in asymmetric systems, start from the construction of the primitive admittance matrix of the transformer, passing then through the calculation of the admittance matrices of the transformer without considering the connections, arriving finally to the application of the connections between the phases with a specific matrix that characterizes the group of the transformer [73].

To generalize to the multiphase system, it is necessary to start from the equivalent single-phase representation of a two windings transformer as reported in Fig. 3-3, thus allowing to characterize the impedances between primary and secondary. In this case, the magnetization and short-circuit impedances, respectively $\mathbf{z_0}$ and $\mathbf{z_{cc}}$, are reported to the primary side.

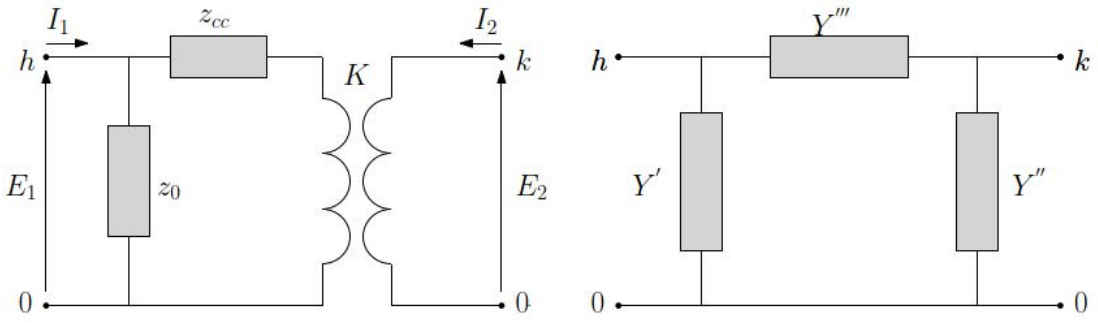

Figure 3-3: Equivalent single-phase representation of a two windings transformer; E vectors are phase-to-ground potentials of each node [73].

An alternative option to represent these impedances is the π-model, which allows switching from mutual and auto impedances to a scheme with three admittances which, in a p.u. system, are defined as:

$$\boldsymbol{Y'} = \frac{1-\boldsymbol{m}}{\boldsymbol{z_{cc}}} \tag{3.19}$$

$$\boldsymbol{Y''} = \frac{\boldsymbol{m}\,(\boldsymbol{m}-1)}{\boldsymbol{z_{cc}}} \tag{3.20}$$

$$\boldsymbol{Y'''} = \frac{\boldsymbol{m}}{\boldsymbol{z_{cc}}} \tag{3.21}$$

with $\boldsymbol{m} = K\frac{\boldsymbol{E_1}}{\boldsymbol{E_2}}$ transformation ratio and $K = \frac{N_1}{N_2}$ turns ratio. These equations do not include the effects of the magnetizing admittances since it involves only the primary side.

Once the single-phase model has been defined for each phase, the primitive admittance matrix for the multi-phase transformer can be built by placing the admittances computed with eq. 3.19-21 on the diagonal, leading to a squared diagonal matrix of dimensions 4n by 4n (with n number of phases):

$$\boldsymbol{Y_p} = \begin{bmatrix} \boldsymbol{Y_a'} & 0 & \cdots & \cdots & \cdots & \cdots & \cdots & 0 \\ 0 & \ddots & 0 & \cdots & \cdots & \cdots & \cdots & 0 \\ \vdots & 0 & \boldsymbol{Y_a''} & 0 & \cdots & \cdots & \cdots & 0 \\ \vdots & \vdots & 0 & \ddots & 0 & \cdots & \cdots & 0 \\ \vdots & \vdots & \vdots & 0 & \boldsymbol{Y_a'''} & 0 & \cdots & 0 \\ \vdots & \vdots & \vdots & \vdots & 0 & \ddots & 0 & 0 \\ \vdots & \vdots & \vdots & \vdots & \vdots & 0 & \boldsymbol{Y_{0a}} & 0 \\ 0 & 0 & 0 & 0 & 0 & 0 & 0 & \ddots \end{bmatrix} \tag{3.22}$$

At this point, to obtain the transformer's admittance matrix, a suitable incidence matrix needs to be applied to $\mathbf{Y_p}$: as this incidence matrix adds the information about admittances' positions, it's strictly dependent on the structure used to group the terms in the π-model:

$$\boldsymbol{A} = \begin{matrix} \boldsymbol{Y'} \\ \boldsymbol{Y''} \\ \boldsymbol{Y'''} \\ \boldsymbol{Y_0} \end{matrix} \begin{bmatrix} [\boldsymbol{I}] & [\boldsymbol{0}] \\ [\boldsymbol{0}] & [\boldsymbol{I}] \\ -[\boldsymbol{I}] & [\boldsymbol{I}] \\ [\boldsymbol{I}] & [\boldsymbol{0}] \end{bmatrix} \tag{3.23}$$

As in this matrix the identity and zeros matrices have order equal to the number of phases, for a two windings three-phase transformer **A** dimensions will be *4n* for the rows and *2n* for the columns (the column's index refer to the primary and secondary side of each phase).

Now to complete the transformer model the information about the connections between the buses at the primary and secondary sides and the transformer ports need to be added.

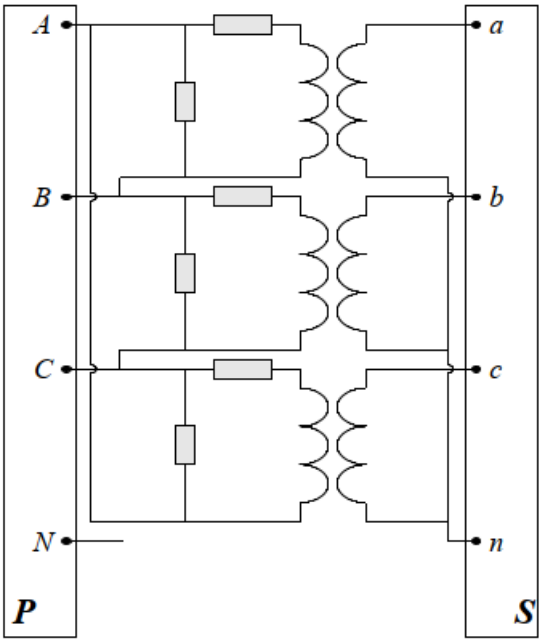

Figure 3-4: Schematic representation of a Delta-Wye Transformer's connections [73].

If to give an example, a Delta-Wye transformer like the one in Fig. 3-4 is considered, the incidence matrix that defines these connections is the following:

$$\boldsymbol{B} = \begin{matrix} A-B \\ B-C \\ C-N \\ a-n \\ b-n \\ c-n \end{matrix} \begin{bmatrix} 1 & -1 & 0 & 0 & 0 & 0 & 0 & 0 \\ 0 & 1 & -1 & 0 & 0 & 0 & 0 & 0 \\ -1 & 0 & 1 & 0 & 0 & 0 & 0 & 0 \\ 0 & 0 & 0 & 0 & 1 & 0 & 0 & -1 \\ 0 & 0 & 0 & 0 & 0 & 1 & 0 & -1 \\ 0 & 0 & 0 & 0 & 0 & 0 & 1 & -1 \end{bmatrix}$$

where the columns refer respectively to the ports A, B, C and N on the primary side and a, b, c, and n on the secondary side; the presence of the column referred to the port N enhance how the number of phases can be chosen independently from the number of ports that are employed.
The complete transformer admittance matrix is then obtained by:

$$\boldsymbol{Y_T} = \boldsymbol{B^T}\{\boldsymbol{A^T}\,\boldsymbol{Y_{prim}}\,\boldsymbol{A}\}\,\boldsymbol{B} \tag{3.24}$$

With a procedure very similar to the one just exposed, but with the addition of appropriate expedients, the model of a three-winding transformer can be computed.

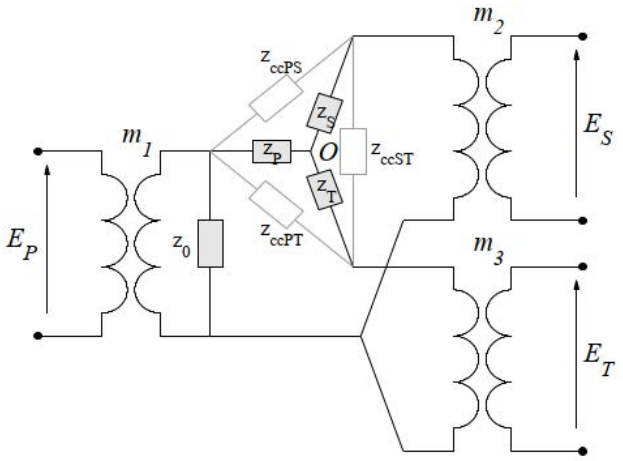

Figure 3-5: Single-phase equivalent circuit of a three-windings transformer with the shift from short circuit impedances to sides' ones [73].

The first modification to be made, as shown in Fig. 3-5, is to pass from the short-circuit impedances Delta-connected to a system of impedances relative to each side (primary P, secondary S and tertiary T) star-connected, applying the formula whereby each impedance relative to a side is equal to half the sum of the two short-circuit impedances connected to the same side minus the short-circuit impedance that instead connects the other two sides; for example:

$$\boldsymbol{Z_P} = \frac{1}{2}\left(\boldsymbol{z_{ccPS}} + \boldsymbol{z_{ccPT}} - \boldsymbol{z_{ccST}}\right) \tag{3.25}$$

The primitive matrix is built as before by inserting in the diagonal the admittances obtained as reciprocal of the side impedances just calculated, taking now into account also the node O, necessary to have a ground connection of the common node and which admittances are very small values (in the order of 10^{-10} compared to the other terms) to avoid the occurrence of problems when the matrix is inverted. Each diagonal submatrix has order 3 (number of coupled single-phase circuits):

$$\boldsymbol{Y_{prim}} = \begin{bmatrix} [\boldsymbol{Y_P}] & [\boldsymbol{0}] & [\boldsymbol{0}] & [\boldsymbol{0}] & [\boldsymbol{0}] \\ [\boldsymbol{0}] & [\boldsymbol{Y_S}] & [\boldsymbol{0}] & [\boldsymbol{0}] & [\boldsymbol{0}] \\ [\boldsymbol{0}] & [\boldsymbol{0}] & [\boldsymbol{Y_T}] & [\boldsymbol{0}] & [\boldsymbol{0}] \\ [\boldsymbol{0}] & [\boldsymbol{0}] & [\boldsymbol{0}] & [\boldsymbol{Y_0}] & [\boldsymbol{0}] \\ [\boldsymbol{0}] & [\boldsymbol{0}] & [\boldsymbol{0}] & [\boldsymbol{0}] & [\boldsymbol{Y_O}] \end{bmatrix} \tag{3.26}$$

$\mathbf{Y_{prim}}$ is now in order 5n.

Subsequently, the incidence matrix **A** can be built with identity and zeros matrices properly positioned; this matrix, now that considers also the new reference O and its admittance, is now of order 5n times 4n:

$$\boldsymbol{Y_{prim}} = \begin{matrix} \boldsymbol{Y_P} \\ \boldsymbol{Y_S} \\ \boldsymbol{Y_T} \\ \boldsymbol{Y_0} \\ \boldsymbol{Y_O} \end{matrix} \begin{bmatrix} [\boldsymbol{I}] & [\boldsymbol{0}] & [\boldsymbol{0}] & -[\boldsymbol{I}] \\ [\boldsymbol{0}] & [\boldsymbol{I}] & [\boldsymbol{0}] & -[\boldsymbol{I}] \\ [\boldsymbol{0}] & [\boldsymbol{0}] & [\boldsymbol{I}] & -[\boldsymbol{I}] \\ [\boldsymbol{I}] & [\boldsymbol{0}] & [\boldsymbol{0}] & [\boldsymbol{0}] \\ [\boldsymbol{0}] & [\boldsymbol{0}] & [\boldsymbol{0}] & [\boldsymbol{I}] \end{bmatrix} \tag{3.27}$$

where the columns represent respectively the three sides and the common node.

Since the common node O is not present in the complete system, before proceeding, it is necessary to carry out a reduction. First of all, calculate the transformer matrix without connections with the following:

$$\overline{Y_T} = \boldsymbol{A^T\, Y_{prim}\, A} \tag{3.28}$$

obtaining an admittance matrix of order 15. This will then be inverted to obtain the relative impedance matrix, from which the rows and columns relative to node O are removed reducing the order to 12; finally, the new matrix is inverted to obtain the reduced admittance matrix of the transformer without connections, which will be indicated with $\overline{\boldsymbol{Y_{T(reduced)}}}$.

Having followed a different procedure than in the two windings case, the impedance definition does not contain information about the transformation ratio, which will therefore be inserted later together with the connections to the external doors. In doing so, the turns ratios are defined as:

$$\begin{cases} m_P = k_P \\ m_S = \frac{1}{k_S} \\ m_T = \frac{1}{k_T} \end{cases} \quad where \quad k_X = \frac{E_{XRated}}{E_{XBase}} \quad with\ X = P, S, T \tag{3.29}$$

At this point, to insert the information regarding the connections with the ports of the various phases and the values of the transformation ratio, the matrices **B** and **C** are formulated:

$$\boldsymbol{B} = \begin{bmatrix} [\boldsymbol{B_P}] & [\boldsymbol{0}] & [\boldsymbol{0}] \\ [\boldsymbol{0}] & [\boldsymbol{B_S}] & [\boldsymbol{0}] \\ [\boldsymbol{0}] & [\boldsymbol{0}] & [\boldsymbol{B_T}] \end{bmatrix} \tag{3.30}$$

$$\boldsymbol{C} = \begin{bmatrix} m_P & 0 & \cdots & \cdots & \cdots & \cdots \\ 0 & \ddots & 0 & \cdots & \cdots & \cdots \\ \vdots & 0 & m_S & 0 & \cdots & \cdots \\ \vdots & \vdots & 0 & \ddots & 0 & \cdots \\ \vdots & \vdots & \vdots & 0 & m_T & 0 \\ \vdots & \vdots & \vdots & \vdots & 0 & \ddots \end{bmatrix} \tag{3.31}$$

where **B** sub-matrices contain the topology of each side as in the two windings case, and the total dimensions of **B** will be $3n \times 4n$, keeping the same choice made previously to insert all the phases of the 4-wire system for the external connections. **C**, instead, is a square matrix of order $4n$.

The complete admittance matrix for a three windings transformer is then obtained by:

$$\boldsymbol{Y_T} = \boldsymbol{B^T}\left\{\boldsymbol{C^T}\ \overline{Y_{T(reduced)}}\ \boldsymbol{C}\right\}\boldsymbol{B} \tag{3.32}$$

It is worth noting that the same procedure can be applied even for a higher number of windings, requiring only the addition of more ports and the appropriate calculation of the impedances in the single-phase circuit.

3.3 Source and shunt element model

As it will be explained in more detail in the dedicated section, each shunt element, and in our case in particular loads and generators, can be represented by a constant admittance and an appropriate correction by current injection. For a generic shunt element between nodes k and h the nominal complex admittance is calculated through:

$$\boldsymbol{Y_{kh}} = \frac{\boldsymbol{S^*_{kh(0)}}}{\left|\boldsymbol{U_{kh(0)}}\right|^2} \tag{3.33}$$

where $\mathbf{S_{kh(0)}}$ is the element's rated power and $U_{kh(0)}$ is the difference between nodes' potentials; the subscript 0 represents the starting nominal values.

The equation above can be further developed by separating the constant term and allowing to specify the vector of the correction current **ΔI**, which, as it is evident in the following formula referred to the i-th iteration, introduces a voltage dependency:

$$\boldsymbol{S^*_{kh(i)}} = \boldsymbol{Y_{kh}} \left|\boldsymbol{U_{kh(i)}}\right|^2 - \boldsymbol{U_{kh(i)}}\boldsymbol{\Delta I_{kh(i)}} \tag{3.34}$$

Considering the same equation but applied for the ZIP model, the same approach can be applied to introduce separated voltage dependencies (respectively constant impedance, current and power):

$$\boldsymbol{S^*_{kh(i)}} = \boldsymbol{S^*_{kh(0)}} \left[k_Z \left(\frac{\left|\boldsymbol{U_{kh(i)}}\right|}{\left|\boldsymbol{U_{kh(0)}}\right|}\right)^2 + k_I \left(\frac{\left|\boldsymbol{U_{kh(i)}}\right|}{\left|\boldsymbol{U_{kh(0)}}\right|}\right) + k_P\right] \tag{3.35}$$

where the sum of the constants is one.

While the **ΔI** component referred to the constant impedance term is set to 0 in eq. 3.34, the correction current vector relative to the constant current of the model (linear voltage dependence) can be obtained from the following equation:

$$\boldsymbol{S^*_{kh(i)I\%}} = k_I \left(\frac{\left|\boldsymbol{U_{kh(i)}}\right|}{\left|\boldsymbol{U_{kh(0)}}\right|}\right) \boldsymbol{Y_{kh}} \left|\boldsymbol{U_{kh(0)}}\right|^2 = k_I \left(\boldsymbol{Y_{kh}} \left|\boldsymbol{U_{kh(i)}}\right|^2 - \boldsymbol{U_{kh(i)}}\, \boldsymbol{\Delta I_{kh(i)I\%}}\right) \tag{3.36}$$

which has been rewritten to have a shape similar to that of eq. 3.34 and from which it can be obtained:

$$\boldsymbol{\Delta I_{kh(i)I\%}} = k_I \frac{\boldsymbol{Y_{kh}}}{\boldsymbol{U_{kh(i)}}} \left(\left|\boldsymbol{U_{kh(i)}}\right|^2 - \boldsymbol{U_{kh(i)}}\boldsymbol{U_{kh(0)}}\right) \tag{3.37}$$

The same procedure can be applied for the expression of the current correction term referred to the constant power share, leading to:

$$\boldsymbol{S^*_{kh(i)P\%}} = k_P \boldsymbol{Y_{kh}} \left|\boldsymbol{U_{kh(0)}}\right|^2 = k_P \left(\boldsymbol{Y_{kh}} \left|\boldsymbol{U_{kh(i)}}\right|^2 - \boldsymbol{U_{kh(i)}}\, \boldsymbol{\Delta I_{kh(i)P\%}}\right) \tag{3.38}$$

with:

$$\boldsymbol{\Delta I_{kh(i)P\%}} = k_P \frac{\boldsymbol{Y_{kh}}}{\boldsymbol{U_{kh(i)}}} \left(\left|\boldsymbol{U_{kh(i)}}\right|^2 - \left|\boldsymbol{U_{kh(0)}}\right|^2\right) \tag{3.39}$$

Finally, the complete equation for the ZIP model can be composed, highlighting how the various voltage dependencies are represented by different current injectors:

$$S^{*}_{kh(i)} = Y_{kh} \left|U_{kh(i)}\right|^{2} - \left(\Delta I_{kh(i)I\%} + \Delta I_{kh(i)P\%}\right) U_{kh(i)} \tag{3.40}$$

3.4 Grounding conditions

One of the most important features of this method for power flow calculation is the possibility to customize the connection between phases and ground at any point of the system.

In this way, all connection types and grounding options can be replicated without having to use the sequence components. As well as for the representation of the shunt elements, where the system is created by simply taking into account the admittance that defines the coupling between phases, in the same way, the connection between neutral and ground can be represented through a self-admittance at the grounded bus, as it can be seen from Fig. 3-6 where a generic system is represented.

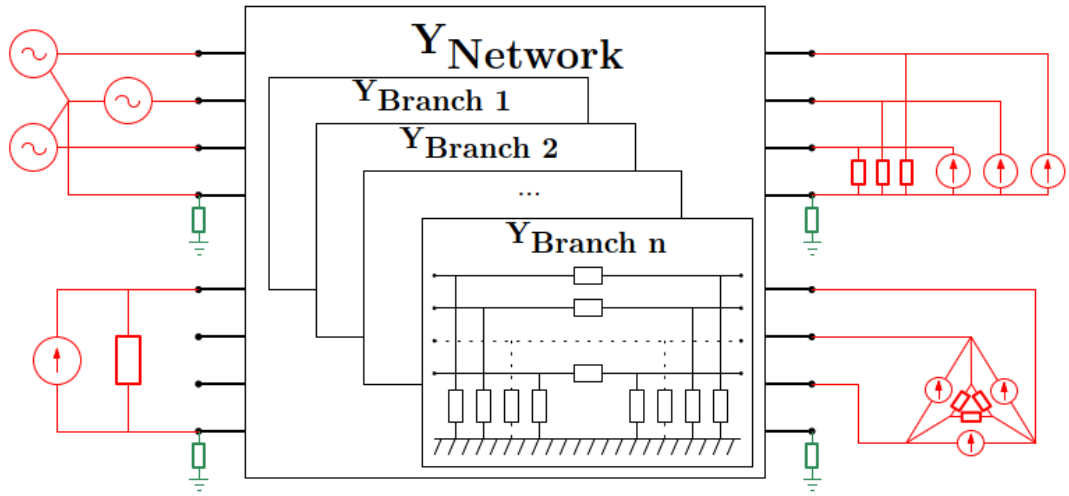

Figure 3-6: Schematic representation of the whole system; red elements are shunt elements connected to external ports, green elements are the earth connection [72].

3.5 Fringing current correction method (FCC)

Due to the aforementioned limitations of the matrix approaches, some modifications have been proposed to try to partially solve the problems, such as the addition of fixed load impedances to the ground to reduce the ill-conditioning typical of circuits with very small shunt admittances compared to branch admittances, or the use of various types of equations for network characterization, since the number of iterations required for convergence varies according to their form.

The novelty that this method introduces is the representation of both loads and generators (excluding the slack bus) as shunt elements, subsequently integrated into the network matrix: the modelling of generators as shunt elements, as will be shown later, is one of the key factors for the reduction of the number of iterations necessary for the convergence method [74]. Overall, we can therefore think of the system as something "inert" which is then "excited" by the voltage phasor applied to the slack bus, establishing the nodal voltages from which the powers absorbed and injected by loads and generators can be obtained. This method normally requires an iterative process of matrix modification to adjust the

value of the shunt admittances according to the constraints imposed by voltages and powers; however, this correction can also be obtained by injecting appropriate current values in parallel to the shunt admittances without modifying the initial values and allowing, like the standard technique, a resolution in complex form without having to separate the real and imaginary quantities. Moreover, the consideration of loads and generators as shunt elements avoids numerical complications and ill-conditioning singularities, thanks to the presence of all these strong ground connections at their buses.

To describe the method, let us consider a generic three-phase system, whose steady-state regime is characterized by the voltage phasor imposed on the slack bus, by the generator voltage modules (from *b* to *g*), by the active power injected at generator buses and by the complex power absorbed by load buses (from *h* to *m*).

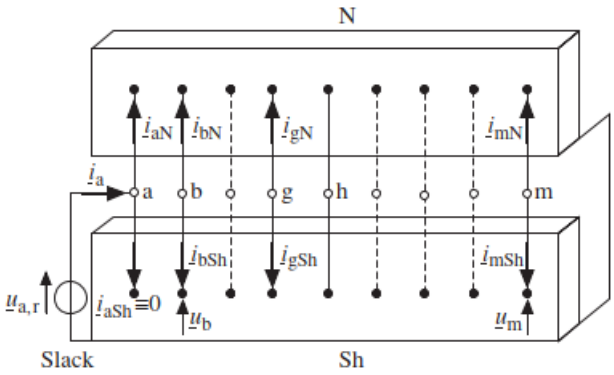

Figure 3-7: Separation of the system in a passive network N and a shunt network Sh; the slack bus is external to both [74].

Considering the system represented in the figure, the power flow calculation is developed as a series of non-linear equations that can be expressed in the following form:

$$\boldsymbol{I = Y * E} \quad \rightarrow \quad \boldsymbol{i_N = Y_n * u} \; ; \; \boldsymbol{i_{Sh} = Y_{Sh} * u} \tag{3.41}$$

which, as shown, can be split in two matrix equation, one for each "part" of the system, where $\mathbf{u}$, $\mathbf{i_N}$ and $\mathbf{i_{Sh}}$ have m elements and $\mathbf{Y_n}$ and $\mathbf{Y_{Sh}}$ are $(n_G + n_L) \times (n_G + n_L)$ nodal admittance matrix, and the latter is a square diagonal matrix; of course when applying this technique to a generic multi-phase network the number of elements in vector and matrices will be multiplied by the number of phases.

The single elements in the shunt admittance matrix can be computed through the following, valid respectively for generic loads and generators:

$$\boldsymbol{S_m = u_m * i^*_{mSh}} \; ; \; \boldsymbol{i_{mSh} = y_m * u_m} \rightarrow \; \boldsymbol{y_m = \frac{p_m - jq_m}{|u_m|^2}} \tag{3.42}$$

$$\boldsymbol{S_g = -u_g * i^*_{gSh}} \; ; \; \boldsymbol{i_{gSh} = y_g * u_g} \rightarrow \; \boldsymbol{y_g = \frac{-p_g + jq_g}{|u_g|^2}} \tag{3.43}$$

where the difference between injected and absorbed power has been taken into account by the sign of the first equation. The power flow equation can be written also as:

$$\begin{bmatrix} \boldsymbol{i_a} \\ \mathbf{0} \\ \vdots \\ \mathbf{0} \\ \mathbf{0} \\ \vdots \\ \mathbf{0} \end{bmatrix} = \begin{bmatrix} \boldsymbol{Y_{GG}} & \boldsymbol{Y_{GL}} \\ \boldsymbol{Y_{LG}} & \boldsymbol{Y_{LL}} \end{bmatrix} \begin{bmatrix} \boldsymbol{u_a} \\ \boldsymbol{u_b} \\ \vdots \\ \boldsymbol{u_g} \\ \boldsymbol{u_h} \\ \vdots \\ \boldsymbol{u_m} \end{bmatrix} \tag{3.44}$$

where for each vector the first g elements form $\mathbf{i}_G$ and $\mathbf{u}_G$, and the others $\mathbf{i}_L$ and $\mathbf{u}_L$; $\mathbf{Y}_{GG}$ and $\mathbf{Y}_{LL}$ are two squared sub-matrices and $\mathbf{Y}_{LG}$ and $\mathbf{Y}_{GL}$ are two rectangular sub-matrices.

Referring to the two equations that can be obtained with this partition, from the second one we get:

$$\boldsymbol{u_L} = -\boldsymbol{Y_{LL}^{-1} Y_{LG} u_G} \tag{3.45}$$

that, replaced in the first, provides:

$$\boldsymbol{i_G} = \left[\boldsymbol{Y_{GG} - Y_{GL} Y_{LL}^{-1} Y_{LG}}\right] \boldsymbol{u_G} = \boldsymbol{Y_{Geq} u_G} \tag{3.46}$$

This system can be further partitioned as shown in Fig. 3-8; and as the current vector has only one non-null element, it can be easily obtained:

$$\boldsymbol{u_x} = -\boldsymbol{D^{-1} C u_{a,r}} \tag{3.47}$$

Therefore, known the generator voltage vector, the load voltage vector can be obtained by applying eq. 3.45.

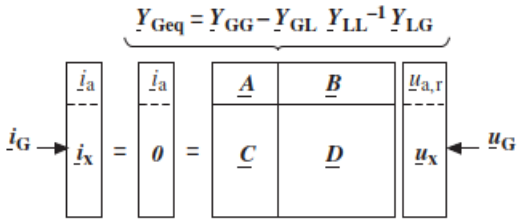

Figure 3-8: The partitioned form of eq. 3.46 [74].

The iterative algorithm can now be implemented, starting from the setting of the initial values of the load admittances (obtained by fixing the voltage module equal to 1 p.u.) and of the equivalent generator admittances (to set the initial values of q at the generation nodes the network is considered as ideal, and the voltage phasors of the generators, which are not inserted in the $\mathbf{Y}_{Sh}$, lie on the real axis and have the amplitude provided by the data, so through the current value $\mathbf{i}_G$, obtained using the eq. 3.46, the first estimate of q is obtained).

At this point, keeping unchanged $\mathbf{u}_{a,r}$, the new $\mathbf{Y}_{Sh1}$ matrix based on the estimation of the initial values determines the new $\mathbf{Y}$ and the new $\mathbf{Y}_{Geq1}$, with their respective sub-matrices, which allow us to write the eq. 3.46 and 3.47 for the first iteration, obtaining the vectors $\mathbf{u}_{G1}$ and $\mathbf{u}_{L1}$. Both vectors' elements are complex voltages whose magnitudes will be different from the scheduled values, resulting in different p and q.

Now, to proceed with iterations, one more direct way is to continue varying the shunt admittances derived at the grid buses until the provided values are met. This method, called admittance matrix correction (AMC), has an excellent convergence speed but requires at each iteration the inversion of the

modified matrix, a heavy procedure especially in the resolution of large networks. This drawback can be overcome by the following presented fringing current correction method (FCC), which fundamentally applies the same kind of correction avoiding the need for inverting the admittance matrices [74].

The AMC method consists of updating the value of generators susceptances, taking into account that q variations mostly affect bus voltage magnitudes and only minimally the phase angles. Through an appropriate transformation we pass from the vector of estimated values $\mathbf{u_{x1}}$ to a similar vector $\mathbf{u_{x1,c}}$ with the same phase angles but amplitudes equal to the scheduled values, from which we can obtain a new vector through the already seen equation:

$$\Delta \boldsymbol{i_{x1,c}} = \boldsymbol{C_1 u_{a,r} + D_1 u_{x1,c}} \tag{3.48}$$

whose current vectors, which must be injected at the generation nodes, represent variations in active and reactive power. As each generator injects its p, to the eq. 3.43 only the new term needs to be added:

$$\Delta \boldsymbol{q_{x1,c}} = Im(\boldsymbol{u_{x1,c}} * \Delta \boldsymbol{i_{x1,c}}^{*}) \tag{3.49}$$

where the operation is an element by element array multiplication. Then the new equation for the generator admittances values is:

$$\boldsymbol{y_g} = \frac{-\boldsymbol{p_g} + j(\boldsymbol{q_g} + \Delta \boldsymbol{q_{x1,c}})}{|\boldsymbol{u_g}|^2} \tag{3.50}$$

The load admittances vary as a consequence of the variation of the $\mathbf{u_{x1,c}}$ vector, which implies the variation of the generator buses' voltages and so of the new vector $\mathbf{u_{L1,c}}$.

The FCC method, on the other way, avoids the updating of $\mathbf{Y_G}$ and $\mathbf{Y_L}$ matrices and the inversions of $\mathbf{Y_{LL}}$ and $\mathbf{D}$, starting from a model equivalent to the AMC's one but considering the current correction vectors both for generators and loads at the respective buses. Based on the two equations that can be derived from eq. 3.44 in generic form, i.e. with a $\mathbf{\Delta i_L}$ vector with non-zero values, the following equation can be derived from the second one (as previously done):

$$\boldsymbol{u_{L,c}} = -\boldsymbol{Y_{LL1}^{-1} Y_{LG} u_{G,c}} + \boldsymbol{Y_{LL1}^{-1} \Delta i_{L,c}} \tag{3.51}$$

that, replaced in the first, provides:

$$\boldsymbol{i_G} = \left[\boldsymbol{Y_{GG1}} - \boldsymbol{Y_{GL} Y_{LL1}^{-1} Y_{LG}}\right] \boldsymbol{u_G} + \boldsymbol{Y_{GL} Y_{LL1}^{-1} \Delta i_L} \tag{3.52}$$

This equation can again be partitioned as shown in Fig. 3-9.

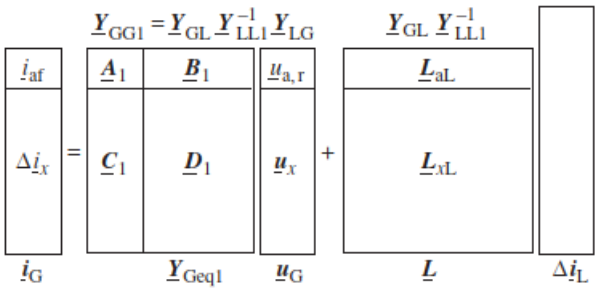

Figure 3-9: Partition of the generic form of eq. 3.44 [74].

This leads to two different equations, from which the second one is:

$$\Delta \boldsymbol{i_x} = \boldsymbol{C_1 u_{a,r} + D_1 u_{x1,c} + L_{xL} \Delta i_L} \tag{3.53}$$

that, solved for $\mathbf{u_x}$, leads to:

$$\boldsymbol{u_x} = \boldsymbol{-D_1^{-1} C_1 u_{a,r} + D_1^{-1} (\Delta i_x - L_{xL} \Delta i_L)} \tag{3.54}$$

where the following equations are valid for the current correction vectors:

$$\Delta \boldsymbol{i_{xq1,c}} = \frac{-j[Im(\boldsymbol{u_{x1,c}} * \Delta \boldsymbol{i_{x1,c}}^*)]}{\boldsymbol{u_{x1,c}^*}} \tag{3.55}$$

$$\Delta \boldsymbol{i_{L,c}} = \left(\frac{diag(\boldsymbol{Y_L})}{\boldsymbol{u_{L,c}^*}}\right) * (\left|\boldsymbol{u_{L,c}}\right|^{\mathbf{2}} - \mathbf{1}) \tag{3.56}$$

obtained respectively from the already seen formulas for the additional reactive power component and from the definition of variation of **ΔS** at the input of a load node, as represented in Fig.3-10 [74].

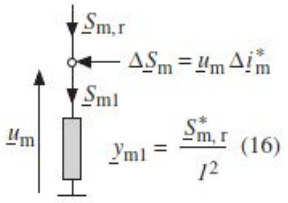

Figure 3-10: Standard load bus defined by its nominal admittance and scheduled $S_{m,r}$ [74].

The sequential application of the above formulas in the following order (eq. 3.54, eq. 3.51, eq. 3.56, eq. 3.53 and eq. 3.55) allows the same result as the AMC method to be achieved in the same number of iterations but with a calculation time reduced in proportion to the $\mathbf{Y_{LL}}$ size. In the first iteration, for the first passage the current correction vectors are imposed null and then, from the second equation which is about $\mathbf{U_{L1,c}}$, the correction current $\mathbf{\Delta i_{L2,c}}$ is obtained, and successively the new values of $\mathbf{\Delta i_{x2,c}}$ are computed; both vectors are then injected in the second cycle.

4 Ground return current distribution in power systems

4.1 Fault regime calculation: comparison between three software

In this section, a comparison of the fault regime calculation results using three software is presented, considering the system shown in Fig. 4-1, for which the main data are reported in Appendix A: upstream, there is a three-phase generator followed by a transformer (the transformation ratio is unitary: the purpose of this part of the comparison is to validate the representation of the various elements, and for this, the whole network is kept at the same voltage level). From node 4, where the secondary side of the transformer is connected, it starts a 120 km line which, for this simplified analysis with parallel lines, is divided into 10 sections of 12 km each represented with the respective nodes at the ends (substations), which are further divided in spans of 200 m. Although this last information is not fundamental for the three-phase fault, the possibility of subdividing the line into spans without detailing physical nodes significantly reduces computational effort by reducing the overall admittance matrix size. In addition, it allows defining the tower footing resistances, hence providing an accurate grid model that exhaustively computes the actual current paths. A second generator, connected to the same node as the main one, is added to the circuit, to have the possibility of having one main generator (which performs the function of a slack bus, or PV node) and another one which is considered as a PQ bus for the Load Flow analysis, and whose influence is however negligible as the size is set hundreds of times smaller. At the end of the line, there is a symmetric wye-connected load.

The line is a double-circuit three-phase line with a earthwire placed above the phase conductors. As detailed in the previous chapter, grounding conditions are explicitly defined for the grid buses, to better represent the connection of the nodes (substations) to the ground through suitable impedances. Since, to define the characteristic impedance and admittance values of the lines, it is necessary to specify conductors' main data and the subsequent geometry of the line (in this case the arrangement of the conductors is considered equal to the section seen in correspondence of the pylon all along the line; this means that no variations in the height of the conductors are currently taken into consideration, simulating an ideal case of perfectly thigh conductors), to implement the phase transposition it is necessary to specify 3 different geometries, one for each configuration and different order of the phases (which are always in opposition to minimize mutual coupling). It's also for this reason that the line has been divided into smaller pieces with nodes, and not simple towers, to allow a decent application of the transposition between phases' conductors.

This is an overview of the main procedures for the definition of the network on the Matlab script. Particular attention must be paid to the definition of the start and arrival ports of the lines: when characterising the circuit, the matrix must specify, in addition to the start and arrival ground ports, which coincide for both three-phase systems, the start and arrival ports for each three-phase system, named respectively as nodes a and b. This feature is necessary to have the opportunity to insert the presence of busbar in correspondence of the node inside the model. By specifying these connections when defining the circuit, the configuration of the lines can be changed from an open busbar (two separated lines, that

can eventually be connected at the beginning or at the end to achieve a series connection) to a closed busbar (two lines that are parallel connected at each substation to reduce the total impedance of the network). This procedure is useful for real-time management during faults because, by suitably modifying the connections, the fault current can be modified by varying impedance values seen in correspondence of the fault. For the first comparison that will be carried out, the lines have been arranged on a single series of nodes that are the same for both, thus leading to a parallel configuration of the lines; subsequently, to evaluate the different behaviour in the fault regime, the same network will be modelled by halving the number of nodes of a single line and arranging the two lines on a different series of nodes: in this way, the two lines will normally be separated, with the possibility of inserting specific connections with negligible impedance in the substations to connect the conductors of the different circuits.

In order to compare the differences between single element's characteristics and validate the outcomes of the self-developed model in Matlab, the first commercial software adopted is Neplan (version 557), which makes use of the sequence components theory, as stated by the relevant standards. Of course, the considered version is the one based on the electricity tool: this software allows, through a particularly intuitive and easy to handle user interface, the representation of an electricity network composed of lines and numerous elements that can be taken from the several available libraries through their graphic icon. Behind the graphic elements, there are windows in which the main parameters need to be specified and which allow different customizations to reach a model as accurate as possible. Besides, all network elements, once connected to the system, can be quickly disconnected via the appropriate connection box allowing a high elasticity to system variations.

From here, the first differences in the settings for both the calculation method and the modelling of the individual network elements can be noticed. First of all, regarding the type of study to be carried out with Neplan, the selected solution chosen is the Superimposition with Loadflow. Even though Neplan is widely developed for calculations and analysis based on the standards addressed in chapter 2, with several settings available for the definition of all parameters according to different standard versions, this method is closer to the one carried out in Matlab as it is designed for computing the fault regime rather than the sole fault current. Using this method, it is possible to simulate the same procedure on which the procedure developed in Matlab is based, that first carries out the calculation of a load-flow in steady-state conditions to obtain the voltages at the nodes and then apply the failure. In this way, more similar results are obtained compared to the use of IEC 60909, which instead provides higher values.

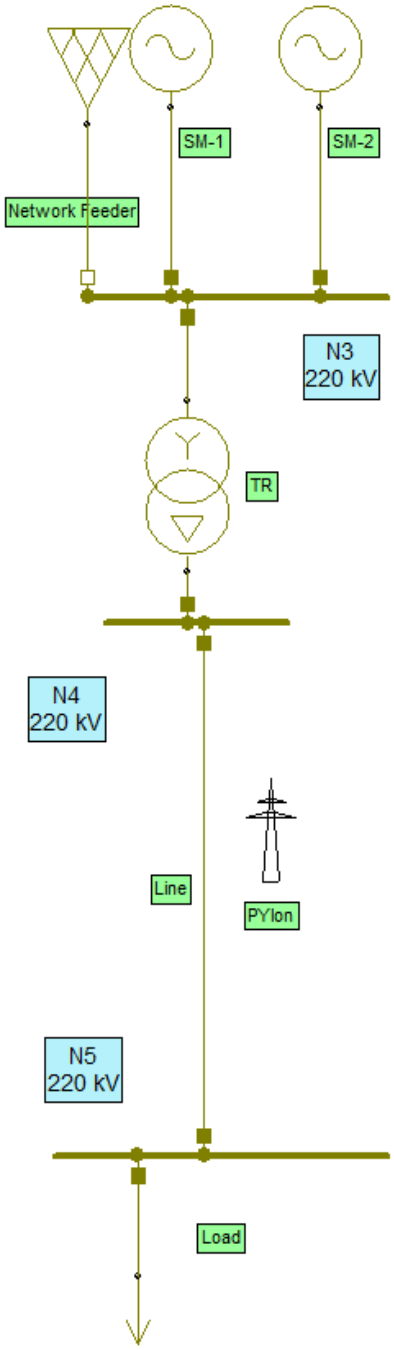

Figure 4-1: Graphic representation of the circuit under examination, taken from the Neplan interface.

As far as the network elements are concerned, it is necessary to make the following considerations:

- Synchronous Machine: The generator in Neplan is modelled according to sequence theory, which is why it requires, in addition to the standard rating values, the value of direct, transient and sub-transitory reactances. This introduces the first big difference between the two systems since in Matlab the generator in the fault regime is directly modelled as a sub-transitory reactance, with the circuit powered by the voltages calculated in the pre-fault regime or the fault regime depending on the situation. Moreover, as explained in the section of the Neplan's

user guide manual [75] dedicated to the model of synchronous machines during faults, Neplan always considers the generator impedance as a full impedance, meaning that even if no resistance values are specified, leaving empty the appropriate box, the program inserts a resistance value which is proportional to the sub-transitory reactance, varying the proportionality coefficient according to voltage level and power. To take this into account, although the results do not vary significantly, it was necessary to modify the impedance and resistance values of the generators initially used in Matlab. As for the values entered for the reactances, these were taken from the table in [76], based on the size and checking what were the range values recommended in the Neplan user manual [75]. Since the program performs a Loadflow analysis before the fault calculation, it is also necessary to specify in the data that the largest size generator is a balance node while the other generator is of PQ type. Let's mention, since it will be needed later, that in Neplan the generator can be replaced by the Network Feeder element, adapting the data so that the two sources are characterized by the same values even though they have different input data. The following relations need to be considered:

$$\boldsymbol{Z_d} = \frac{\boldsymbol{V_{base}^2}}{\boldsymbol{MVA_3}} = \boldsymbol{Z_{sc}} = \frac{\boldsymbol{V_{1n}^2}}{\boldsymbol{S_n}}\, v_{sc} \tag{4.1}$$

to compute the values of short-circuit powers or currents for the Network Feeder characterization.

- Transformer: For the transformer, there are no particular expedients to take into account as the modelling is quite similar between the two software.
- Line: In Matlab, the lines' impedances are built knowing the conductors' characteristics and spatial position, creating matrices for resistance, reactance, capacitance and conductance. The procedure in Neplan requires the definition of lines' impedances for the positive-sequence and for the zero-sequence, according to the already mentioned symmetry assumptions. To obtain these values for the sequence components, the Matlab Power_lineparam tool has been used starting from the detailed characteristics used in the Matlab script. Based on a single window, as shown in Fig. 4-2, the tool computes the sequences values of the line starting from the specification of the types of conductors, the main physical characteristics and the relative position. Such a procedure would have been possible also with the Neplan pylon function, which however does not allow the representation of a double-circuit three-phase line for data calculation so it will be implemented only in the single-phase to ground fault section to evaluate the effects of the presence of towers and ground conductors.

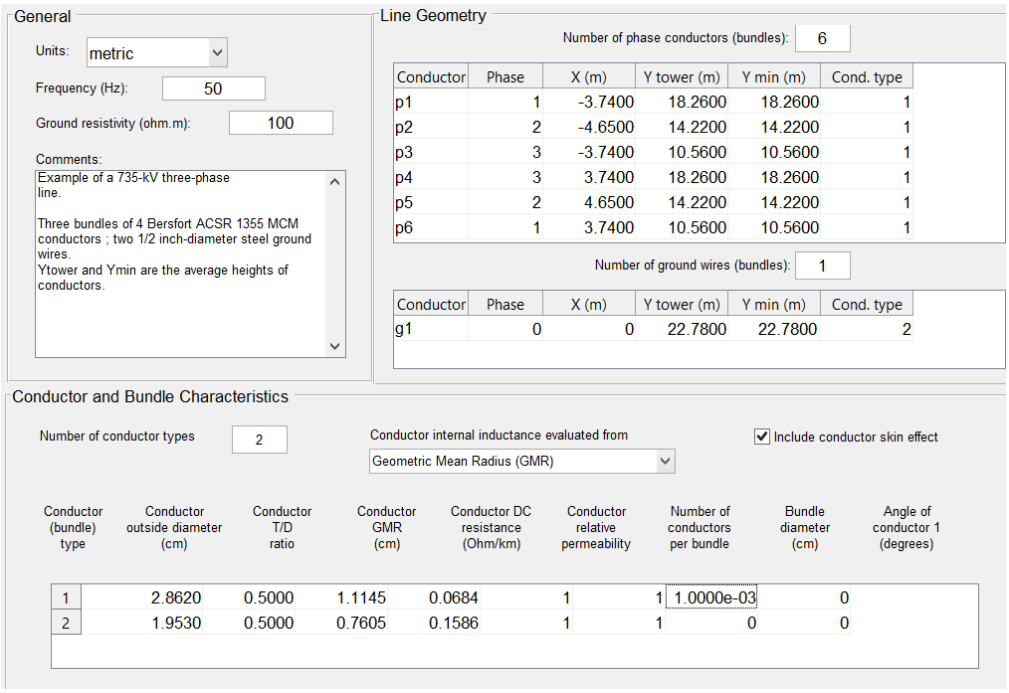

Figure 4-2: Interface of the Matlab's tool Power_lineparam, used for the computation of the line's sequence parameters.

The main difference that is automatically inserted by the program is to consider the conductors as bundled conductors, both for phases and neutral conductors: the inconvenience is that, while it accepts a null value as input for the ground wire bundle diameter, it does not accept it in the phase conductors, forcing the insertion a very small value that still leads to very similar results. Furthermore, the T/D ratio is set with the standard value for a solid conductor (0.500, as suggested in the Matlab link related to this tool) and the GMR is calculated accordingly.

Since the line is modelled according to the sequence components theory, Neplan considers the system as symmetrical, which is often a not valid assumption: for this reason, to have a comparison as much accurate as possible, the system is represented in Matlab as a transposed line, where the transposition is applied at each substation. Beyond this detail, which is far from negligible for this kind of analysis, it must also be noted that on Neplan it is not possible to model the spans along the line efficiently. To do such a thing in the system, it would be necessary to insert a node or a pylon at each tower, which, although being feasible for these simple tests, would complicate unnecessarily the model in bigger networks, therefore making this approach impracticable when dealing with real transmission systems.

In addition to this, the insertion of nodes in correspondence of the towers still would not lead to a better representation of the network because the software does not allow to customize the ground connections of the substations and therefore it would require the use of pylon element, at least to insert ground wire and ground parameters. Apart from this, the software allows the customization of machines and transformers groundings and has a dedicated grid element

which collects information on the grounding of the elements of the represented system. This will have a great influence in the comparison in case of single-phase to ground fault, as will be shown later on, not too much in the fault current values as in its distribution.

Finally, the line is modelled as a single circuit in order to get a closer model to the one assumed in Neplan (single-phase equivalent with sequence components). In this way, it is possible to set a suitable phase geometry so to maintain symmetry. For this reason, the maximum current values of the line have been doubled.

- Load: Also in this case there are no differences compared to the Matlab model which requires the same data, needing the specification of the PQ type for the Loadflow analysis.

The comparison is then made with respect to a second software, which is OpenDSS [77]: a program whose development started in April 1997 at Electrotek Concepts by the minds of Roger Dugan and Tom McDermott, intending to build a tool, initially dedicated only to simulation in distribution systems, that was not based only on conventional analysis methods for distributed generation system, whose limitations were well known, but that would allow the realization of a powerful and flexible instrument, minimizing the difficulties of data conversion between various systems, avoiding limitations for the type of analysis carried out, able to simulate circumstances influenced both by the position of the network and by the temporal development (therefore the possibility to model the temporal behaviour of loads and generation), leaving the user the possibility to design through the interface any network he wants.

In this case, the procedure is much more similar to the developed one because the program implements all types of calculations and element models through the construction of the admittance matrix. The procedure for the definition of lines, loads, generators and transformers is also very similar, leaving the user the freedom to use the desired number of nodes to effectively represent any line without constraints on the number of phase or earth conductors. The main difference between the two systems, however, is that, to initialise a network in OpenDSS, an equivalent external circuit is required. This element, characterised by short circuit powers, fault currents or sequence parameters based on the available data, will act as a balance node for the grid, i.e. an equivalent ideal voltage generator. While designing this element through the definition of MVA short-circuit power for three- and single-phase faults, converting the synchronous machine parameters as previously done also for Neplan, it has to been considered, as explained in the OpenDSS help section (where this element is referred as Vsource), that the results of the division between the squared base kV and MVA_{sc1} is the single-phase impedance Z_s, and that to obtain the zero-sequence value for a better comparison with other software the equation is the following:

$$\boldsymbol{Z}_{(\mathbf{0})} = 3\,\boldsymbol{Z}_{\boldsymbol{s}} - 2\,\boldsymbol{Z}_{(\mathbf{1})} \tag{4.2}$$

As for Neplan, the only way to take into account the effects of towers grounding would be to model a node at the start or the end of every single span, a solution that has a complexity proportional to the size of the system. However, unlike Neplan, the program allows modifying the grounding parameters at each node because, by default, each one has port 0 solidly grounded, therefore the grounding impedance can

be defined, at each node, as the passive element connecting the neutral (in this case the 7th conductor) and port 0. In a very similar way, it is possible to carry out the parallel or series connections of the two circuits in correspondence of the buses. By default, multiple circuits lines are modelled by the software as a set of conductors having a spatial geometry which defines the mutual couplings. However, no reference is provided on the circuits connections, so they are considered as separated lines lying on the same pylons. However, through the insertion of conductors of negligible resistance between the corresponding phases of one circuit and the other, it is possible to represent the parallel, as it will be shown in the first examples. This procedure is better to be achieved through the definition of single-phase conductors between two ports, so to avoid the appearance of mutual couplings with conductors of different phases, as it would happen defining this bonding element (jumper) as a three-phase one. OpenDSS allows to follow an alternative approach to operate the parallel of lines' circuits, which consists of reducing the number of ports from 7 to 4 in the case of the busbar switch being closed, resulting in the electrical parallel of the two circuits. This solution would avoid the definition of the above mentioned jumpers, but increases the data definition process since the number of ports changes for each of the grid buses.

As far as the calculation of fault currents is concerned, the program offers several choices. The standard function is to carry out a completely automatic study of the network fault regime: this solution, obtained by setting "solve mode = faultstudy" and then exporting the relative values, applies different types of fault on the network buses with default fault resistance values. It will produce a single-phase earth fault for each conductor, a two-phase fault for each possible pair of conductors at the same bus, and a fault that includes all the ports present in a bus, all these for each bus where a conductor of any type is defined. As will be shown in the relative image further on, the buses involved with the transmission line connection in our system have 7 ports (2*3 phases + ground wire), while others, involved with the connection of the external circuit, a generator and the transformer (nodes 3 and 4 respectively) have only 3 ports, dedicated to the three phases. For this reason, the last case of failure simulated by the software would represent a three-phase failure condition involving simultaneously both circuits, a condition hardly found in practice and, therefore, not in the scope of this analysis.

The alternative for this calculation is to manually enter the faults within the network since they can be considered as a resistance with an adjustable value: for this reason, the software allows defining a shunt element as "fault", a component implicitly grounded, whose sending and receiving nodes and ports can be specified, together with the number of phases involved and the fault resistance. Once this has been done, the simulation can be carried out normally with the solve command, hence performing the analysis of the fault regime. If the dynamics of the circuit are of interest, it is advisable to solve the circuit in dynamic mode (specifying the number of steps to be carried out and the time of one step), thus effectively obtaining, as in the case of Matlab, first a pre-fault condition, as a result of a Loadflow study and then the calculation of the fault currents. In this way, it is possible to save and display the variation of the data in the simulation interval by placing a monitor tool in the appropriate points. By establishing the comparison in this way it is also possible, through the definition of various samples, to show the

current variation in one point of the circuit by varying the position of the fault along a line and varying the resistance value until it is negligible (high resistance) and the grid returns to a steady state.

First case: Three-phase fault with parallel-connected circuits

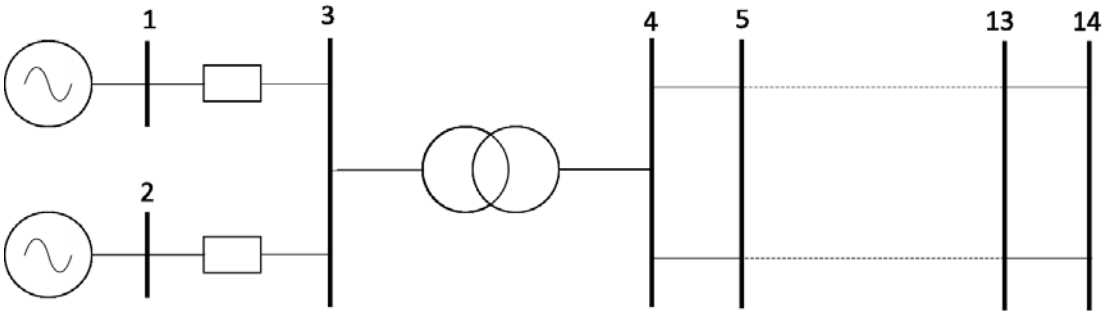

Figure 4-3: Schematic representation of the analysed network, represented in the configuration with parallel connections between the two circuits.

For this first simulation, the faults were carried out inside the only line present in the network and schematically represented in Fig. 4-3, starting from the node at the secondary side of the transformer (node 4) up to the last node of the line (node 14) and simulating a fault every 12 km up to the final distance of 120 km. This is done in the Matlab script by shifting the position of the two nodes for the faults (one for each circuit) is automatically shifted at each cycle. Then in the appropriate section of the fault function is specified in which circuit the fault is simulated, allowing, of course, the selection of both circuits: in all the tests that will be presented, the faults were simulated on the first circuit.

In Neplan it is possible to simulate several faults in a single calculation routine by selecting the nodes where the fault occurs and the faulty lines; there is also the possibility of simulating special faults, more customizable than standard ones. The software will not carry out the calculations as if the faults were simultaneous but will treat them individually; each calculation routine, therefore, requires to manually change the distance of the fault along the line. There is, therefore, the possibility of simulating the fault in any position of the selected line, setting the distance from the starting node as a percentage of the total length: from this, the choice of the number of nodes, to avoid approximation errors by simulating faults respectively at distances of 10, 20, 30 % and so on. The only exceptions are in the positions close to the initial and final node of the line since for distances of less than 2% or more than 98% the software does not allow the calculation on the line but refers directly to the fault on the node.

In OpenDSS the fault can be applied to any bus and between any couple of ports by specifying the involved phases. Since this case is symmetrical, there is no difference in applying the fault condition on one circuit's phases rather than the other, so the values shown below refer to the first one (which corresponds in each line's buses to ports.1.2.3). As already mentioned, there would also be the possibility, through the use of a monitor on the fault, to define several samples and save the values for each simulation, shifting in a single simulation the fault location as it's done in Matlab: unfortunately, this would require to model the line with only two buses as done in Neplan while, to perform the phases'

transposition while keeping similarity with the circuit built by the Matlab program, in case of single-phase faults, 10 buses were maintained and at each simulation the fault element was moved from bus to bus keeping the same nodes.

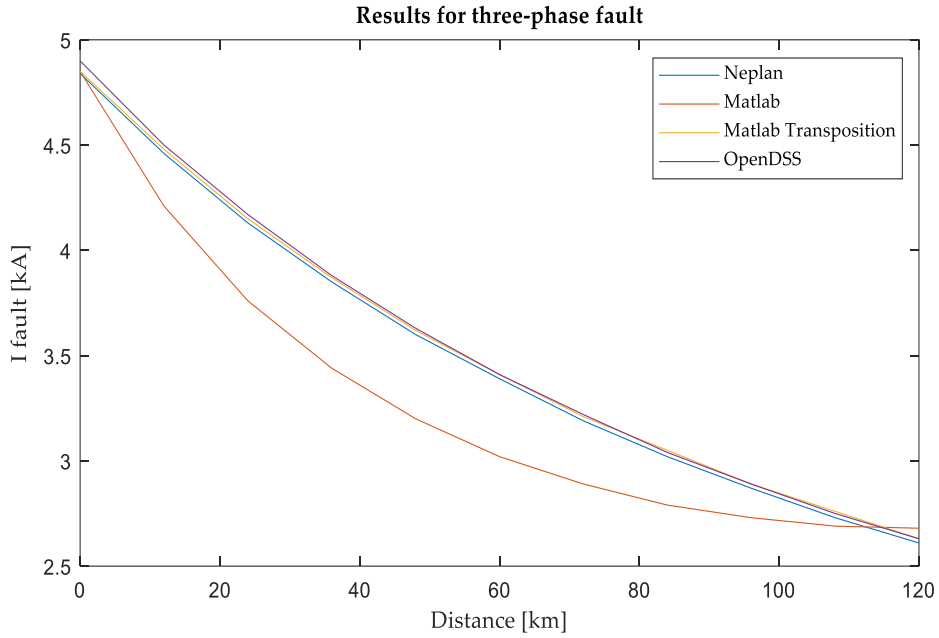

Figure 4-4: Results for three-phase fault simulations; the reason of the values that are most different from the others is the absence of phase transposition that, when has been applied, has led to much more similar results.

In the graph reported in Fig. 4-4, it can be noticed that the values obtained for the three-phase fault along the line are practically the same for the three software. The fourth set of data, the orange one, which differs more from the others in terms of values and "slope", shows the results obtained by Matlab simulating the same circuit but without the transposition on phases' conductors; in fact, the values vary considerably as the line length increases, as a result of its asymmetry. It can be seen how, by transposing the phases, the results get closer to those obtainable with Neplan and OpenDSS, in which the system is assumed symmetrical, using the sequence components to represent lines' impedances. Of course, the more often the phases are transposed in correspondence of the substations, the closer the result will be. A further test, which results are presented in Table 4-1, was carried out by performing the transposition of phases every 40 km, showing a clear difference compared to the case without transposition.

In the same table, the values obtained through the OpenDSS automatic fault study mode are shown as well: unfortunately, as already explained, this mode is set to carry out a fault including all the conductive phases and not directly a three-phase fault, meaning that the values obtained by the program refer to a simultaneous fault on both circuits, leading to current values which, of course, are about half compared to all the other values obtained except for the case of buses 4 which has the peculiarity already described above. For the only purpose of this comparison, the values obtained have therefore been multiplied by two.

	Matlab			Neplan	OpenDSS	
Location	Fault currents [kA]					
[km]	without transposition	40 km transposition	12 km transposition	Sovrapposition +Loadflow	mode = Fault Study	Fault elements
0	4,85	4,85	4,85	4,84	4,91	4,90
12	4,21	4,25	4,48	4,46	4,56	4,50
24	3,76	3,93	4,15	4,13	4,23	4,17
36	3,44	3,81	3,87	3,85	3,92	3,88
48	3,20	3,51	3,62	3,60	3,66	3,63
60	3,02	3,26	3,41	3,39	3,45	3,41
72	2,89	3,13	3,21	3,19	3,26	3,22
84	2,79	3,00	3,05	3,02	3,09	3,04
96	2,73	2,78	2,89	2,87	2,94	2,89
108	2,69	2,66	2,76	2,73	2,80	2,75
120	2,68	2,64	2,63	2,61	2,67	2,63

Table 4-1: Table containing the results for the three-phase faults simulated in the different software with different conditions.

These same values obtained through the fault study function can also be achieved by manually entering two fault elements, one per circuit, in the same bus in each simulation and adding the values of the fault currents obtained. This same numerical result can also be obtained in the case of lines not connected in parallel but with simultaneous three-phase faults on the same bus for both lines: since the fault element is modelled as a resistance with a selectable value, its "insertion" between the phases of each circuit and the common ground leads to a parallel configuration which gives the same results as those achieved by inserting the jumpers directly into the network definition.

Second case: Three-phase fault without parallel connections

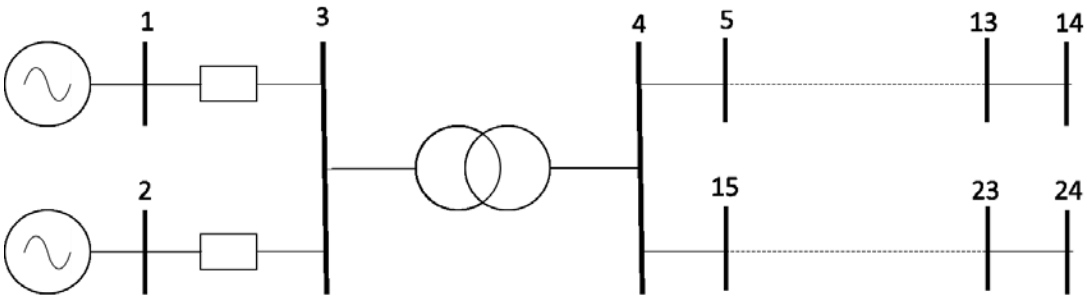

Figure 4-5: Schematic representation of the analysed network, represented in the configuration without the parallel connections between the two circuits.

As counter-evidence, the same fault test (this time on a single circuit), was carried out on the same network but with a series configuration as schematically represented in Fig. 4-5, therefore expecting smaller values of fault currents. In fact, as the fault position moves away from the generation and the line impedance plays an increasingly important role, they become closer to half the values obtained in the previous case, as shown in Fig. 4-6. To obtain this configuration, these passages have been needed

in the different software: in Matlab, different node numbers have been defined for the passage of the single three-phase line (as if it there were two separated lines lying on the same pylons and with the common ground but no phase-connections); in OpenDSS, the jumpers have been removed; in Neplan, the values entered to define line's impedance and admittance have been simply adapted respectively multiplying and dividing them by two and rearranging the current limits for the conductors.

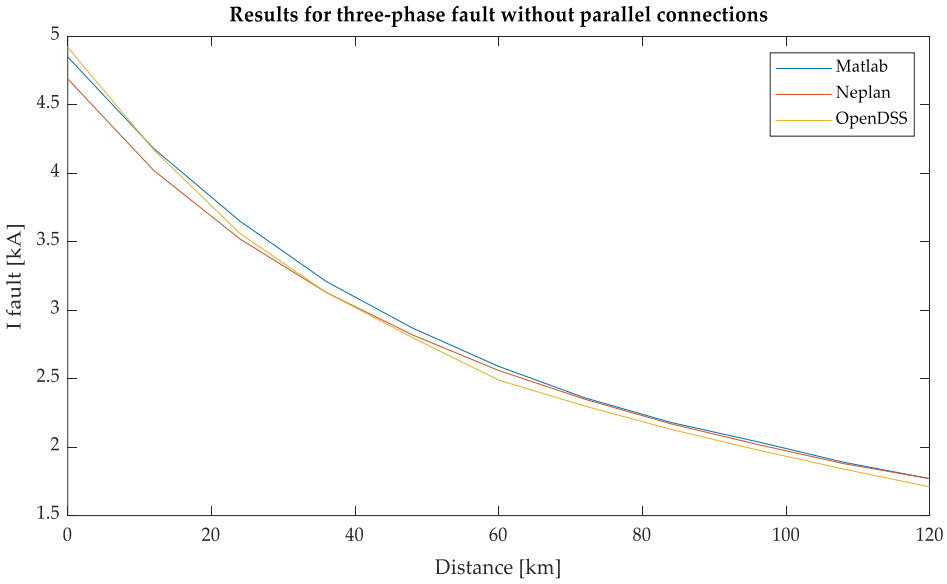

Figure 4-6: Results for three-phase fault simulations without parallel connections between the two circuits, a condition that leads to higher values of the line's impedances and lower values of fault currents.

Third case: Single-phase to ground fault with varying busbar switch status at both ends of the line

To carry out this comparison, with the idea of investigating, later on, more in detail the distribution of the single-phase to ground or single-phase to neutral fault current, the line has been shortened and brought to a total length of 12 km, and the load has been removed from the last node. In order to perform a simulation including busbar switches (putting in parallel the two circuits) at either end of the line, and remembering that the nodes along the line represent pylons on which all the conductors lie, different ports are assigned to each of the conductors, keeping them separated (although being part of the same system through mutual impedances). The busbar switch at the end of the line, which could be realised simply by modifying the port number for the phases at the sending and receiving nodes of the circuits, was instead realised by keeping different ports for all the conductors, as if there were two parallel three-phase circuits, connected successively by a 1 m long line, to operate the busbar switch status change by just including or excluding this jumper (in the Matlab code, this is done by simply commenting the relative command line). Moreover, in this test, the phases were not transposed, but it was chosen to reduce the line length, hence reducing the risk of results misinterpretation due to the model.

The same test was performed twice, once defining the line by using the cell-modelling approach (implicitly accounting for the towers' grounding conditions in the admittance matrix) assuming a grounded tower every 1 km, which is the where the fault is simulated, and then by defining a set of

additional nodes representing the tower groundings at the same distance, to demonstrate that there are no differences in the results, verifying the validity of the cell-modelling approach, bringing the already mentioned advantages in terms of system complexity reduction. The program is written in such a way as to insert the tower resistance in the starting section of the pi-model in the line's admittance matrix, and only if the number of spans per section is greater than 1: in this way, the values of the earth impedances of the substations, which are defined in another sub-matrix, are never overwritten.

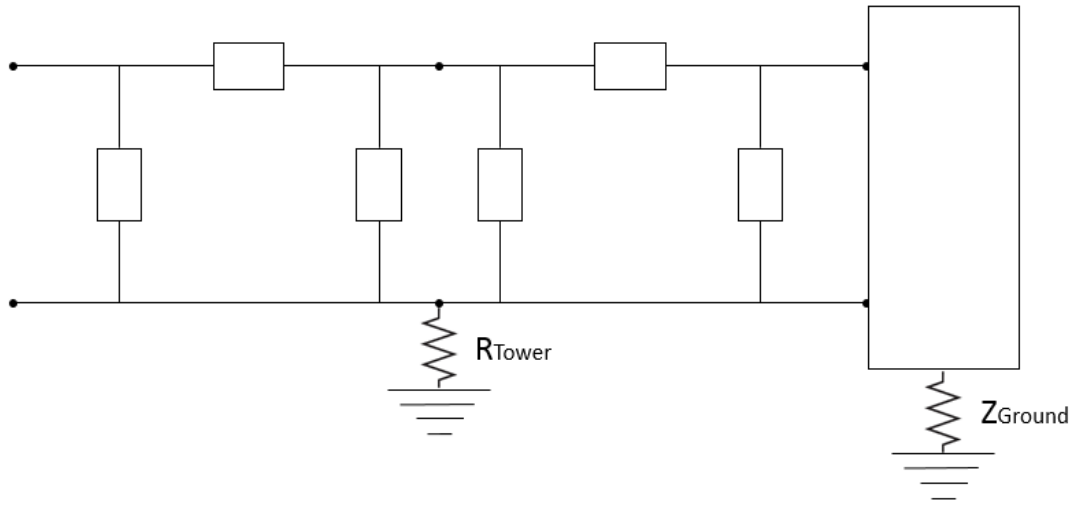

Figure 4-7: Schematic representation of the grounding systems realized by the Matlab script for towers and substations.

In Neplan, on the other hand, the representation of the network is significantly different: in order to make the results comparable to those deriving from the multi-conductor study for single-phase failure, instead of directly specifying the parameters of the double circuit line inside the specific settings window, it has been used the possibility to calculate, through the insertion of the pylon element on the working space, the parameters of the line, by inserting some specific properties of the conductor wires and their position in space, exactly like in the procedure performed through Matlab's tool Power_lineparam. With the same reasoning applied to the other tool, the settings of the bundled conductors and the variation in the height of the conductors along the line according to the actual tensile force, which are not simulated in the other software, are neglected: however, unlike the Matlab tool, in this case, it is possible to specify only the position of three phases conductors plus one or two ground conductors, without being able to calculate the parameters of a double circuit. To obtain something similar it is necessary to set the number of lines equal to two in the line data window so that the program automatically modifies the impedance and admittance values, but still, this does not allow the same representation as in the multi-conductor approach. As it will be seen from the results, it is necessary to take into account that by calculating the mutual reactances in this way, mutual couplings among the conductors in the two circuits of the line are not computed, with no influence due to the mutual phases' position. For this reason, the reactance values will generally be higher when not considering for the actual spatial location and the consequent higher symmetry obtained by suitably locating the phases on the towers. Due to this aspect, although the line length is relatively short (12 km), the fault current

values will decrease faster in the Neplan calculation, rather than in the other software. It should be also considered that, although with this tool there are now pylons every km with a ground conductor and parameters for the modelling of the earth system, it is still not possible to define an earth impedance between neutral and ground, an element that is present in the other two software and that will not allow the analysis of the ground current distribution.

Also, as it is not possible to specify in correspondence of the busbar whether the busbar switch is open or closed, to realize the connection at the beginning and the end of the lines, so, with the open switches, the line length has been doubled to take into account that in reality, the current in the faulted phase flows through a higher impedance path. A similar condition could have been achieved also with the definition of two different single circuit lines with a connecting line of negligible impedance at the final nodes.

Another element that needs to be accurately defined for this test is the network feeder, as for the single-phase faults the zero-sequence is involved together with the positive- and negative- ones. To make a comparison with the Matlab generator model, the consideration carried out is the one schematically shown in Fig. 4-8: at the zero-sequence, when three voltages with the same phase are imposed, three equal currents circulate on each phase and sum up at the neutral point which is then connected to ground through the Z_{ground} impedance.

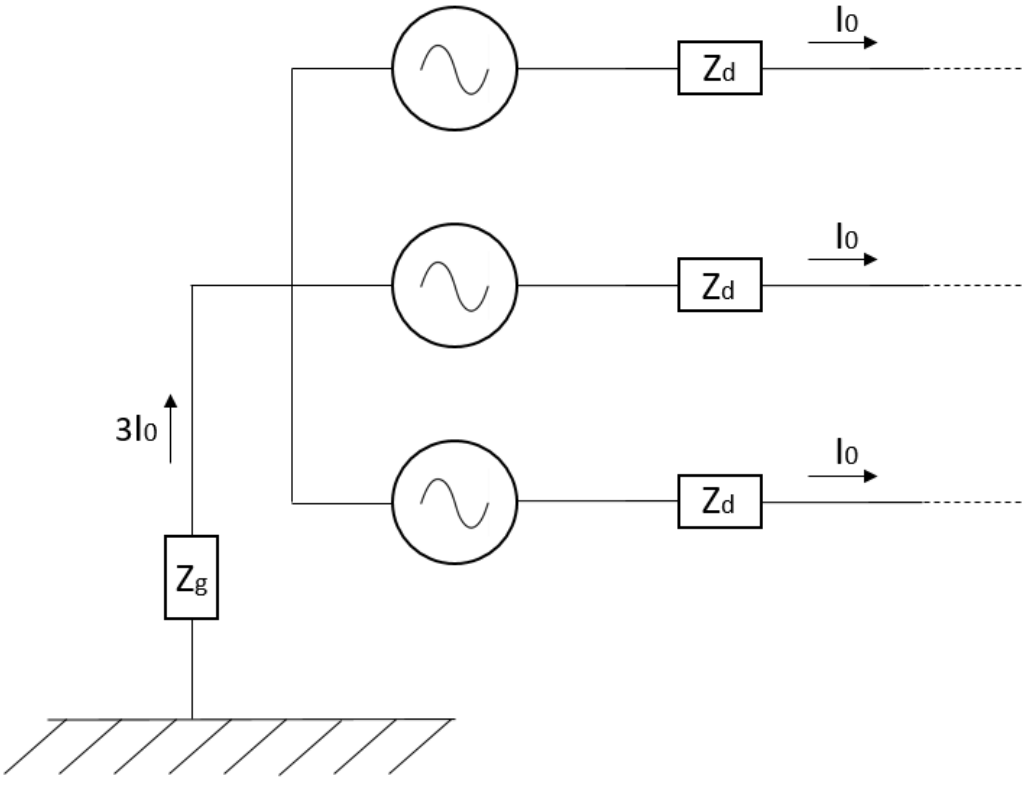

Figure 4-8: Zero-sequence representation of the generator in the Matlab script.

This leads to the following equation valid for the zero-sequence behaviour of the network feeder:

$$\boldsymbol{Z}_{(\mathbf{0})} = \boldsymbol{Z}_{\boldsymbol{d}} + 3\boldsymbol{Z}_{\boldsymbol{g}} \tag{4.3}$$

from which it is possible to compute the required impedance value that, inserted in the setting window, provides the values of short circuit currents and MVA powers for the feeder model. Inside the network feeder customization window, it has also been removed the tick from the setting “calculation of Ik" according to IEC”, just as the calculation of the maximum Ik" has also been removed in the short circuit calculation parameters window, to prevent the automatic change of parameters by Neplan, modifying the study assumptions with respect to the models in the other software.

In OpenDSS, as already mentioned, the jumpers which previously were used to connect phases conductors at the same bus have been removed, and the connection between the two circuits has been represented exactly as in the same bus of the line, meaning a 4 ports bus where both circuits convey as shown in Fig 4-9, where is also given an idea of the general representation of the elements.

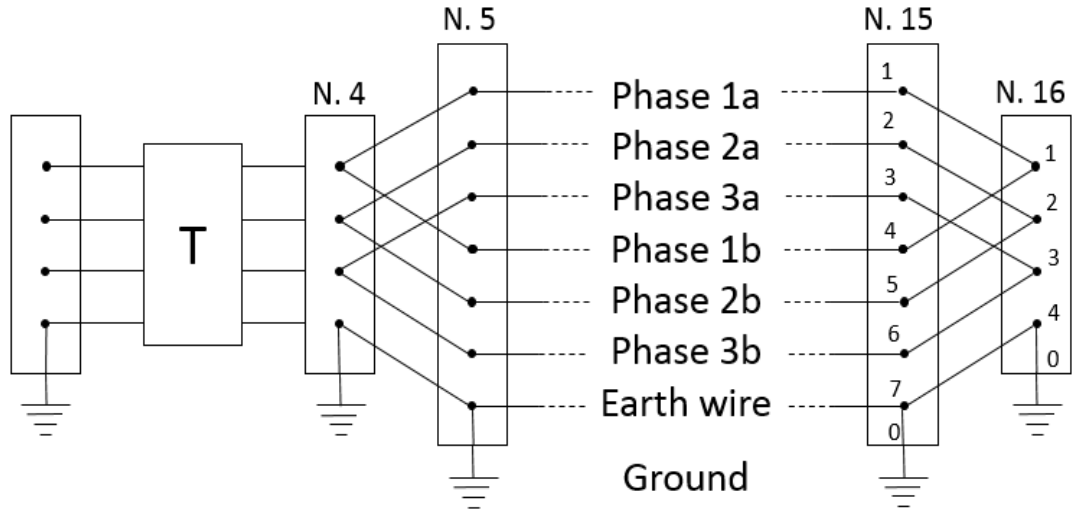

Figure 4-9: Schematic representation of the considered network with the same configuration used by OpenDSS, to highlight conductors disposition and references.

In the above image, all the conductors, and also the ground, are represented (ground current values are calculated as the sum of all the other vectors changed of the sign and are referred by the program as I residual, a parameter which is exported only if the correct function is applied): as shown in the line buses, a conductor has been inserted between the ground and neutral in such a way that the ground impedance value can be defined and the value of the current passing through it can be seen in the analysis of the fault current distribution. Here, to simulate the single-phase to ground fault, for each simulation the fault element has been inserted in the first conductor of each node, without specifying the second node of the element, which by default is port 0 of the same bus.

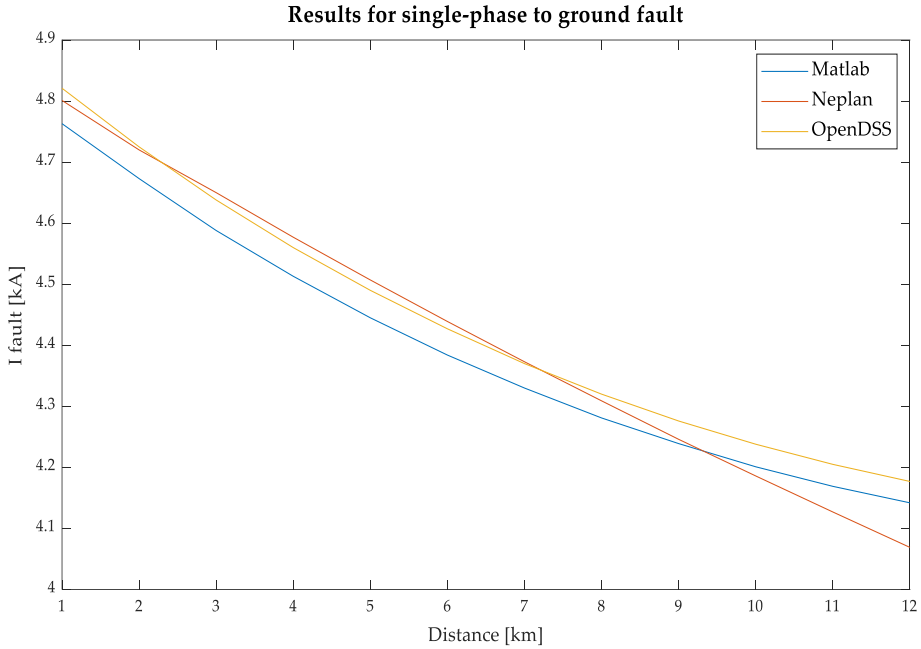

Figure 4-10: Results for SLG fault simulation; the linear trend of Neplan's results is probably related to the short distances.

It can be noted from Fig. 4-10 that, moving the fault point along the 12 km line length, the trend of the results obtained using Neplan, in which it was not possible to define a tower footing impedance, is different and has a more linear behaviour compared to the those obtained through a calculation based on a multi-conductor representation: this is mainly because in the other two software, as the fault location moves away from the beginning of the line, the influence of grounding impedances of the nodes and the resistances of the towers increases, making the linearity assumptions made in Neplan less and less valid. This linearity effect is not due to the use of the parameters calculated using the pylon element in Neplan, because the same simulation, carried out with the line parameters defined as in the other cases (calculated through Power_lineparam), therefore without specifying in Neplan the presence of the neutral that is already considered in the sequences values, has led to slightly higher values (for the reasons already explained above), but with the same slope.

4.2 Detailed assessment of the ground-fault current distribution

Fourth case: Ground current distribution in single-phase to ground fault

In making this comparison, the values reported are those obtained through Matlab and OpenDSS as Neplan does not allow to know the exact current distribution over the conductors and the earth path when the fault condition is applied. In the two software it was not necessary to make any changes to the previous case because OpenDSS calculates the current in every single port of the circuit's buses, thus allowing to know the module and phase of the current in phase conductors, in the earth wire and the ground (obtained monitoring the earth-connection elements as mentioned above). Furthermore, the results are saved from the program for each circuit elements, and there is the possibility through the

selection of the desired element to see current (and voltage and power as well) values at the entrance and exit port of the element, obviously paying particular attention to vectors' phases in carrying out the comparison and considering their direction. The same thing is valid for Matlab, where the current values can be easily computed for every single span or line section, according to how the network has been defined, calculating the relative admittance matrix and applying properly the faults condition. The current in the ground is also calculated as the vector sum, with changed sign, of the other conductors' currents.

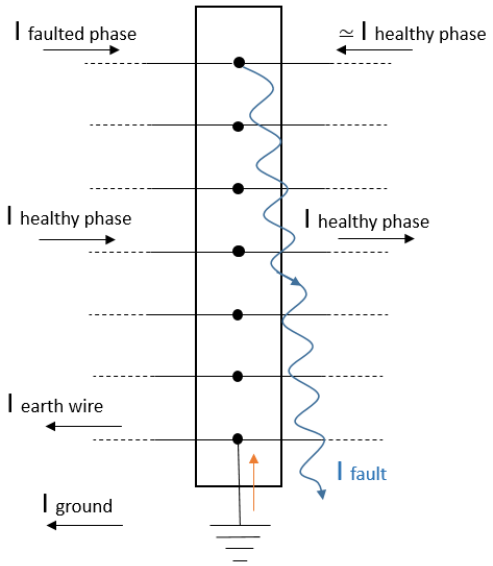

Figure 4-11: Schematic representation of a faulted bus in OpenDSS to show the several paths of the current and to provide a visual reference for the name that will be used in the following tables.

In Fig. 4-11 is represented the fault simulation at the node, specifying the names by which the various currents will be referred to. Below are reported the values of the currents in all conductors and the ground for all circuit nodes in the case of a fault at a distance of 1 (Table 4-2) and 12 (Table 4-3) km respectively from the beginning of the line, only to enable a more accurate and complete comparison by showing also values that are not useful for fault analysis purposes. The current magnitudes are expressed here in kA.

I_fault	4,7633											
I_faulted_phase	4,5715	0,1917	0,1916	0,1916	0,1915	0,1914	0,1913	0,1913	0,1912	0,1911	0,1910	0,1910
	0,0047	0,0044	0,0040	0,0037	0,0033	0,0030	0,0026	0,0023	0,0019	0,0016	0,0014	0,0011
	0,0096	0,0094	0,0092	0,0091	0,0089	0,0088	0,0087	0,0086	0,0085	0,0085	0,0084	0,0084
I_healthy_phase	0,1902	0,1902	0,1903	0,1904	0,1905	0,1905	0,1906	0,1907	0,1908	0,1908	0,1909	0,1910
	0,0036	0,0033	0,0029	0,0026	0,0022	0,0019	0,0016	0,0013	0,0011	0,0010	0,0010	0,0011
	0,0091	0,0089	0,0088	0,0087	0,0086	0,0085	0,0085	0,0084	0,0084	0,0084	0,0084	0,0084
I_earth-wire	1,7997	0,2083	0,0318	0,0137	0,0110	0,0109	0,0111	0,0112	0,0113	0,0115	0,0116	0,0111
I_ground	3,1290	0,2056	0,0331	0,0162	0,0132	0,0128	0,0126	0,0124	0,0122	0,0121	0,0120	0,0111

I_fault	4,8207											
I_faulted_phase	4,6266	0,1941	0,1940	0,1940	0,1939	0,1938	0,1937	0,1937	0,1936	0,1935	0,1934	0,1934
	0,0052	0,0048	0,0045	0,0041	0,0038	0,0034	0,0031	0,0027	0,0024	0,0020	0,0017	0,0014
	0,0104	0,0102	0,0100	0,0098	0,0096	0,0094	0,0092	0,0091	0,0089	0,0088	0,0087	0,0086
I_healthy_phase	0,1924	0,1924	0,1925	0,1926	0,1927	0,1928	0,1928	0,1929	0,1930	0,1931	0,1931	0,1932
	0,0038	0,0034	0,0031	0,0027	0,0024	0,0021	0,0017	0,0014	0,0012	0,0010	0,0009	0,0010
	0,0087	0,0086	0,0085	0,0084	0,0084	0,0083	0,0083	0,0083	0,0083	0,0083	0,0084	0,0084
I_earth-wire	1,8211	0,2107	0,0323	0,0139	0,0112	0,0111	0,0112	0,0113	0,0114	0,0116	0,0118	0,0112
I_ground	3,1672	0,2075	0,0332	0,0165	0,0135	0,0131	0,0129	0,0128	0,0126	0,0124	0,0123	0,0115

Table 4-2: Tables reporting currents magnitude for the several conductors and the ground in case of fault at the beginning of the line, in which are reported also negligible values (such as the current in the phases different from the faulted one) just to show the output of Matlab's script calculations. The first table is for Matlab results, the second one is for OpenDSS values, which have been exported from the program in excel and then re-elaborated.

I_fault	4,1424											
I_faulted_phase	2,1551	2,1552	2,1554	2,1555	2,1556	2,1557	2,1558	2,1559	2,1560	2,1561	2,1561	2,1562
	0,0146	0,0143	0,0141	0,0138	0,0136	0,0133	0,0131	0,0129	0,0126	0,0124	0,0122	0,0120
	0,0913	0,0913	0,0913	0,0913	0,0913	0,0913	0,0913	0,0913	0,0913	0,0913	0,0913	0,0913
I_healthy_phase	1,9854	1,9855	1,9856	1,9857	1,9858	1,9859	1,9860	1,9861	1,9862	1,9863	1,9864	1,9865
	0,0103	0,0104	0,0105	0,0106	0,0108	0,0109	0,0111	0,0112	0,0114	0,0116	0,0118	0,0120
	0,0915	0,0915	0,0915	0,0915	0,0915	0,0914	0,0914	0,0914	0,0914	0,0914	0,0913	0,0913
I_earth-wire	1,5440	1,6383	1,6283	1,6257	1,6254	1,6253	1,6252	1,6250	1,6250	1,6274	1,6372	1,5427
I_ground	2,6616	2,5281	2,5339	2,5362	2,5362	2,5360	2,5358	2,5356	2,5352	2,5325	2,5262	2,6592

I_fault	4,1767											
I_faulted_phase	2,1728	2,1729	2,1730	2,1732	2,1733	2,1734	2,1735	2,1736	2,1737	2,1738	2,1739	2,1740
	0,0153	0,0150	0,0147	0,0144	0,0142	0,0139	0,0136	0,0133	0,0131	0,0128	0,0125	0,0123
	0,0927	0,0926	0,0925	0,0925	0,0924	0,0924	0,0923	0,0923	0,0923	0,0922	0,0922	0,0921
I_healthy_phase	2,0018	2,0019	2,0020	2,0021	2,0023	2,0024	2,0025	2,0026	2,0027	2,0028	2,0028	2,0029
	0,0098	0,0099	0,0100	0,0102	0,0104	0,0105	0,0107	0,0109	0,0111	0,0114	0,0116	0,0118
	0,0918	0,0918	0,0918	0,0918	0,0919	0,0919	0,0919	0,0920	0,0920	0,0920	0,0920	0,0921
I_earth-wire	1,5565	1,6515	1,6414	1,6387	1,6385	1,6384	1,6383	1,6381	1,6382	1,6406	1,6504	1,5553
I_ground	2,6842	2,5497	2,5556	2,5579	2,5579	2,5577	2,5575	2,5573	2,5569	2,5542	2,5480	2,6820

Table 4-3: Tables with the same characteristics of the previous ones but reporting the results of the fault simulated at the end of the line.

As it can be noticed from the last table, and could be seen even better in case of a fault simulated at the middle of the line, the most relevant current exchanges between the neutral conductor and the ground are in correspondence of a couple of grounding systems from the fault location, highlighting that, when the effect of the earthing systems is considered, typically only a couple of towers before and after need to be taken into account. In Fig. 4-12 are reported the graphs computed by Matlab each time a fault is simulated to give a graphical representation of the current distribution variation along the line; Figg. 4-13 and 4-14

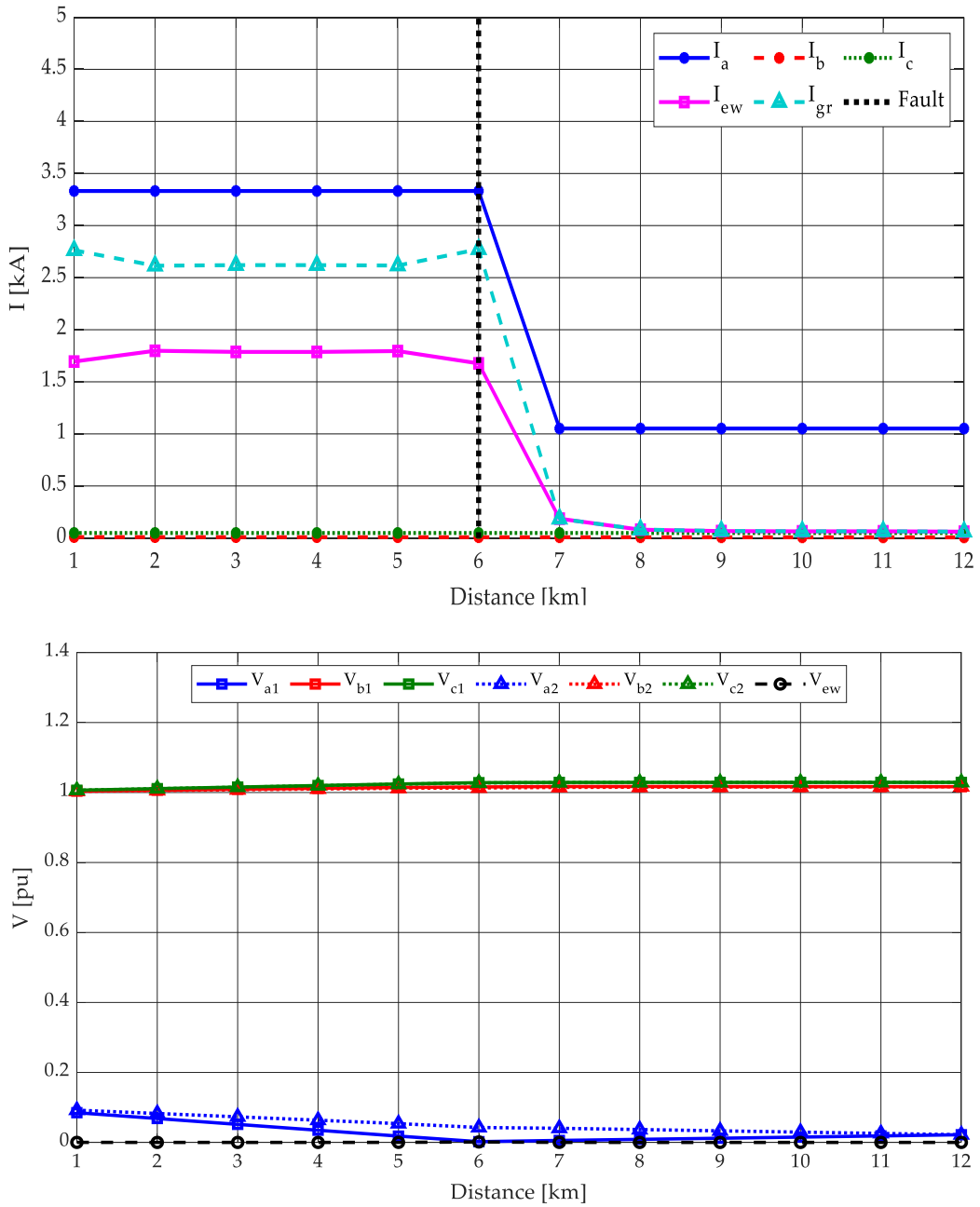

Figure 4-12: Graphical outputs of the Matlab's script for ground-fault current distribution in case of SLG fault simulated at the middle of the line, as reported in the first graph; as can be understood from the legends, the first graph represents currents magnitude for all the main involved conductors and paths, to underline the differences in the sections “before” and “after” the fault, and the second one represents the p.u. voltages.

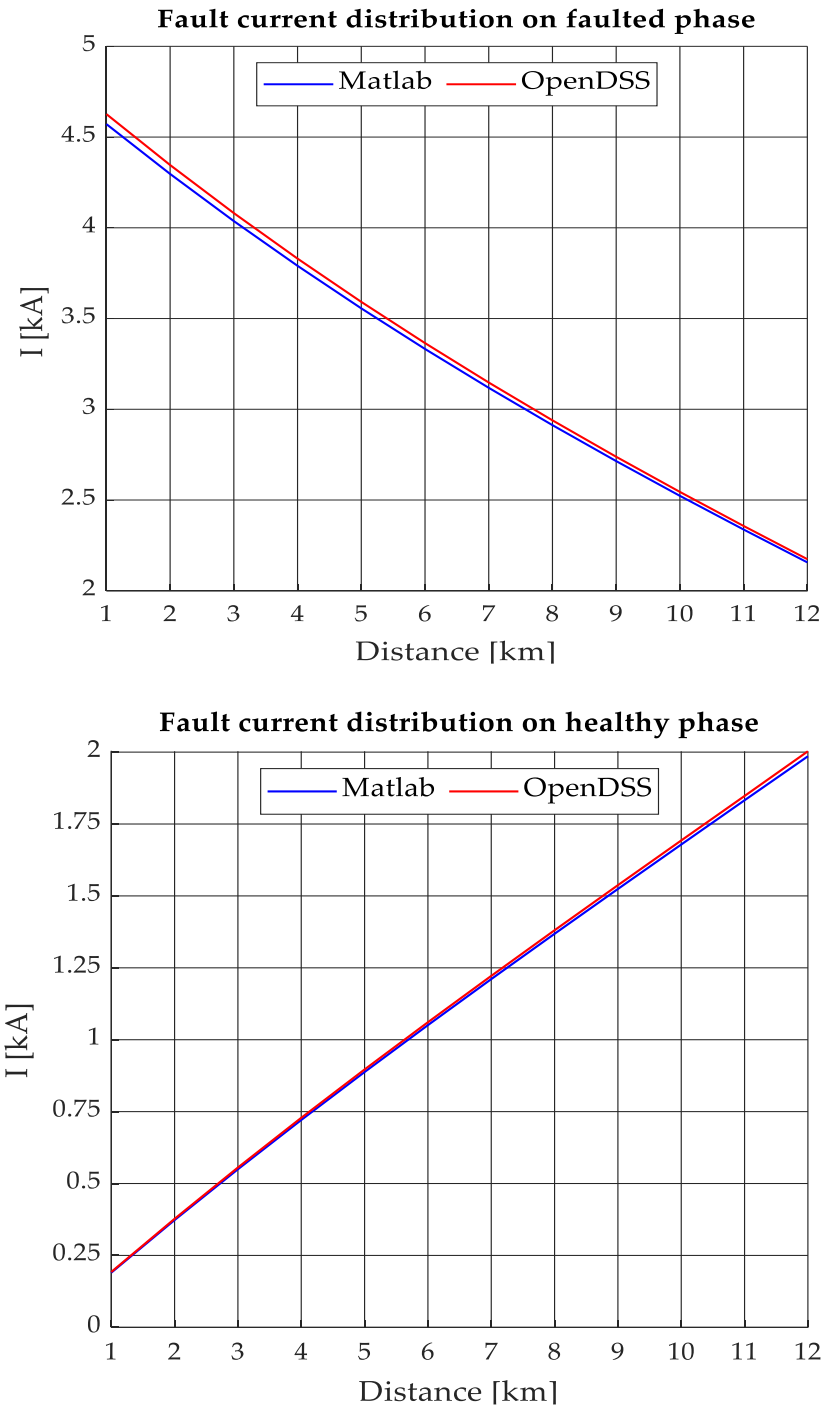

Figure 4-13: These graphics represent the comparison between the values of fault current on the faulted and healthy conductor of the same phase for the two circuits; as can be seen the results are quite similar.

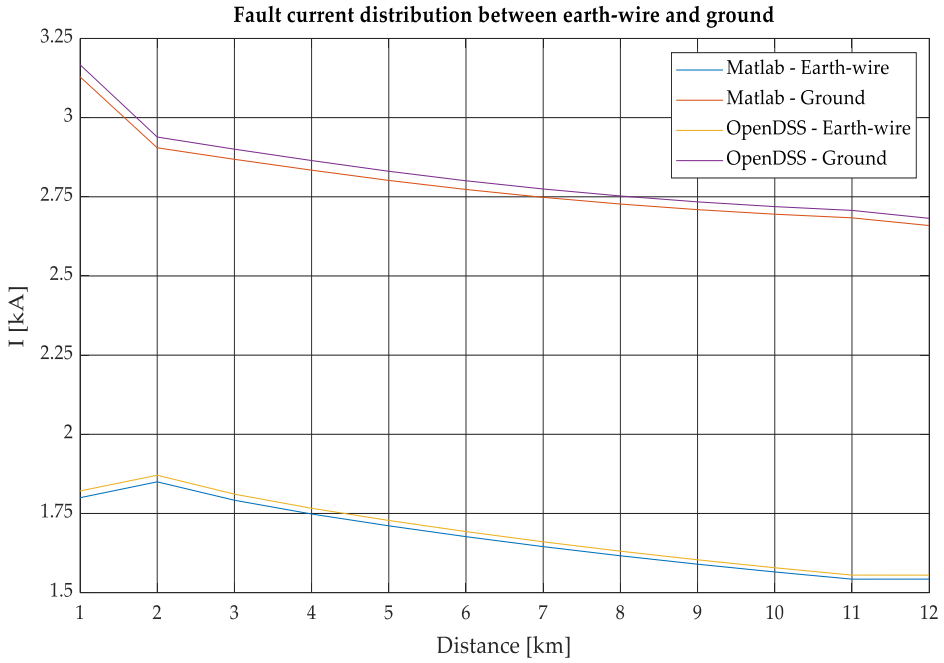

Figure 4-14: This graphic represents the comparison between the values of ground-fault current distribution in the EW and the ground paths for Matlab's and OpenDSS' values; these have been reported in the same graph to underline how the two variables are almost complementary as the line is short; the initial behaviour it's due do the different values of resistance between substation and towers' footing that leads to higher variations of the current which successively re-enters through the grounding of the generation nodes.

Fifth case: Ground current distribution in single-phase to neutral fault

With the same parameters and methods as in the previous case, a comparison was made on the values of the fault current and its distribution between neutral and ground paths also in the case of single-phase to neutral fault. This involves a variation in the arrangement of the values in the fault matrix and, consequently, concerning the previous case, the fault current values and the distribution in healthy phases remains practically unchanged, while the distribution of the current between earth wire and ground paths is modified with a greater share flowing into the neutral conductor. To achieve this new fault situation in OpenDSS, in the code line in which the fault element is defined, the receiving bus must be specified as it is the port, in the respective bus, dedicated to the earth wire (port 7 or 4 depending on how many phase conductors pass through the bus).

I_fault	4,7656											
I_faulted_phase	4,5739	0,1916	0,1916	0,1915	0,1914	0,1913	0,1913	0,1912	0,1911	0,1911	0,1910	0,1909
	0,0047	0,0044	0,0040	0,0037	0,0033	0,0030	0,0026	0,0023	0,0019	0,0016	0,0014	0,0011
	0,0099	0,0097	0,0095	0,0094	0,0092	0,0091	0,0090	0,0089	0,0088	0,0088	0,0087	0,0087
I_healthy_phase	0,1901	0,1902	0,1902	0,1903	0,1904	0,1905	0,1905	0,1906	0,1907	0,1908	0,1908	0,1909
	0,0036	0,0033	0,0029	0,0026	0,0022	0,0019	0,0016	0,0013	0,0011	0,0010	0,0010	0,0011
	0,0092	0,0091	0,0090	0,0089	0,0088	0,0087	0,0087	0,0087	0,0086	0,0086	0,0086	0,0087
I_earth-wire	2,0072	0,3275	0,0308	0,0068	0,0108	0,0110	0,0111	0,0112	0,0113	0,0114	0,0116	0,0111
I_ground	2,7734	0,3294	0,0300	0,0090	0,0129	0,0129	0,0126	0,0124	0,0122	0,0121	0,0119	0,0111

I_fault	4,8224											
I_faulted_phase	4,6284	0,1940	0,1939	0,1939	0,1938	0,1937	0,1936	0,1936	0,1935	0,1934	0,1933	0,1933
	0,0052	0,0048	0,0045	0,0041	0,0038	0,0034	0,0031	0,0027	0,0024	0,0020	0,0017	0,0014
	0,0107	0,0105	0,0103	0,0101	0,0099	0,0097	0,0095	0,0094	0,0092	0,0091	0,0090	0,0089
I_healthy_phase	0,1923	0,1924	0,1924	0,1925	0,1926	0,1927	0,1927	0,1928	0,1929	0,1930	0,1930	0,1931
	0,0038	0,0034	0,0031	0,0027	0,0024	0,0021	0,0017	0,0014	0,0012	0,0010	0,0009	0,0010
	0,0088	0,0087	0,0087	0,0086	0,0086	0,0085	0,0085	0,0085	0,0085	0,0086	0,0086	0,0087
I_earth-wire	2,0305	0,3309	0,0308	0,0070	0,0109	0,0111	0,0112	0,0113	0,0114	0,0116	0,0117	0,0112
I_ground	2,8073	0,3335	0,0306	0,0092	0,0132	0,0132	0,0129	0,0127	0,0126	0,0124	0,0123	0,0114

Table 4-4:Tables reporting currents magnitude for the several conductors and the ground in case of fault at the beginning of the line; the first table is for Matlab results, the second one is for OpenDSS values.

I_fault	4,1431											
I_faulted_phase	2,1567	2,1568	2,1570	2,1571	2,1572	2,1573	2,1574	2,1575	2,1576	2,1577	2,1577	2,1578
	0,0146	0,0143	0,0141	0,0138	0,0136	0,0133	0,0131	0,0129	0,0126	0,0124	0,0122	0,0120
	0,0918	0,0918	0,0918	0,0919	0,0919	0,0919	0,0919	0,0919	0,0919	0,0919	0,0920	0,0920
I_healthy_phase	1,9845	1,9846	1,9847	1,9848	1,9849	1,9850	1,9851	1,9852	1,9853	1,9854	1,9855	1,9855
	0,0103	0,0104	0,0105	0,0106	0,0108	0,0109	0,0111	0,0112	0,0114	0,0116	0,0118	0,0120
	0,0923	0,0923	0,0922	0,0922	0,0922	0,0921	0,0921	0,0921	0,0921	0,0920	0,0920	0,0920
I_earth-wire	1,5445	1,6388	1,6288	1,6261	1,6259	1,6258	1,6257	1,6256	1,6253	1,6212	1,6009	1,7400
I_ground	2,6618	2,5283	2,5341	2,5364	2,5364	2,5362	2,5360	2,5357	2,5357	2,5395	2,5546	2,4072

I_fault	4,1771											
I_faulted_phase	2,1742	2,1743	2,1745	2,1746	2,1747	2,1748	2,1749	2,1750	2,1751	2,1752	2,1753	2,1754
	0,0153	0,0150	0,0147	0,0144	0,0142	0,0139	0,0136	0,0133	0,0131	0,0128	0,0125	0,0123
	0,0932	0,0931	0,0931	0,0931	0,0930	0,0930	0,0929	0,0929	0,0929	0,0928	0,0928	0,0928
I_healthy_phase	2,0007	2,0008	2,0009	2,0010	2,0011	2,0012	2,0013	2,0014	2,0015	2,0016	2,0017	2,0018
	0,0098	0,0099	0,0100	0,0102	0,0104	0,0105	0,0107	0,0109	0,0111	0,0114	0,0116	0,0118
	0,0925	0,0926	0,0926	0,0926	0,0926	0,0926	0,0926	0,0927	0,0927	0,0927	0,0927	0,0927
I_earth-wire	1,5568	1,6518	1,6417	1,6391	1,6388	1,6387	1,6386	1,6385	1,6382	1,6342	1,6137	1,7536
I_ground	2,6841	2,5497	2,5555	2,5579	2,5579	2,5577	2,5575	2,5572	2,5573	2,5610	2,5763	2,4279

Table 4-5: Tables with the same characteristics of the previous ones but reporting the results of the fault simulated at the end of the line.

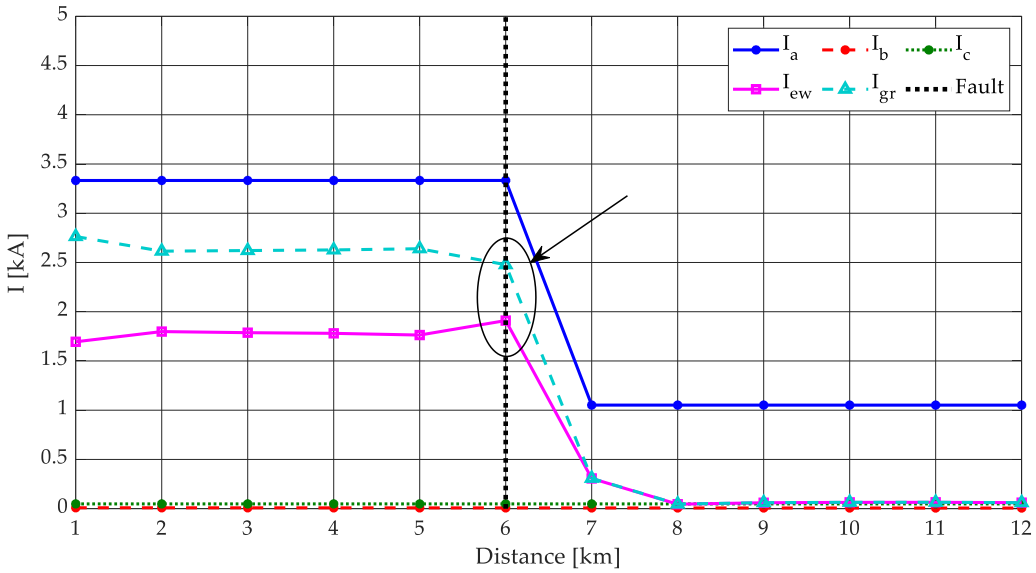

Figure 4-15: Graphical representation of ground-fault current distribution in case of a single line to earth-wire fault simulated at the middle of the line; the main difference from the SLG fault is circled, while the same graphic for the voltages has not been reported as there were no relevant differences.

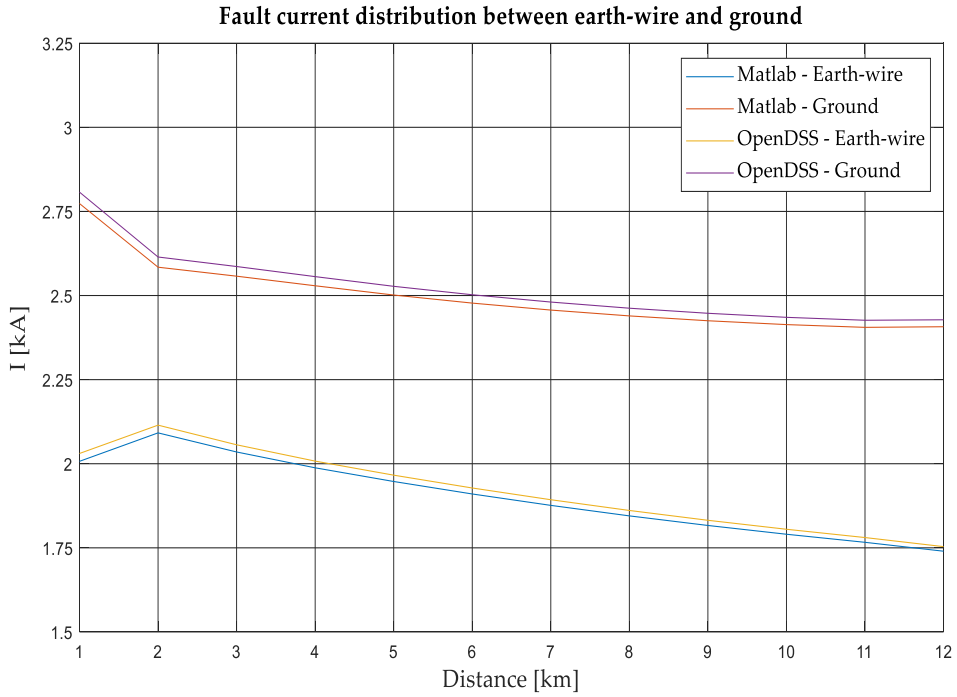

Figure 4-16: This graphic represents the comparison between the values of ground-fault current distribution in the EW and the ground paths for Matlab's and OpenDSS' values; as can be seen, a line to EW fault results in higher shares of current flowing through the neutral conductor than the ground.

All the simulated fault cases, as reported in the Tables 4-4 and 4-5 and shown in the Figg. 4-15 and 4-16, have confirmed the validity of the script developed according to the methodology described in chapter 3: the values of the short circuit currents are always practically the same between the programs and, even looking in more detail at the distribution of the fault current between ground and neutral, the values obtained are confirmed by OpenDSS.

This confirms the various advantages due to the multi-conductor representation of the system and to the script structure, such as the already mentioned possibility to customize the busbar connector configuration without having to insert further elements, the automatic modification of fault location along a line and the wide possibility to customize the earthing parameters.

4.3 Synchronous machine representation

Particular attention must be paid to the generator element, which is the one that presents the most differences between the used software. Focusing on the generator as a synchronous machine and not as an equivalent circuit for the slack bus or network feeder as in OpenDSS and Neplan (elements used to obtain the values presented for single-phase failures), the main difference lies in the fact that in Matlab the generator is modelled in phase components while, in most of commercial software as Neplan, it is modelled based on the symmetrical sequences theory. In the Matlab model, therefore, regardless of the fault type (three-phase symmetrical or single-phase asymmetrical), the generator impedance would be exactly the same, behind sub-transitory voltage, while the neutral point management (i.e. grounding impedance) can be adjusted to replicate the zero-sequence behaviour defined in the commercial software. If the generator is represented through the network feeder model or equivalent circuit in the relative programs, the reasoning explained above is carried out, which leads to very similar impedance values to the sequences between positive- and zero- sequence. All this has been performed to make a comparison as truthful as possible with OpenDSS, but to validate the model of generator representation at the phases, a special analysis has been carried out comparing it with the synchronous machine model in Neplan.

No significant difference is found when evaluating the fault regime with three-phase symmetrical faults in the three software, since grounding conditions do not influence the calculation and the generator model in phase components can be easily represented as a series of ideal voltage generator and internal impedance (usually the sub-transient one, X_d"). The situation changes in the case of asymmetrical faults, because the X_0 values for synchronous machines with turbo rotor are typically in the range (1-10%) X_d" (Neplan manual suggests values in the range (40-80%) X_d"). Taking, for example, the values used in the simulations here presented, for a value of X_d"=12%, the corresponding X_0 would be 7.2%, therefore lower than the value of series impedance alone.

Setting the synchronous generator's X_0 value to 12% (i.e. X_0=X_d") in Neplan, the single-phase to ground fault current values between Matlab and Neplan are very similar as shown in Fig. 4-17, whose values have been obtained considering the system in which line impedances have been set according to the outcomes of the Power_lineparam tool. Very similar results can be observed in the same conditions but using the network feeder, as in all cases the positive- and zero-sequence impedances are kept almost identical: the most marked differences, although still of marginal relevance, are at the very beginning of the line, where the presence of the synchronous machine grounding (included in the modelling of the zero-sequence impedance of the machine as 3 times the value defined in the earthing box) and the fault resistance R_f automatically set by Neplan, lead to slightly lower values. As mentioned in the previous

case, the single-phase fault calculation, is carried out without phase transposition to avoid misinterpretation.

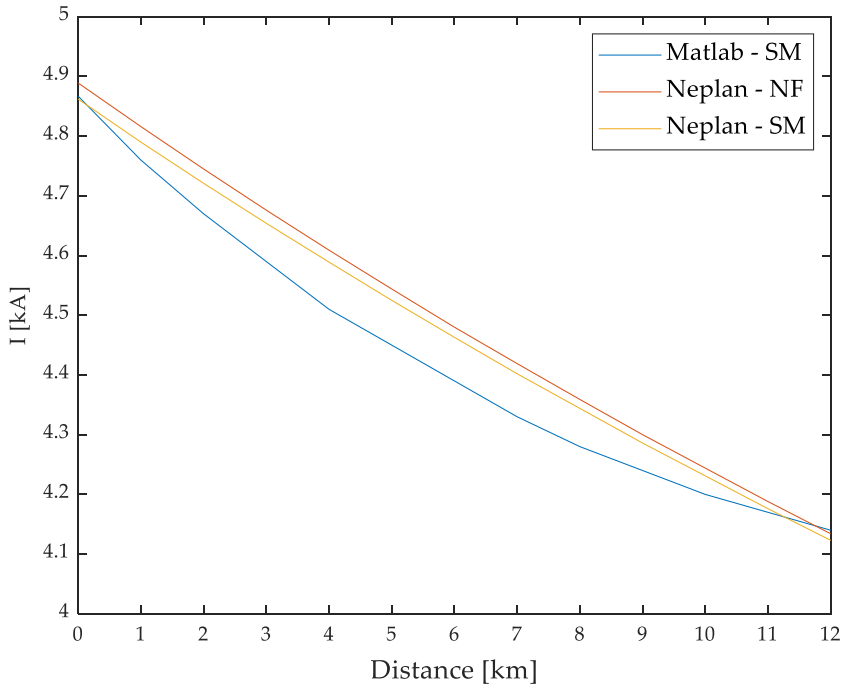

Figure 4-17: This graphic represents the values useful for a comparison between the different strategies used to model the generator, where SM stands for Synchronous Machine while NF stands for Network Feeder.

The question is therefore how to represent, in the generator model in phase components, this behaviour at the zero-sequence, i.e. how to modify the overall impedance in the equivalent zero-sequence circuit so that the value decreases reaching 60% X_d" as simulated in Neplan. To replicate this value without changing the value of the series reactance, a modification has been applied to the ground impedance at the generator's connection bus. For this comparison, the change is made concerning the generator which does not act as slack for the Load Flow because in that case the voltage is fixed, preventing any effect of the grounding impedance settings. Since the objective is to reduce the grounding reactance, in the definition of the Z_{ground} the real part has been set in such a way as to obtain the same value that is imposed in Neplan (3 R_{earth} + R_f), while the imaginary part has been set with a negative sign (representing a capacitive reactance), whose value has been computed such as to return to the same percentages of Neplan through the following:

$$X_{(0)} = 0.6\, X_d^{"} = X_d^{"} + 3\, X_g \tag{4.4}$$

which represents the equality between the zero-sequence reactance as obtained in Neplan and Matlab. By solving this equation and considering the above mentioned resistive part, the grounding impedance is defined for the generator's neutral point according to the desired zero-sequence impedance. The results of the generator's contribution to the fault current for both models are reported in Fig. 4-18, highlighting a similar behaviour having the larger discrepancy in the central part of the line where the absence of the transposition is more influent.

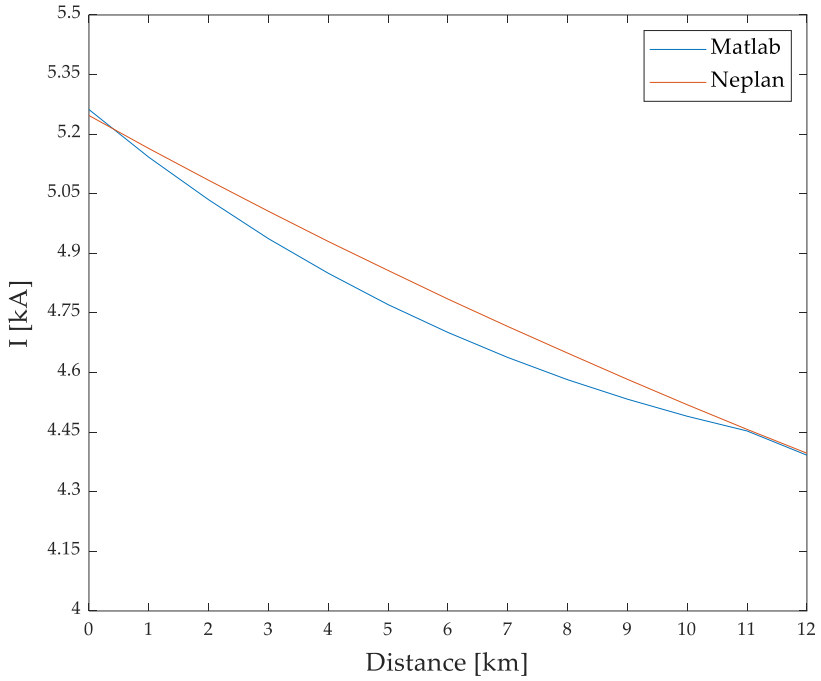

Figure 4-18: This graphic represents the magnitudes of the currents for SLG fault simulated in Matlab and in Neplan with the generator modelled as a Synchronous machine to validate the generator's phase representation applied in Matlab's script; the main difference, which is obtained at the middle of the line, could be due both to the absence of tower earthing resistance in Neplan and to the absence of phase transposition in the Matlab model.

4.4 Modelling of a portion of a real Transmission Network

After having demonstrated the validity of the script developed in Matlab on a simple line, to show how each element's model behaves compared with a software based on similar procedures or with a software based on symmetrical components (sequences) calculation, the same comparison is carried out on a portion of a real transmission network, being a portion of the English transmission network, derived from public data. The network has therefore been modelled in the three software according to the same strategies already applied in the previous case. The main data used for the circuit are reported in Appendix B.

In Matlab, the lines continue to be modelled as in the real case (i.e. detailing the single conductors), therefore, almost all of them as double circuit lines with the possibility of operating the busbar switch in correspondence of some of the substations; two of the lines of the network are instead in a single circuit, so the relevant sending and receiving buses have been defined to represent the same situation that is simulated in Neplan and that will be presented later. The main difference with respect to the previous case is, in addition to the greater quantity of loads, which, however, do not imply any complications as they are modelled at constant impedance/admittance by all the software used for fault regime calculation, is the presence of several generation sources. While in the previous case only one generator was effectively sourcing the fault condition as the second one was modelled as electrically far from the system under study, now there are four energy sources in the network, of which one will be

considered as Slack Bus for the Load-Flow calculation and the others will be modelled as synchronous machines. As already mentioned, since Neplan includes small series resistors in the generator model in case of failure if these are not specified, the corresponding percentage values have also been included in the Matlab model because, even though their effects continue to be practically negligible, their influence is higher than the previous case.

In Neplan, the network, whose complete representation has been captured in Fig. 4-19 has been modelled by building two different nodes in the cases where the busbar switch is operated normally open, and as a single node in the case of a substation with closed busbar. It would, of course, be possible to model each substation as two separate nodes connected by a short line with negligible impedance to make the connection and have greater flexibility in the cases, but for the first tests, it was chosen to keep the configuration as close as possible to the supplied data. The parameters of the sequence components of line impedances are again calculated using Power_lineparam, adapting the model to take into account that all the lines were represented in Neplan as single circuit lines so the values to be inserted for impedances, admittances and maximum conductor current were doubled or halved according to the specific case. As far as the generation is concerned, the Slack Bus was modelled with the Network Feeder element with the supplied parameters while all the other sources were represented as synchronous motors whose parameters were set as discussed in the relative section and were considered as PV nodes during the Load-Flow calculation carried out by the program.

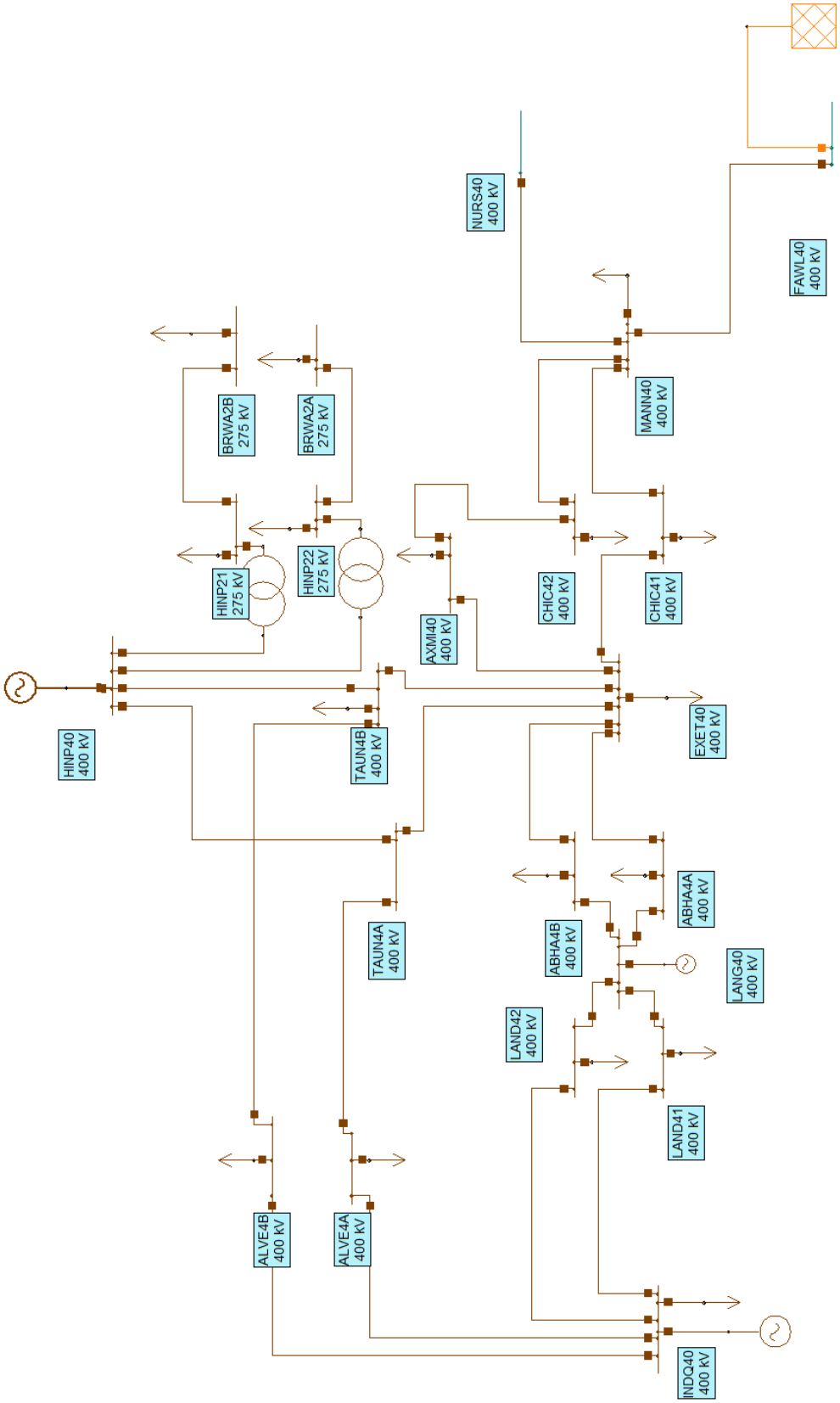

Figure 4-19: Representation of a portion of the English grid in Neplan; in orange is represented the Network Feeder, which is the equivalent model of the remaining grid, while in brown are presented all the other elements.

In OpenDSS there is no need for model simplifications as far as the definition of the lines is concerned, therefore they are all built as double circuit apart from the two single circuit lines that are modelled in the same way (of course the parameters' values are different) but, suitably defining the ports connections at the respective buses. As in Neplan, the main difference is about the sources: apart from the Slack Bus, introduced through the Circuit element previously discussed and required by the program to define a new grid, there are now three other generators with an influential contribution.

Initially, these were represented with the generator element: this is the basic element for the modelling of a synchronous machine, and can be defined in a quite simple way through the voltage values (phase-neutral by default, for a three-phase wye connected generator, or phase-phase for delta connected plants which generate a currents triplet displaced by 30°), three-phase power, power factor and the appropriate selection of the model. To ensure that the Load-Flow carried out before the short circuit analysis converges and to maintain similarity with the other programs, model 2 is selected for both generators and loads, i.e. constant impedance/admittance.

Since the failure situation is a generally transitory circumstance, it is explained in the manual how the machine is modelled in case of Solve mode=dynamics: in fact, the latter is represented as a voltage source behind a sub-transitory reactance at the positive-sequence, while a further impedance value can be specified for the negative-sequence, which allows for a greater precision in the case of unbalanced grid conditions; the model does not, however, provide for an explicit representation of the zero-sequence impedance. To take it into account, the generator connection through a transformer with the secondary side grounded is needed. The grounding impedance has to be set according to the parameters representing the generator's behaviour at zero-sequence; the series of the internal generator impedance and the grounding conditions provides the total impedance of the synchronous machine. Since the reaction of the machine to the fault is characterised by an oscillatory trend, to simulate and analyse the contribution of the generator to the fault current the parameters regarding step size and number of iterations are set as very small to verify the behaviour of the machines in the moments immediately following the fault.

However, after carrying out the first tests to verify the results of both the Load-Flow and the fault currents (a procedure carried out as before with the manual insertion of the fault element because the automatic procedure using the faultstudy does not allow the analysis of the sub-transitory period), it has been noted that these generator elements have a different behaviour compared to the model realised in Matlab and Neplan: in both cases, in fact, the voltage applied to the nodes where the generators are located is kept fixed at 1 p.u.; in Neplan this, in fact, is implemented in order to carry out the calculations according to the standards, using the voltage set at the node and the sub-transitory reactance defined in the parameters. In Matlab, the generator element, as discussed in chapter 3, is modelled as an ideal voltage generator connected to the grid by means of a transformer, representing the generator's series impedance and providing the grounding port at the connection bus.

To be able to simulate this circumstance also in OpenDSS it was then necessary to replace the generator elements with Vsource elements, i.e. ideal voltage generators. In this way, the Vsource element maintains fixed the rated voltage at the generator's bus in the fault current calculation, while a

transformer interfaces the network and the Vsource whose parameters have been set as can be seen in Fig. 4-20 to have the same impedance values that the machine would have during the sub-transitory.

```
New Vsource.Gen_1     Bus1=   GEN_1.1.2.3.0   basekV=          400
Phases=3        MVAsc1=10000000 MVAsc3=10000000
New transformer.GEN1 buses=[   GEN_1.1.2.3     HINP4.1.2.3     ]
Conns=[Delta Wye] Kvs=[400 400] Kvas=[1261000 1261000] xhl=20.4    %loadloss=1

New Vsource.Gen_2     Bus1=   GEN_2.1.2.3.0   basekV=          400
Phases=3        MVAsc1=10000000 MVAsc3=10000000
New transformer.GEN2 buses=[   GEN_2.1.2.3     INDQ4.1.2.3     ]
Conns=[Delta Wye] Kvs=[400 400] Kvas=[1000000 1000000] xhl=15.24    %loadloss=0.75

New Vsource.Gen_3     Bus1=   GEN_3.1.2.3.0   basekV=          400
Phases=3        MVAsc1=10000000 MVAsc3=10000000
New transformer.GEN3 buses=[   GEN_3.1.2.3     LANG4.1.2.3     ]
Conns=[Delta Wye] Kvs=[400 400] Kvas=[ 905000 905000] xhl=25    %loadloss=1.25
```

Figure 4-20: Lines of code inserted in the OpenDSS subscript concerning the generation; it can be seen that the parameters of the generators have been set to be practically ideal while those of the transformers represent the real parameters.

From the picture, it can be noticed also that the standard connection of the Vsource is delta, so the values for the comparison need to be taken from the secondary side of the transformer to avoid phase shifts. In this way, it has been possible to simulate more accurately the procedure carried out in the other software which has led to more similar values not only in the value of the fault currents, whose effect of the generator model is limited by the presence of the lines, but more in the module and in the phase of the currents supplied by Vsource in case of a fault, as will be shown in the results.

First case: Three-phase fault on the first circuit of the line between TAUN and EXET

The first case is, as before, the case of a three-phase fault to verify the behaviour of the network model in the three software at the positive-sequence alone. The fault was therefore simulated in the first circuit of the transmission line between the EXET and TAUN substations, with a length of 38.232 km. In OpenDSS and Matlab this is obtained by defining the fault element in correspondence of a fault position moving along the first circuit of the considered line, while in Neplan (where the two circuits are represented as separated lines) the calculation was carried out in the line having as receiving bus TAUN4A.

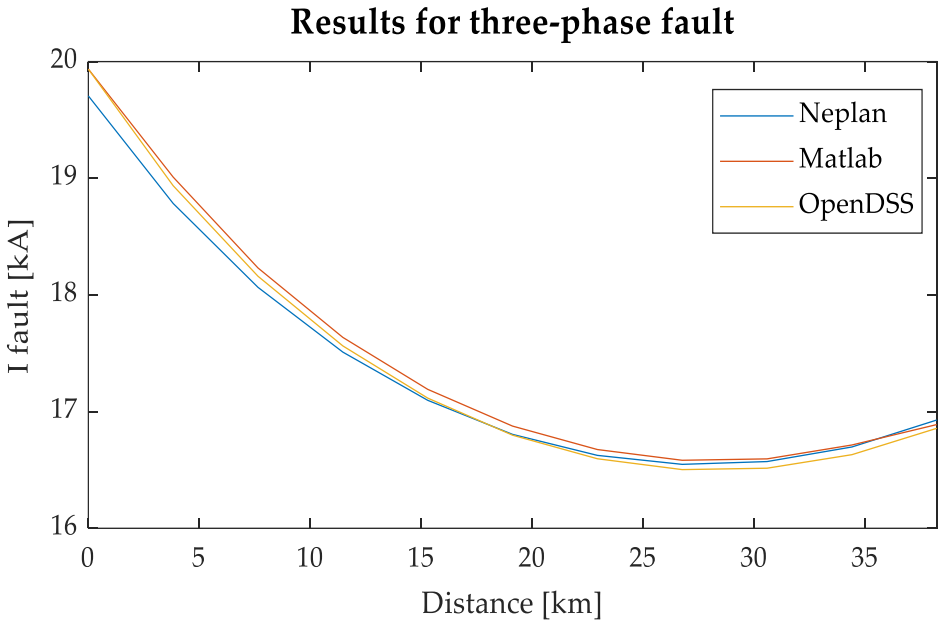

Figure 4-21: Results of the three-phase fault along the line EXET-TAUN where 0 km corresponds to EXET substation.

From the above results shown in Fig. 4-21, it can be seen that the values obtained by the three software are very similar, therefore validating the positive-sequence impedance modelling of the elements with respect to the commercial software.

Concerning the generator's model, a comparison between the OpenDSS results and those coming from the Matlab program based on the methodology described in chapter 3 is reported in the following. Table 4-6 reports the contribution of the four energy sources in the grid modelled in the two software, in terms of current (amplitude and phase angle) and voltage, in the case of a fault at the EXET substation. The results show the achievement of a high level of precision: the biggest difference, however very small in percentage, is in the values of the network feeder but this is due to the presence between fault and source of a single-circuit line that is modelled differently in the two software.

		Matlab				OpenDSS			
		Slack	Gen_1	Gen_2	Gen_3	Slack	Gen_1	Gen_2	Gen_3
Current	Amplitude [kA]	5,0764	4,9916	3,5706	6,2174	5,225	5,052	3,592	6281
		5,3102	5,0242	3,562	6,2783	5,237	5,05	3,593	6288
		5,0643	4,9961	3,5754	6,2341	4,984	4,923	3,541	6172,3
	Angle [°]	98,2049	98,957	95,5763	96,1019	103,2	98,2	94,9	95,7
		-23,4834	-22,6494	-25,5469	-24,8696	-19,9	-23,5	-26	-25,4
		-144,949	-144,107	-146,623	-145,815	-138,5	-142,6	-145,6	-144,9
Voltage	p.u.	0.6273	0.4793	0.3190	0.3069	0,6381	0,4788	0,3193	0,3074
		0.6763	0.4730	0.3191	0.2982	0,6552	0,4700	0,3135	0,2933
		0.6402	0.4741	0.3158	0.3019	0,6385	0,4728	0,3138	0,3009

Table 4-6: In this table are reported the main values to make a comparison between the two software's models of the generators; to understand the position of the source, the couple of nodes in which the generators and transformers are defined in OpenDSS are GEN_1 for HINP, GEN_2 for INDQ and GEN_3 for LANG.

Second case: Single-phase to ground fault on one line

As previously done, also with this portion of a real transmission grid, to continue to demonstrate the numerical validation of the results obtained through the Matlab script, the second step consists in carrying out the single-phase to ground fault in one of the lines of the network with all three software. By applying the same considerations made for the simpler case study described above, a comparison is reported in the following, noting that grounding conditions have been suitably adapted in the phase-components models to represent the zero-sequence impedance adopted in Neplan. In particular, the generator grounding at the grid side node foresees the presence of a capacitive component added to compensate the phase reactance of the generator to represent generator's zero-sequence impedance (the same used in Neplan) without changing its behaviour in case of three-phase failure.

The same procedure has been applied also in OpenDSS where a transformer is placed between the generator bus and the grid, making the ground connection available at its secondary side and allowing the setting of grounding impedance through the R_{neut} and X_{neut} commands, referring to the impedance placed between the neutral point and ground. However, the specification of these values within the definition folders of these elements has not led to the desired impedance variations within the values calculated by the program in the network's primitive admittance matrix. To overcome this problem, probably linked to the default connections to the earth of generators and transformers, the star-centre of the transformer has been connected to the dedicated port in the node (port 7 is the same used for earthwires connection), and then, inside the node, a conductor has been defined, with negligible resistance both to the positive- and the zero-sequence, null inductive reactance in all the sequences, and capacitive reactance of such value to compensate the phase impedance and obtain the real impedance value of the generator at the zero-sequence. The values of the capacities to be inserted have been subsequently doubled because it was not possible to define two different capacity values for positive- and zero-sequences, and therefore the phase capacity matrix of the conductor has been directly defined, so that the software, by placing the two equal capacity values in series, has obtained the correct admittance values.

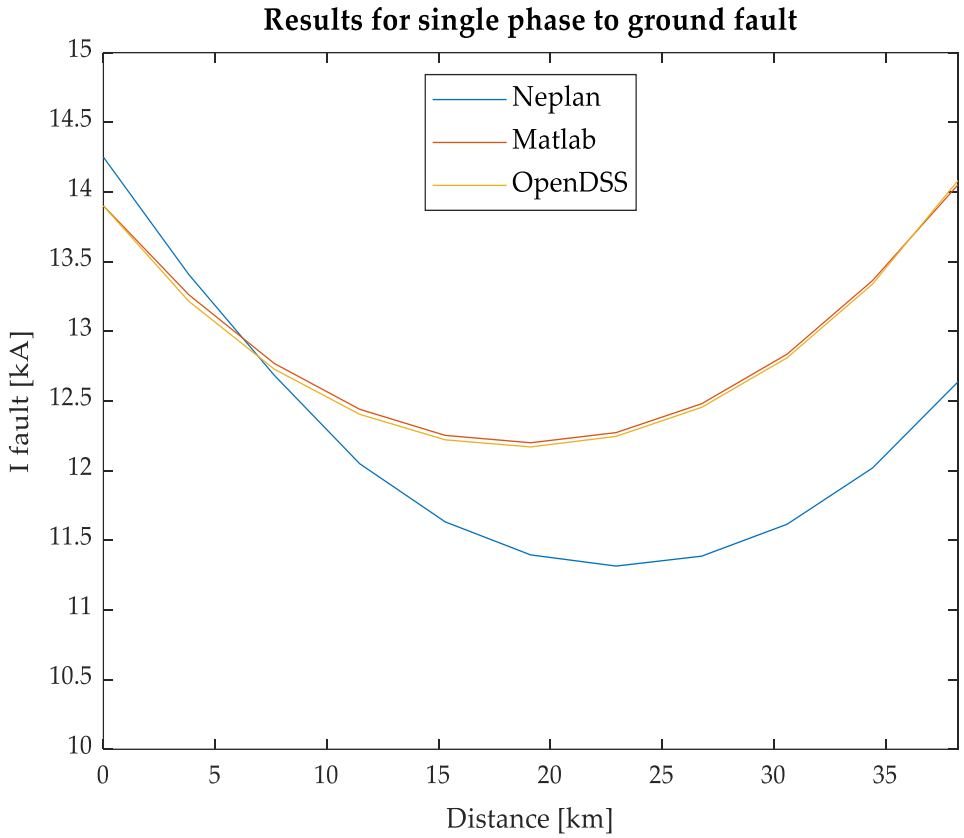

Figure 4-22: Results of SLG fault along the line EXET-TAUN where 0 km corresponds to EXET substation.

From the results reported in Fig.4-22 it can be seen how, moving from substation EXET (where the busbar switch is closed) towards substation TAUN (where the busbar switch is open), the results obtained through a phase-components model, i.e. with OpenDSS and the developed Matlab program, are sufficiently close (with a maximum deviation of about 50 A over 12.5-14 kA, i.e. 0.35-0.4%). By comparing these results with those obtained in Neplan, applying the symmetrical components approach, an increasing difference can be noticed as the fault gets closer to the TAUN substation, where there is a relative percentage error close to 10%.

Besides the differences mentioned above between the two modelling methods, which is mainly due to the two different systems for the geometrical and physical parameterization of the conductors (one uses the actual line geometry, while the other relies on symmetry assumptions), another factor is the approach to double circuit lines. While with the multi-conductor method the two circuits are part of the same line (with mutual coupling terms), in Neplan this was realised by defining two separated lines with no influence on one another. This difference is made clear by observing that the fault current magnitude results tend to diverge increasingly for faults located closer to the substation operated with the opened busbar switch.

To confirm the weight of these parameters, the same fault simulation between the three programs was carried out along the only portion of double circuit lines of the network that was enough far away from

the feeder network to see all the sources contributions and where both the busbar switch, at the sending and receiving buses, were closed: i.e. the 36.315 km line between EXET and AXMI.

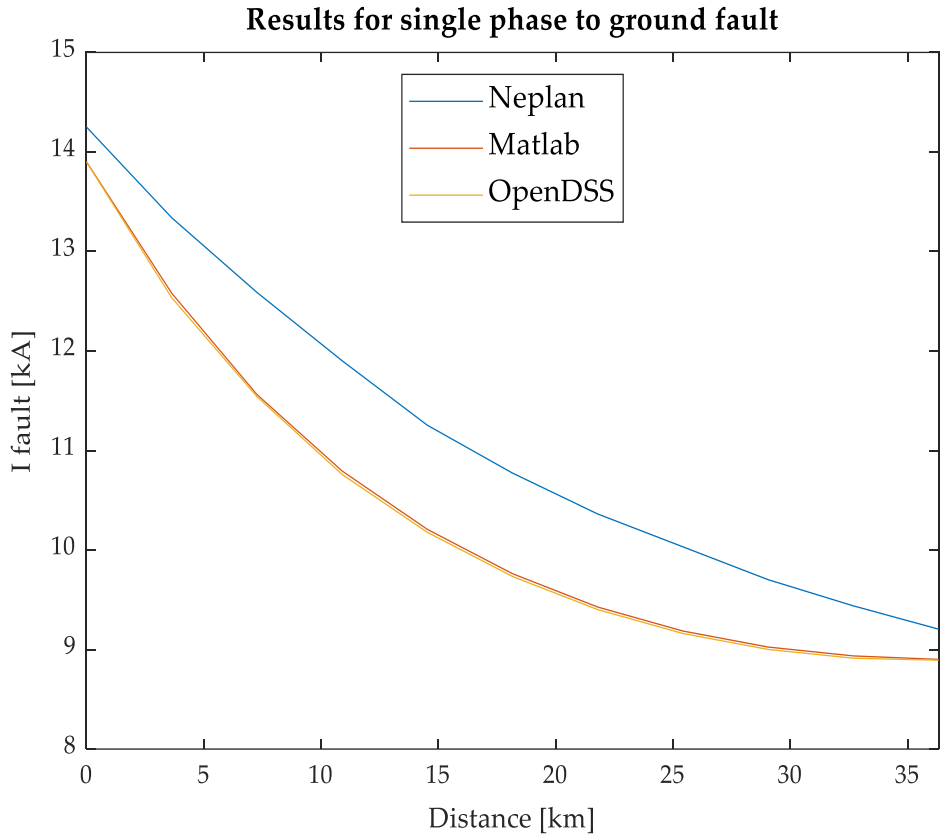

Figure 4-23: Results of SLG fault along the line EXET-AXMI where 0 km corresponds to EXET substation.

The results of the single-phase ground-fault current for faults occurring along the line in this case highlight the already mentioned reasoning as it can be seen in Fig. 4-23: in this example, no influence is associated to the different status of busbar switches, while sources contribution can be assumed being almost the same in the various software. The reason for the difference observed in Fig. 4-23 is, therefore, mainly due to the absence of mutual coupling in the Neplan model, as the relative error passes from 2.5% to 3.4% at the two ends, respectively, but reaches its maximum (10%) for faults occurring in the farthest point with respect to the substations (where the two circuits reconnect). As the last verification of this effect, the same fault with the same conditions was carried out between the INDQ substation, which hosts a generator and is operated with closed busbar switch, and ALVE, operated with the open busbar switch. This one is the longest line in the network, so starting from a node where there is a generator and a load, elements that are modelled with the same assumptions in the three software, as confirmed by the values of current supplied or absorbed both in pre-fault and in case of failure, and arriving at a node that instead is more than 90 km from this source of energy and more than 100 km from the generator with the largest size, the effect of the line should influence the results even more than in the previous case.

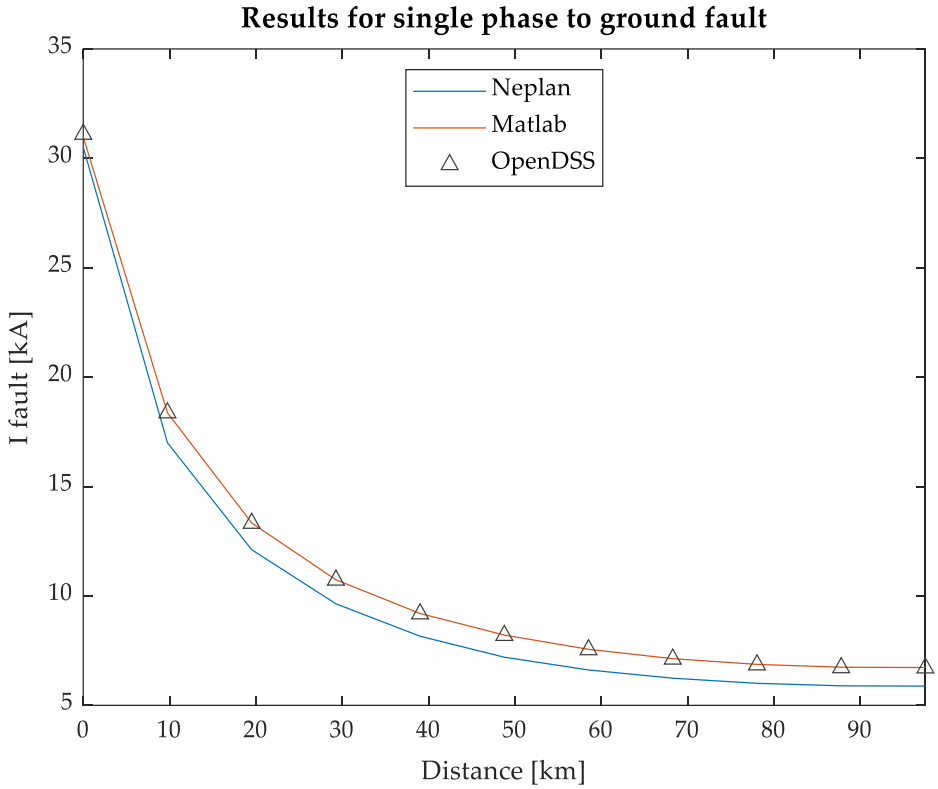

Figure 4-24: Results of SLG fault along the line INDQ-ALVE where 0 km corresponds to INDQ substation.

This last test, which results are reported in Fig. 4-24, again shows how the component that mostly influences the results is the different parameterization of the lines as confirmed by the relative percentage error ranging from about 1.5% and reaching about 10%. On the other hand, the relationship between the parameters in Matlab and OpenDSS (both based on phase-components modelling) is always very good, in this particular case with so much accuracy that in this graph the series of values obtained with the latter software has been represented only with markers to avoid the complete overwriting of the series obtained with Matlab.

5 Influence of grid configurations and of tower ground resistance on fault current magnitude and its distribution

5.1 Influence of the busbar switch

To demonstrate the flexibility of the program in passing from one configuration to another, considering that it has been developed to take into account the busbar configuration and that it shows a great precision in the computation of the distribution of the fault current between the lines' phases (faulty and healthy), earthwire and ground path, further tests have been carried out modifying the state of the busbar collectors. Still considering the portion of the English transmission line as the network for the tests and carrying out the modifications in such a way as to replicate the circumstances that can actually occur on these lines, the new tests are conducted considering the INDQ-ALVE and EXET-TAUN lines. First, three-phase fault studies are performed to verify the amplitude of the fault current and its distribution between the phases varies according to whether or not the two circuits are connected in parallel. Then SLG faults are simulated to discuss about the current distribution among phases, earthwire and ground path. It is worth noting that, since a power station is connected to the INDQ substation, its configuration has not been modified so the variations have been carried out on the other end of the line.

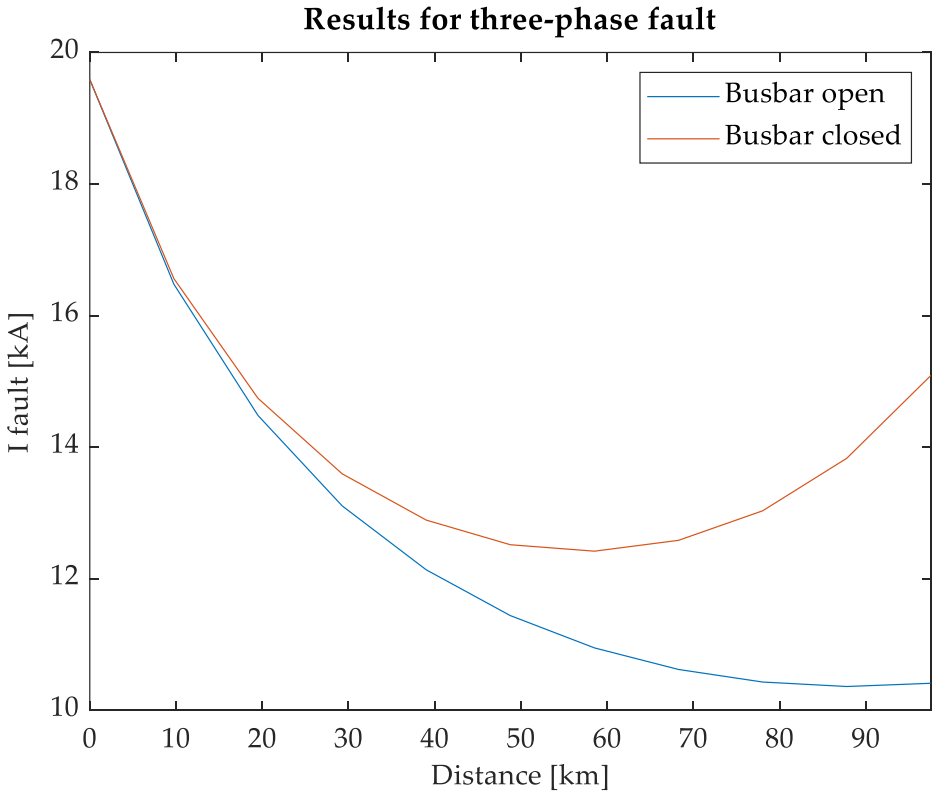

Figure 5-1: Values of short-circuit currents' amplitude for three-phase faults simulated along the INDQ-ALVE line, once with the busbar in ALVE substation closed and once with the busbar open.

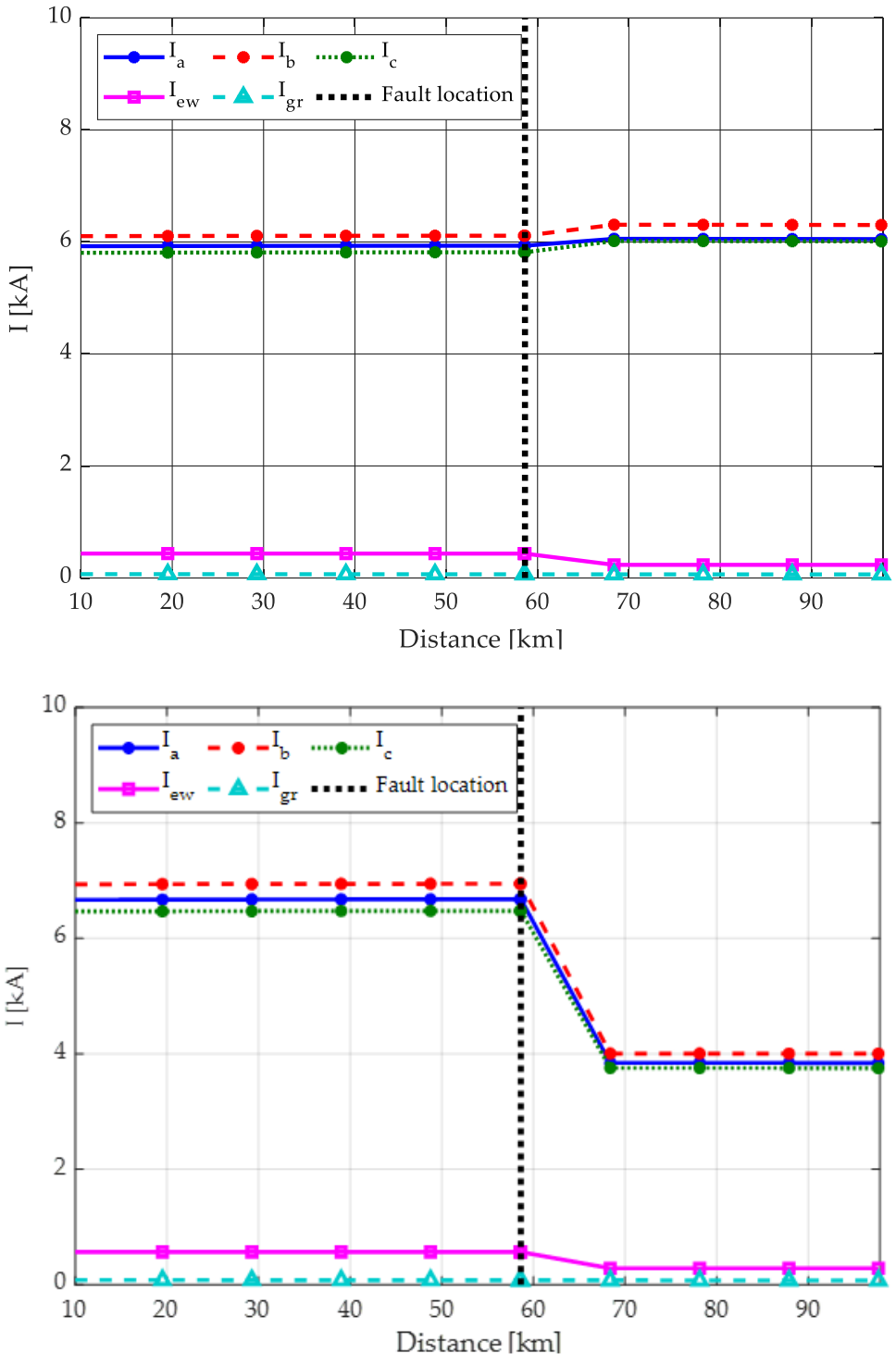

Figure 5-2: Fault current distribution among faulted line's conductors in case of three-phase fault simulated at 60 % of the line length; on the top, the results with closed busbar, below the results with open busbar.

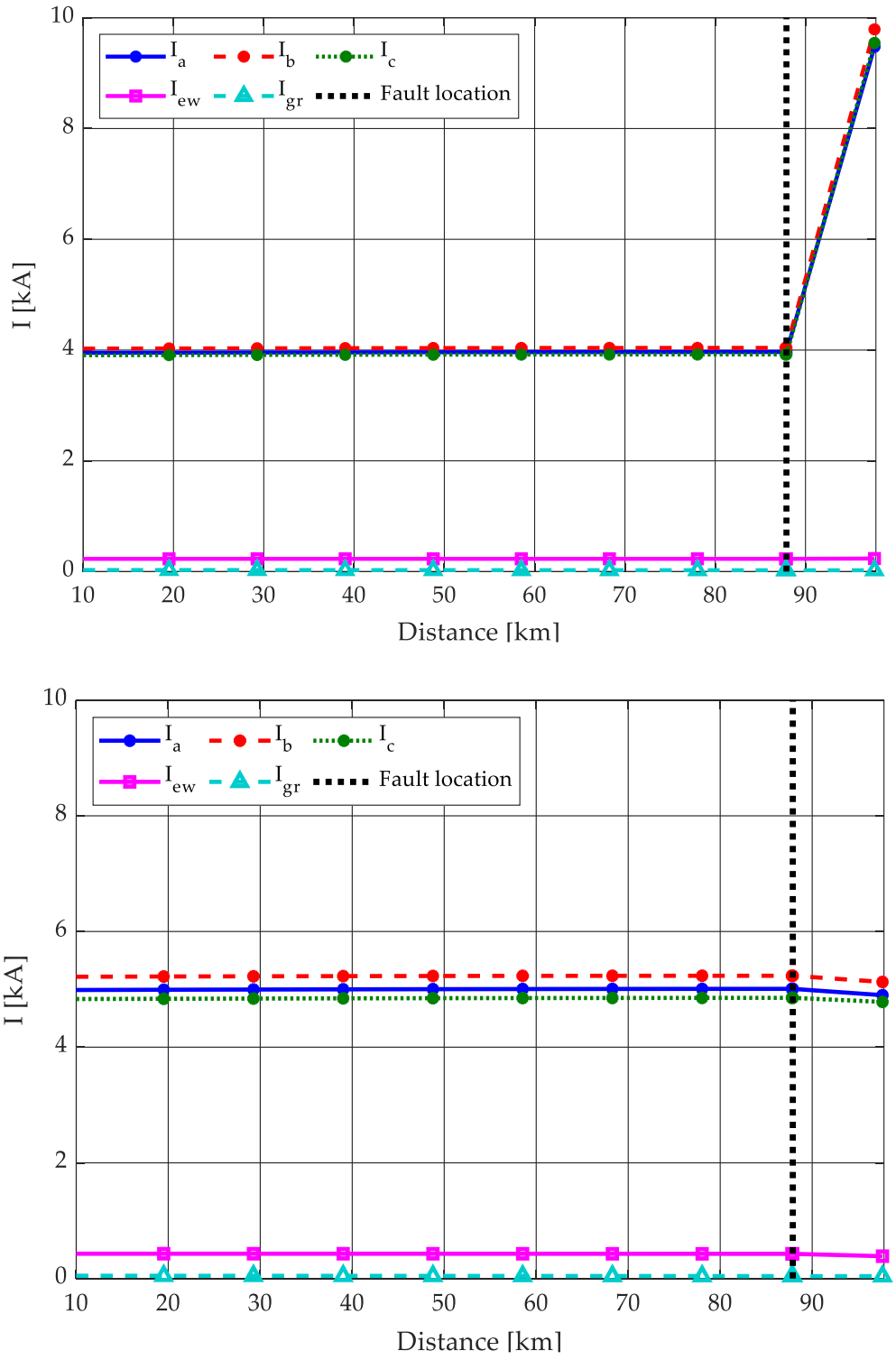

Figure 5-3: Fault current distribution among faulted line's conductors in case of three-phase fault simulated at 90 % of the line length; on the top, the results with closed busbar, below the results with open busbar.

As it can be seen from the results reported in Figg. 5-1 to 5-3, the location of the fault greatly influences the effect of the change in the busbar status. Moving away from the INDQ node, the more the fault location gets closer to the substation with closed busbar switch, the more the value of the fault current

increases: in fact, the closer the fault happens to the node where the interactions between the two circuits change, the greater is the effect of the busbar switch operation. With the busbar switch closed, on one hand, this causes a reduction of the overall grid impedance, and on the other hand, it has the consequence of getting the generators electrically closer to the fault point, hence increasing considerably their contribution to the fault current.

In Table 5-1 are reported the magnitude values of the generators' contributions to the fault current for the fault simulated at 90% of the line length (with respect to the sending bus INDQ), which is one of the points where the trend of the currents is more diversified between the two cases: the strong effect of having put the two lines in parallel is immediately evident from the numbers as the contribution of the generators increases as the fault point gets electrically closer. Generators' contributions to the fault current vary between 27. 6% and 35.9%, the latter being reached by the generator in INDQ which is electrically the closest to the fault point.

	Busbar closed				Busbar open			
Generators	FAWL	INDQ	LANG	HINP	FAWL	INDQ	LANG	HINP
Currents'	2,4955	4,9261	2,2426	4,0878	1,982	3,6743	1,7014	3,0721
Amplitude	2,5738	5,0137	2,2737	4,1675	2,0509	3,7922	1,7314	3,1691
[kA]	2,4145	4,872	2,2083	4,0451	1,8319	3,4369	1,5728	2,879

Table 5-1: Amplitude of the generation systems contribution to the fault current in case of fault simulated at the 90% of the length of the line, for both configurations.

The same tests have been carried out along the EXET-TAUN line, where the busbar configurations have been switched only on the TAUN node because in the EXET substation is connected one of the two single circuit lines so that the contribution of the change of the busbar state in that node would have been strongly influenced by this line's presence. All other variables have remained unchanged and the busbar on ALVE has been set open as in the original configuration.

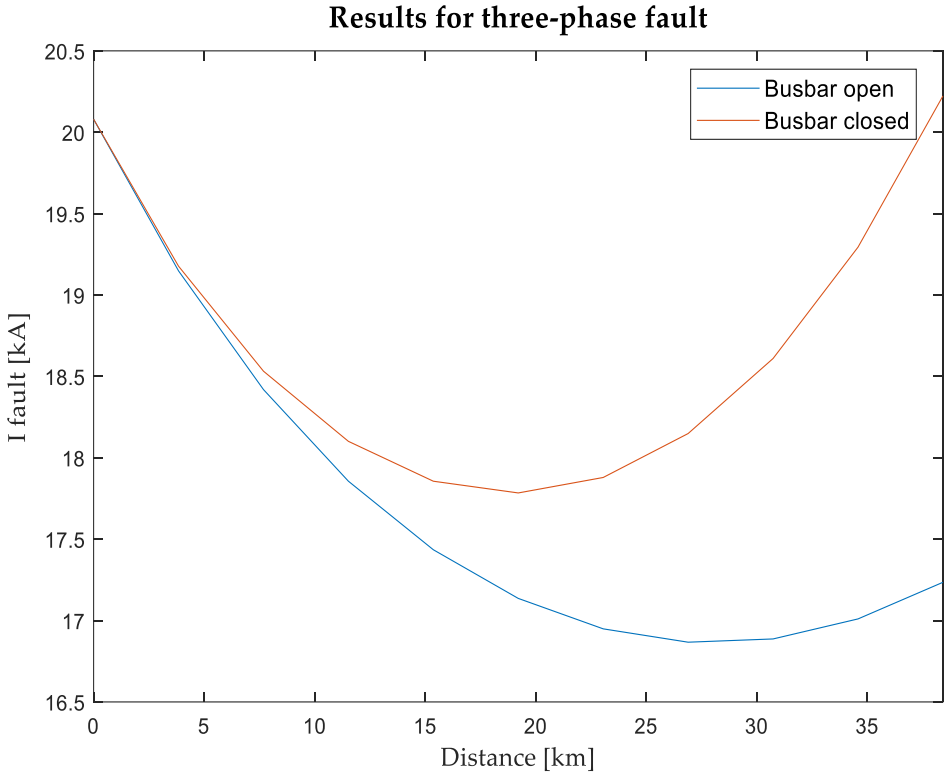

Figure 5-4: Values of short-circuit currents' amplitude for three-phase faults simulated along the EXET-TAUN line, once with the busbar in TAUN substation closed and once with the busbar open.

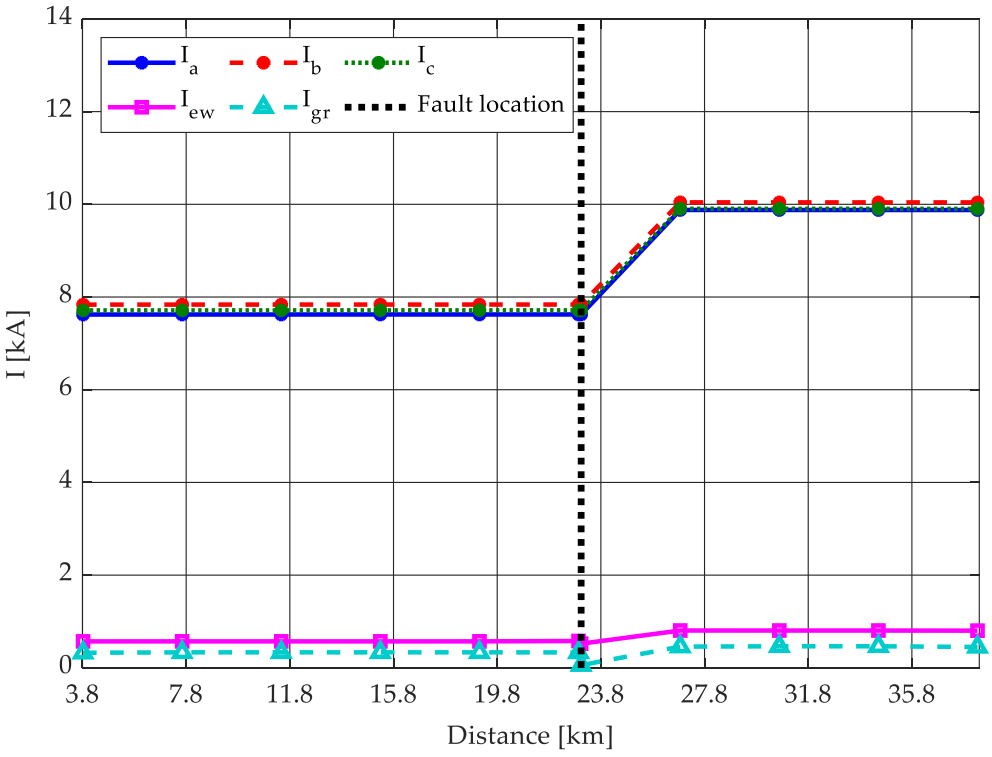

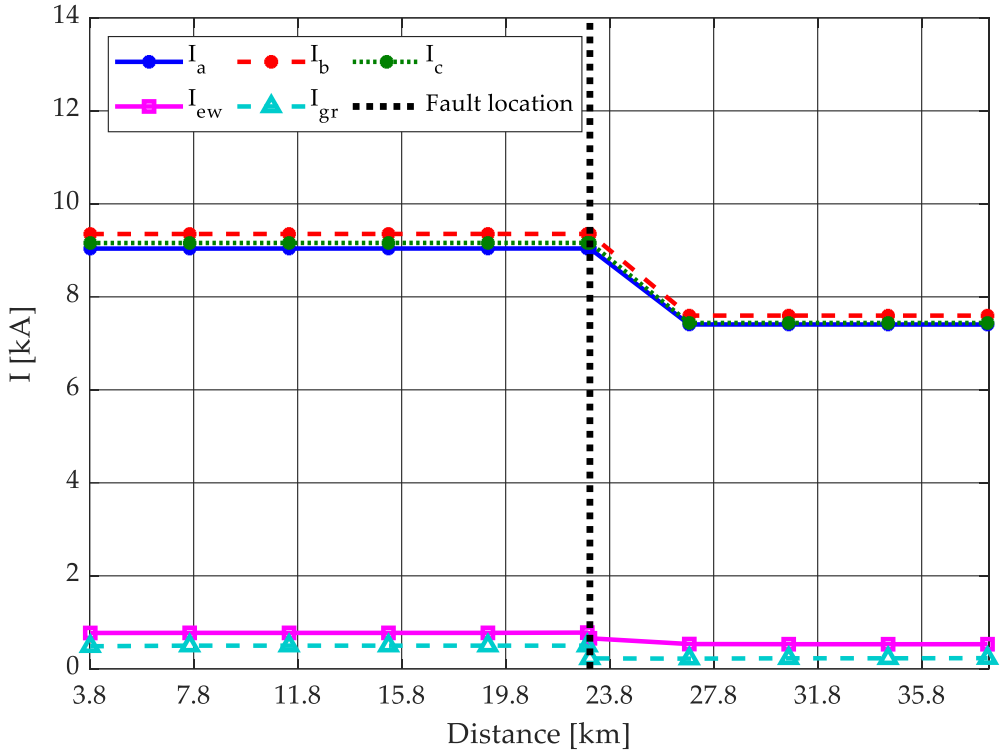

Figure 5-5: Fault current distribution among faulted line's conductors in case of three-phase fault simulated at 60 % of the line length; on the top, the results with closed busbar, below the results with open busbar.

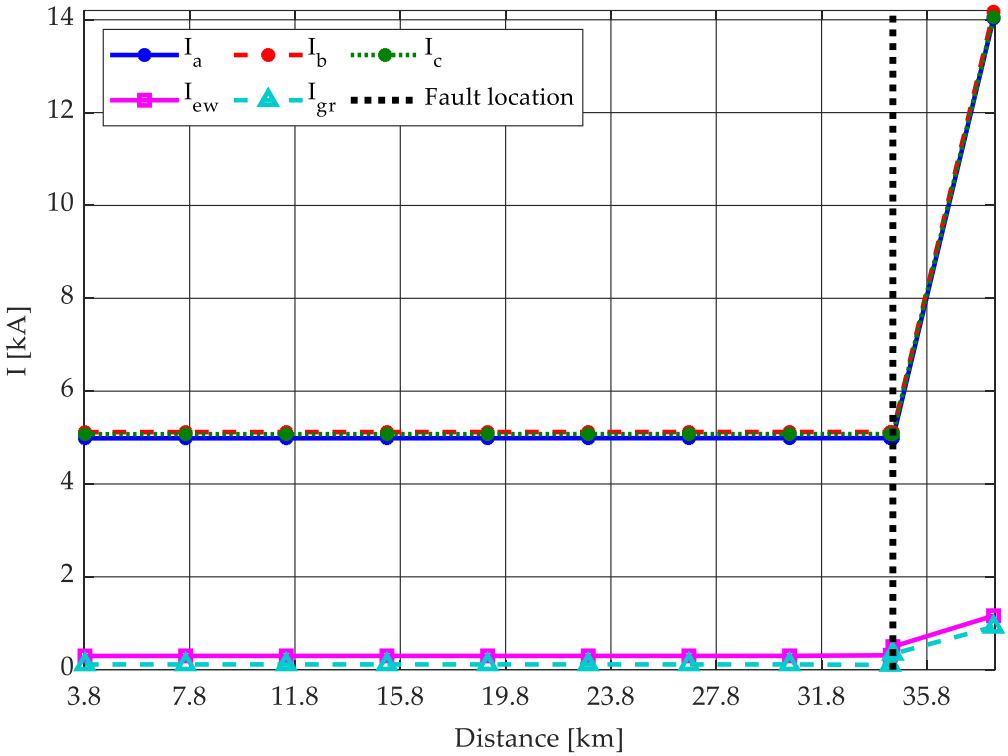

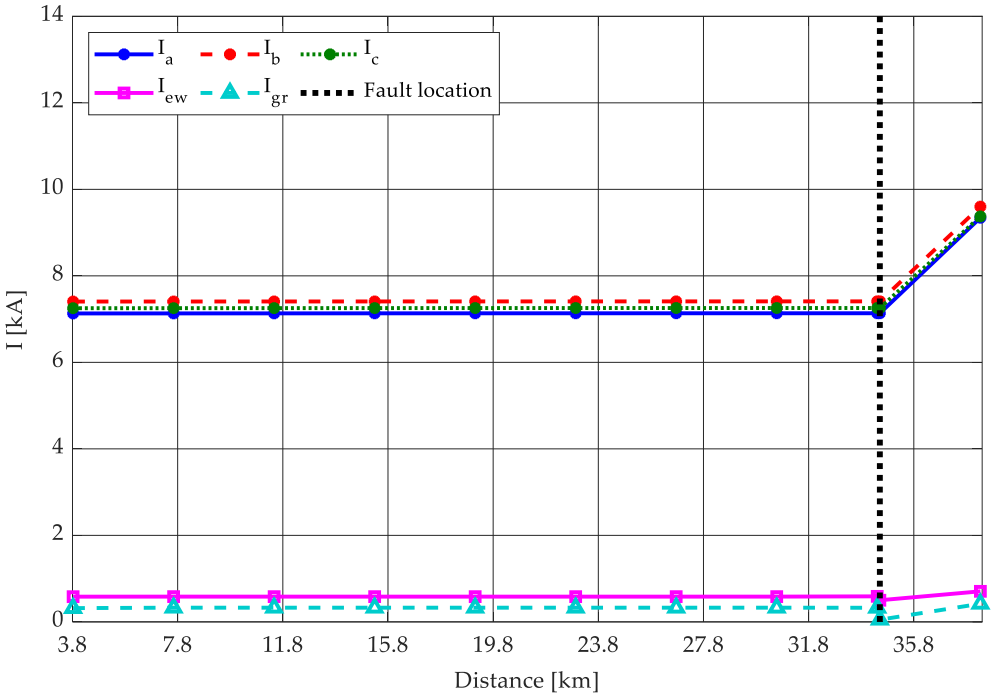

Figure 5-6: Fault current distribution among faulted line's conductors in case of three-phase fault simulated at 90 % of the line length; on the top, the results with closed busbar, below the results with open busbar.

Simulations' results reported in Figg. 5-4 to 5-6, show the same trend respect to the previous case, still highlighting a strong variation when approaching the TAUN substation, also thanks to the proximity to the source. As it can be seen from Table 5-2 showing the contributions of the generators to the fault currents, significantly different contributions are found with the two busbar switch configurations and with respect to the actual fault position, in particular at 60% and 90% of line path with respect to the sending bus EXET. As in the previous case, the maximum variation is obtained on the electrically closest generator, which in this case it the one connected at HINP substation, even if in this case the variations are much more homogeneous because the generators are located at similar distance from the point of failure compared to the previous test where the equivalent external network was much further away than the generators.

	Busbar closed				Busbar open			
Generators	FAWL	INDQ	LANG	HINP	FAWL	INDQ	LANG	HINP
Currents'	4,0278	4,4338	2,8913	6,3173	3,8115	4,1899	2,7312	5,918
Amplitude	4,1839	4,4979	2,9469	6,3736	3,9793	4,268	2,7929	6,061
[kA]	3,9797	4,4089	2,8912	6,2549	3,7464	4,1384	2,7153	5,8985

	Busbar closed				Busbar open			
Generators	FAWL	INDQ	LANG	HINP	FAWL	INDQ	LANG	HINP
Currents'	4,0769	4,8149	3,0011	7,2747	3,5817	4,2093	2,6215	6,2903
Amplitude	4,2074	4,8436	3,0408	7,2957	3,7458	4,2839	2,6848	6,458
[kA]	4,04	4,8081	3,008	7,2409	3,51	4,1485	2,5994	6,285

Table 5-2: Amplitude of the generation systems contribution to the fault current in case of fault simulated respectively at the 60% of the length of the line (above) and the 90% (below), for both configurations.

It should be noted, however, that a higher overall variation was seen in the test on the previous line (INDQ-ALVE), which has an extension of about 98 km, considerably greater than about 40 km of this last case. Therefore, the variation in the overall impedance of the network can be seen more clearly in the first case: although the fault currents have the same trend, in the first test there is an increase of about 40% comparing the fault current amplitudes in case of fault simulated in the substation with the busbar switch closed, while in the second case there is an increase of about 15%.

In general, it can be noted that operating the circuits in parallel configuration reduces the value of the current circulating in the lines before reaching the point of failure on the side where the collector is always kept closed, while, of course, on the other side there is a considerable increase of the current flowing through the phase conductors.

The same analysis concerning the value and distribution of the fault current and the contribution of the generators by varying the network configuration is now carried out in the event of a single-phase ground fault, along the same lines considered previously. Now the analysis focuses on analysing the influence of substations grounding. While in the previous cases these resistive terms were set at very high values, simulating insulation of the substations' neutral point (in order to compare the results with Neplan, in which no bus grounding impedance can be set), now a typical value of 10 Ω is used. The earthing impedance values for nodes where generators or transformers are connected have not been modified and the variations inserted for the zero-sequence behaviour of the generators have been maintained.

No changes have been made to the line towers that are still isolated from ground since their influence on the value and distribution of the fault current will be analysed in detail in the next section.

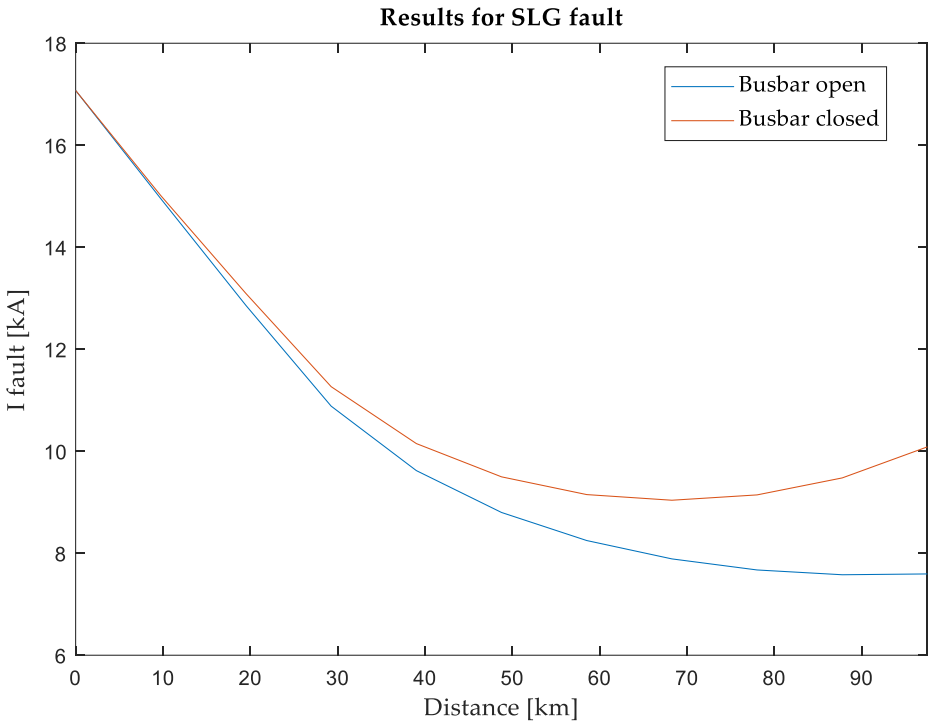

Figure 5-7: Values of short-circuit currents' amplitude for SLG fault simulated along the INDQ-ALVE line, once with the busbar in ALVE substation closed and once with the busbar open.

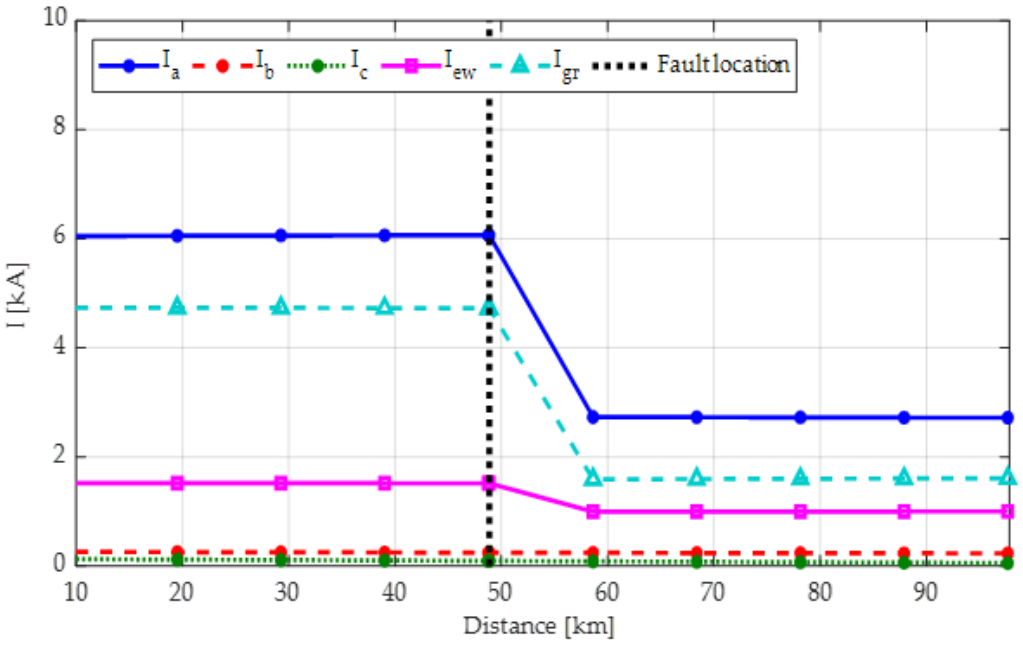

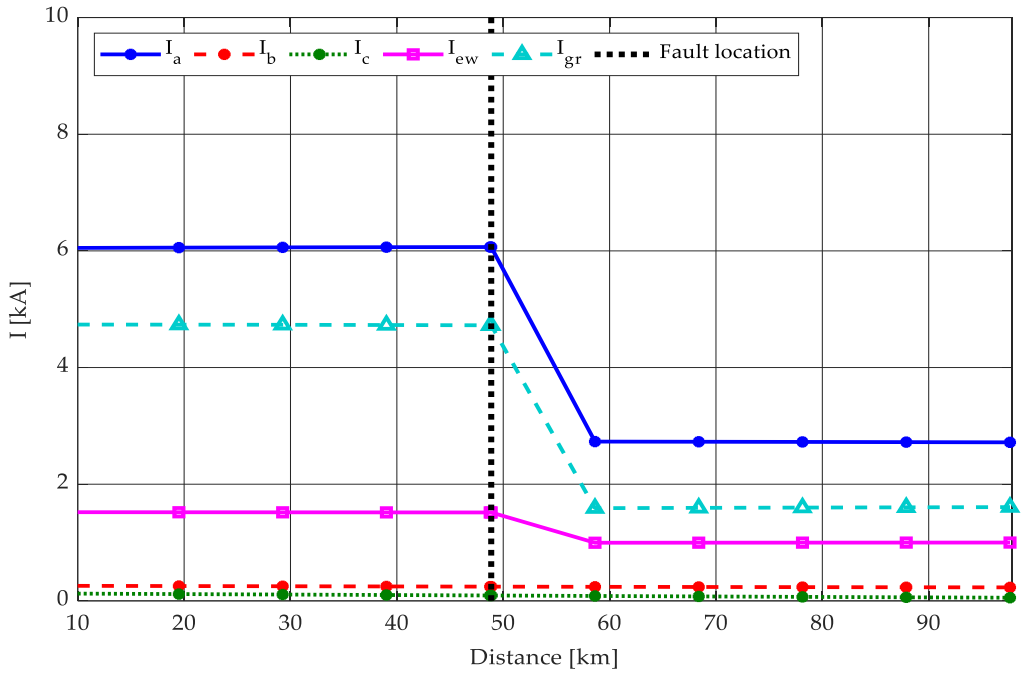

Figure 5-8: Fault current distribution among faulted line's conductors, earth wire and ground in case of SLG fault simulated at 50 % of the line length; on the top the results with closed busbar, below the results with open busbar.

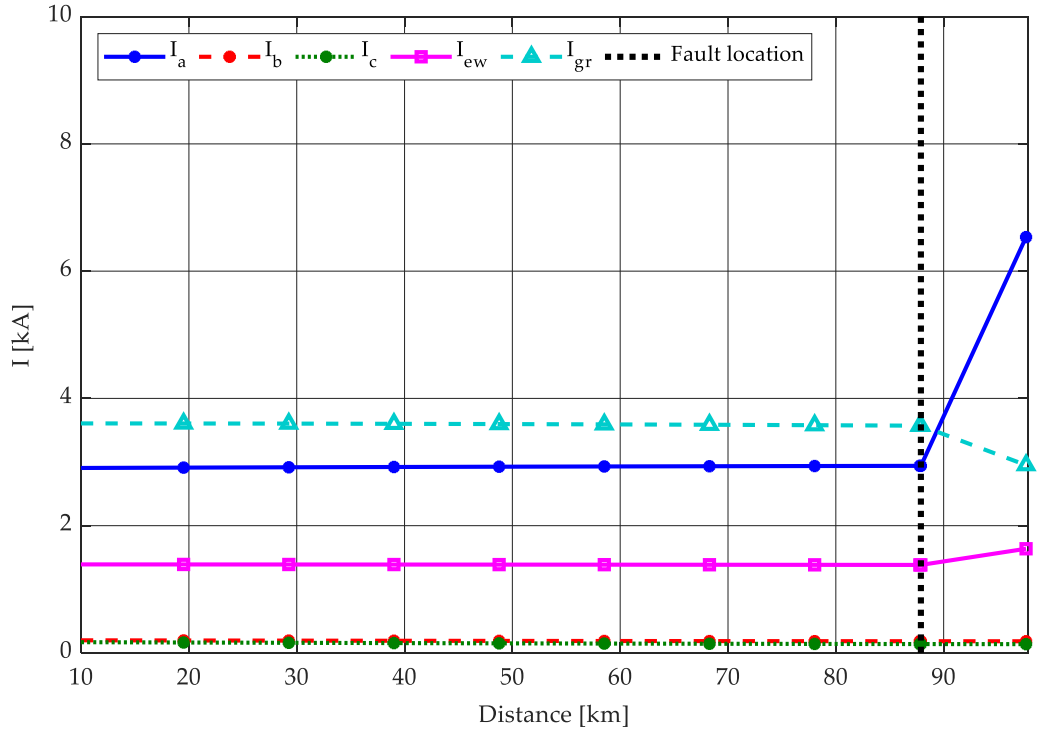

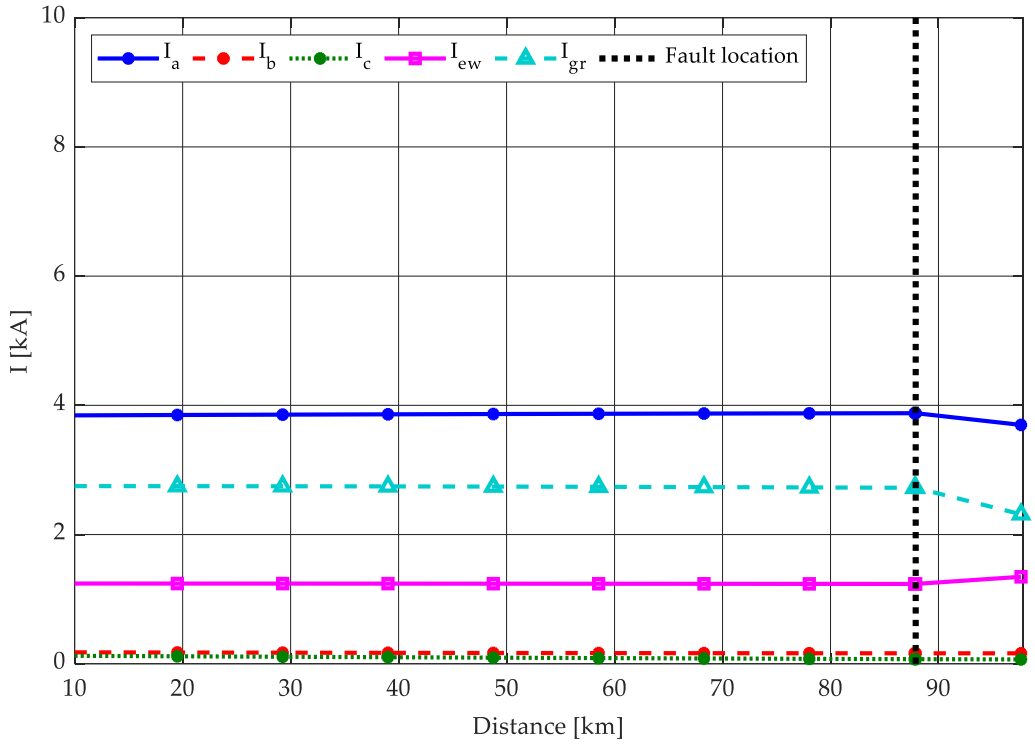

Figure 5-9: Fault current distribution among faulted line's conductors, earth wire and ground in case of SLG fault simulated at 90 % of the line length; on the top the results with closed busbar, below the results with open busbar.

As shown from the results reported in the Figg. 5-7 to 5-9, the trend of the currents is the same as in the case of a three-phase fault, i.e. the result of the parallel configuration of the lines shifts the minimum point of the fault currents between one case and another with a consequent increase in the fault current as the fault get closer to the ALVE substation. Compared to the case of single-phase ground tests discussed previously, it can be verified that the value of the currents is higher due to a lower impedance of the system with respect to ground, apart from the first value which, however, being a fault simulated very close to the generator, is particularly affected by the contribution of the latter and by its grounding conditions. It should be noted, however, that the percentage variation of the fault current between open and closed busbar is less than that in the three-phase fault calculation because the switch operation has a greater influence on the positive-sequence and negative-sequence impedance compared to zero-sequence one (ground and neutral conditions have not changed), also because the tower footing resistance is still neglected.

In this case, there is no need to report the contributions by generators, because the results are very close to those obtained in the previous case, still having a larger variation as the generator is electrically closer to the fault, hence more and more marked getting close to the ALVE substation.

More interesting is instead the distribution of the fault current in the fault section when this occurred at 90% of the total length of the line: in addition to the direct consequence of having put the two circuits in parallel, i.e. the fact that, with the switch closed, a significant current circulates on the first phase of the healthy circuit, too (about 1.77 kA compared to 2.93 kA of the faulty phase, along the line starting from INDQ), there is also a slight variation in the distribution of the fault current between neutral and

earth. In the case of parallel circuits, the fraction of current flowing on the earth conductor is lower by a few percentage points: this effect is linked to the presence of the connection with the healthy phase of the second circuit which contributes to the distribution of the current in the fault section. In this regard, the values of the phase angles of the currents in the first phase of the faulted circuit, in the first phase of the healthy circuit, the neutral conductor and the ground are shown below in Table 5-3; remembering the definition of the direction of the vectors in the π model of the network, since these current calculations are carried out in the second port of the model, the phase values on the INDQ node side result rotated by 180° as the currents are taken as positive if entering the fault section, by convention.

Fault section: INDQ side	Fault section: ALVE side
[°]	
95	94
95	-85
-87	-90
-90	-88

Table 5-3: Value expressed in degrees of the phase angle of the current vectors that arrives at the faulted section (90% of the length of the line); these values refer respectively to the faulted phase, the same phase but in the healthy circuit, the earthwire and the ground.

The same test was then carried out on the EXET-TAUN line maintaining the same assumptions made for the three-phase fault analysis, and the results are reported in the Figg. 5-10 to 5-12.

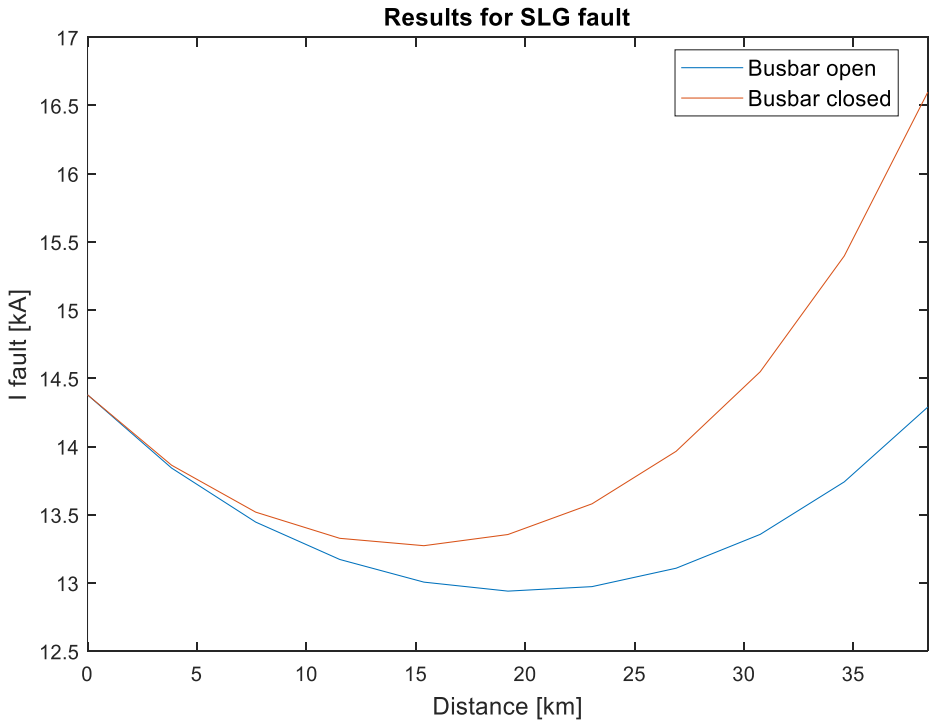

Figure 5-10: Values of short-circuit currents' amplitude for SLG fault simulated along the EXET-TAUN line, once with the busbar in TAUN substation closed and once with the busbar open.

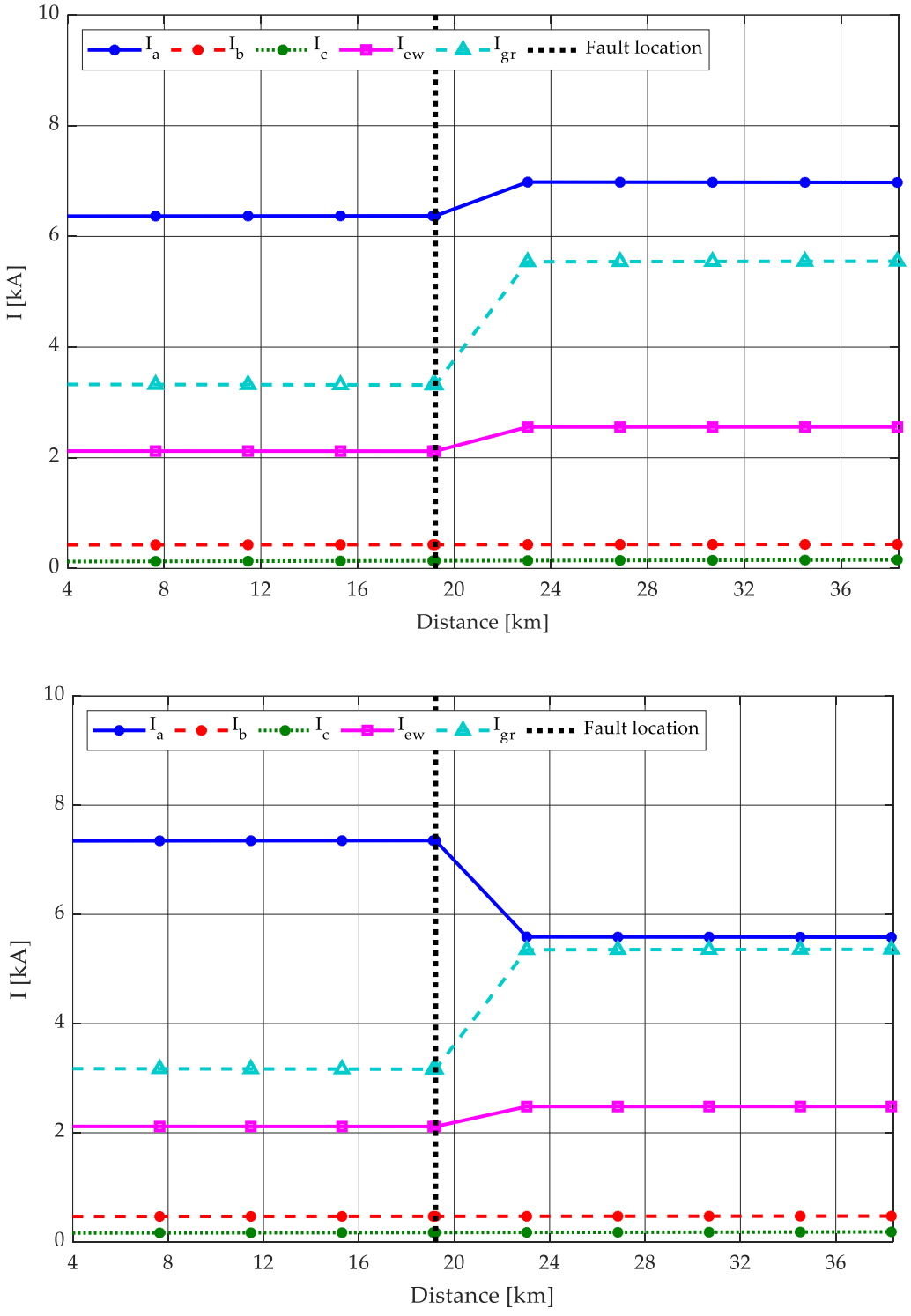

Figure 5-11: Fault current distribution among faulted line's conductors, earth wire and ground in case of SLG fault simulated at 50 % of the line length; on the top the results with closed busbar, below the results with open busbar.

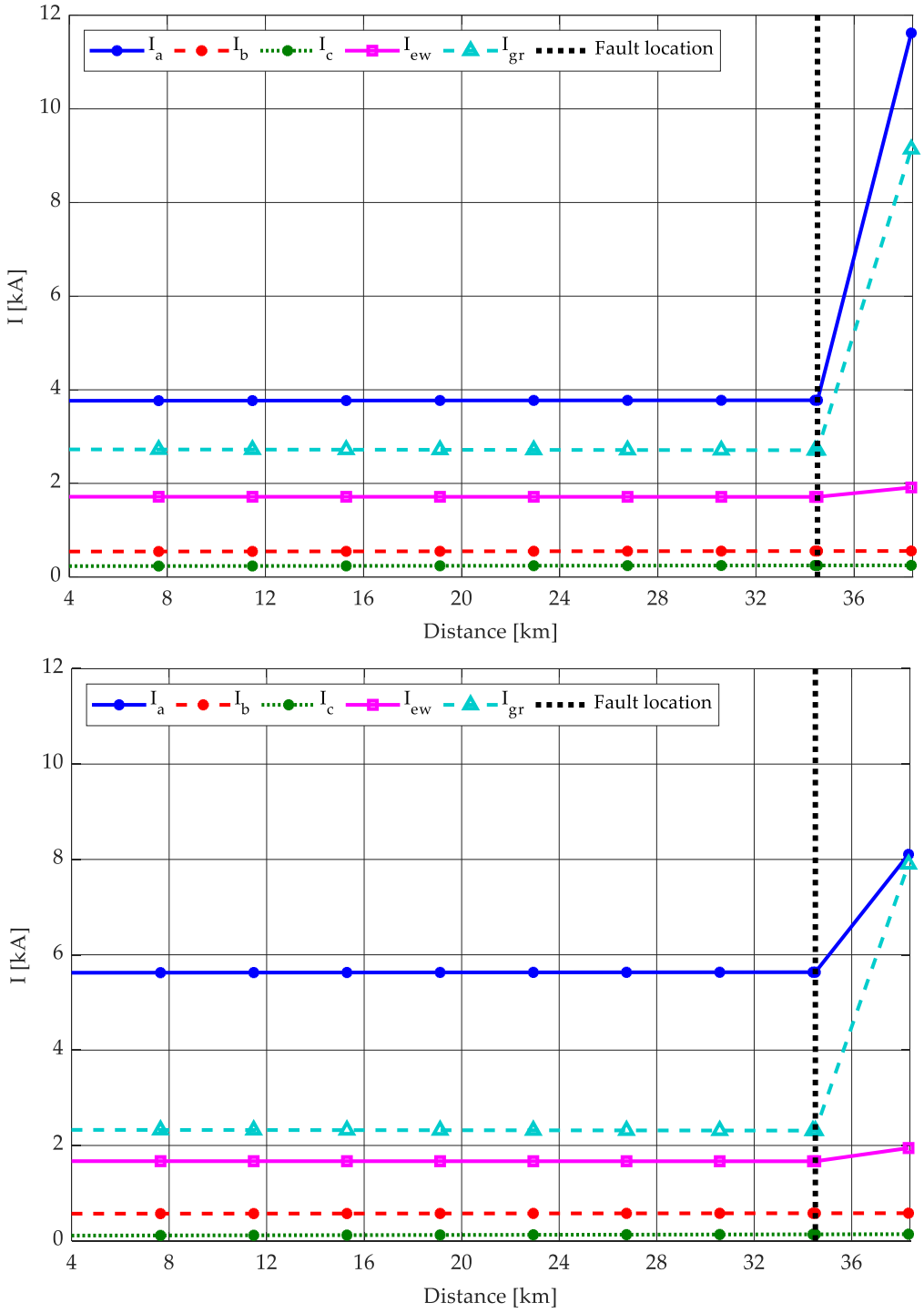

Figure 5-12: Fault current distribution among faulted line's conductors, earth wire and ground in case of SLG fault simulated at 90 % of the line length; on the top the results with closed busbar, below the results with open busbar.

The same behaviour is verified concerning generation and the distribution of the current in the fault section, as shown below in Table 5-4. The variation in the amplitude of the currents between vectors entering the EXET side and the TAUN side, respectively, is the same verified also in the three-phase simulations, i.e. a lower current amplitude is seen on the EXET side with closed busbar switch and

higher values on the TAUN side where there is the contribution of the generator on HINP, which for faults along this line is the one that has the higher contribution and percentage variation between closed/open busbar.

Even in the case of single-phase failure, the influence of busbar switch operation is lower than in the other line for the reasons already seen above. More evident in this line, on the other hand, even if it is an effect present in both cases, is the effect of the insertion of the real values of the grounding at the substations, which not only has as a consequence an increase in the value of the fault currents compared to the "isolated" case but also modifies the trend according to the fault position, making the fault current values increase near the TAUN node as the fault current can flow to ground through a much smaller resistance.

Fault section: EXET side	Fault section: TAUN side
[°]	
94	95
92	-88
-73	-78
-84	-89

Table 5-4: Value expressed in degrees of the phase of the current vectors that arrives at the faulted section (90% of the length of the line); these values refer respectively to the faulted phase, the same phase but in the healthy circuit, the earthwire and the ground..

5.2 Influence of the grounding system

A peculiarity of this script developed in Matlab is the possibility to analyse the current distribution along the line not only at the nodes but also at the towers, computing the values of current and voltages for phase conductors, earth wire and the return path in the ground, allowing great flexibility in the grounding parameters: for this, in this section, various configurations of the pylons' grounding have been simulated.

Evaluating the current distribution over all available paths is of great importance in the analysis of fault regime, since it is strongly involved in the substation grounding design. As it will be shown below, the specification of tower footing impedances influences mainly the currents distribution, rather than the value of the fault current, modifying the share of current circulating in the earthwire and through the ground path. Therefore, the tower footing resistances have been included only to the line where the fault is simulated, keeping the rest of the network model unchanged. The following graphs display the current distribution trend in case of single-phase failure along the EXET-TAUN line, showing the dependence on the ground resistance value, on the fault type from phase-to-phase to phase-to-ground and on the length of the spans.

It has been chosen to simulate both types of single-phase faults that may occur along the line (ground fault, e.g. in the case of a tree's branch hitting the line, and fault between phase and pylon, which is

electrically connected to the neutral) to highlight the effect on the current distribution between the ground and the earth wire.

The following tests, which results are reported in Figg. 5-13 to 5-16, have been carried out with a fault simulated at 50% of the line length; the influence of the fault position on the fault current distribution will be shown successively.

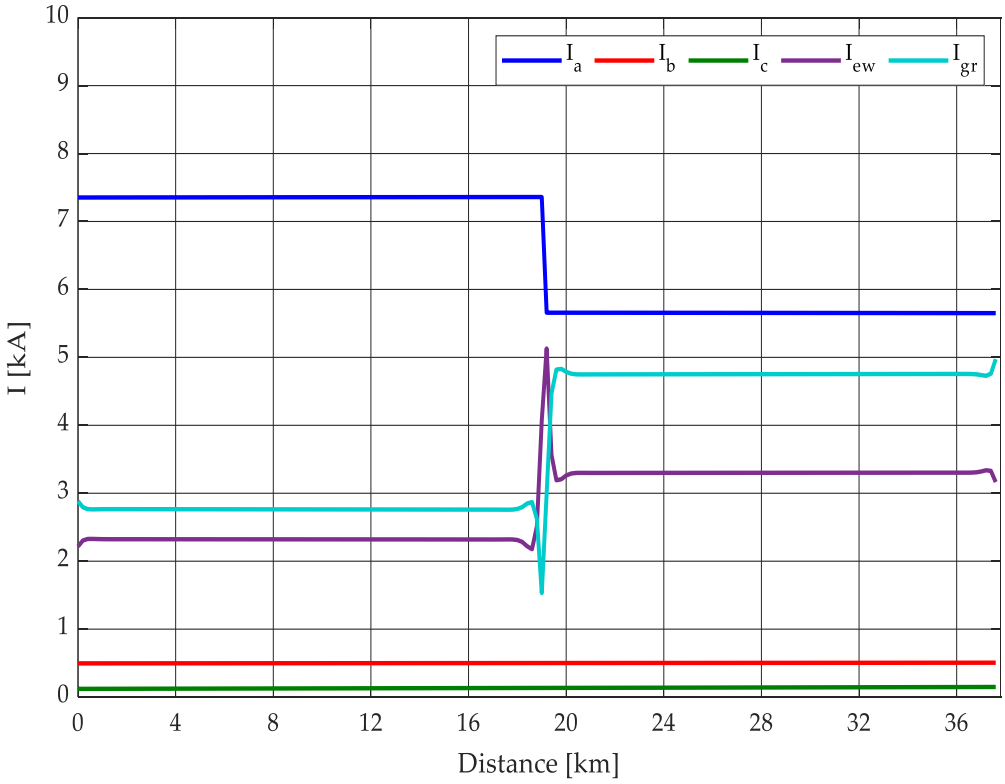

Figure 5-13: Fault current distribution in case of a phase-to-neutral fault with an earthing resistance of the tower of 0.1 Ω.

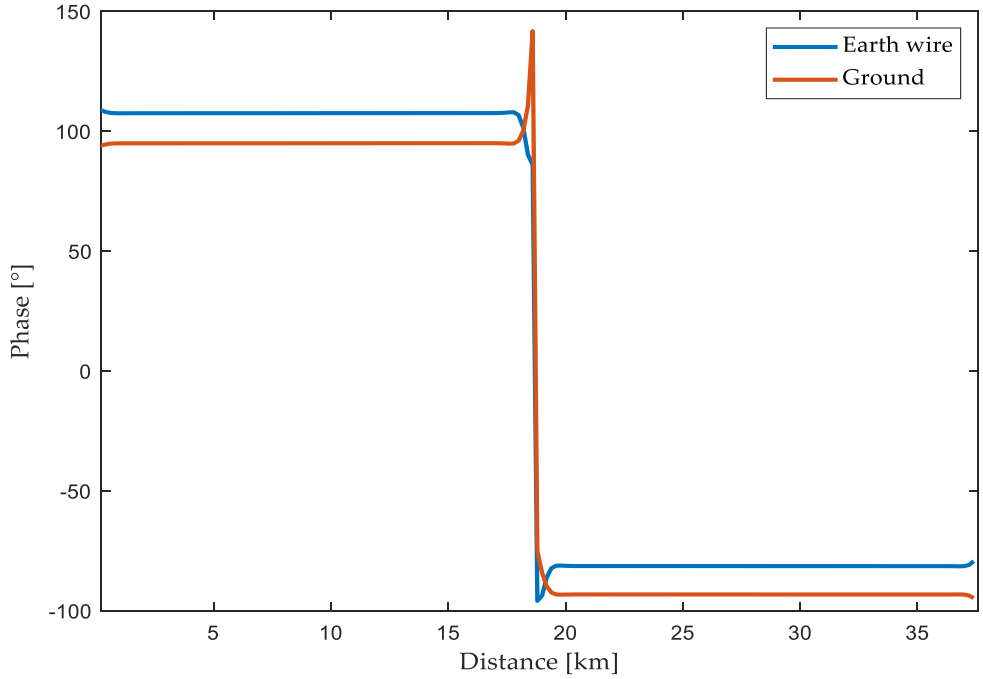

Figure 5-14: Phase angle of the fault current components in case of a phase-to-neutral fault with an earthing resistance of the tower of 0.1 Ω.

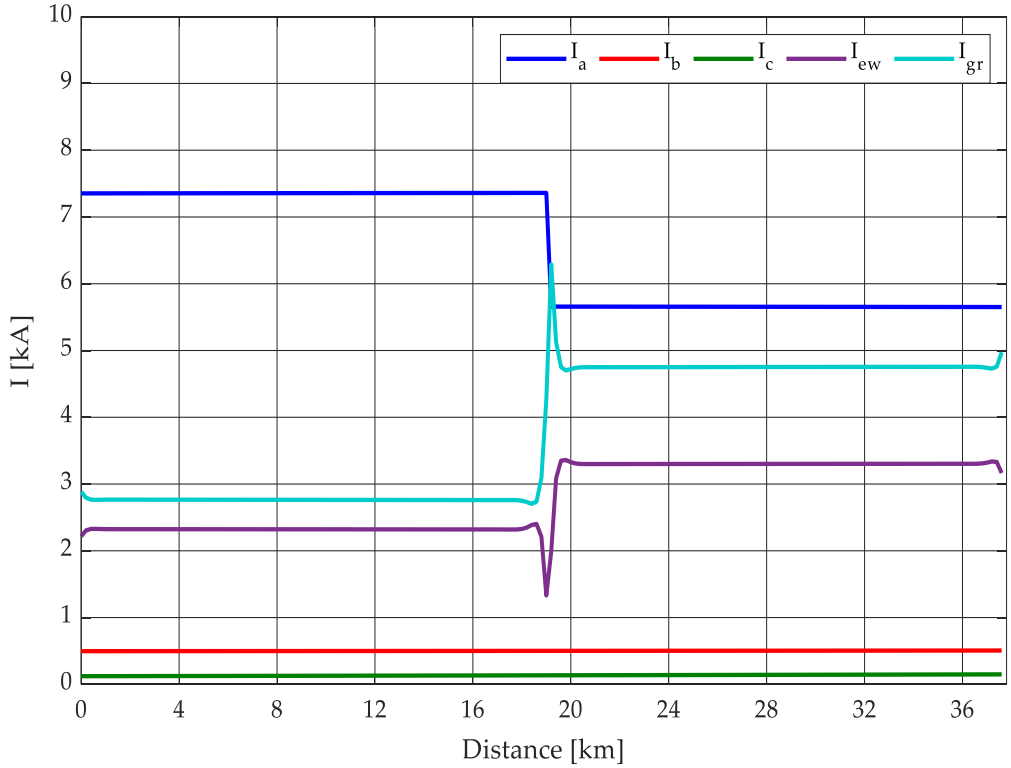

Figure 5-15: Fault current distribution in case of a phase-to-ground fault with an earthing resistance of the tower of 0.1 Ω.

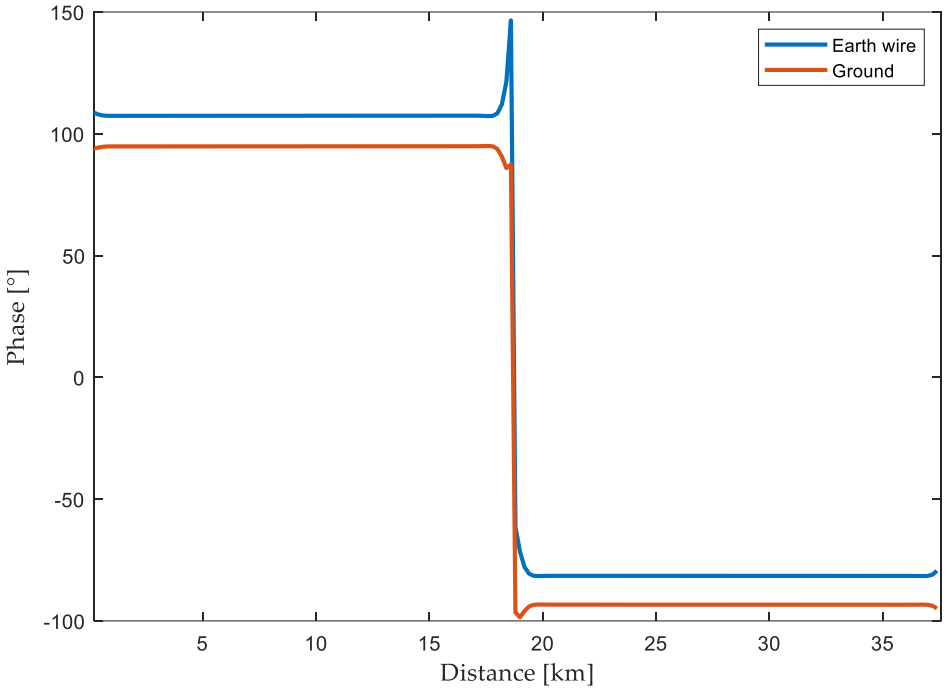

Figure 5-16: Phase angle of the fault current components in case of a phase-to-ground fault with an earthing resistance of the tower of 0.1 Ω.

In the first test, the main difference between the two types of failure is shown, as there is a dual behaviour of the current peaks at the failure section with an obvious increase of the respective current amplitude in the mostly interested part (i.e. the earthwire in case of phase-tower fault, the ground path in case of phase-ground fault). Observing the current shares at increasing distance from the fault location, after a significant variation in the vicinity of the fault point, it tends to assume an approximately constant value that is equal regardless of the fault type.

Only for this test, also the phase angle values of the currents have been reported, which on the one hand also show the dual behaviour between the two types of fault, and on the other hand show, apart from the fault section where the fault resistance influences the value, the phase opposition of the current vectors on the two sides of the fault location, as the currents' components flow in opposite directions, according to the convention used in the lumped parameters line model described in section 3.

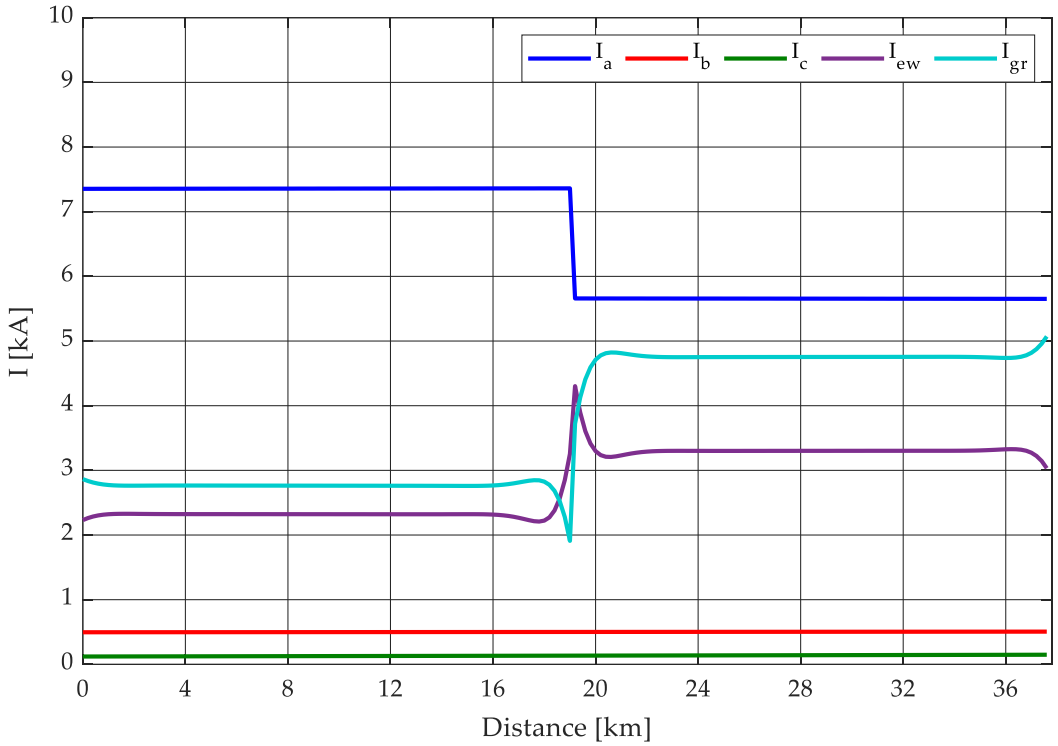

Figure 5-17: Fault current distribution in case of a phase-to-neutral fault with an earthing resistance of the tower of 1 Ω.

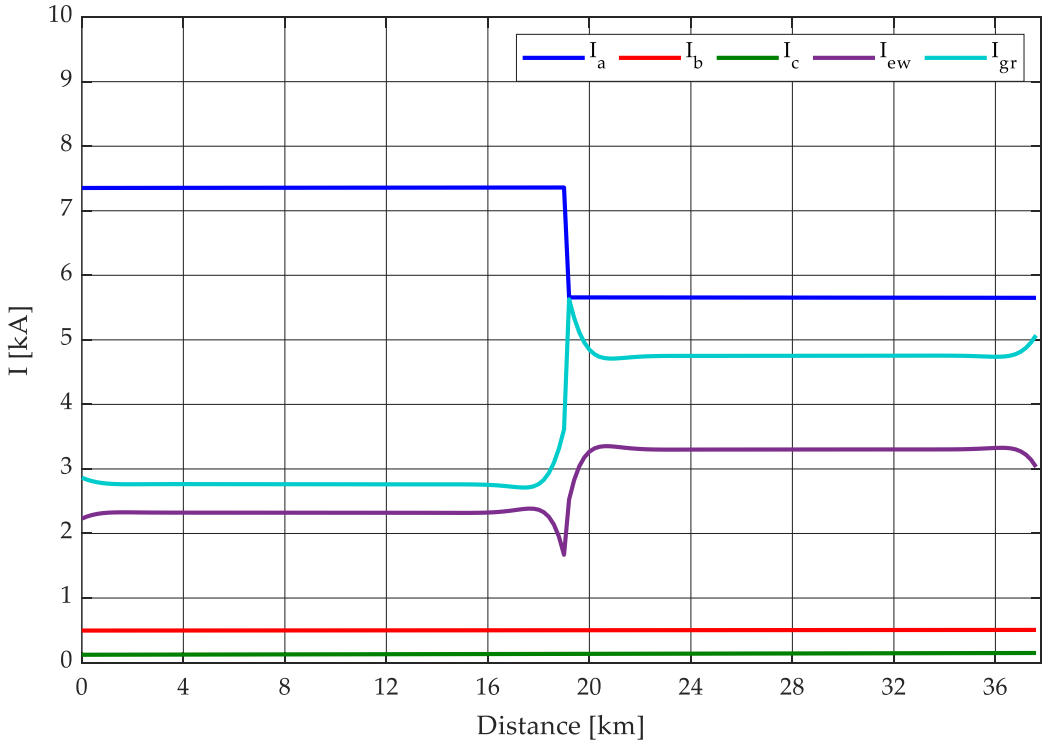

Figure 5-18: Fault current distribution in case of a phase-to-ground fault with an earthing resistance of the tower of 1 Ω.

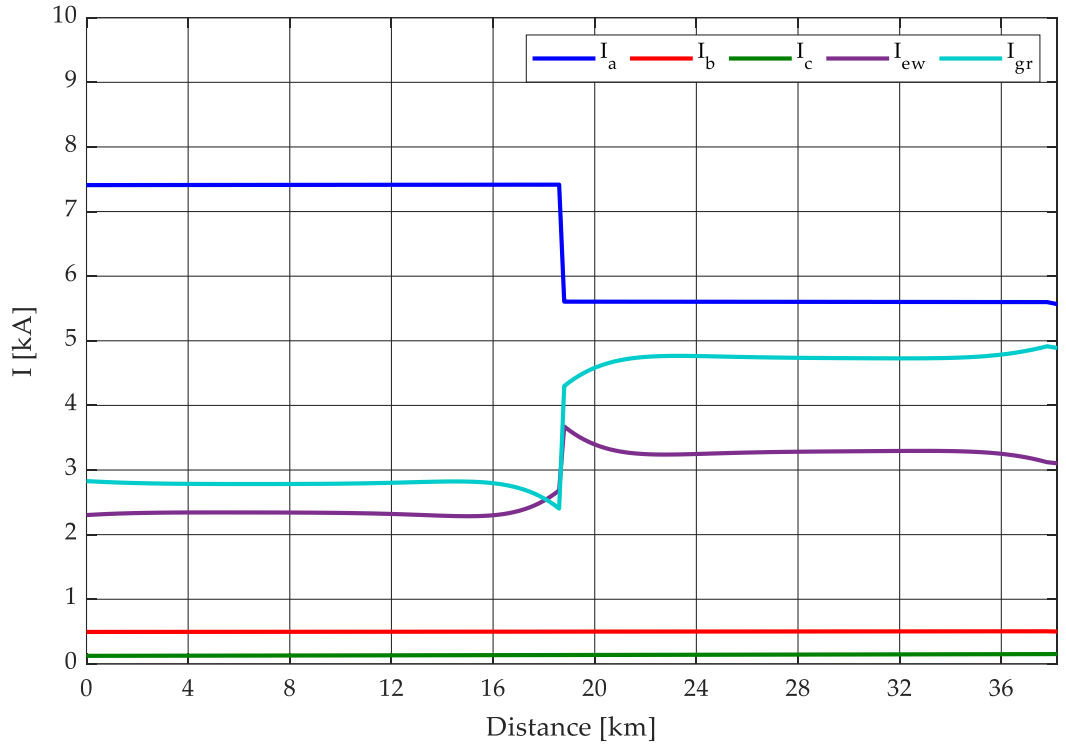

Figure 5-19: Fault current distribution in case of a phase-to-neutral fault with an earthing resistance of the tower of 10 Ω.

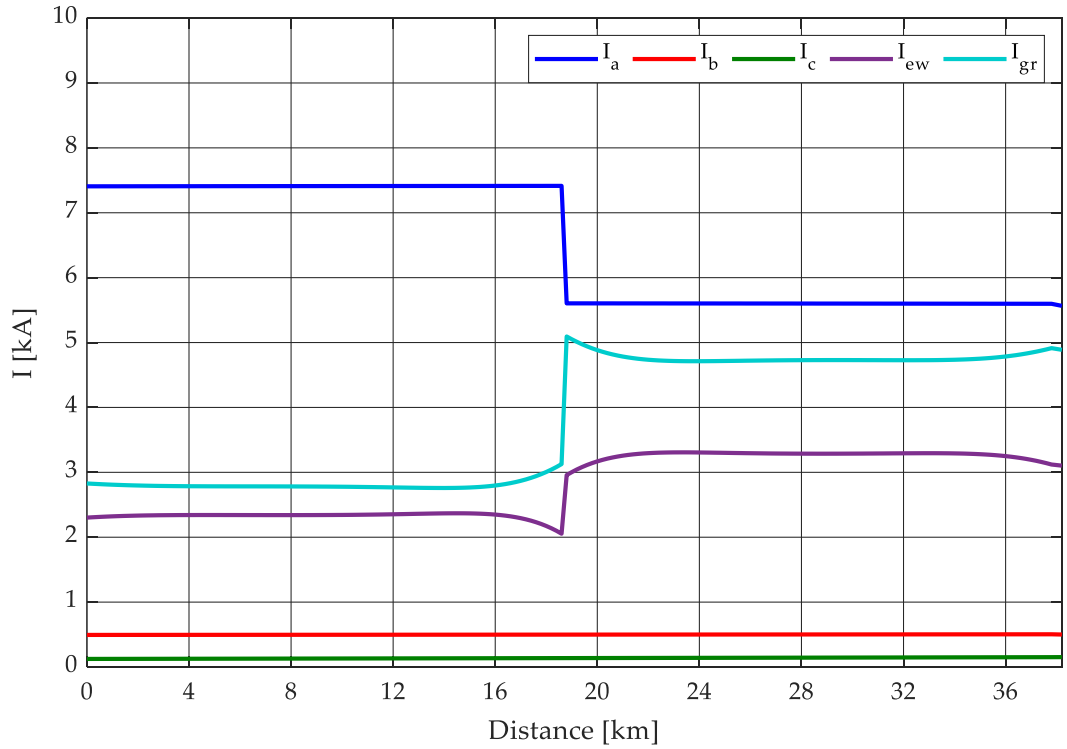

Figure 5-20: Fault current distribution in case of a phase-to-ground fault with an earthing resistance of the tower of 10 Ω.

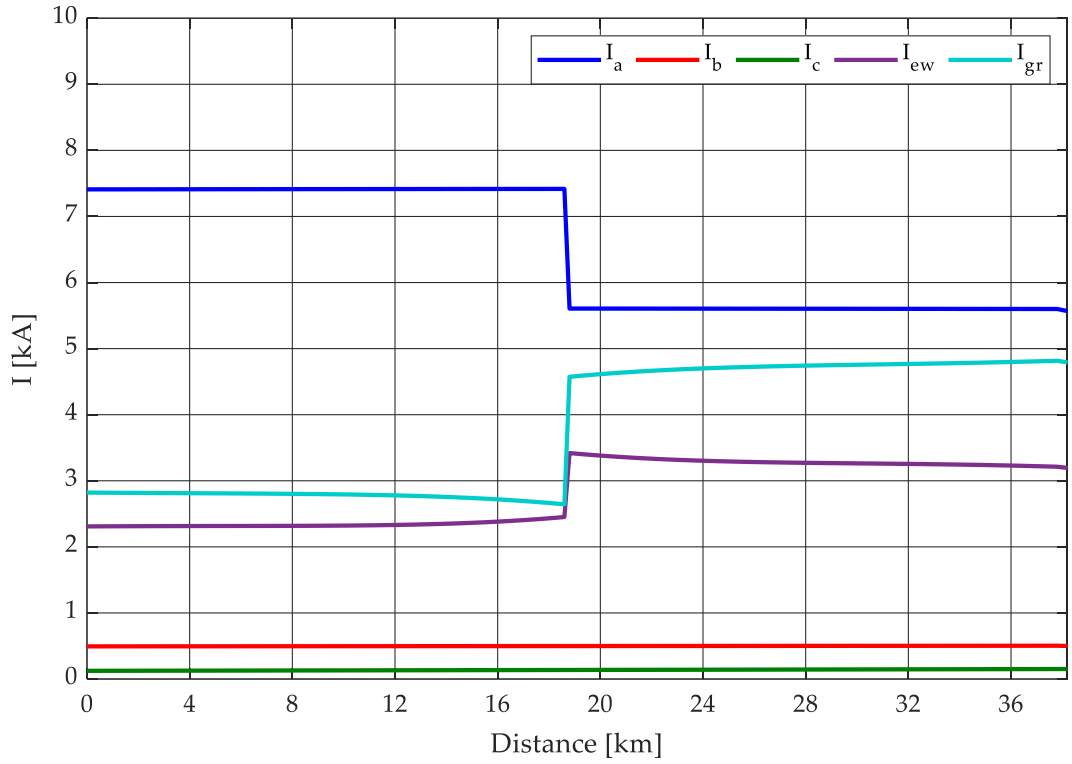

Figure 5-21: Fault current distribution in case of a phase-to-neutral fault with an earthing resistance of the tower of 100 Ω.

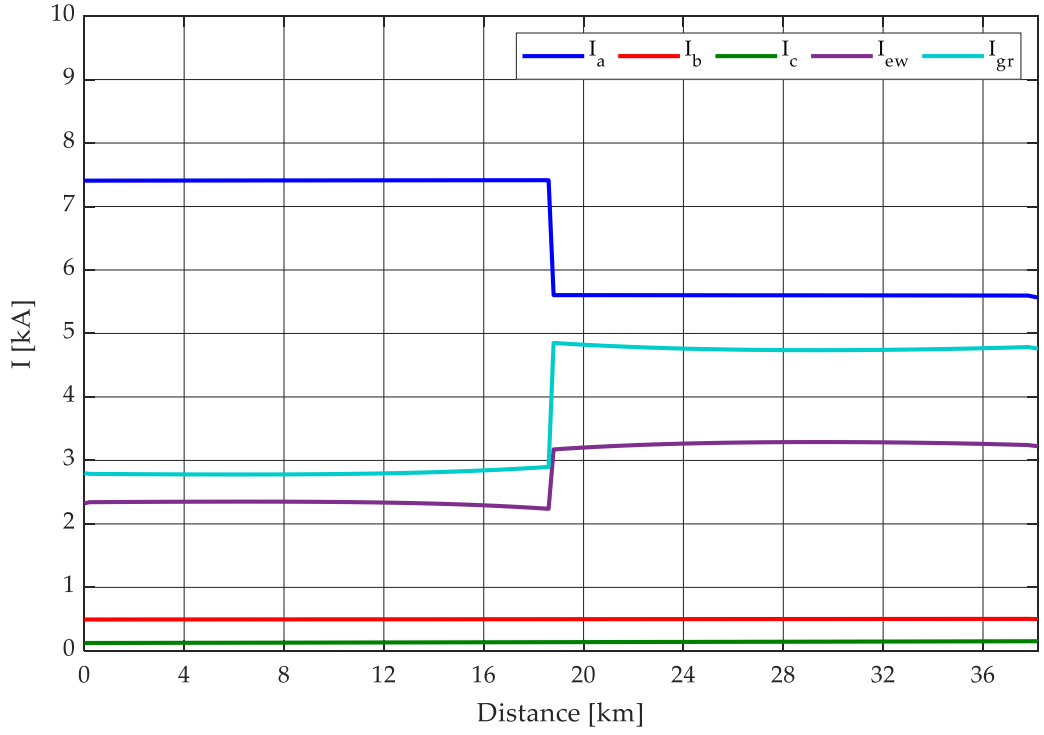

Figure 5-22: Fault current distribution in case of a phase-to-ground fault with an earthing resistance of the tower of 100 Ω.

The analysis which results are shown in Figg. 5-17 to 5-22 considered different values of the tower footing resistance. As it can be seen, a higher value of such resistances leads to a lower peak current at the fault section for both fault cases and to a longer space required for the achievement of constant current amplitude in both the ground and the earthwire. On the other hand, low values involve a great variation of the current amplitude in the fault section and the closer pylons and a quick stabilization of current magnitudes in terms of distance from the fault position.

It is worth noting the slight variations of the currents' amplitude in the proximity of the substations where, in the various tests, the earthing resistance has been kept constant at 0.1 Ω, thus lower than the towers' one (substations are typically grounded through earth grids). The contribution of loads and, most importantly, the busbar switch status need to be considered; their effect is less evident at higher earthing resistances where the currents on the earthwire and ground have not yet reached a constant value, near the substations or in any case that involves a larger number of spans to achieve this stabilization.

The values of the fault current are not reported here as there is just a small decrease of about 0.6% passing from the case with ground resistance value of 0.1 Ω to the value of 1 Ω, while it remains the same in the other cases.

The effects of fault location on power distribution are now analysed with simulations at the beginning and at the end of the line, which results are reported in Figg. 5-23 to 5-26.

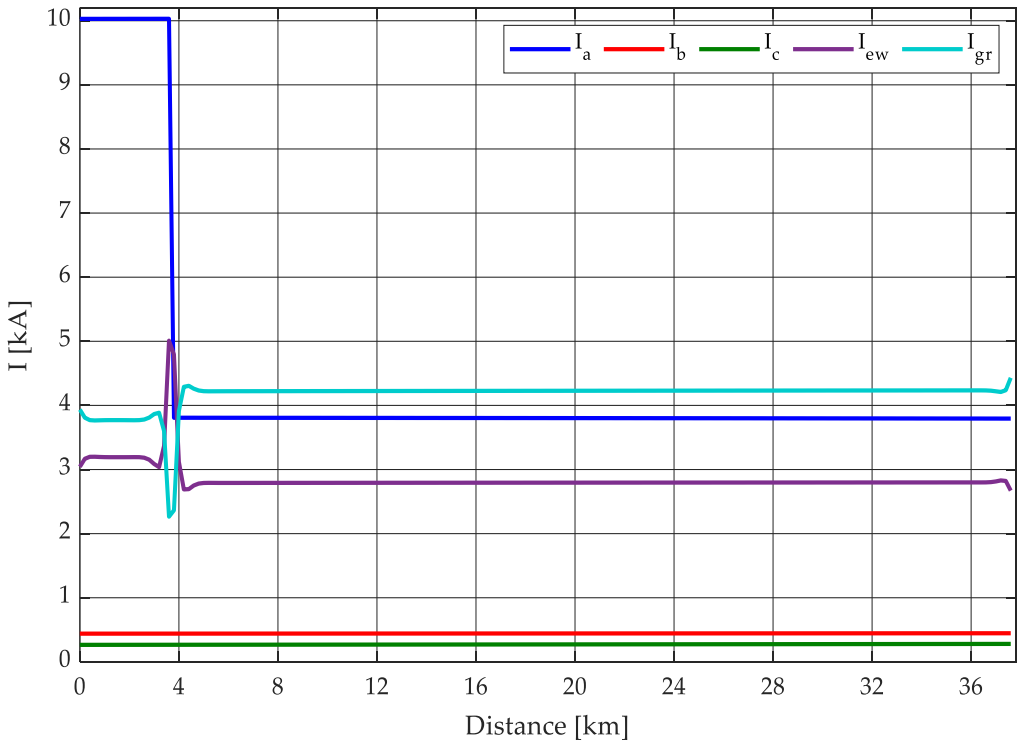

Figure 5-23: Fault current distribution in case of phase-to-neutral fault at the 10% of the line length with an earthing resistance of the tower of 0.1 Ω.

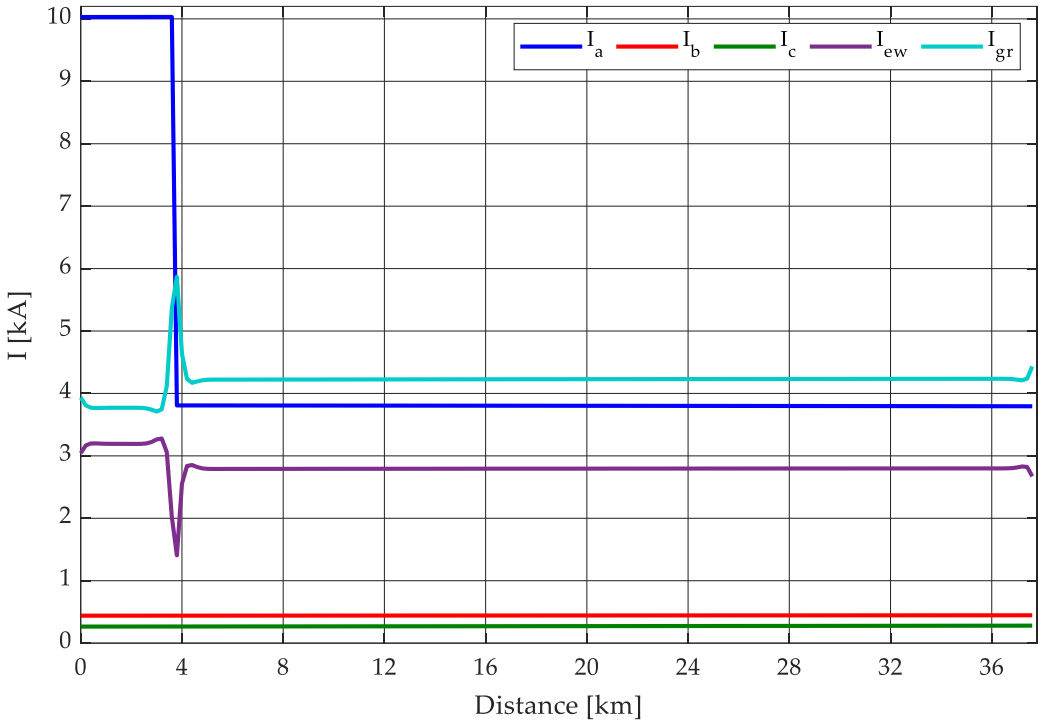

Figure 5-24: Fault current distribution in case of phase-to-ground fault at the 10% of the line length with an earthing resistance of the tower of 0.1 Ω.

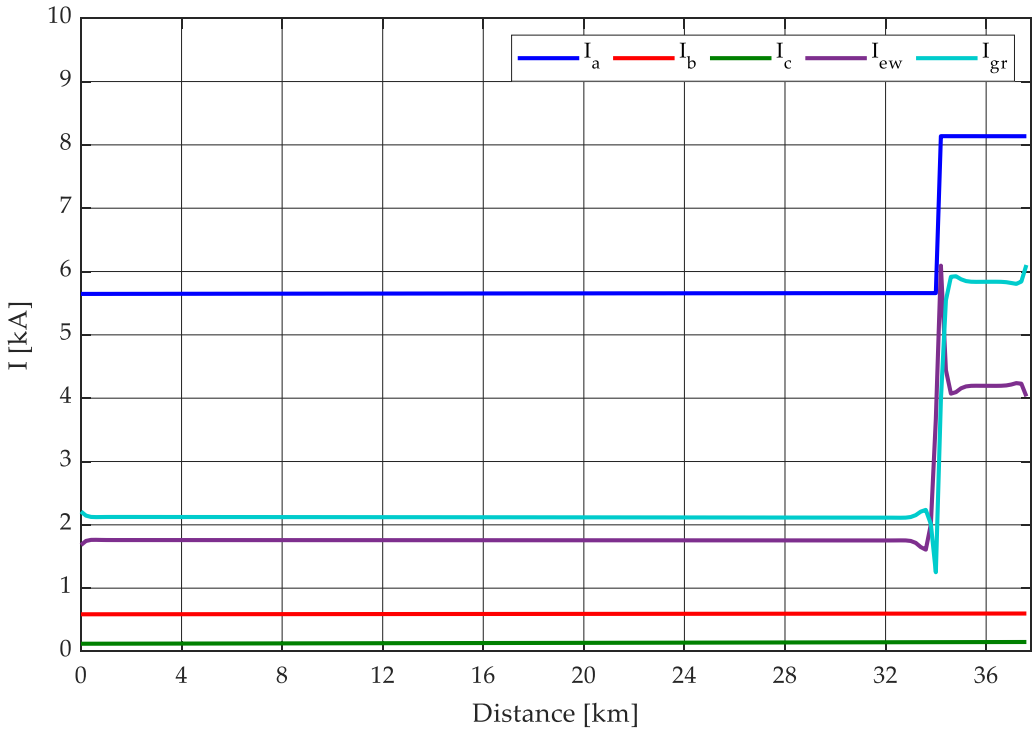

Figure 5-25: Fault current distribution in case of phase-to-neutral fault at the 90% of the line length with an earthing resistance of the tower of 0.1 Ω.

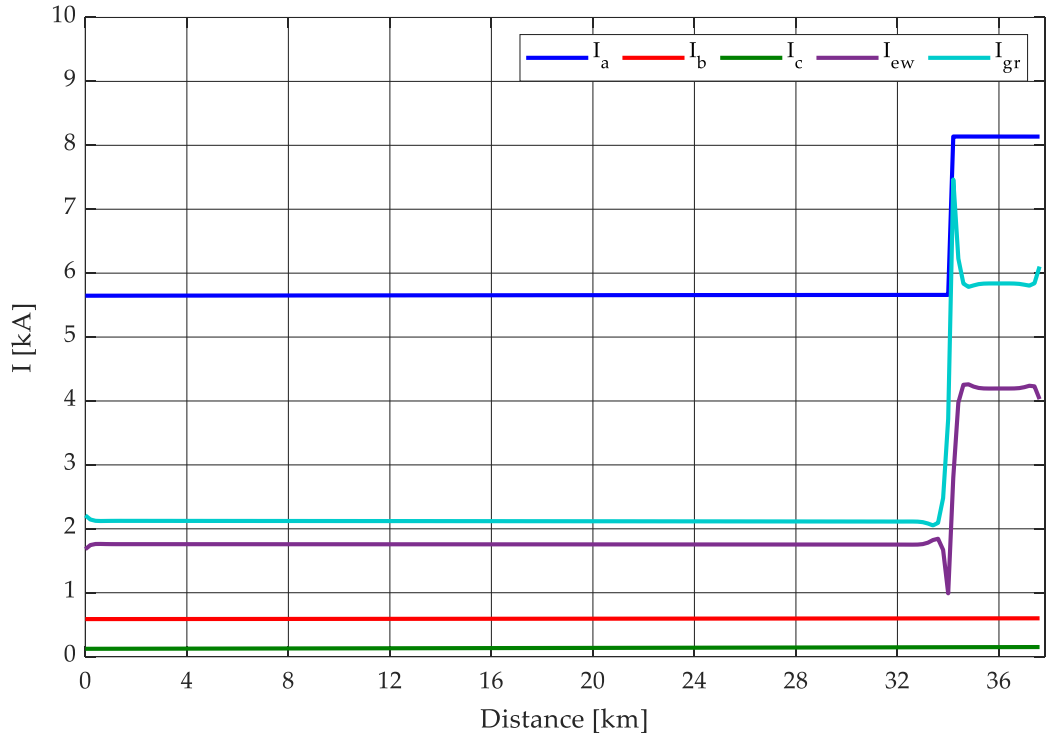

Figure 5-26: Fault current distribution in case of phase-to-ground fault at the 90% of the line length with an earthing resistance of the tower of 0.1 Ω.

Regarding the influence of the fault location on the fault current distribution, the above graphics show that there is not a direct correlation between these parameters: the only differences are those highlighted in the previous chapter regarding the fault current values before and after the fault section and in its correspondence (from left to right, the effect are a higher peaks rise, a lower current value before the fault location and a higher current value after the fault location). The currents distribution, in fact is mostly related to the electrical distance between the fault location and the generators' buses.

The variation of the distribution in the proximity of the substation is not particularly dependent on the distance of the fault from the substation itself; it is only affected by the distance when the fault happens very close to the substation (in the graph in Fig. 5-27, the fault is simulated at two spans from TAUN substation) where the variation of the currents between earth-wire and ground is such as to mask this effect.

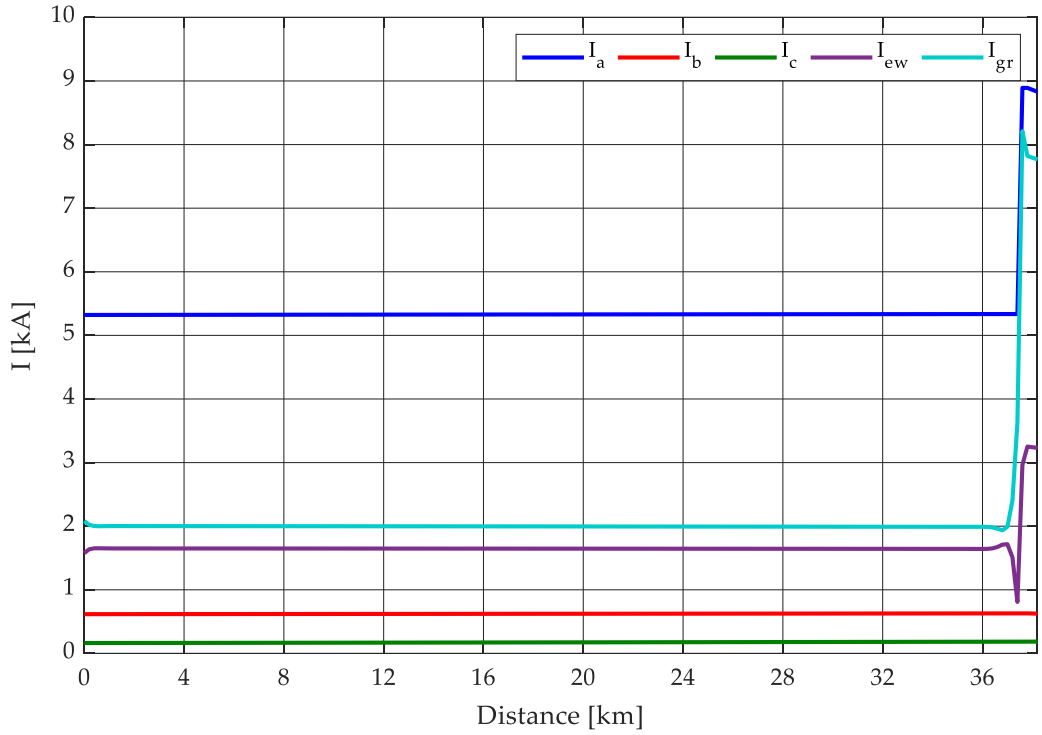

Figure 5-27: Fault current distribution in case of phase-to-ground fault at the 95.5% of the line length with an earthing resistance of the tower of 0.1 Ω.

The last parameter whose influence on fault current distribution has been analysed is the span length: for this, three cases of single phase-to-neutral faults have been simulated at half of the line length, with a span length of respectively 200, 400 and 800 m.

To obtain these results reported in Figg. 5-28 to 5-30, the fault has always been simulated near pylons with 0.1 Ω grounding resistance to maintain a similar trend at the fault sections, while of course, a simulation of the fault in the middle of a span involves lower peak values for both the current in the neutral and in the ground as the first grounding resistances that allow current exchanges are physically further away.

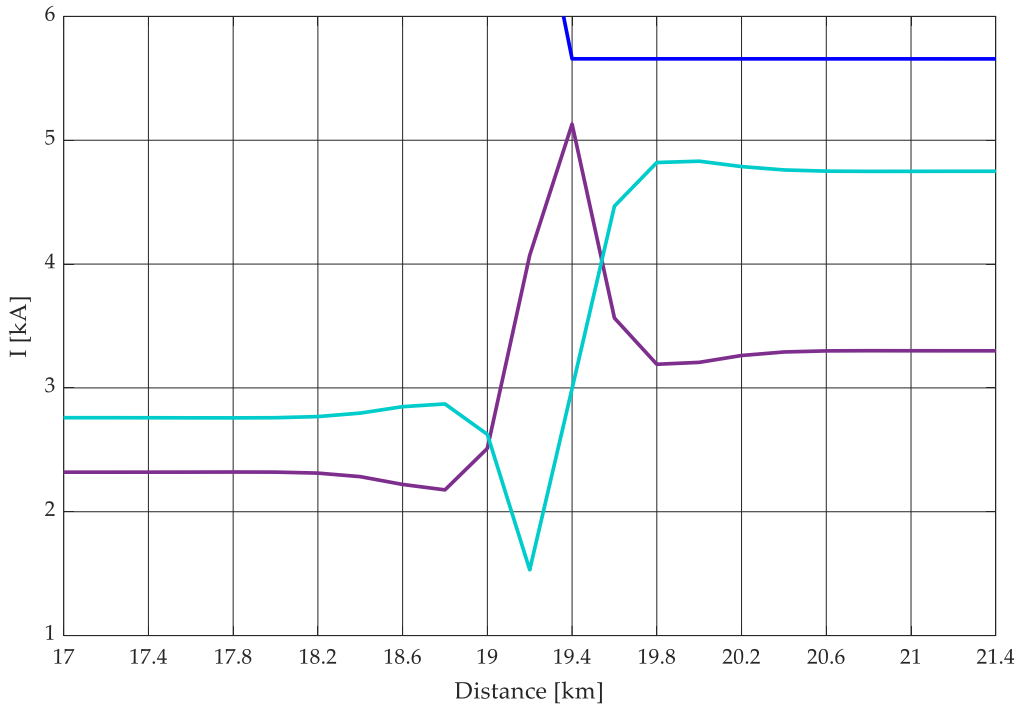

Figure 5-28: Zoom of Figure 5-13 to highlight the distribution of the fault current between ground paths and neutral conductor in the proximity of the fault section.

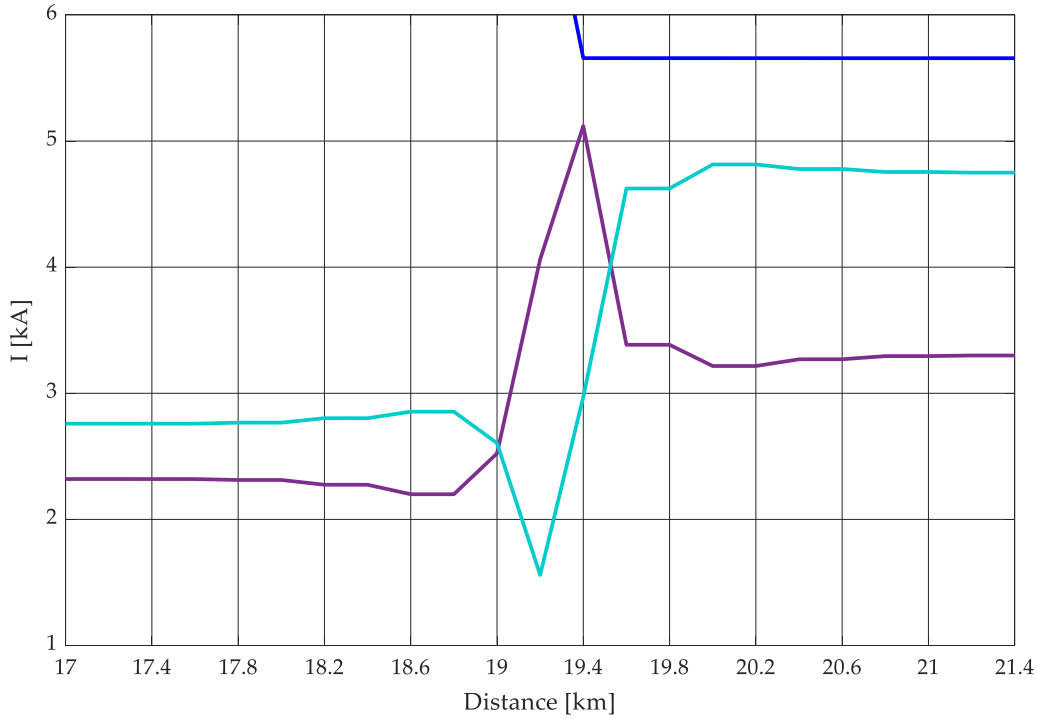

Figure 5-29: Distribution of the fault current between ground paths and neutral conductor in the proximity of the fault section, with 400 m spans.

The graphs show the different trend of the fault current distribution in case of failure at half of the line, resistance 0.1 Ω but with spans of 200 m in the first case and 400 m in the other. It should be noted that

the main difference is neither in the value of the fault current nor in its distribution in correspondence of the fault section, but what varies is the distribution in the adjacent areas: since in the second case there are half of spans and towers, the current requires more space to carry out the exchanges between neutral and ground (as a result of the slower variations in the voltage potential due to a weaker grounding) and therefore, although the number of towers influencing this distribution is about the same, a constant value is reached at greater distances. While in the first case already at 18.2 and 20.4 km the current has a uniform value along the line sections before and after the fault, in the second case the same effect with the same values is obtained at 17.4 and 21.2 km. In both cases, the contribution is in any case provided by the first 3-4 spans that on both sides are closer to the fault section.

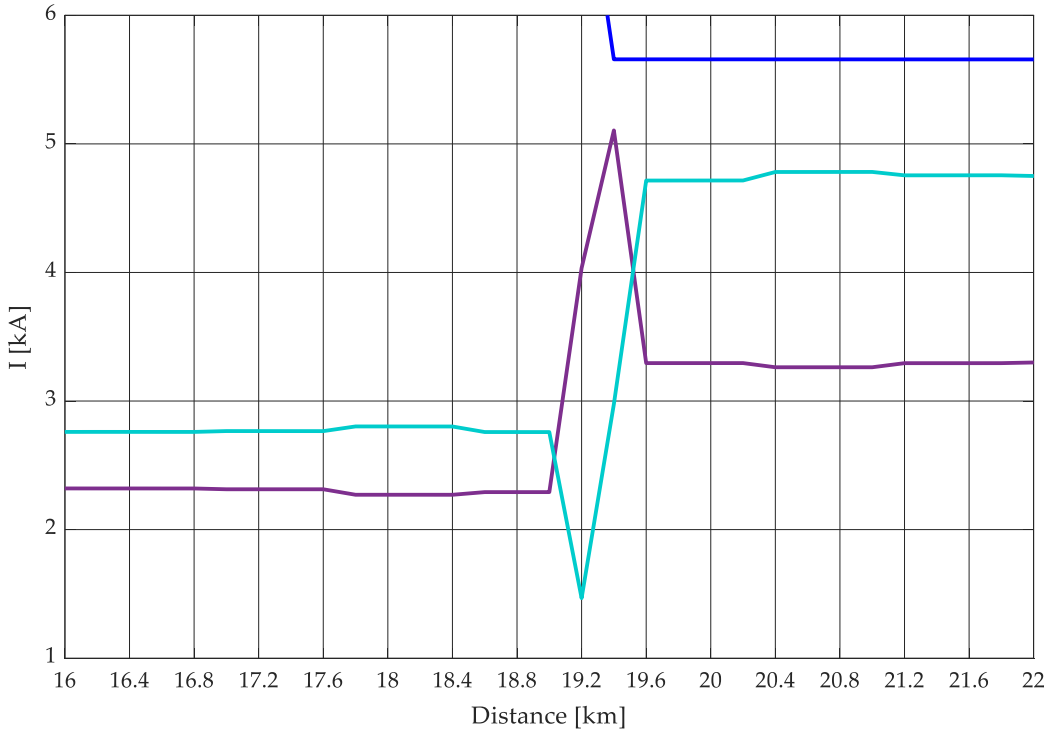

Figure 5-30: Distribution of the fault current between ground paths and neutral conductor in the proximity of the fault section, with 800 m spans.

A very similar effect is also achieved in the case of 800 m long spans, where the almost constant values are reached at 16.8 and 21.8 km. In the latter case, the fluctuation of the current value near the fault sections is reduced due to the greater distance the current has to travel before reaching the connection points between neutral and ground.

6 Conclusions

The main objective of the thesis is to present and validate numerically a Matlab script based on multi-conductor representation and phase analysis, able to model and simulate asymmetric networks with different conductor numbers between one section and another.

The comparison was carried out with Neplan software, based on a representation of the network through sequence theory, and OpenDSS, a software based on multi-conductor representation and nodal admittance matrix construction as in Matlab. The main elements on which the comparison between the modelling approaches in the three software is focused are generators, transformers, load, lines and grounding systems.

Two case study systems have been considered for the analysis. The first is a simple line with unidirectional feeding and a single load, while the second is a portion of a real transmission network. Simulations on both cases have shown that, for three-phase faults, the results of the three programs are the same, validating the phase-components approach with respect to positive-sequence representation, in the case of symmetrical transmission lines.

For single-phase failures, the results obtained in Matlab were sufficiently close to those obtained in OpenDSS for both cases, while those obtained in Neplan differ by a maximum of 10% in the real grid case. This difference has been demonstrated being due to symmetry assumptions being made in Neplan, since they were found, in particular, for very long double circuit lines. This effect is mainly due to the lack of possibility of customisation of the earthing systems of substations and towers on Neplan; as proof of this, tests have been simulated near the generation and transformation nodes where the contribution values of the generators, being equal between the three software, validate the correspondence between symmetrical components model and multi-conductor model of the generator.

Once the model has been validated numerically, further simulations have been carried out to show the advantages of the multi-conductor approach used in Matlab: a particularly useful feature is the possibility to simply model the busbar switch configurations, whose state greatly affects the amplitude and the distribution of the fault current, since it influences the electrical distance between the fault and the sources. Another great advantage is the possibility to widely customize the grounding conditions, allowing, on the one hand, to better represent the real systems and, on the other hand, to know not only the fault current value at the fault point but also its distribution between neutral and ground paths. This made it possible to analyse the influence of parameters such as busbar switch status, grounding resistance at both the substations and at towers, fault position and span length on fault current distribution. This feature allows to investigate how much these parameters affect the fault current distribution, highlighting the necessity of a detailed system modelling approach, in order to analyse the consequence of the fault in the larger areas rather than just in the vicinity of the fault location.

This method also allows a better evaluation of the GPR than the non-probabilistic maximum failure current method currently used by the standards that refers to the worst case, to better quantify the phenomenon for the human safety and to avoid unnecessary and extremely expensive measures.

Appendix

For the sake of completeness and replicability of the tests, the appendix contains the data needed to reconstruct the two networks used for the fault simulations, i.e. the simple double circuit line empowered just by one side, used for the first tests, and the data of a portion of the UK National Grid transmission network that can also be found on the nationalgrid site.

Appendix A

This appendix shows the data of the simple line used for the first tests. The grounding values have not been reported because they have been described in the appropriate section, as well as the transformer connections that are only needed to make the connections to the primary and secondary side because then the grounding is set in other scripts of the code. As also reported in the section of single-phase faults simulated on this line, the length of the line has been reduced to 12 km and consequently, the names of the nodes have also changed because in the three-phase case the line ends at the FOURTEEN node while in the single-phase one it ends at SIXTEEN.

V_{1n} [kV]	V_{2n} [kV]	S_n [MVA]	v_{cc} [%]	p_{cc} [%]	Conn.
220	220	500	12	0.1	Yy0

Table A-1: Transformer's data for the first test.

Node	V [kV]	S_n [MVA]	P [MW]	Q [Mvar]	X_d %	X_d" %	x(2) %	x(0) %
TREE	220	400	400	0	160	12	12	6

Table A-2: Generator's data for the first test.

Node	P [MW]	Q [Mvar]
FOURTEEN	1	0

Table A-3: Load's data for the first test.

Wire Type	r [mm]	GMR [mm]	R [ohm/km]	g	I_{max} [A]
1	28.62	11.14	0.0684	0	1000
2	19.53	7.60	0.1586	0	1000

Table A-4: Conductors' data for the first test.

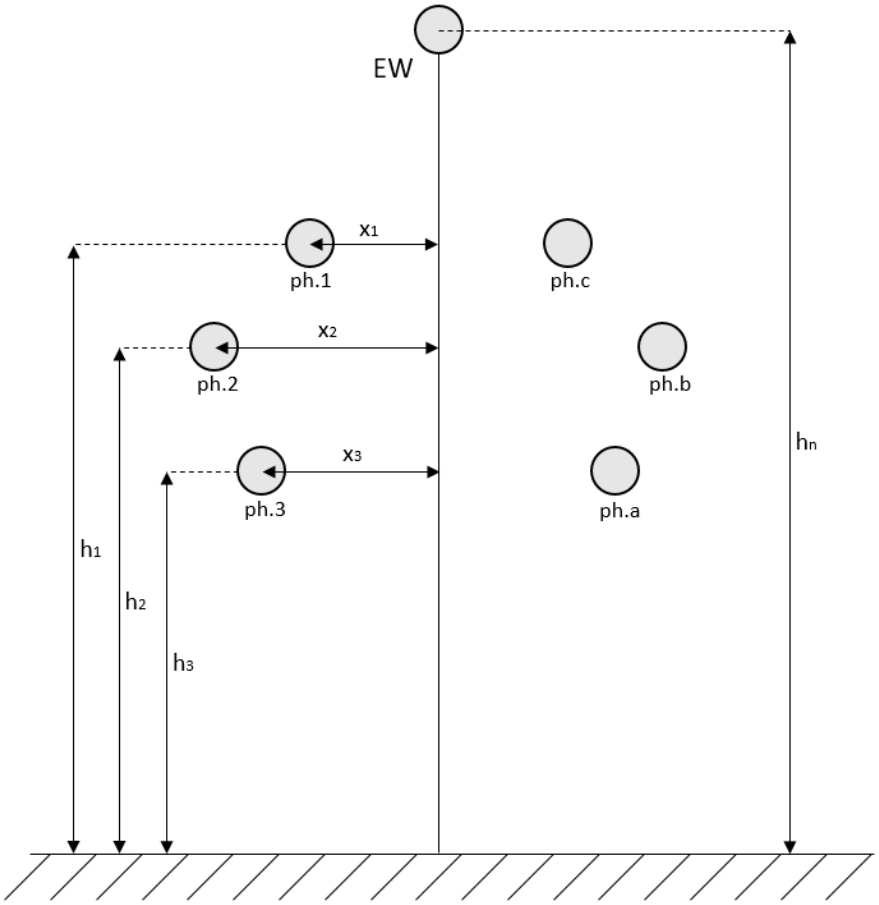

Table A-5: Tower layout in case of double circuit line to understand the distance parameters inserted in the lines' data tables; in case of single circuit line the values refer to the unique line, while for double circuit line the parameters of the second circuit are the same for the height and need to be changed of sign for the distance on the x-axis.

n° ph.	ph. cond	EW	x_1	x_2	x_3	x_n	h_1	h_2	h_3	h_n
6	1	2	-3.74	-4.65	-3.74	0	18.26	14.22	10.56	22.78

Table A-6: Line's data for the first test.

From Node	To Node	Line Type	Length [km]
FOUR	FOURTEEN	1	120

Table A-7: Network's branches composition and length for the first test.

Appendix B

This appendix contains the data of a portion of the UK National Grid transmission network. No particular changes have been made between the three-phase fault and the SLG fault; all the data have the same meaning as the other test, it has been added only a dedicated table for the external equivalent grid as it needs different parameters from the generators to be defined in Neplan.

V_{1n} [kV]	V_{2n} [kV]	S_n [MVA]	v_{cc} [%]	p_{cc} [%]	Conn.
400	275	500	12.2	0.2	Yy0

Table B-1: Transformer's data for the portion of the UK National Grid transmission network; as the nodes to which is connected are the nodes of two double circuit lines, in the software two transformers have been modelled, defined by the same data.

Node	V [kV]	S_n [MVA]	P [MW]	Q [Mvar]	X_d %	X_d'' %	x(2) %	x(0) %
HINP	400	1261	1261	0	180	20.4	20.4	1.464
INDQ	400	1000	1000	0	180	15.24	15.24	1.464
LANG	400	905	905	0	180	25	25	2.382

Table B-2: Generators' data for the portion of the UK National Grid transmission network.

Node	V [kV]	S_n [MVA]	P [MW]	Q [Mvar]	v_{cc} [%]	p_{cc} [%]	$I_k''_{max3f}$	$I_k''_{max1f}$
FAWL	400	10000	10000	0	100	0	14434	14434

Table B-3: External circuit equivalent grid's data for the portion of the UK National Grid transmission network.

Node	P [MW]	Q [Mvar]
ABHA.A	141.6	0
ABHA.B	98.4	0
ALVE.A	101	0
ALVE.B	102	0
AXMI	105	26.315
BRWA.A	114.5	33.396
BRWA.B	114.5	33.396
CHIC.A	52.2	17.157
CHIH.B	52.2	17.157
EXET	300	0
HINP2.A	1	0.512
HINP2.B	1	0.512
INDQ	420	0
LAND.A	126.5	0
LAND.B	126.5	0
MANN	727.8	147.786
TAUN.B	127	17.669

Table B-4: Loads' data for the portion of the UK National Grid transmission network; the characterization of NODE A and NODE.B has been introduced to distinguish the two different circuit of the double circuit lines.

Wire Type	r [mm]	GMR [mm]	R [ohm/km]	g	I_{max} [A]
1	24.71	9.62	0.0878	0	1000
2	19.53	7.60	0.1654	0	1000
3	131.04	51.03	0.0342	0	1000
4	19.53	7.60	0.1586	0	1000
5	137.48	53.53	0.0279	0	1000
6	134.88	52.52	0.02945	0	1000

Table B-5: Conductors' data for the portion of the UK National Grid transmission network.

n° phases	ph. cond	EW	x_1	x_2	x_3	x_n	h_1	h_2	h_3	h_n
6	1	2	-2.8	-4.2	-3.2	0	19.87	16.12	12.37	23.79
6	3	4	-3.12	-4.7	-3.48	0	20.06	15.64	11.93	24.27
6	3	4	-5.48	-5.71	-6.09	0	28.57	20.8	12.96	34.94
6	3	2	-5.48	-5.71	-6.09	0	29.86	22.09	14.25	35.6
3	6	4	-5.48	-5.71	-6.09	0	27.7	19.93	12.09	35.6

Table B-6: Lines' data for the portion of the UK National Grid transmission network.

From Node	To Node	Line Type	Length [km]
FAWL	MANN	3	60.65
MANN	NURS	3	39.68
MANN	CHIC	3	53.784
CHIC.A	AXMI	5	39.697
CHIC.B	EXET	5	76.088
AXMI	EXET	3	36,315
EXET	TAUN	2	38.232
EXET	ABHA	4	49.15
ABHA	LANG	4	24.63
LANG	LAND	1	21.47
LAND	INDQ	1	49.55
INDQ	ALVE	4	97.543
ALVE	TAUN	4	72.867
TAUN	HINP	2	26.694
HINP2	BRWA	1	18.953

Table B-7: Network's branches composition and length for the portion of the UK National Grid transmission network.

Bibliografia

[1] A. Administration, “U.S. Department of Energy Washington DC,” 24 September 2019. [Online]. Available: https://www.eia.gov/outlooks/ieo/pdf/ieo2019.pdf.

[2] IPCC, October 2013. [Online]. Available: https://www.ipcc.ch/site/assets/uploads/2018/03/ar5-wg1-spmitalian.pdf.

[3] E. Commission, “European Commission website,” [Online]. Available: https://ec.europa.eu/clima/policies.

[4] E. Commission, “European Commission website,” [Online]. Available: https://ec.europa.eu/info/news/clean-energy-all-europeans-package-completed-good-consumers-good-growth-and-jobs-and-good-planet-2019-may-22_en.

[5] R. Turri, *Corso di Sistemi Elettrici per l'Industri e i Trasporti - Qualità del Servizio,* Padova, 2019.

[6] R. Benato and L. Fellin, Impianti elettrici, Milano: Wolters Kluwer, 2014.

[7] IEEE, *Recommended Practice for Monitoring Electric Power Quality, IEEE Std. 1159,* 2009.

[8] Y. Wang, H. Luo and X.-Y. Xiao, “Voltage sag frequency kernel density estimation method considering protection characteristics and fault distribution,” *Electric Power Systems Research,* no. 170, pp. 128-137, 2019.

[9] J. V. Milanovic, M. T. Aung and C. P. Gupta, “The influence of fault distribution on stochastic prediction of voltage sags,” *IEEE Transactions on Power Delivery,* no. 20, pp. 278-285, 2005.

[10] U. A. Bordalo, A. B. Rodrigues and M. G. Da Silva, “A New Methodology for Probabilistic Short-Circuit Evaluation With Applications in Power Quality Analysis,” *IEEE TRANSACTIONS ON POWER SYSTEMS ,* vol. 21, no. 2, pp. 474-479, 2006.

[11] Terna, *Criteri generali di protezione delle reti a tensione uguale o superiore a 110 kV,* 2018.

[12] Enel, *Guida per le connessioni alla rete elettrica di Enel Distribuzione,* 2015.

[13] W. A. Chisholm, J. A. Jardini, P. E. Freire, G. Watt, L. Figueroa and O. Regis, “Global and Brazilian Perspectives on Managing Ground Potential Rise at Overhead AC Transmission Structures during Power Frequency Faults: Invited Lecture: CIGRE Technical Brochure 694 Tutorial,” in *International Symposium on Lightning Protection*, Sao Paulo, 2019.

[14] H. H., G. H., H. A. and A. A., “Safety-limit Curves for Earthing System Designs: Appraisal of Standard Recommendations,” *IEEE Proceedings - Generation, Transmission and Distribution,* vol. 152, pp. 871-879, 2005.

[15] S. Mangione and L. Mineo, *Safety Concerns on Ground Fault Application Transfer Phenomenon in HV Installations,* Palermo, 2005.

[16] S. Mangione, “A Simple Method for Evaluating Ground-Fault Current Transfer at the Transition Station of a Combined Overhead-Cable Line,” *IEEE TRANSACTIONS ON POWER DELIVERY,* vol. 23, no. 3, pp. 1413-1418, 2008.

[17] V. Torres-Garcia, D. Guillen, J. Olveres, B. Escalante-Ramirez and J. R. Rodriguez-Rodriguez, “Modelling of high impedance faults in distribution systems and validation

based on multiresolution techniques," *Computers and Electrical Engineering,* vol. 83, pp. 1-15, 2020.

[18] J. J. Burke and D. J. Lawrence, "Characteristics of faults current on distribution systems," *IEEE Transactions on Power Apparatus and Systems,* vol. 103, no. 1, pp. 1-6, 1984.

[19] L. M. Popovic, "Practical method for evaluating ground fault current distribution in station supplied by an unhomogeneous line," *IEEE Transactions on Power Delivery, Vol. 12, No. 2, April 1997,* vol. 12, no. 2, pp. 722-727, 1997.

[20] M. Nassereddine, J. Rizk, A. Hellany and M. Nagrial, "Relation between transmission lines coupling factor and over head earth wire length: its impacts on fault current distributions," *IET Generation, Transmission & Distribution,* 2013.

[21] M. G. Unde and R. N. Maske, "Analysis of Fault Current Distribution," in *International Conference on Information, Communication, Engineering and Technology (ICICET)*, Pune, India, 2018.

[22] L. Qi, H. Yuan, L. Li and X. Cui, "Calculation of Interference Voltage on the Nearby Underground Metal Pipeline due to the Grounding Fault on Overhead Transmission Lines," *IEEE TRANSACTIONS ON ELECTROMAGNETIC COMPATIBILITY,* vol. 55, no. 5, pp. 965-974, 2013.

[23] N. Haddad and M. Cucchiaro, *Ground potential rise calculation applied to a multiconductor network of a railway system,* Saint-Denis, 2012.

[24] M. El Kady, "Probabilistic short circuit analysis by Monte-Carlo simulations," *IEEE Transactions on Power Apparatus and Systems,* vol. 102, no. 5, pp. 1308-1316, 1983.

[25] F. Dawalibi, "Ground fault current distribution between soil and neutral conductors," *IEEE Transactions on Power Apparatus and Systems,* vol. 99, no. 2, pp. 452-461, 1980.

[26] Y. Lim and G. Strbac, "Analytical approach to probabilistic prediction of voltage sags on transmission networks," *IEEE Proceeding: Generation Transmission and Distribution,* vol. 149, no. 1, pp. 7-14, 2002.

[27] M. B. Bastian, W. D. Carman and D. J. Woodhouse, "Real-Time Monitoring of Substation Ground Potential Rise and Grounding System Impedance Using Power System Faults," *IEEE TRANSACTIONS ON INDUSTRY APPLICATIONS,* vol. 51, no. 6, pp. 5298-5304, 2015.

[28] T. Radošević, K. Musulin and B. Dikić, "Earth potential rise influence in high voltage substations with long cable and transmission lines in rural areas," in *ENERGYCON*, Dubrovnik, Croatia, 2014.

[29] M. Talaat, M. Farahat, M. A. Essa and M. Maowwad, "Simulation of the electric field and the GPR resulting from vertical-driven rods earthing system in a multi-layers earth structure," *Measurement,* vol. 132, pp. 387-401, 2019.

[30] T. Ayodele, A. Ogunjuyigbe and O. Oyewole, "Comparative assessment of the effect of earthing grid configurations on the earthing system using IEEE and Finite Element Methods," *Engineering Science and Technology, an International Journal,* vol. 21, pp. 970-983, 2018.

[31] P. Sebire, W. D.J. and W. Tocher, *Effective Management Of Earth Potential Rise Through Alternative Installation Strategies For Counterpoise Conductors,* Warners Bay, NSW, Australia, 2016.

[32] S. IEEE, *IEEE Recommended Practice for Determining the Electric Power Station Ground Potential Rise and Induced Voltage from a Power Fault,* 2012.

[33] R. Benato, *Appunti del corso di Sistemi Elettrici Per l'Energia,* Padova, 2019.

[34] D. J. Woodhouse and R. H. Middleton, *Assessment of Analysis Techniques used in determining Grounding System Potential Rise from the Fall of Potential Method,* New South Wales, Australia, 2000.

[35] X. Liang and C. Wang, *Factors Affecting Ground Potential Rise and Fault Currents along Transmission Lines with Multi-Grounded Shield Wires,* Canada, 2016.

[36] S. C. Malanda, E. Buraimoh, I. Davidson and E. Singh, "Analysis of Soil Resistivity and its Impact on Grounding Systems Design," in *Power Africa*, 2018.

[37] M. Nassereddine, J. Rizk and G. Nasserddine, "Soil Resistivity Data Computations; Single and Two-Layer Soil Resistivity Structure and Its Implication on Earthing Design," *World Academy of Science, Engineering and Technology International Journal of Electrical and Computer Engineering,* vol. 7, no. 1, pp. 35-40, 2013.

[38] M. Mitolo, P. E. Sutherland and R. Natarajan, "Effects of High Fault Currents on Ground Grid Design," *IEEE TRANSACTIONS ON INDUSTRY APPLICATIONS,* vol. 46, no. 3, pp. 1118-1124, 2010.

[39] W. K. Daily and F. Dawalibi, "Cost Reduction and Minimization of Land Based on an Accurate Determination of Fault Current Distribution in Shield Wires and Grounding Systems," *IEEE Transactions on Power Delivery,* vol. 8, no. 1, pp. 97-103, 1993.

[40] R. Narayan and S. Harshavandhana, *Earth Potential Rise in Public Spaces Near Telecommunications Facilities.*

[41] M. B. Bastian, W. D. Carman and D. J. Woodhouse, "Real-Time Monitoring of Substation Ground Potential Rise and Grounding System Impedance Using Power System Faults," *IEEE TRANSACTIONS ON INDUSTRY APPLICATIONS,* vol. 51, no. 6, pp. 5298-5304, 2015.

[42] A. Demazy, T. Alpcan, I. Mareels and S. Saha, *Assessment of Voltage Stability Risks under Stochastic Net Loads using Scalable SVM Classification,* Melbourne, 2016.

[43] D. Nordgård, K. Sand and I. Wangensteen, *Risk assessment methods applied to electricity distribution system asset management,* Trondheim, Norway, 2009.

[44] J. Stowe, *Managing Health and Safety Risk Assessment Effectively; Cost Effective Compliance,* The Stationary Office, 2001.

[45] J. Hewitt and J. Pham, *Qualitative Versus Quantitative Methods in Safety Risk Management,* 2017.

[46] J. G. Sverak, W. Wang, Y. Gervais, H. Dai Do and D. Mukhedar, "A probabilistic method for the design of power grounding systems," *IEEE Transactions on Power Delivery,* vol. 7, no. 3, pp. 1196-1206, 1992.

[47] CENELEC, *Power Installations Exceeding 1 kV a.c., European Committee of Electrotechnical Standardization,* 1999.

[48] I. S. 80, *IEEE guide for safety in AC substation grounding,* 2000.

[49] M. El-Kady, P. Hotte and M. Vainberg, "Probabilistic Assessment of Step and Touch Potentials Near Transmission Line Structures," *IEEE Transactions on Power Apparatus and Systems,* vol. 102, no. 3, pp. 640-645, 1983.

[50] A. Dimopoulos, H. Griffiths, N. Harid, A. Haddad, A. Ainsley and G. Mpofu, "Probability Surface Distributions for Application in Grounding Safety Assessment," *IEEE TRANSACTIONS ON POWER DELIVERY, VOL. 27, NO. 4, OCTOBER 2012,* vol. 27, no. 4, pp. 1928-1936, 2012.

[51] *IEC 60909-0: Short-circuit currents in three-phase a.c. systems - calculation of currents,* 2001.

[52] *IEC 60050(131): International Electrotechnical Vocabulary - Chapter 131: Electric and magnetic circuits,* 1978.

[53] *An American National Standard: IEEE Application Guide for AC High-Voltage Circuit Breakers Rated on a Symmetrical Current Bass,* 1979.

[54] A. Berizzi, S. Masucco, A. Silvestri and D. Zaninelli, "Short-circuit current calculation: a comparison between methods of IEC and ANSI standards using dynamic simulations as reference," *IEEE TRANSACTIONS ON INDUSTRY APPLICATIONS,* vol. 30, no. 4, pp. 1099-1106, 1994.

[55] B. Bridger, "All amperes are not created equal: a comparison of current ratings of high-voltage circuit breakers rated according to ANSI and IEC standards," *IEEE TRANSACTIONS ON INDUSTRY APPLICATIONS,* vol. 29, no. 1, pp. 195-201, 1993.

[56] G. Knight and H. Sieling, *Comparison of ANSI and IEC 909 short-circuit current calculation procedures.,* Manhattan, 1991.

[57] A. Rodolakis J., "A comparison of North American (ANSI) and European (IEC) fault calculation guidelines," *IEEE TRANSACTIONS ON INDUSTRY APPLICATIONS,* vol. 29, no. 3, pp. 515-521, 1993.

[58] A. Heyduk and J. Joostberens, "Comparative analysis of European and American standards for maximum fault current calculations on medium voltage mine power networks," *ELEKTRONIKA IR ELEKTROTECHNIKA,* vol. 22, no. 2, pp. 13-20, 2016.

[59] V. Lackovic, *Introduction to short circuit current calculations,* New York.

[60] S. L. Sankar and M. M. Iqbal, "ANSI and IEC standards based short circuit analysis of a typical 2x30MW thermal power plant," *Middle-East Journal of Scientific Research,* vol. 23, no. 8, pp. 1617-1625, 2015.

[61] D. Nedic, G. Bathurst and J. Heath, "A comparison of short circuit calculation methods and guidelines for distribution networks," in *19th International Conference on Electricity Distribution*, Vienna, 2007.

[62] J. Das and D. C. Mohla, *Harmonization of ANSI/IEEE standards for high-voltage circuit breakers with IEC and its impact on application and analysis,* 2011.

[63] C. F. De Sieno, P. P. Marchenko and G. S. Vassell, "General Equations for Fault Currents in Transmission Line Ground Wires," *IEEE Transactions on Power Apparatus and Systems,* vol. 8, no. 86, pp. 1891-1900, 1969.

[64] S. A. P. Meliopoulos and J. E. B., "Analysis of grounding systems," *IEEE Transactions on Power Apparatus and Systems,* vol. 100, no. 3, pp. 1039-1048, 1981.

[65] F. P. Dawalibi and G. Niles, "Measurements and computations of fault current distribution on overhead lines," *IEEE Transactions on Power Apparatus and Systems,* vol. 103, no. 3, pp. 553-560, 1984.

[66] L. M. Popovic, "Practical method for evaluating fault current distribution in station, towers and ground wires," *IEEE Transactions on Power Delivery,* vol. 13, no. 1, pp. 123-128, 1998.

[67] G. Weizenfeld, "Power system ground fault current distribution using the double-sided elimination method," *IEEE Transactions on Power Systems,* vol. 1, no. 1, pp. 17-25, 1986.

[68] J. Nahman and V. Dordevic, “Earth fault currents and potentials distribution in composite systems,” *IEEE Proceedings - Generation Transmission Distribution,* vol. 142, no. 2, pp. 135-142, 1995.

[69] G. M. Casolino and A. Losi, *On Eigenvalues of the Three-Phase Nodal Admittance Matrix,* Cassino: AEIT, 2019.

[70] A. M. Kettner, “On the Properties of the Compound Nodal Admittance Matrix of Polyphase Power Systems,” *IEEE Transactions on Power System,* vol. 34, no. 1, pp. 444-453, 2019.

[71] A. Marini, S. Mortazavi, L. Piegari and M.-S. Ghazizadeh, “An efficient graph-based power flow algorithm for electrical distribution systems with a comprehensive modeling of distributed generations,” *Electric Power Systems Research,* vol. 170, pp. 229-243, 2019.

[72] K. Sunderland, M. Coppo, R. Turri and M. Conlon, “A correction current injection method for power flow analysis of unbalanced multiple-grounded 4-wire distribution networks,” *Electric Power Systems Research,* vol. 132, pp. 30-38, 2016.

[73] M. Coppo, F. Bignucolo and R. Turri, “Generalised transformer modelling for power flow calculation in multi-phase unbalanced networks,” *IET Generation, Transmission & Distribution,* vol. 11, no. 15, pp. 3843-3852, 2017.

[74] R. Benato, A. Paolucci and R. Turri, “Power Flow Solution by a Complex Admittance Matrix Method,” *ETEP,* vol. 11, no. 3, pp. 181-188, 2001.

[75] Busarello, Cott, P. Gmbh and A. Utilities, *Neplan User's Guide Electrical.*

[76] R. Roeper, Le correnti di corto circuito nelle reti trifasi, Milano: Editoriale Delfino, 1965.

[77] R. C. Dugan and D. Montenegro, *The Open Distribution System Simulator (OpenDSS),* Electric Power Research Institute, 2020.